Distributed Control for Wind Farm Power Output Stabilization and Regulation

Submitted in partial fulfillment of the requirements for
the degree of
Doctor of Philosophy
in
Electrical and Computer Engineering

Stefanos Baros

Diploma, ECE, National Technical University of Athens (NTUA), 2011
M.Sc., ECE, Carnegie Mellon University, 2012

Carnegie Mellon University
Pittsburgh, PA

May 2016

Keywords: Distributed control, wind farm power output regulation, consensus-based control, nonlinear control.

To my parents,
who inspire me to pursue knowledge in my life,
a more lasting possession than anything else

S. B.

ΚΡΕΣΣΟΝΕΣ ΕΙΣΙ ΑΙ ΤΩΝ ΠΕΠΑΙΔΕΥΜΕΝΩΝ ΕΛΠΙΔΕΣ Η Ο ΤΩΝ ΑΜΑΘΩΝ ΠΛΟΥΤΟΣ

Δημόκριτος

“The visions of educated people are more important than the wealth of the uneducated”

Democritus

Abstract

Modern power systems are characterized by an increasing penetration of renewable energy generating units. These aim to reduce the carbon emissions in the environment by replacing conventional energy generating units which rely on fossil fuels. In this new power systems composition, wind generators (WGs) dominate, being one of the largest and fastest-growing sources of renewable energy production. Nevertheless, their unpredictable and highly volatile power output hinders their efficient and secure large-scale deployment, and poses challenges for the transient stability of power systems. Given that, we identify two challenges in the operation of modern power systems: rendering WGs capable of regulating their power output while securing transient stabilization of conventional synchronous generators (SGs). This dissertation makes several contributions for effectively dealing with these major challenges by introducing new distributed control techniques for SGs, storage devices and state-of-the-art (SoA) WGs.

Initially, this dissertation introduces a novel nonlinear control design which is able to coordinate a storage device and a SG to attain transient stabilization and concurrent voltage regulation on their terminal bus. Thereafter, it proposes control designs that SoA WGs can adopt to effectively regulate their power output to meet local or group objectives. In this context, the first control design is a decentralized nonlinear energy-based control design, that can be employed by a wind double-fed induction generator (DFIG) with an incorporated energy storage device (namely a SoA WG) to regulate its power output by harnessing stored energy, with guaranteed performance for a wide-range of operating conditions. Recognizing that, today, albeit wind farms (WFs) are comprised of numerous WGs which are sparsely located in large geographical areas, they are required to respond rapidly and provide services to the grid in an efficient, reliable and timely fashion. To this end, this dissertation proposes distributed control methods for power output regulation of WFs comprised of SoA WGs. In particular, a novel distributed control design is proposed, which can be adopted by SoA WGs to continuously, dynamically and distributively self-organize and control their power outputs by leveraging limited peer-to-peer communication. By employing the proposed control design, WGs can exploit their storage devices in a fair load-sharing manner so that their total power output tracks a total power reference under highly dynamical conditions. Finally, this dissertation proposes a distributed control design for wind DFIGs without a storage device, the most common type of WGs deployed today. With this control design, wind DFIGs can dynamically, distributively and fairly self-dispatch and adjust the power they extract from the wind for the purpose of their total power tracking a dynamic reference. The effectiveness of the control designs proposed in this dissertation is illustrated through several case studies on a 3-bus power system and the IEEE 24-bus Reliability Test System.

Acknowledgments

I wish to express my deep gratitude and appreciation to everyone that contributed to making my PhD journey a wonderful experience.

Foremost, to my advisor, Marija Ilić. Marija's passion, endless energy and striving for excellence in research have been a constant source of inspiration and motivation for me. Marija nurtured and enlightened me academically throughout these years in the best possible way. She would always enthusiastically share her own unique ideas and deep understanding of power system problems while at the same time giving me the freedom to explore and develop my own research ideas, enabling me that way to realize my own potential. Through her careful guidance, patience, continuous encouragement and support she made me mature as a researcher, while many times she had gone beyond the role of the advisor offering me her friendly advice when its was highly needed. I feel very fortunate and privileged to have been advised by Marija whose deep influence on both my professional and personal life I will always carry with me.

My gratitude also extends to the other members of my committee: to Prof. Soummya Kar, for always being eager to discuss and share his ideas with me and for providing me with valuable insight on my thesis topics that initiated new research directions; to Prof. Bruno Sinopoli, for his useful comments regarding my research, valuable advice about my future career path and for always being open to interesting nonacademic discussions; to Prof. Erik Ydstie for sharing with me his constructive comments on my PhD research.

Among my friends that are not in Pittsburgh, I wish to particularly thank and express my deepest possible appreciation and gratitude to Paris Syminelakis. Although on the west coast, he was always there for me, constantly supporting, encouraging and offering me his advice on both my academic and personal life matters throughout these years. Our friendship has been invaluable to me in succesfully completing this journey, and taking the right decisions in my life. For all these and many more, countless to remember, I am forever indebted.

Among my Pittsburgh friends, I wish to first thank my close friend Antonis Tasoglou for the numerous fun moments, friendly discussions and advice that we shared all these years that made me feel like I never left home.

Suprisingly, the last year of my PhD journey was the most enjoyable one. This is due to many wonderful moments of fun, joy and excitement over Italian, Greek and Serbian dinners and espressos that I shared with my amazing friends, Nicola Forti, Corrin Trombley, Walter Lucia, Ana Jevtić, Stefania Pellegrinelli, Javad Mohammadi, Martin Wagner and Elias Bou-Harb. Thank you all for being there for me, for making me smile during my toughest PhD moments, and for filling my last year at CMU with so many unforgettable moments.

I could not forget to thank my early-years officemates and friends, Nikos Arechiga and Milos Cvetković: Nikos, for the deep discussions about life, math and sciences as well as about the many other interests that we share; Milos, for being a true friend, a constant source of help and advice, and always willing to brainstorm with me on interesting research ideas.

I also wish to thank Claire Bauerle and Carol Patterson for always being willing to assist me with the procedural matters of my PhD life. Moreover, I would like to thank all the colleagues and friends of the B-level at Porter Hall for the many intriguing discussions that we had and the useful advice, words of comfort, fun and tough moments that we shared. This includes Sanja Cvijić, Jhi-Young Joo, Antonio Damião Rodrigues, Jonathan Donadee, Joya Deri, Xia Miao, Rupamathi Jaddivada, Irfan Khan, Joao Saude, Sergio Pequito, Kevin Bachovchin, Xiaoqi Yin, Yang Weng, Chin Yen, John Costanzo, Dinghuan Zhu, Kyri Baker, Subhro Das, Jonathan Mei, Qixing Liu and others too numerous to name.

Last but not least, I wish to express my love, gratitude and appreciation to my family; to my wonderful parents, Alexandros and Frosoula and my brothers, Andreas and Dimitris, for always inspiring me to pursue my dreams passionately throughout my life while standing by my side and supporting me all the way. Finally, to Irene, for sharing this journey with me and supporting me in every possible way all these years.

I wish to thank PSERC and NIST for financially supporting my PhD research.

Contents

List of Figures

*

List of Tables

*

Chapter 1

Introduction

Modern power systems are characterized by both the influx of advanced control, sensing, communications, information technologies as well as the penetration of high levels of renewable energy resources. On one side, advanced technologies provide new sources of information, and new means of contributing to power systems control and maintaining secure normal operation of power systems. On the other side, the volatile nature of renewable energy resources causes fast and unpredictable variations on the generation side that challenge normal operation of power systems.

In this thesis, we develop advanced distributed nonlinear control designs for conventional and new power systems technologies like synchronous generators, energy storage devices and state-of-the-art wind generators. These control designs exploit communication, sensing and information technologies to accomplish several objectives with guaranteed performance and stability in power systems with high levels of renewable power generation.

1.1 Motivation

In this new power systems environment, wind power dominates the renewable power generation portfolio worldwide. In the U.S., wind power is one of the fastest growing sources of new electricity capacity and the largest source of new renewable power generation added since 2000, according to a U.S. Department of Energy (DOE) study [1]. Specifically, as pointed out in this study, by 2020, the total generated wind energy per year (coming from offshore and onshore wind farms) is expected to cover 10% of the total U.S. electricity demand. Projecting further into the future, the DOE study envisions that by 2030, the generated wind energy would cover 20% of the total U.S. electricity demand, and by 2050, this percentage could even reach 35%.

In Europe and other countries all over the world, the ratio of wind generation capacity over the total generation capacity and the ratio of yearly generated wind energy over the total electricity demand already reached higher values [2]. Furthermore, these ratios are increasing according to a much steeper growth curve. If this global trend of integrating high amounts of wind power generation into modern power systems remains consistent it will cause WGs to become core generating units along with synchronous generators (SGs) in the near future. In this scenario, they will contribute with a significant share in the total power generation portfolio while they will dominate the renewable power generation portfolio along with hydro power generators.

Although integration of high levels of wind power into modern power systems is very desirable from an environmental viewpoint, it raises some critical challenges to be tackled on the secure operation of power systems.

Two aspects of wind power generation can affect power systems operation in detrimental ways: it can cause reduction of the total system's effective rotational inertia and it is highly variable and unpredictable. We explain the former as follows. Wind Double-fed Induction Generators (DFIGs) also have significant amount of kinetic energy stored in their rotating blades, and therefore inertia, which, in fact, is comparable to the inertia of conventional generators. However, in the case of conventional synchronous generators, immediately after a grid disturbance, e.g a load increase, the electrical torque of each generator will increase to supply the load, causing its rotor speed to decrease. The decrease of the rotor speed releases the kinetic energy stored in the shaft of the generator and causes a corresponding decrease in the electrical torque. In fact, the electrical torque decrease will be caused by the decrease of the physical angular position of the rotor flux vector which follows the decrease of the rotational speed of the rotor. That is because the flux vector is fully aligned with the physical position of the rotor. To summarize, the above sequence of actions leads to a self-stabilizing mechanism on the generator speed dynamics called "inertial response", and is an inherent characteristic of their dynamic behavior. On other hand, DFIGs lack this innate "inertial response" capability due to their asynchronous operation (their rotor speed differs from the synchronous speed $2\pi 60$ (rad/s)), realized by electrical decoupling from their power electronics (particularly the rotor-side converter (RSC)). Because of that, during grid disturbances, although the rotor speed and rotor angle position of DFIGs will vary, that will not significantly and directly affect the rotor flux vector position and correspondingly the generator electrical torque, since, these are independently controlled by the power electronics. In other words, the rotor flux vector position and the electrical torque are not dependent on the physical position of the rotor. However, DFIGs can release their kinetic energy and provide inertial response when their power electronic controllers are designed appropriately.

With the majority of the new WGs replacing SGs today in power systems being DFIGs, a total reduction of the total systems' effective inertias will inevitably be observed in power grids worldwide.

The reduction of this effective inertia can challenge transient and frequency stability of power systems. More so the frequency stability, since the reduced effective inertia can make the frequency more sensitive to disturbances, therefore prone to faster and greater variations around the equilibrium, for a given set of power system disturbances. Furthermore, the reduced effective inertia can affect transient stability, which is characterized by SGs retaining their synchronism with the grid after being subjected to a large disturbance. This will happen in power grids with high wind power integration since the reduction of the effective inertia will cause large disturbances to have a pronounced impact on the SGs' dynamics, so maintaining their synchronism with the grid will become a challenging task.

At the same time, the highly variable and unpredictable power output of WGs can challenge frequency and transient stability of power systems even more, if it is not effectively managed. The reason is that the highly variable wind power initiates new power disturbances that can lead to imbalance between power generation and demand, and respectively to frequency variations. In addition, these imbalances can lead to SGs losing their synchronism with the grid.

We underline that, today, wind power output variability is mainly managed by operating SGs such that they withhold certain "spinning reserve" levels, so that they are able to counteract power imbalances, caused by the variable wind generation in real time. SGs can maintain "spinning reserves" when they are underoperated, so that they can increase their power output to maintain supply-demand balance in response to wind power variations. However, operating conventional SGs in such a way leads to a number of inefficiencies. For instance, since these SGs are operated below their nominal power output values, their power output is not the maximum that could be used for base load supply. From an economic point of view, this is highly inefficient and constitutes one of the main reasons hampering integration of high amounts of wind power generation today.

From the above discussion, we identify two main challenges for modern power systems with high wind power integration: to guarantee their transient and frequency stability.

In this thesis, we address these challenges by developing novel nonlinear control laws for SGs and energy storage devices to guarantee transient stabilization of the SGs, and novel distributed nonlinear control laws for state-of-the-art (SoA) WGs to enable them to regulate their power output.

1.2 Problem Statement

1.2.1 Transient Stability

Transient stability, is a term specifically devised for power systems to characterize the state in which all generators retain their synchronism with the grid after a system is subjected to a large disturbance [3], e.g. disconnection of a line, tripping of generator, etc. On the other hand, transient instability describes the state in which one or more generators lose synchronism with the grid and is often the main cause of wide-spread blackouts [4].

We underline the significance of transient stability in modern power systems by analyzing the mechanism through which transient instabilities can lead to a series of catastrophic cascading events and eventually to a wide-spread blackout. Consider a power system in which a contingency (i.e a large disturbance), such as a disconnection of a transmission line, occurs. Immediately after such a disturbance, three main events will take place. The first is redistribution of the powers flowing through the lines in the vicinity to the disturbance. This will be experienced by each of the synchronous generators in close physical proximity with the fault as a power imbalance between its mechanical and electrical power, causing its rotational speed to vary. This leads to the second event. Let $\mathcal{G}$ represent the set of synchronous generators, and consider the rotor speed dynamics of a SG i given as [3, 5]:

$$\dot{\omega}_i = \frac{(P_{m,i} - P_{e,i})}{2H_i}, \quad \forall i \in \mathcal{G} \tag{1.1}$$

The variables $P_{m,i}, P_{e,i}, H_i$ denote mechanical power, electrical power and inertia of the generator, respectively. During and right after a fault, $P_{m,i}$ is not changing significantly due to the slow response of the governor (main controller of the mechanical power), whereas $P_{e,i}$ is varying according to the grid conditions. Hence, in the second event generators that experience a power imbalance, i.e $P_{m,i} \neq P_{e,i}$, either accelerate or decelerate with respect to the synchronous speed of the grid.

When generators accelerate/decelerate, there is a great risk of damage to the physical equipment. For this reason, generators are always equipped with a specific type of protection scheme, namely an out-of-step protection scheme. The sole purpose of this scheme is to detect when generators accelerate/decelerate and disconnect them from the grid when their speeds greatly deviate from the synchronous speed [3]. The action of these protection schemes initiates the third event in which generators disconnect from the grid. In some of the most widely known blackouts [4], the latter event led to several generators being taken offline.

When generators disconnect from the grid, the imbalance between total load and generation becomes even greater. This, in turn, leads to new redistribution of power flows, more generators accelerating/decelerating and finally getting disconnected from the grid. In other words, the three main events we just described continue repeating in the same sequence.

Another important aspect of power systems operation is voltage regulation. Formally, voltage regulation is the regulation of the terminal voltages of all buses in a power system at an acceptable level [6], [3] which, for transmission systems, is any value within $\pm 5\%$ of the nominal value.

Today, the main means to effectively counteract transient instabilities and retain the synchronism of SGs with the grid are control of conventional SGs (exciter, governor) and control of new technologies interfaced through power electronics, such as storage devices, wind generators (WGs), photovoltaics (PVs) and Flexible AC Transmission Systems (FACTS).

1.2.2 Power Output Regulation of Wind Generators

Today, the ongoing integration of high amounts of wind power led us to take the concerns, associated with the impact of wind power on power systems, more seriously. This can be realized from the technical regulations regarding the integration and operation of WGs which are becoming very demanding. In the current status of these regulations, WGs are required to provide several capabilities and support to the grid, ranging from voltage/frequency regulation and ability to stay connected with the grid during disturbances, to the ability to regulate their power output [2].

The inability of WGs to generate predictable power through power output regulation is the main reason that slows down the integration of more wind power into power systems. This can be realized by analyzing the impact that unpredictable wind power generation has on today's power system operations. In the slow time-scale (several minutes) of operations, at which the economic dispatch (ED) is conducted, time-delays arise from the moment system operators gather information (e.g wind speed) and issue scheduled power outputs for the WFs, until the moment these schedules are actually implemented by the WFs. Thus, by the time WFs receive their scheduled powers they might not be able to meet them due to the minute-to-minute wind variability. Consequently, that leads to the increase of the total generation cost since expensive conventional synchronous generators are called in real-time to compensate the power mismatch between scheduled and real available wind power. In addition, as already mentioned, the unpredictable wind power forces system operators to operate online SGs below their maximum capabilities, maintaining in that way spinning reserves, or to add online generation capacity that otherwise would be offline. In the fast time-scale of operations, wind power variability causes supply-demand imbalances that can challenge frequency and transient stability. In this case, fast regulating SGs are required to compensate these power imbalances.

When integrating very high amounts of wind power in power systems, the economic inneficiency that comes from underoperating generators such that they withhold spinning reserves, as well as the great challenge of securing the stability of these systems may together outweigh the benefits of such integration. In these cases, the integration levels become infeasible due to both economic and technical reasons.

Currently used wind DFIGs can provide power output regulation when they operate in a deloaded regime. When DFIGs operate in this regime, they extract mechanical power less than the maximum possible for given wind-speed conditions. This gives them the flexibility to control their power to meet several power demands, given that these demands lie in the feasible power range. On the other hand, WGs could provide power output regulation and many other capabilities, presuming that they exploit some kind of energy storage within their system. Unfortunately, the DFIGs integrated today into power systems lack this capability.

On the bright side, General Electric recently announced the commercialization of their "brilliant" wind DFIG [7]. The brilliant wind DFIG is a DFIG that incorporates an energy storage device, in particular a battery, into its system. This type of wind DFIGs is now considered to be the gold standard for WG technology, being studied in the literature over the last decade. With the integrated storage device, these WGs can realize many of the already discussed capabilities, including power output regulation, without resorting to the energy stored in their shafts. In other words, they can provide these capabilities by relying on their electrical and not on their mechanical part.

1.3 Background and Related Work

1.3.1 Industry Practice

a) **Transient Stability**

The current industry practice for securing transient stability is purely heuristic and based on extensive trial and error procedures [8]. Specifically, in this practice, system operators (SO) execute the following steps before finalizing and communicating the scheduled power outputs to generators.

- First, they conduct the economic dispatch (ED) process in order to compute the optimal power outputs of generators with respect to total generation cost for serving a given load.
- Then, they perform contingency analysis for a given set of faults with the ED power outputs assigned to generators.

- If the contingency analysis shows transient instabilities, they alter the dispatch obtained from ED, i.e they re-distribute generation from critical (for being transiently unstable) to not critical generators using knowledge of the system and reconduct the contingency analysis with the new dispatch.
- If the contingency analysis with the new dispatch results to a transiently stable system for the studied set of faults, then it is regarded as secure.

The logic behind executing the above heuristic approach is to exhaustively assess whether a system is transiently stable/unstable after it is subjected to various disturbances through numerical simulations. Thus, the above process terminates when simulations lead to a secure/stable power system response. The aforementioned steps describe today's industry practice for securing transient stability [8].

b) **Voltage Regulation**

Today, one of the main means for ensuring voltage regulation in power systems are the excitation controllers of conventional generators [3], [9]. These controllers are based on approximate linearizations and they control the DC voltage of the generator's rotor field windings in order to regulate its terminal voltage to a specific value.

1.3.2 Related Work - Transient Stability

In the literature, the line of research that was followed by researchers for addressing transient stability and voltage regulation was based on nonlinear control theory. The reason that motivated researchers to resort to nonlinear control theory is that power systems are inherently nonlinear dynamical systems, and large disturbances, such as faults, trigger their nonlinear dynamic behavior. Since the states move away from their equilibrium during large disturbances, standard linear controllers are not able to guarantee stabilization or performance [10]. On the other hand, nonlinear controllers can guarantee stabilization and performance for a wide range of operating conditions that correspond to a wide range of state-variables' deviations around equilibrium.

In [11] the authors proposed a feedback linearizing excitation controller for accomplishing concurrent transient stabilization and voltage regulation. This controller is shown to be able to avoid break-down of a large real-world system during a major disturbance. Nevertheless, a shortcoming of this approach is that during transience, voltage can vary greatly outside the acceptable limits and can trigger the generator voltage protection. In [6], the authors proposed a switching excitation controller to achieve transient stability and post-fault voltage regulation. Specifically, during the transient period, this controller uses the electromechanical states as feedback signals in order to ensure transient stability, while during the post-transient period, it uses voltage as a feedback signal in order to ensure voltage regulation. The smooth transition among the different feedback signals is realized through appropriate membership functions. A drawback of this approach is that the membership functions need to be carefully designed based on simulations and trial and error procedures.

In general, guaranteeing concurrent transient stabilization and voltage regulation with the excitation controller is challenging since these two objectives become conflicting for the controller. Simply put, since the excitation controller adjusts the voltage to ensure transient stabilization, regulating the voltage to an equilibrium rapidly (voltage regulation) will lead to the controller losing the capability for transient stabilization. To overcome this limitation, researchers proposed coordinated control of a storage device and a generator. In this direction the authors in [12] proposed a multi-index nonlinear coordinated control approach for a storage device and an exciter. The main drawback of this approach is that the rotor angle position and the rotor acceleration are not exploited as feedback signals by the controller. According to [11], these two variables can be very effective feedback signals for controllers that aim to ensure transient stabilization. In particular, the acceleration signal as a feedback signal can enable the controller to increase the transfer capability of the system while the rotor angle can provide high synchronizing torque to the generator, critical for avoiding first swing instability [3].

In this thesis, we develop a nonlinear coordinated controller for a generator and a storage device that are on the same bus, able to effectively guarantee concurrent transient stabilization and voltage regulation without the limitations discussed above. This, given that the storage device has sufficient stored energy.

1.3.3 Related Work - Power Output Regulation of Wind Generators

WGs without energy storage can regulate their power output when they operate in a deloaded regime. On the other hand, when WGs are equipped with energy storage they can exploit the storage device to regulate their power output. The literature related to the problem of enabling a group of deloaded DFIGs (without storage devices) to attain power output regulation is not very broad.

Specifically, distributed approaches for dispatching and regulating the power output of WGs were considered in [13] and [14]. In [13], a multi agent systems-based (MAS) control strategy for wind DFIGs in a microgrid was proposed. Each bus is assumed to have an agent that is allowed to communicate with its neighboring agents according to two consensus protocols. That way, each agent can retrieve the ratio defined by the total demand over the total available wind power in a distributed fashion. Subsequently, this information can be used by each DFIG to define its set-point. The drawback of this method is that it is quasistatic. In other words, the set-points are computed and communicated to the respective controllers at discrete time instants. Since the DFIGs' controllers have to wait until the protocols converge before implementing their new set-points, it means that their power output is also controlled in a quasistatic fashion. Therefore, in settings where DFIGs have to control their power outputs rapidly and under highly and fast-varying dynamical conditions, e.g in microgrids, DFIGs may not be able to respond timely. In [14], the authors proposed two controllers for WGs operating in a deloaded mode, a centralized and a distributed controller. Both controllers aimed to regulate the set-points of the individual WGs such that the fatigue on the wind turbines is minimized, and at the same time the total power demand is met. In this work, linear WG models were considered, therefore, the performance of the controllers on regulating the power set-points can only be guaranteed close to the operating point around which the linear model is valid. This limits the operating region in which the power set-points could be controlled making the approach unsuitable in cases where the power set-points have to vary greatly in order to meet large variations in the total power demand.

To the best of our knowledge, [13] and [14] are the only references that presented distributed control methods for dispatching WGs according to a total power demand, therefore enabling deloaded WGs to regulate their power output. In both of them, the controllers for the DFIGs were derived based on approximate linearizations around specific operating points, therefore their performance can be guaranteed only in a small neighborhood around these operating points. Thus, with these controllers, the domain of capabilities that DFIGs can offer is limited since the rotor-speed and the capacitor dynamics are highly nonlinear.

The idea of integrating an energy storage device into a wind DFIG scheme dates back at least a decade. Several researchers suggested the integration of an energy storage device into the DFIG system as a way of increasing the range of capabilities that the DFIG can provide to the grid [15, 16, 17]. Particularly in [16] a PI controller for the grid side converter (GSC) and a PI controller for the DC-DC converter of a DFIG/energy storage system were presented. Jointly, the two controllers can enable the WG to provide constant power output while improving the transient voltage response. In a similar line of research, the authors in [17] proposed a multi-mode control strategy for SoA WGs that can enable them to manage intermittency as well as to improve their dynamic response during faults. In [15], a two-layer centralized constant power control architecture for SoA WGs (with integrated storage) was introduced. In the higher layer, a wind farm supervisory controller computes the power set-points for the individual WGs. Specifically, the set-point for the power extracted from the wind as well as the storage device's power output in order to meet a total WF power demand. In the lower layer, local controllers guarantee that the power set-points are met. Centralized control approaches such as the one in [15] require high computational effort, are not robust to single-point failures and run in a quasistatic time domain that might hamper a fast WF response under fast-varying dynamical conditions.

1.4 Thesis Contributions

The contributions of this dissertation are analyzed below.

- **Nonlinear Coordinated Control Scheme for a Generator and an Energy Storage Device that Guarantees Transient Stabilization and Voltage Regulation.** We develop a nonlinear coordinated control architecture for a SG and an energy storage device using results from Multi-Input Multi-Output (MIMO) feedback linearization theory. Concretely, we first introduce a novel output vector that leads to the generator-storage subsystem dynamics having full relative degree. Thereafter, we use this output vector to recast the generator-storage dynamics to a new form in which these dynamics inherit several desired properties. We accomplish that by explicitly deriving a full state transformation. In the new state-space form, the first property is that, the relevant variables for accomplishing transient stability and voltage regulation become state-variables. The second property is that the state transformation is full, i.e the dimension of the new state-space matches that of the initial one. This comes from the fact that with the proposed output vector the system has full relative degree and has the following implication. The particular choice of the output vector makes it possible to explicitly design a full MIMO feedback linearizing controller for the generator-storage dynamics that causes the closed-loop system to be linear and controllable without zero dynamics. This proposed controller for the generator-storage set-up is the first one to guarantee concurrent transient stability and voltage regulation by coordinating a SG and an energy storage, and in that way exploiting their full potential in a cooperative way.

- **Decentralized Nonlinear Energy-based Control Scheme Enabling SoA WGs to Guarantee Maximum Power Point Tracking (MPPT) and Power Output Regulation.** We develop a nonlinear energy-based control scheme for all three converters of a DFIG with energy storage, namely the RSC, GSC and DC-DC converter. Initially, we recast the SoA WG standard state-space model into a new form where some critical energy variables become state-variables. Subsequently, we form and translate the main control objectives, Maximum Power Point Tracking (MPPT) and predictable power output, into tracking objectives of asymptotically stable equilibria for these new energy state-variables. Lastly, we design nonlinear Control Lyapunov Function (CLF) Energy-based control laws for its rotor-side converter (RSC) to guarantee MPPT, and for its grid-side converter (GSC) and DC-DC converter (that controls the storage power) to jointly guarantee power output regulation by exploiting the energy storage device.

  This is the first comprehensive nonlinear control scheme for all three converters of a SoA WG. Hence, it is the first control scheme to guarantee MPPT from the WG under nonlinear rotor speed dynamics and power output regulation during large variations of the power set-point. Finally, our approach is the first to leverage energy state-space modeling for control of SoA WGs that facilitates a more intuitive understanding of the control objectives using energy variables, which eventually leads to a more intuitive controller design.

- **Methodology for Compositional Stability Analysis and for Deriving Suffi-**

cient Stability Conditions of a Specific Class of Leader-follower Consensus Protocols. For a specific class of leader-follower consensus protocols (e.g with a specific communication architecture), we combine singular perturbation and Lyapunov theories with the Gershgorin circle theorem to perform compositional stability analysis and derive sufficient stability conditions for their control gains. Further, by employing a Lyapunov-Krasovskii functional we establish time-delay independent asymptotic stability of their equilibria, guaranteeing their robustness with respect to communication delays. Combining all these tools, we provide a new methodology to stability analysis for a particular class of distributed protocols that is: 1) *intuitive* - it exploits singular perturbation theory to reveal the local and global control objectives accomplished by the protocol in different time-scales; 2) *computationally efficient* - it is based on Lyapunov functions for lower-dimensional subsystems; 3) provides an explicit way of deriving *sufficient conditions* for stability of this class of protocols through the use of Gershgorin's circle theorem.

- **Distributed Control for Power Output Regulation of Wind Farms with SoA WGs**. We establish a novel distributed control architecture for SoA WGs that enables them to self-organize and control their storage devices under dynamical conditions such that their total power output tracks a given varying reference. At the same time, it enables their storage devices to contribute in a equal sharing fashion, i.e all storage devices provide the same amount of power. The details of this work can be found in [18]. We first pose the main problem as a *constrained consensus problem* for the power electronics controllers of SoA WGs, specifically the GSCs, and introduce a distributed leader-follower consensus protocol that WGs can adopt to distributively and asymptotically achieve the above control objectives. Further, by applying our proposed methodology we employ singular perturbation and Lyapunov theories to perform compositional stability analysis and prove that the desired equilibrium point of the consensus protocol is asymptotically stable, explicitly deriving sufficient conditions under which this is guaranteed. Lastly, we design distributed control laws for the GSC and the DC-DC converter that realize the protocol in practice and accomplish the desired control objectives. The distributed power-electronics control architecture: 1) can lead to *total generation cost reduction*, especially when it is deployed in large-scale applications, since it enables SoA WGs to regulate their power output using stored wind energy, therefore eliminating the need for utilizing fast ramping-up SGs to compensate wind power variability; 2) is *practically realizable*, requiring WGs to exchange feedback signals that can be easily measured locally; 3) leads to guaranteed *stability and performance* of the associated dynamics with and without communication delays.

The proposed distributed control laws for the GSC and DC-DC converter are the first advanced, distributed controllers for WGs with integrated storage to reveal and exploit their full potential for accomplishing complex capabilities. Specifically, they are the first controllers of their kind to enable SoA WGs to self-organize and provide WF power output regulation with load sharing among their the storage devices, under dynamical conditions. We emphasize that, since these WGs will be main energy generating units in the coming years, systematic and distributed methods for controlling them, that are practical and mathematically rigorous, are needed before their large-scale application. This contribution paves the way toward this direction.

- **Distributed Torque Control Scheme of Deloaded Wind DFIGs for Wind Farm Power Output Regulation**. We establish a novel distributed control architecture that WGs can adopt to dynamically self-dispatch in an equal loading manner. In our context that means their loading levels have to be equal, while their total power extracted from the wind tracks a given power reference. The details related to this contribution can be found in [19]. We first formulate this problem as a constrained consensus problem where the WGs have to agree on their utilization levels (that depend on local wind-speed conditions) while their total power is constrained to match a reference. We *propose a leader-follower consensus protocol* that WGs can incorporate into their rotor-side converter (RSC) control scheme to accomplish the above objectives in a distributed and coordinated fashion. By applying our proposed methodology for stability analysis, we study the asymptotic behavior of the protocol and establish certain stability properties as follows. We start by employing singular perturbation theory to perform temporal decomposition of the protocol dynamics. Subsequently, we perform compositional stability analysis and establish (using Lyapunov-like arguments) asymptotic stability of the equilibria of the corresponding fast and slow decoupled subsystems. Then, we combine these stability certificates through a composite Lyapunov function and derive conditions on the time-scale separation parameter under which asymptotic stability of the equilibrium of the full protocol dynamics is guaranteed. Further, we extend these results and establish, using a Lyapunov-Krasovskii functional, that the stability property is time-delay-independent. Lastly, we develop a CLF-based torque controller for the rotor-side power electronics (RSC) of WGs that realizes the protocol in practice through peer-to-peer communication. The proposed control architecture: 1) can dynamically dispatch and control the power output of a group of WGs based on local wind-speed conditions and in a distributed fashion, eliminating the need for a central wind farm controller that has to gather information from all WGs and perform extensive computations; 2) *requires minimum peer-to-peer communication* among neighboring WGs; 3) *enables WGs to be dispatched timely* which is critical when dispatching has to be performed under fast-varying dynamical wind and loading conditions to balance supply-demand, especially in autonomous power systems such as microgrids; 4) leads to *guaranteed stability and performance* of the associated dynamics.

It is the first control scheme for the RSC to systematically and effectively solve the problem of dispatching and regulating the power output of a group of deloaded WGs in a *distributed, dynamic and efficient manner*. In contrast to previous work [13], our method is dynamic in the sense that the proposed power electronics WG controllers reach consensus dynamically according to a given reference. We emphasize that, in the near future, the *problem of dispatching and controlling the power outputs of WGs efficiently and distributively will become as critical as the distributed Economic Dispatch (ED) problem for SGs*, which has already attracted a lot of attention in the power systems and control communities [20, 21, 22]. Therefore, this work provides first steps in this direction.

1.5 Thesis Organization

In *Chapter 2*, we present an analytical approach of a nonlinear coordinated MIMO feedback linearizing control law for a conventional SG and an energy storage device. The control objective for the SG/energy storage scheme is concurrent transient stabilization of the SG and voltage regulation of the terminal bus after a large disturbance.

In *Chapter 3*, a wind double-fed induction generator (DFIG) with an energy storage system (SoA WG) is studied. We present the design of nonlinear CLF Energy-based feedback control laws for the rotor-side converter (RSC) to guarantee MPPT and for the grid-side converter (GSC) and DC-DC converter to jointly guarantee power output regulation by deploying the energy storage.

In *Chapter 4*, we consider a WF comprised of a group of SoA WGs. The control objectives for the WGs are to self-organize and control their storage devices in an equal sharing fashion under dynamical conditions in order for the WF power output to track a given varying reference, i.e WF power output regulation. We propose a leader-follower consensus protocol that WGs can adopt to distributively and asymptotically achieve these control objectives.

Further, in the same chapter, we introduce a methodology for compositional stability analysis and for deriving sufficient stability conditions for this particular class of protocols. By employing our methodology we establish conditional asymptotic stability of the protocol's equilibrium point. Lastly, we design distributed control laws for the GSC and the DC-DC converter that realize the protocol in practice through peer-to-peer communication and accomplish the desired objectives.

In *Chapter 5*, a WF comprised of conventional DFIGs without storage devices operating in a deloaded mode, is considered. The control objective for the WGs is to dynamically self-dispatch in an equal loading manner, i.e for their relative loading levels to have the same value while their total power output is regulated to a given power reference. We introduce a leader-follower consensus protocol that WGs can incorporate into their RSC control scheme to accomplish the above objectives in a distributed, coordinated and dynamical fashion. We study the asymptotic behavior of the protocol and establish conditional asymptotic stability of its equilibrium point by employing the methodology introduced in chapter 4. Further, we extend these results and establish, using a Lyapunov-Krasovskii functional that this stability property is time-delay-independent. Lastly, we develop a distributed CLF-based torque controller for the RSC that realizes the protocol in practice through peer-to-peer communication.

In *Chapter Conclusions and Future Work*, the results presented in this thesis are summarized and new research directions for future work are pointed out.

Chapter 2

Coordinated Nonlinear Control of a Generator and a Storage Device

2.1 Introduction

As elaborated in the introduction of the thesis, transient stability is defined as the property of a power system to withstand large disturbances (e.g disconnection of a line, short-circuit in a line) and retain its normal operation. In more detail, it is the property of power system to retain synchronism of all of its synchronous generators after a disturbance. Securing transient stability is traditionally considered one of the main problems that system operators have to address, while with the expected future high levels of wind power penetration, solving this problem will become even more challenging. Consequently, guaranteeing transient stability will arise as an even more critical problem for power systems operations that demands a lot of attention.

Traditionally, transient stability property is granted to power systems through proper control design of the synchronous generators. In particular, through proper control of the excitation controllers, which are the ones that regulate the terminal voltages and indirectly the electrical torques of the generators. Through these, SGs can ensure stability of their swing dynamics or equivalently, that they will remain in synchronism with the grid after a disturbance. However, although the excitation controllers, when suitably designed, can be very effective in maintaining transient stability of power systems, it is very challenging to enable them to achieve that concurrently with terminal voltage regulation which stands as their main functionality. The reason is that when transient stability is the main control objective to be accomplished, the terminal voltage has to be a free variable that can vary accordingly to ensure stable rotor angle/speed dynamics. Hence, when voltage regulation is also one of the control objectives for the exciter, both objectives are realized as conflicting for the excitation controller which leads to a challenging control design problem.

In modern power systems, many diverse types of new technologies are integrated. To name a few, storage devices, photovoltaics (PVs), wind generators etc. These technologies can be leveraged through advanced control designs to contribute, together with the existing excitation controllers of SGs, to the maintainance of transient stability and ensuring voltage regulation in power systems. Here, storage devices, concretely batteries, are considered for this particular purpose. Coordinating the controller of a battery storage device with an excitation controller emerged in the literature as a promising direction for concurrently ensuring transient stability and voltage regulation. This is because of the capability of battery storage devices to control independently both their real and their reactive power at the same time. In fact, by exploiting, through suitable control, the potential of both a SG and a battery, the two main objectives can be effectively attained.

The design of a coordinated controller for a SG and a battery storage (that lie at the same bus) that achieves concurrent transient stabilization and voltage regulation can be posed as a nonlinear control design problem with the nonlinearities emerging in the generator dynamics. Suprisingly, this problem has not been rigorously addressed in the literature, as it will be further discussed in the literature review section below.

This Chapter is dedicated to solving this particular problem. Our main contribution is a nonlinear coordinated control design for a generator-battery storage system that can effectively guarantee concurrent transient stabilization of the SG and regulation of their common bus' voltage.

2.2 Literature Review

In the literature, the line of research that is followed by researchers for addressing transient stability and voltage regulation together is grounded on nonlinear control theory. The reason that motivated researchers to resort to nonlinear control theory is that power systems are inherently nonlinear, and large disturbances, as the ones considered during contingencies, trigger a highly nonlinear dynamic behavior. In this case, the states move away from their equilibrium operating points around which, standard linear controllers can guarantee stabilization and performance [10]. On the other hand, nonlinear controllers can guarantee stabilization and performance for a wide range of operating conditions. The authors in [11] proposed a feedback linearizing excitation controller to accomplish transient stabilization and voltage regulation concurrently, and is able to avoid break-down of a large real-world system during a major disturbance. However, a concern with this approach is that, during transience, voltage can vary greatly outside the acceptable limits and might trigger the generator protection. In [6], the authors proposed a switching excitation controller to achieve transient stability and post-fault voltage regulation. Specifically, during the transient period, this controller uses feedback from electromechanical states to retain transient stability, and during the post-transient period, it uses voltage feedback to ensure voltage regulation. The smooth transition among the different feedback signals is realized through membership functions. A weakness of this approach is that the membership functions need to be carefully designed based on simulations and trial and error procedures. To overcome the limitations that come along with using only the excitation controller to jointly guarantee transient stability and voltage regulation, as we already mentioned, researchers proposed coordinated control of a generator and a storage device. In more detail, in [12], the authors introduced a multi-index nonlinear coordinated control design for a generator and a storage device. The drawback of this approach is that feedback signals from the rotor angle position and the rotor acceleration are not incorporated in the control design. According to [11] the acceleration signal as a feedback variable is important for increasing the transfer capability of the system and the rotor angle signal for enabling the generator to exhibit a high synchronizing torque response, critical for avoiding first swing instability [3].

Our proposed control design that will be analyzed in forthcoming sections is free of the limitations discussed above.

2.3 Modeling

2.3.1 Load Model

In this thesis, we assume that loads behave as constant impedances during transience and adopt this modeling type. Accordingly, we eliminate load buses to obtain a reduced representation of the system [9].

2.3.2 Generator Model

Each synchronous generator is modeled with the standard model for transient stability studies, namely the one axis or flux-decay model. In this model, a generator is represented as a voltage behind the direct axis transient reactance. Denoting the set of generator-storage systems by the set $\tilde{\mathcal{G}}$, the following dynamical equations fully describe the generator model:

$$\dot{\delta}_i = \omega_s(\omega_i - \omega_0), \qquad \forall i \in \tilde{\mathcal{G}} \tag{2.1}$$

$$\dot{\omega}_i = \frac{1}{2H_i}(P_{m,i} - P_{e,i}), \qquad \forall i \in \tilde{\mathcal{G}} \tag{2.2}$$

$$\dot{E}'_{q,i} = \frac{1}{T'_{d0,i}}(E_{fd,i} - E'_{q,i} + (X'_{d,i} - X_{d,i})I_{ds,i}), \qquad \forall i \in \tilde{\mathcal{G}} \tag{2.3}$$

$$P_{e,i} = E'_{q,i} I_{qs,i} \tag{2.4}$$

The generator state-variables $\delta_i,\ \omega_i,\ E'_{q,i} \in \mathbb{R}$ denote the rotor angle position, angular speed and voltage behind transient reactance, respectively. Further, the variables $P_{e,i},\ P_{m,i} \in \mathbb{R}$ denote electrical and mechanical powers of the generator and $I_{ds,i}, I_{qs,i} \in \mathbb{R}$, the currents of the generator in a $d{-}q$ reference frame. The generator control input is given by the excitation voltage $E_{fd,i} \in \mathbb{R}$. The constants $\omega_s,\ \omega_0$ denote the synchronous speed $\omega_s = 2 \cdot \pi \cdot 60\ (rad/s)$ and the per unit synchronous speed $\omega_0 = 1$. The constants $T'_{d0,i}, X_{d,i},\ X'_{d,i}, H_i \in \mathbb{R}$ denote the transient open-circuit time constant, the stator reactance, the stator transient reactance and the inertia of the generator, respectively.

2.3.3 STATCOM/Battery Energy Storage Model

As a storage device, we consider a Battery Energy Storage (BES) that is interfaced by a Static Synchronous Compensator (STATCOM). Its full model can be described by the dynamics of the current components in the synchronous reference frame [16]. In particular by the following two dynamical equations:

$$\dot{I}_{db,i} = -\omega_s \frac{R_{b,i}}{L_{b,i}} I_{db,i} + \omega_s I_{qb,i} + \omega_s \frac{(u_{\alpha,i} - V_{sd,i})}{L_{b,i}}, \qquad \forall i \in \tilde{\mathcal{G}} \tag{2.5}$$

$$\dot{I}_{qb,i} = -\omega_s \frac{R_{b,i}}{L_{b,i}} I_{qb,i} - \omega_s I_{db,i} + \omega_s \frac{(u_{\beta,i} - V_{sq,i})}{L_{b,i}}, \qquad \forall i \in \tilde{\mathcal{G}} \tag{2.6}$$

The state-variables in the above model are $I_{db,i}, I_{qb,i} \in \mathbb{R}$ which denote the current output of the STATCOM/BES system. In addition, the control inputs are $u_{\alpha,i}, u_{\beta,i} \in \mathbb{R}$ which denote the voltage components directly controlled by the STATCOM, whereas the variables $V_{sd,i}, V_{sq,i} \in \mathbb{R}$, denote the terminal voltage components in the synchronous reference frame. It is important to note that the generator reference frame and the synchronous reference frame are rotating with the same speed but with a phase angle difference δ_i. The constants

$R_{b,i}, L_{b,i} \in \mathbb{R}$ denote the resistance and the reactance of the transformer connecting the STATCOM/BES to the grid.

We specifically considered battery storage devices since they have appealing characteristics; they can respond rapidly, they have high efficiency and they have the capability to provide both real and reactive power in the fast time scale relevant for transient stabilization and voltage regulation [23].

With the necessary modeling presented above, we now proceed to rigorously formulate our main problems.

2.4 Problem Formulation

2.4.1 Transient Stability

Transient stability can be mathematically defined in the context of *Lyapunov stability theory* [10]. Consider a power system whose dynamics are generically described by the following differential equation:

$$\dot{x} = f(x), \quad x \in D \subseteq \mathbb{R}^n \tag{2.7}$$

where $f : D \mapsto \mathbb{R}^n$ is a vector field and x is a state vector. Before stating our problem, we introduce some necessary definitions starting from the definition of an asymptotically stable equilibrium x_e.

Definition 2.1 ([10]). *An equilibrium point x_e of (2.7) is asymptotically stable if it is **stable** and if:*

$$\exists\delta \text{ such that } \quad ||x(0) - x_e|| \leq \delta \Rightarrow \lim_{t\to\infty} x(t) \to x_e \tag{2.8}$$

where $x(0)$ denotes the initial condition of x. Moreover, $\phi(t; x)$ is the solution of the system (2.7) that starts at the initial state x at $t = 0$ while R_A is the region for which the asymptotically stable equilibrium point attracts all the solutions, and is called *region of* *attraction (ROA)*. This region, is defined as follows.

Definition 2.2 ([10]). *The ROA of x_e is defined by the following set*

$$R_A = \{x \in D \mid \ \phi(t;x) \text{ is defined } \forall t \geq 0 \text{ and } \phi(t;x) \to x_e \text{ as } t \to \infty\}$$

Consider now that the power system defined by the dynamics in (2.7) is initially operating at equilibrium when subjected to a disturbance at the time instant t_f, which is cleared at t_{cl}. Let pr, f, ps denote the pre-fault, faulted and post-fault operating conditions, respectively. The effect of the disturbance can be seen in the vector field that changes from f^{pr} to f^f. After a temporary disturbance which is cleared at t_{cl}, the system will evolve according to the same pre-fault vector field i.e $f^{ps} = f^{pr}$. In each time range, the system (2.7) can be compactly described as:

$$\dot{x} = f^{pr}(x), \quad 0 \leq t < t_f \tag{2.9a}$$

$$\dot{x} = f^{f}(x), \quad t_f \leq t < t_{cl} \tag{2.9b}$$

$$\dot{x} = f^{ps}(x), \quad t_{cl} \leq t \tag{2.9c}$$

The following definition gives the conditions that lead to the system (2.9a)-(2.9c) being *transiently stable.*

Problem Formulation 1 (**Transient stability**, [9]). *The power system given by* (2.9a)-(2.9c) *will be transiently stable after a disturbance when the following two conditions are met:*

- *The equilibrium x_e^{ps} of* (2.9c) *is asymptotically stable.*
- *$x(t_{cl}) \in R_A^{ps}$ i.e in the time instant the fault is cleared, the state-vector lies inside the ROA of the post-fault system dynamics.*

It springs from the above definition that two factors play a key role in maintaining transient stability of a power system. In particular, the type of the equilibrium point (e.g asymptotically stable, stable), and how large the region of attraction of the post-fault equilibrium is. From these, we identify two causes that can lead to a *transiently unstable* power system.

- **Case 1**. The post-fault equilibrium is identical to the pre-fault equilibrium i.e $x_e^{ps} = x_e^{pr}$, and the disturbance moves the state-variable x outside of the region of attraction when the fault is cleared, i.e $x(t_{cl}) \notin R_A^{ps}$ [9, 3, 10].
- **Case 2**. The post-fault equilibrium is different from the pre-fault equilibrium, i.e $x_{e,ps} \neq x_{e,pr}$, and the disturbance moves the state-variable x when the fault is cleared outside the region of attraction of the post-fault equilibrium, i.e $x(t_{cl}) \notin R_A^{ps}$ [9, 3, 10].

In this thesis and without loss of generality, we particularly study *Case 1.* This case emerges when the topology of the power grid remains intact after a disturbance. Maintaining transient stability in this set-up solely depends on whether the equilibrium point has a R_A large enough so that the state will remain inside it at the moment the fault is cleared. When that is the case, the state will converge to the equilibrium point asymptotically. In power systems terminology, the time interval measured from the onset of the fault until the moment that the state-vector exits the R_A is called the *Critical Clearing Time* (t_{CCT}). In conclusion, to guarantee transient stability in the particular *Case 1* is equivalent to having a t_{CCT} large enough (equivalently R_A large enough), so that, for a given set of disturbances, the state-vector lies inside the R_A at the moment the fault is cleared.

2.4.2 Voltage Regulation

Problem Formulation 2 (**Voltage regulation**). *Voltage regulation is guaranteed when the following conditions hold for the voltage $V_{s,j}$ of each bus $j \in \mathcal{B}$:*

- $V_{s,j0} \in [\underline{V}_{s,j}, \overline{V}_{s,j}]$
- $V_{s,j0}$ *is asymptotically stable.*

where $\underline{V}_{s,j} = 0.95 \cdot V_{s,j}^{nom}$, $\overline{V}_{s,j} = 1.05 \cdot V_{s,j}^{nom}$. *The constant* $V_{s,j}^{nom}$ *denotes the nominal voltage.*

From the above, we can conclude that the voltage regulation functionality is realized

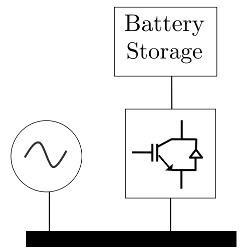

Figure 2.1: Generator/storage subsystem

when the voltage equilibrium $V_{s,j0}$ of each bus j meets the two requirements listed above.

2.5 MIMO Feedback Linearizing Controller

We consider the generator-storage set-up (as in Fig. 2.1) with a battery energy storage system. For this set-up, the main contribution of this thesis is a novel nonlinear Multi-input Multi-output (MIMO) coordinated control design that guarantees transient stability of the generator and voltage regulation of the terminal bus [24].

Our proposed methodology can be outlined as follows. First, we begin with the state-space model (2.1)-(2.3), (2.5), (2.6) and define an objective manifold, which, if tracked, leads to provable transient stability and voltage regulation. Thereafter, we define an output vector and a corresponding state-space transformation that recasts the state-space model in a new form that possesses some desired properties. Specifically, the relevant variables for accomplishing the main objectives, namely rotor angle, rotor acceleration and terminal voltage appear as state-variables in this new state-space. Finally, for the generator and storage system in this new form, we develop a MIMO feedback linearizing controller which attains transient stability and voltage regulation by rendering desired equilibria for these state-variables asymptotically stable. In particular, asymptotic stability of the rotor angle and acceleration equilibria leads to transient stability, while asymptotic stability of the terminal voltage equilibrium to voltage regulation.

2.5.1 State-space Model in Input-affine Form

The first step in our analysis is to bring the system (2.1)-(2.3), (2.5), (2.6) in the standard state-space form. To do that, let x_i, η_i be the state vector and the output vector of the generator/storage subsystem i:

$$x_i = [\delta_i,\ \omega_i,,\ E'_{q,i},\ I_{db,i},\ I_{qb,i}]^\top,\ x_i \in \mathbb{R}^5 \tag{2.10}$$

$$\eta_i = [I_{ds,i},\ I_{qs,i}]^\top,\ \eta_i \in \mathbb{R}^2 \tag{2.11}$$

With these, the system (2.1)-(2.3), (2.5), (2.6) can be written in input-affine state-space form as:

$$\dot{x}_i = f_i(x_i, \eta_i) + g_i u_i, \tag{2.12}$$

$$f_i : \mathbb{R}^5 \times \mathbb{R}^2 \mapsto \mathbb{R}^5,\ g_i \in \mathbb{R}_+^{5\times 3},\ u_i \in \mathbb{R}^3$$

$$f_i(x_i, \eta_i) \triangleq \begin{pmatrix} \omega_s(\omega_i - \omega_0) \\ \frac{1}{2H_i}(P_{m,i} - E'_{q,i} I_{qs,i}) \\ \frac{1}{T'_{d0,i}}(-E'_{q,i} + (X'_{d,i} - X_{d,i}) I_{ds,i}) \\ \omega_s(\frac{-R_{b,i}}{L_{b,i}} I_{db,i} + I_{qb,i}) \\ \omega_s(\frac{-R_{b,i}}{L_{b,i}} I_{qb,i} - I_{db,i}) \end{pmatrix},\ g_i \triangleq \begin{pmatrix} 0 & 0 & 0 \\ 0 & 0 & 0 \\ \frac{1}{T'_{d0,i}} & 0 & 0 \\ 0 & \frac{\omega_s}{L_{b,i}} & 0 \\ 0 & 0 & \frac{\omega_s}{L_{b,i}} \end{pmatrix},\ u_i \triangleq \begin{pmatrix} E_{fd,i} \\ u_{\alpha,i} - V_{sd,i} \\ u_{\beta,i} - V_{sq,i} \end{pmatrix}$$

Recall that $\mathcal{G}$, $\tilde{\mathcal{G}}$ denote the sets of generator and generator/storage systems respectively. By extending the expressions for the generator currents $I_{ds,i}, I_{qs,i}$ to accommodate the effect of the energy storage devices results to:

$$
\begin{aligned}
I_{ds,i} = &\sum_{k\in\mathcal{G}} \Big[G_{ik}E^{'}_{q,k}\sin(\delta_i-\delta_k) - B_{ik}E^{'}_{q,k}\cos(\delta_i-\delta_k)\Big] \\
&+ \sum_{l\in\tilde{\mathcal{G}}} \Big[G_{il}E^{'}_{q,l}\sin(\delta_i-\delta_l) - B_{il}E^{'}_{q,l}\cos(\delta_i-\delta_l) \\
&\underbrace{-(G_{r,il}I_{db,l} - B_{r,il}I_{qb,l})\sin(\delta_i) + (B_{r,il}I_{db,l} + G_{r,il}I_{qb,l})\cos(\delta_i)}_{\text{effect of energy storage } l \text{ on generator } i}\Big]
\end{aligned}
\tag{2.13}
$$

$$
\begin{aligned}
I_{qs,i} = &\sum_{k\in\mathcal{G}} \Big[G_{ik}E^{'}_{q,k}\cos(\delta_i-\delta_k) + B_{ik}E^{'}_{q,k}\sin(\delta_i-\delta_k)\Big] \\
&+ \sum_{l\in\tilde{\mathcal{G}}} \Big[G_{il}E^{'}_{q,l}\cos(\delta_i-\delta_l) + B_{il}E^{'}_{q,l}\sin(\delta_i-\delta_l) \\
&\underbrace{-(G_{r,il}I_{db,l} - B_{r,il}I_{qb,l})\cos(\delta_i) - (B_{r,il}I_{db,l} + G_{r,il}I_{qb,l})\sin(\delta_i)}_{\text{effect of energy storage } l \text{ on generator } i}\Big]
\end{aligned}
\tag{2.14}
$$

The terms $G_{ik},\ B_{ik},\ G_{il},\ B_{il} \in \mathbb{R}$ denote the conductances and the susceptances of the elements $Y_{e,ik},\ Y_{e,il}$ of the reduced admittance matrix $Y_e \in \mathbb{C}^{(|\mathcal{G}|+|\tilde{\mathcal{G}}|)\times(|\mathcal{G}|+|\tilde{\mathcal{G}}|)}$ [5]. The terms $G_{r,il}, B_{r,il}$ denote the conductance and the susceptance of the element $Y_{r,il}$. The matrix Y_r is given as $Y_r = I_{(|\mathcal{G}|+|\tilde{\mathcal{G}}|)} - Y_e\ \mathrm{diag}\{\jmath \cdot X'_{d,i}\},\ Y_r \in \mathbb{C}^{(|\mathcal{G}|+|\tilde{\mathcal{G}}|)\times(|\mathcal{G}|+|\tilde{\mathcal{G}}|)}$.

2.5.2 Control Objectives

The next task is to pose the main problem as a *tracking control problem* which involves a *target manifold* that we wish to drive our state-variables x_i to. We first define the target manifold by identifying the variables of interest for our problem. These are the rotor angular speed of generator i, ω_i, its angular acceleration $\dot{\omega}_i$, and its terminal voltage $V_{s,i}$. We assemble these variables into the vector $y_i = [\omega_i,\ \dot{\omega}_i,\ V_{s,i}]^T$, $y_i \in \mathbb{R}^3$ (with equilibrium

$y_{i0} = [\omega_0, 0, V_{s,i0}]^T$), and define the target manifold $\mathcal{O}_i$ as:

$$\mathcal{O}_i := \{x_i \in \mathbb{R}^5 \mid y_i = y_{i0}, \quad y_i \in \mathbb{R}^3\} \tag{2.15}$$

We now analyze the state constraints to provide more insight on why tracking of the above manifold realizes the control objectives. Consider the first constraint on $\mathcal{O}_i$ which imposes $\dot{\omega}_i = 0$ and the corresponding equation (2.2). From these two, it can be inferred that, on $\mathcal{O}_i$, $P_{m,i} = P_{e,i}$ holds, which corresponds to the mechanical and electric power of generator i being equal. Further, the second constraint $\omega_i = \omega_0$, mandates that generator i be in synchrony with the grid on $\mathcal{O}_i$, with its rotational speed being equal to the synchronous. When the state-variables respect these two constraints, the transient stabilization objective is realized. On the other hand, the last constraint, $V_{s,i} = V_{s,i0}$, imposes $V_{s,i}$ to be at its equilibrium on $\mathcal{O}_i$, realizing the voltage regulation objective. Altogether, by driving the states to the target manifold $\mathcal{O}_i$ the desired objectives can be accomplished. To this end, we employ MIMO feedback linearization theory to design a nonlinear controller.

2.5.3 MIMO Feedback Linearization Theory

In this section, we review some theoretical results from Multi-Input Multi-Output (MIMO) feedback linearization theory which form the basis for designing our proposed controller [25]. In doing that, we abuse the notation slightly and reuse some of the already defined indices in a different context with sole purpose of being consistent with the reference [25]. First, consider a MIMO system in the form:

$$\dot{x} = f(x) + \sum_{i=1}^{m} g_i(x)u_i \quad x \in \mathbb{R}^n \tag{2.16}$$

$$y_1 = h_1(x)$$

$$\vdots$$

$$y_m = h_m(x)$$

where $f(x),\ g_1(x),\ ...,\ g_m(x)$ are vector fields in an open set of $\mathbb{R}^n$. In a more compact form the above system can be written as:

$$\begin{aligned} &\dot{x} = f(x) + g(x)u \\ &y = h(x) \\ &u = [u_1,\ u_2,\ ...,\ u_m]^\top, && u \in \mathbb{R}^m \\ &y = [y_1,\ y_2,\ ...,\ y_m]^\top, && y \in \mathbb{R}^m \end{aligned} \tag{2.17}$$

Let the *Lie Derivative* of h along f be defined as:

$$L_f h(x) = \frac{\partial h}{\partial x} f(x) \tag{2.18}$$

Then, according to [25], the above system has (vector) relative degree $\{r_1, ..., r_m\}$ if the following conditions are satisfied:

i. $L_{g_j} L_f^k h_i(x) = 0$, for all $1 \leq j \leq m$, $k < \ r_i - 1$, $1 \leq i \leq m$ and $\forall x$ in a neighborhood of x_0.

ii. the $m \times m$ matrix

$$A(x) = \begin{pmatrix} L_{g_1} L_f^{r_1-1} h_1(x) & \cdots & L_{g_m} L_f^{r_1-1} h_1(x) \\ L_{g_1} L_f^{r_2-1} h_2(x) & \cdots & L_{g_m} L_f^{r_2-1} h_2(x) \\ \vdots & & \\ L_{g_1} L_f^{r_m-1} h_m(x) & \cdots & L_{g_m} L_f^{r_m-1} h_m(x) \end{pmatrix} \tag{2.19}$$

is nonsingular at $x = x_0$.

The existence of an output y that meets the above two conditions is a *necessary and sufficient* condition for the existence of a coordinate transformation and a state feedback (locally around x_0) that solve the *State Space Exact Linearization Problem* [25]. This is formally stated through the next definition.

Lemma 2.1 ([25])**.** *Suppose the matrix $g(x_0)$ has rank m. Then the State Space Exact Linearization Problem is solvable if and only if there exist a neighborhood V of x_0 and m-real valued functions $h_1(x)$, $h_2(x)$, ..., $h_m(x)$ defined on V such that the system (2.17) has some (vector) relative degree $\{r_1, ..., r_m\}$ at x_0 and $r_1 + r_2 + ... + r_m = n$ (dimension of the state-space).*

In this case the functions:

$$\xi_k^i(x) = L_f^{k-1} h_i(x) \quad \text{for} \quad 1 \leq k \leq r_i,\ 1 \leq i \leq m \tag{2.20}$$

define a local transformation at x_0. Next, we use these results to develop a novel MIMO feedback linearizing controller for the generator-storage system.

2.5.4 Controller Design

We first introduce an output y for the system (2.1)-(2.3), (2.5), (2.6) that fulfills the *conditions* i and ii. Then, we use this output to define a key state-space transformation that recasts the initial state-space, (2.1)-(2.3), (2.5), (2.6) into a new form in which: 1) the relevant variables for achieving transient stability and voltage regulation become state-variables (the rotor angle, the rotor acceleration and the terminal voltage); 2) a coordinated full-state MIMO feedback linearizing controller with no zero dynamics can be explicitly designed. We propose the following output vector.

Proposition 2.1. *The output $y_i = [\Delta\delta_i,\ \Delta I_{qb,i},\ \Delta V_{s,i}]^\top$ solves the state-space exact lin-*

earization problem for the subsystem given by (2.1)-(2.3), (2.5), (2.6).

Proof. Note that the new state variables $\Delta\delta_i$, $\Delta I_{qb,i}$, $\Delta V_{s,i}$ denote deviations from the pre-fault equilibrium values. The first step is to show that the output y_i achieves a vector relative degree $\{r_{1,i}, r_{2,i}, r_{3,i}\}$, where $r_{1,i} + r_{2,i} + r_{3,i} = 5$. To show that, we differentiate each output at least until one input appears:

$$\dddot{\Delta\delta}_i = b_{1,i}(x) + a_{11,i}(x)E_{fd,i} + a_{12,i}(x)(u_{\alpha,i} - V_{sd,i}) + a_{13,i}(x)(u_{\beta,i} - V_{sq,i}) \tag{2.21a}$$

$$\Delta\dot{I}_{qb,i} = b_{2,i}(x) + a_{23,i}(x)(u_{\beta,i} - V_{sq,i}) \tag{2.21b}$$

$$\Delta\dot{V}_{s,i} = b_{3,i}(x) + a_{31,i}(x)E_{fd,i} + a_{32,i}(x)(u_{\alpha,i} - V_{sd,i}) + a_{33,i}(x)(u_{\beta,i} - V_{sq,i}) \tag{2.21c}$$

where the matrices $b_i(x) \in \mathbb{R}^3$ and $A_i(x) \in \mathbb{R}^{3\times 3}$ can be written as:

$$b_i(x) = \begin{pmatrix} b_{1,i}(x) \\ b_{2,i}(x) \\ b_{3,i}(x) \end{pmatrix}, \quad A_i(x) = \begin{pmatrix} a_{11,i}(x) & a_{12,i}(x) & a_{13,i}(x) \\ 0 & 0 & a_{23,i}(x) \\ a_{31,i}(x) & a_{32,i}(x) & a_{33,i}(x) \end{pmatrix} \tag{2.22}$$

The full expressions of the functions $b_{1,i}(x)$, $b_{2,i}(x)$, $b_{3,i}(x)$, $a_{11,i}(x)$, $a_{12,i}(x)$, $a_{13,i}(x)$, $a_{23,i}(x)$, $a_{31,i}(x)$, $a_{32,i}(x)$, $a_{33,i}(x)$ are given at the end of this chapter. From (2.22), observe that the matrix $A_i(x)$ is nonsingular in a neighborhood of x_0 so that condition *ii* is fulfilled. Further, we have that $L_{f_i}(\Delta\delta_i) = \omega_s(\omega_i - \omega_0)$ and $L_{g_{i,z}}L_{f_i}(\Delta\delta_i) = 0$ with $z := \{1, 2, 3\}$ and $g_{i,z}$ being the z-(th) column of g_i. We can show that the latter condition also holds for all other elements of the output vector so that condition *i* is fulfilled as well. Altogether, we can conclude that conditions *i* and *ii* are fulfilled and that the output y_i achieves a vector relative degree $\{r_{1,i}, r_{2,i}, r_{3,i}\} = \{3, 1, 1\}$, where $r_{1,i} + r_{2,i} + r_{3,i} = 5$. By invoking Lemma 1, and because $\operatorname{rank} g_i = 3$ we can conclude that the *State-Space Exact Linearization Problem* for the subsystem i is solvable. $\blacksquare$

Next, we use the output y_i to define a state-space transformation. The new state-variables can be obtained from y_i as [25]:

$$\xi_{1,i} = [\Delta\delta_i,\ \Delta\omega_i,\ \dot{\omega}_i]^\top, \qquad \xi_{1,i} \in \mathbb{R}^3 \tag{2.23}$$

$$\xi_{2,i} = [\Delta I_{qb,i}], \qquad \xi_{2,i} \in \mathbb{R} \tag{2.24}$$

$$\xi_{3,i} = [\Delta V_{s,i}], \qquad \xi_{3,i} \in \mathbb{R} \tag{2.25}$$

$$\xi_i = [\xi_{1,i},\ \xi_{2,i},\ \ \xi_{3,i}]^\top, \qquad \xi_i \in \mathbb{R}^5 \tag{2.26}$$

Let $v_i = [v_{1,i},\ v_{2,i},\ v_{3,i}]^T,\ v_i \in \mathbb{R}^3$ be the control inputs of the linearized system. Then, equations (2.21a)-(2.21c) can be written as:

$$\dddot{\Delta\delta}_i = v_{1,i} \tag{2.27a}$$

$$\Delta\dot{I}_{qb,i} = v_{2,i} \tag{2.27b}$$

$$\Delta\dot{V}_{s,i} = v_{3,i} \tag{2.27c}$$

By combining (2.21a)-(2.21c), (2.27a)-(2.27c), we can obtain the feedback linearizing input vector in compact form as:

$$u_i = A_i^{-1}(x)\Big[v_i - b_i(x)\Big] \tag{2.28}$$

Moreover, with $a_{(\cdot),i}(x) \triangleq a_{(\cdot),i}$, we analytically obtain each input u_i as:

$$\begin{aligned} E_{fd,i} = {} & \frac{(a_{12,i}a_{23,i}b_{3,i} - a_{12,i}a_{33,i}b_{2,i}}{(a_{23,i}(a_{11,i}a_{32,i} - a_{12,i}a_{31,i}))} + \frac{a_{13,i}a_{32,i}b_{2,i} - a_{23,i}a_{32,i}b_{1,i} - a_{12,i}a_{23,i}v_{3,i}}{(a_{23,i}(a_{11,i}a_{32,i} - a_{12,i}a_{31,i}))} \\ & + \frac{a_{12,i}a_{33,i}v_{2,i} - a_{13,i}a_{32,i}v_{2,i} + a_{23,i}a_{32,i}v_{1,i})}{(a_{23,i}(a_{11,i}a_{32,i} - a_{12,i}a_{31,i}))} \end{aligned} \tag{2.29}$$

$$
\begin{aligned}
u_{\alpha,i} &= \frac{-(a_{11,i}a_{23,i}b_{3,i} - a_{11,i}a_{33,i}b_{2,i}}{(a_{23,i}(a_{11,i}a_{32,i} - a_{12,i}a_{31,i}))} + \frac{a_{13,i}a_{31,i}b_{2,i} - a_{23,i}a_{31,i}b_{1,i} - a_{11,i}a_{23,i}v_{3,i}}{(a_{23,i}(a_{11,i}a_{32,i} - a_{12,i}a_{31,i}))} \\
&\quad + \frac{a_{11,i}a_{33,i}v_{2,i} - a_{13,i}a_{31,i}v_{2,i} + a_{23,i}a_{31,i}v_{1,i})}{(a_{23,i}(a_{11,i}a_{32,i} - a_{12,i}a_{31,i}))} + V_{sd,i} \qquad (2.30) \\
u_{\beta,i} &= \frac{(v_{2,i} - b_{2,i})}{a_{23,i}} + V_{sq,i} \qquad (2.31)
\end{aligned}
$$

The transformed closed-loop linearized subsystem i takes the *Brunowsky canonical form*:

$$
\dot{\xi}_i = \bar{A}_i\xi_i + \bar{B}_i v_i \qquad (2.32)
$$

$$
\bar{A}_i = \begin{pmatrix} 0 & 1 & 0 & 0 & 0 \\ 0 & 0 & 1 & 0 & 0 \\ 0 & 0 & 0 & 0 & 0 \\ 0 & 0 & 0 & 0 & 0 \\ 0 & 0 & 0 & 0 & 0 \end{pmatrix}, \quad \bar{B}_i = \begin{pmatrix} 0 & 0 & 0 \\ 0 & 0 & 0 \\ 1 & 0 & 0 \\ 0 & 1 & 0 \\ 0 & 0 & 1 \end{pmatrix}
$$

When full state feedback is available, the input v_i can be expressed as:

$$
\begin{aligned}
v_{1,i} &= k_{1,i}(\Delta\delta_i) + k_{2,i}(\Delta\omega_i) + k_{3,i}(\dot{\omega}_i) \\
v_{2,i} &= k_{4,i}(\Delta I_{qb,i}) \\
v_{3,i} &= k_{5,i}(\Delta V_{s,i}) \qquad (2.33)
\end{aligned}
$$

The gains $k_{1,i} - k_{5,i}$ can be chosen appropriately such that $\bar{A}_i$ is a Hurwitz matrix. When that is true, the equilibrium point $\xi_{i0} = \mathbf{0}_{5\times 1}$ of (2.32) becomes *asymptotically stable* [10] and the initial state-vector x_i is driven to a manifold F_i given below.

$$
F_i := \{x_i \in \mathbb{R}^5 \mid \xi_i = \mathbf{0}_5 \ \} \qquad (2.34)
$$

Further, notice that

$$F_i \subseteq \mathcal{O}_i \tag{2.35}$$

This implies that when $\bar{A}_i$ is *Hurwitz* the state-variables x_i are asymptotically tracking the objective manifold $\mathcal{O}_i$ and accomplishing the desired objectives.

2.6 Case Studies

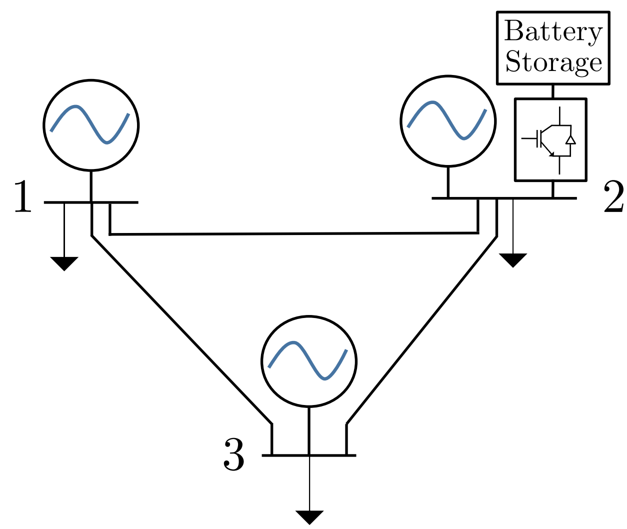

Figure 2.2: 3-bus system

We illustrate the effectiveness of the proposed controller through numerical simulations on the 3-bus power system shown in Fig. 2.2. At bus 2, an energy storage device is placed with the storage and generator controlled according to (2.30), (2.31) and (2.29) respectively. The following two scenarios are explored.

- **Scenario 1**: At $t = 0s$, the system is at equilibrium, when at $t = 0.3s$, a three-phase short-circuit occurs at bus 3 and lasts 200 ms.
- **Scenario 2**: At $t = 0s$, the system is at equilibrium, when at $t = 0.3s$, a three-phase short-circuit occurs at bus 3 and lasts 600 ms.

The system response under these scenarios is depicted in Fig. (2.3), (2.4) below.

2.6.1 Assessment of the Numerical Simulations

From Fig. 2.3a, we observe that, during scenario 1, the rotor angle δ_2 is regulated to its equilibrium rapidly with a low-magnitude first swing and no oscillations, as in the case of generators 1 and 3 (which are controlled through standard AVR controllers). It is important for generators to exhibit low-magnitude first swings in their transient response since then it would be more likely that they will retain their synchronism with the grid after the fault. On the other hand, large-magnitude first swings very often lead to generators losing their synchronism (first swing instability) [3]. From the rotor angle transient response we conclude that under *Scenario 1* the proposed controller ensures transient stabilization of generator 2. Moving to Fig. 2.3b, we observe that the terminal voltage of generator 2 is regulated to its equilibrium rapidly without oscillations, verifying that the controller also ensures voltage regulation of bus 2.

Under the most severe *Scenario 2*, generator 2 behaves again very well during transience. More specifically, its rotor angle response is still very damped as depicted in Fig. 2.4a. In contrast, the rotor angle responses of generators 1 and 3 are very oscillatory. In addition, the voltage at bus 2 is regulated to its equilibrium immediately after the fault without overshoot and oscillations (Fig.2.4b).

In summary, we conclude that the performance of the proposed controller is not compromised in the most severe fault with the controller effectively accomplishing the assigned objectives in both scenarios.

2.6.2 Discussion on the Implementation of the Controller

In order to implement the proposed controller a nonlinear observer is required for retrieving the rotor angle, the rotor acceleration and the voltage E_q'. The reason is that these variables cannot be directly measured. Alternatively, we can compute some of these hard-to-

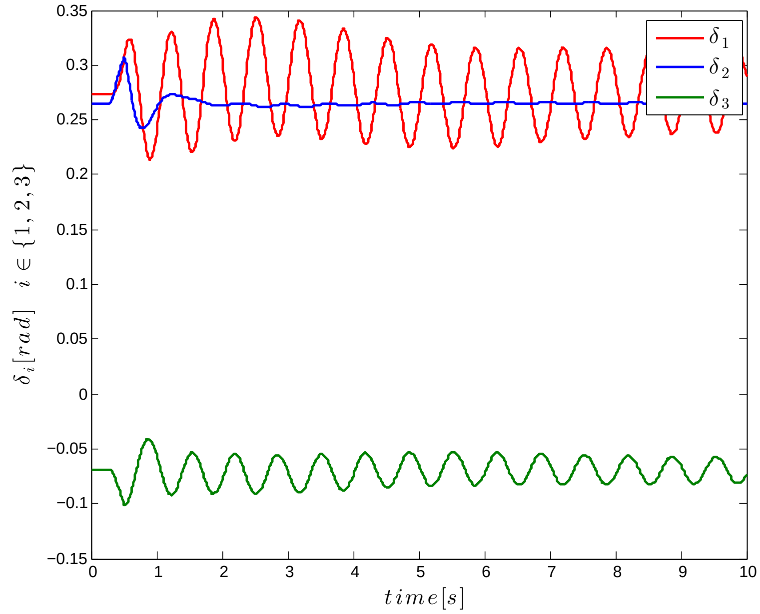

(a) Rotor angle response

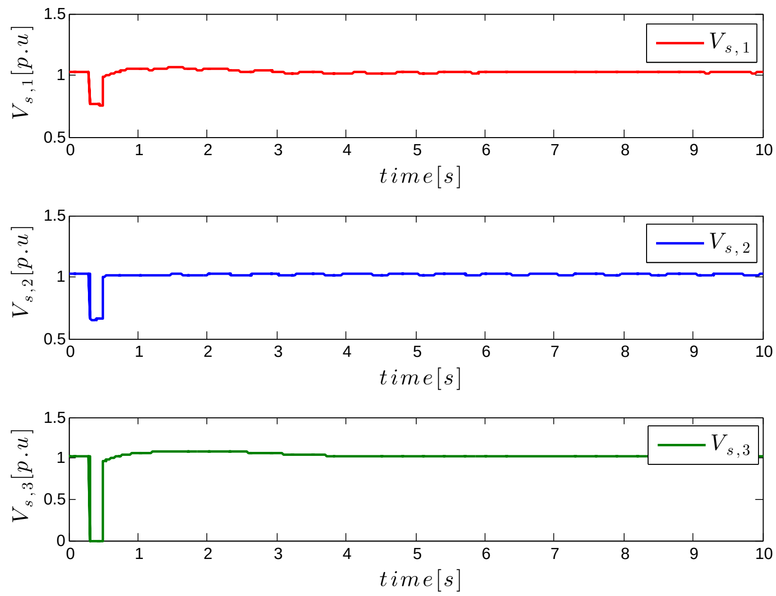

(b) Voltage response

Figure 2.3: System response under scenario 1

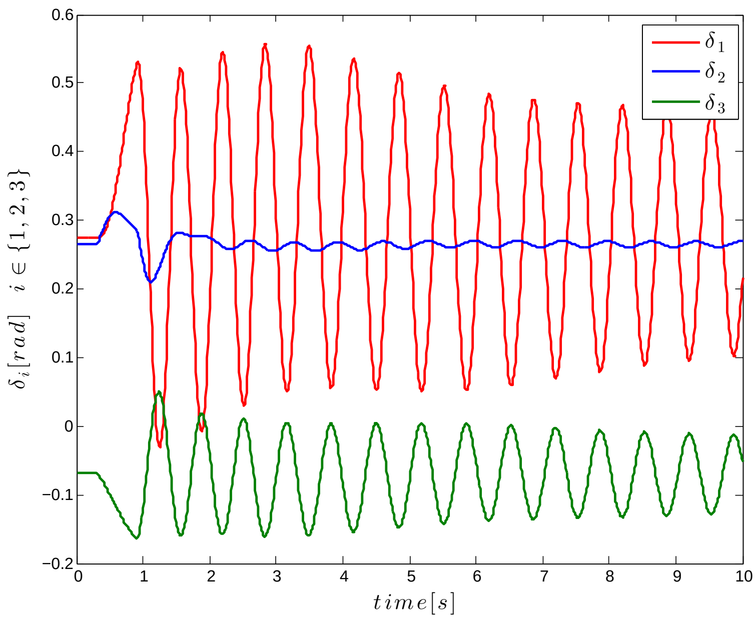

(a) Rotor angles response

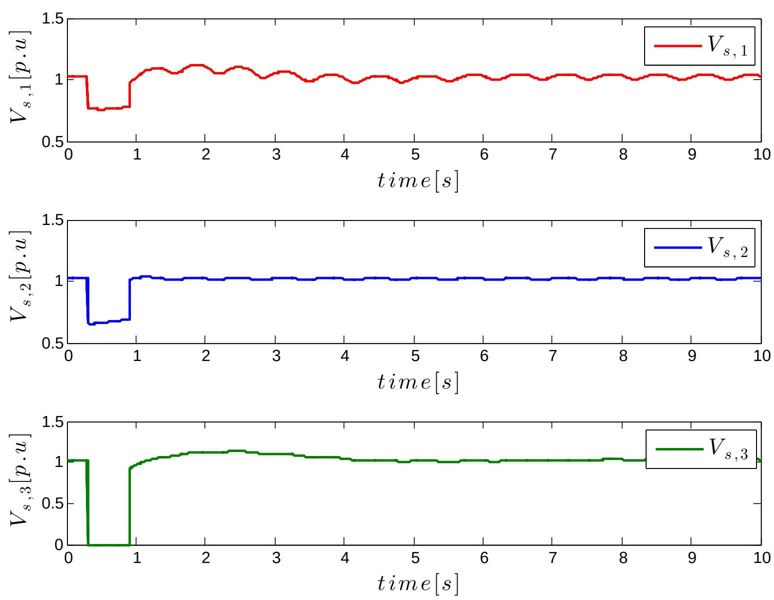

(b) Voltages response

Figure 2.4: System response under scenario 2

measure variables through some other variables that can be measured easily. For instance, acceleration can be computed from ΔP_e when that is available, since $\dot{\omega}{=}\Delta P_e/H$ while $E_q^{'}$ can be computed from the currents I_{ds}, I_{qs} and the voltage V_s when they are available. In general, $\Delta P_e,\ I_{ds},\ I_{qs},\ V_s$ can be easily measured and can be used in the above computations.

2.7 Conclusion

In this chapter, a coordinated nonlinear controller for a generator and an energy storage device is developed. The controller is built upon MIMO Feedback Linearization theory [25] and has two assigned control objectives, transient stabilization of the synchronous generator and voltage regulation of the generator/storage bus. The effectiveness of the proposed controller is demonstrated through numerical simulations on a 3-bus system.

2.8 Appendix

Full Expressions of the Terms Involved in the Derivation of the Controller

$$
\begin{aligned}
b_{1,i} &= -\frac{1}{2H_i}(I_{qs,i} + E_{q,i}^{'}\frac{\partial I_{qs,i}}{\partial E_{q,i}^{'}})\frac{1}{T_{d0,i}^{'}}(-E_{q,i}^{'} + (X_{d,i}^{'} - X_{d,i})I_{ds,i}) - \frac{1}{2H_i}\sum_{k=1,\ k\neq i}^{|\mathcal{G}|+|\tilde{\mathcal{G}}|}[E_{q,i}^{'}(\frac{\partial I_{qs,i}}{\partial E_{q,k}^{'}}\dot{E}_{q,k}^{'} \\
&\quad + \frac{\partial I_{qs,i}}{\partial I_{db,k}}\dot{I}_{db,k} + \frac{\partial I_{qs,i}}{\partial I_{qb,k}}\dot{I}_{qb,k})] - \frac{1}{2H_i}\sum_{k=1}^{|\mathcal{G}|+|\tilde{\mathcal{G}}|}[E_{q,i}^{'}\frac{\partial I_{qs,i}}{\partial \delta_k}\dot{\delta}_k] - \frac{1}{2H_i}E_{q,i}^{'}\frac{\partial I_{qs,i}}{\partial I_{db,i}}(-\omega_s\frac{R_{b,i}}{L_{b,i}}I_{db,i} + \omega_s I_{qb,i}) \\
&\quad - \frac{1}{2H_i}E_{q,i}^{'}\frac{\partial I_{qs,i}}{\partial I_{qb,i}}(-\omega_s\frac{R_{b,i}}{L_{b,i}}I_{qb,i} - \omega_s I_{db,i}) \\
a_{11,i} &= -\frac{1}{2H_i}(I_{qs,i} + E_{q,i}^{'}\frac{\partial I_{qs,i}}{\partial E_{q,i}^{'}})\frac{1}{T_{d0,i}^{'}} \\
a_{12,i} &= -\frac{1}{2H_i}E_{q,i}^{'}\frac{\partial I_{qs,i}}{\partial I_{db,i}}\frac{\omega_s}{L_{b,i}} \\
a_{13,i} &= -\frac{1}{2H_i}E_{q,i}^{'}\frac{\partial I_{qs,i}}{\partial I_{qb,i}}\frac{\omega_s}{L_{b,i}} \\
b_{2,i} &= -\omega_s\frac{R_{b,i}}{L_{b,i}}I_{qb,i} - \omega_s I_{db,i} \\
a_{23,i} &= \frac{\omega_s}{L_{b,i}}
\end{aligned}
$$

$$
\begin{aligned}
b_{3,i} &= \frac{1}{2\sqrt{(E^{'}_{q,i} - I_{ds,i}X^{'}_{d,i})^2 + (I_{qs,i}X^{'}_{d,i})^2}}\Big[- 2X^{'}_{d,i}(E^{'}_{q,i} - I_{ds,i}X^{'}_{d,i})\Big[\sum_{k=1,\ k\neq i}^{|\mathcal{G}|+|\tilde{\mathcal{G}}|}(\frac{\partial I_{ds,i}}{\partial E^{'}_{q,k}}\dot{E}^{'}_{q,k} \\
&+ \frac{\partial I_{ds,i}}{\partial \delta_k}\dot{\delta}_k + \frac{\partial I_{ds,i}}{\partial I_{db,k}}\dot{I}_{db,k} + \frac{\partial I_{ds,i}}{\partial I_{qb,k}}\dot{I}_{qb,k}) + \frac{\partial I_{ds,i}}{\partial \delta_i}\dot{\delta}_i\Big] + 2I_{qs,i}X^{'}_{d,i}\Big[\sum_{k=1,\ k\neq i}^{|\mathcal{G}|+|\tilde{\mathcal{G}}|}(\frac{\partial I_{qs,i}}{\partial E^{'}_{q,k}}\dot{E}^{'}_{q,k} + \frac{\partial I_{qs,i}}{\partial \delta_k}\dot{\delta}_k \\
&+ \frac{\partial I_{qs,i}}{\partial I_{db,k}}\dot{I}_{db,k} + \frac{\partial I_{qs,i}}{\partial I_{qb,k}}\dot{I}_{qb,k}) + \frac{\partial I_{qs,i}}{\partial \delta_i}\dot{\delta}_i\Big] + \Big[2(E^{'}_{q,i} - I_{ds,i}X^{'}_{d,i})(1 - X^{'}_{d,i}\frac{\partial I_{ds,i}}{\partial E^{'}_{q,i}}) \\
&+ 2I_{qs,i}X^{'}_{d,i}\frac{\partial I_{qs,i}}{\partial E^{'}_{q,i}}\Big]\frac{1}{T^{'}_{d0,i}}(-E^{'}_{q,i} + (X^{'}_{d,i} - X_{d,i})I_{ds,i}) + \Big[2(E^{'}_{q,i} - I_{ds,i}X^{'}_{d,i})(-X^{'}_{d,i}\frac{\partial I_{ds,i}}{\partial I_{db,i}}) \\
&+ 2I_{qs,i}X^{'}_{d,i}\frac{\partial I_{qs,i}}{\partial I_{db,i}}\Big](-\omega_s\frac{R_{b,i}}{L_{b,i}}I_{db,i} + \omega_s I_{qb,i}) + \Big[2(E^{'}_{q,i} - I_{ds,i}X^{'}_{d,i})(-X^{'}_{d,i}\frac{\partial I_{ds,i}}{\partial I_{qb,i}}) \\
a_{31,i} &= \Big[2(E^{'}_{q,i} - I_{ds,i}X^{'}_{d,i})(1 - X^{'}_{d,i}\frac{\partial I_{ds,i}}{\partial E^{'}_{q,i}}) + 2I_{qs,i}X^{'}_{d,i}\frac{\partial I_{qs,i}}{\partial E^{'}_{q,i}}\Big]\frac{1}{T^{'}_{d0,i}} \\
a_{32,i} &= \Big[2(E^{'}_{q,i} - I_{ds,i}X^{'}_{d,i})(-X^{'}_{d,i}\frac{\partial I_{ds,i}}{\partial I_{db,i}}) + 2I_{qs,i}X^{'}_{d,i}\frac{\partial I_{qs,i}}{\partial I_{db,i}}\Big]\frac{\omega_s}{L_{b,i}} \\
a_{33,i} &= \Big[2(E^{'}_{q,i} - I_{ds,i}X^{'}_{d,i})(-X^{'}_{d,i}\frac{\partial I_{ds,i}}{\partial I_{qb,i}}) + 2I_{qs,i}X^{'}_{d,i}\frac{\partial I_{qs,i}}{\partial I_{qb,i}}\Big]\frac{\omega_s}{L_{b,i}} \\
\frac{\partial I_{ds,i}}{\partial E^{'}_{q,k}} &= [G_{ik}\sin(\delta_i - \delta_k) - B_{ik}\cos(\delta_i - \delta_k)] \\
\frac{\partial I_{qs,i}}{\partial E^{'}_{q,k}} &= [G_{ik}\cos(\delta_i - \delta_k) + B_{ik}\sin(\delta_i - \delta_k)] \\
\frac{\partial I_{ds,i}}{\partial I_{db,k}} &= [-G_{r,ik}\sin(\delta_i) + B_{r,ik}\cos(\delta_i)] \\
\frac{\partial I_{ds,i}}{\partial I_{qb,k}} &= [B_{r,ik}\sin(\delta_i) + G_{r,ik}\cos(\delta_i)] \\
\frac{\partial I_{qs,i}}{\partial I_{db,k}} &= [-G_{r,ik}\cos(\delta_i) - B_{r,ik}\sin(\delta_i)] \\
\frac{\partial I_{qs,i}}{\partial I_{qb,k}} &= [B_{r,ik}\cos(\delta_i) - G_{r,ik}\sin(\delta_i)] \\
\frac{\partial I_{ds,i}}{\partial \delta_i} &= \sum_{k=1}^{|\mathcal{G}|+|\tilde{\mathcal{G}}|}[G_{ik}E^{'}_{q,k}\cos(\delta_i - \delta_k) + B_{ik}E^{'}_{q,k}\sin(\delta_i - \delta_k) - (G_{r,ik}I_{db,k} - B_{r,ik}I_{qb,k})\cos(\delta_i) - (B_{r,ik}I_{db,k} \\
&+ G_{r,ik}I_{qb,k})\sin(\delta_i)] \\
\frac{\partial I_{ds,i}}{\partial \delta_k} &= [-G_{ik}E^{'}_{q,k}\cos(\delta_i - \delta_k) - B_{ik}E^{'}_{q,k}\sin(\delta_i - \delta_k)]
\end{aligned}
$$

$$
\begin{aligned}
\frac{\partial I_{qs,i}}{\partial \delta_i} &= \sum_{k=1}^{|\mathcal{G}|+|\tilde{\mathcal{G}}|} [-G_{ik}E^{'}_{q,k}\sin(\delta_i - \delta_k) + B_{ik}E^{'}_{q,k} \cdot \cos(\delta_i - \delta_k) + (G_{r,ik}I_{db,k} - B_{r,ik}I_{qb,k})\sin(\delta_i) \\
&- (B_{r,ik}I_{db,k} + G_{r,ik}I_{qb,k})\cos(\delta_i)] \\
\frac{\partial I_{qs,i}}{\partial \delta_k} &= [G_{ik}E^{'}_{q,k}\sin(\delta_i - \delta_k) - B_{ik}E^{'}_{q,k}\cos(\delta_i - \delta_k)]
\end{aligned}
$$

Chapter 3

Nonlinear Control of a Wind Generator with Integrated Storage

3.1 Introduction

As envisioned by a recent U.S. DOE study [1], by 2020, 10% of the annual U.S. electricity demand is expected to be produced by WGs, offshore and onshore. Projecting more into the future, the study envisions that by 2030, 20% of the U.S. electricity demand could be produced from WGs, and by 2050, this percentage could even be 35%. Altogether, this study reveals a trend of increased exploitation of WGs to generate renewable energy in the U.S. Although in general this is highly desirable, on the downside, it renders the stability, robustness and efficiency of power grids more dependent on the control methods used by these WGs. This dependency and the actual impact of wind power on power systems has not yet been quantified and completely understood. However, it is clear that designing more sophisticated and advanced control schemes for state-of-the-art (SoA) WGs should be a high priority task in this new power systems environment.

In the past decade, a new line of research was initiated, with the goal to assess the impact of integrated wind power on power systems stability. One of the related studies concluded that, integrating numerous WGs in particular wind doubly-fed induction generators (DFIGs), can potentially either enhance or deteriorate power systems' transient and small-signal stability [26, 27]. Mainly, this can be attributed to the overall decrease of these systems' inertia caused by the integration of WGs. In other words, wind generators can impact power systems in both beneficial or detrimental ways as pointed out in many of the related studies.

With the actual impact of wind power on power systems being vague, the technical regulations associated with the integration and operation of WGs evolved and became increasingly demanding [28]. In particular, these regulations now mandate that WGs provide many capabilities and ancillary services to power grids, ranging from voltage and frequency regulation to the ability to withstand certain faults while staying connected to the grid [2, 28]. As a reference, we list some of these capabilities below:

- Primary frequency regulation and inertial response to support grid's frequency
- Reactive power control for voltage regulation
- Low Voltage Ride Through (LVRT) for avoiding disconnection during low-voltage conditions
- Power output regulation

The reasoning that drove the changes and developments in the technical regulations is the following. Integrated WGs are replacing synchronous generators (SGs) in the generation portfolio with the latter traditionally providing capabilities that contribute to a stable and robust power systems operation. WGs can also contribute to this, when they provide capabilities akin to the ones provided by the SGs. If that is the case, WGs counteract their negative effects on the grid as well.

From a systems operation perspective, one of the main problems that WGs have to resolve in order to emulate SGs' performance is to counterbalance wind intermittency and somehow generate predictable power output [2]. DFIGs without storage can carry out this when they operate in a deloaded mode, extracting less wind power than the maximum available possible for given wind speed conditions[29]. On the other hand, DFIGs with integrated storage (SoA WGs) can carry out this capability by harnessing their storage devices [16]. In fact, with the integrated storage devices SoA WGs can, not only counterbalance wind intermittency and regulate their power output, but further contribute to frequency regulation as well as many other power systems functionalities. With such flexibility, this technology can become advantageous in the operation of power systems with high wind power integration.

In this day and age, SoA WGs are under commercialization by General Electric with the name *brilliant wind DFIGs.* Brilliant wind DFIGs are consisted of common wind DFIGs with battery storage devices incorporated into their systems [7]. The development of this technology is propelled by the ongoing stringent technical regulations associated with the performance and operation of WGs. Thus, DFIGs with storage are able to comply with strict technical regulations by offering many ancillary services to the grid through capabilities that do not draw on the kinetic energy stored in their rotating shafts.

We envision that, DFIGs with energy storage devices, by possessing all of these appealing characteristics, they will be widely deployed in the future and be very valuable to power systems operation particularly in high wind power integration settings. However, we recognize that this has to be preceded by the development of sophisticated control designs for these WGs that will allow them to effectively and efficiently use their potential to provide advanced services to the grid. These services have to contribute to the secure, efficient and reliable power grid operations.

In this chapter, we make a contribution toward this direction. Our contribution is the development of a decentralized nonlinear energy-based Control Lyapunov Function-based (CLF) control design [30] which guarantees that a WG attains Maximum Power Point Tracking (MPPT) and power output reference tracking by leveraging its storage device. In conclusion, the proposed control design aspires to enable the performance of WGs to emulate that of SGs over a wide range of operating conditions.

3.2 Literature Review

We briefly review the literature on control of wind DFIGs with integrated storage devices. Partly, this has been already presented in the introductory chapter. In [16], a PI controller for the grid side converter (GSC) and a PI controller for the DC-DC converter were introduced, which together enable a SoA WG to generate constant power output and enhanced voltage response during faults. In similar spirit, in [17], a multi-mode control strategy for a SoA WG was developed with aim to counterbalance the variability on the WG's power output and enhance its transient performance during faults. In [15], a two-layer centralized control design for a group of SoA WGs in a WF was presented, that consists of a high-level wind farm controller which issues the real power references for the individual SoA WGs and local low-level controllers which realize them.

In the above literature, the design of the controllers rests on approximate linearization methods which, because of the highly nonlinear rotor-speed and capacitor dynamics of the SoA WG, lead to guaranteed performance only in a small operating region around the equilibrium.

3.3 Wind Generator Modeling

In this section, the detailed model of a wind DFIG with integrated storage, which is shown pictorially in Fig. 3.1, is presented. Further, the stochastic wind-speed model that is extensively used throughout this thesis.

3.3.1 Rotor Voltages Dynamical Model

The rotor-voltages model originates from [5] and is restated here for completeness. It captures the rotor-voltage dynamical equations via two first-order ordinary differential equa-

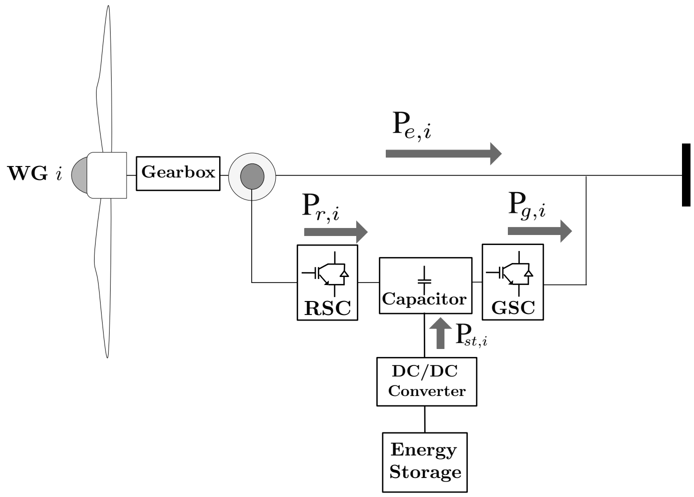

Figure 3.1: Wind generator with integrated storage

tions (ODEs) in a $d - q$ coordinate system. In this coordinate system, the d axis is aligned with the terminal voltage while the q axis is orthogonal to the d axis. That facilitates decoupled real and reactive power control through the rotor-side converter (RSC). Let the set of SoA WGs be denoted by $\mathcal{G}$. The rotor voltages dynamical model, assuming instantaneous stator voltage dynamics, is given by:

$$\dot{E}'_{d,i} = \frac{1}{T'_{0,i}}[-E'_{d,i} + (X_{s,i} - X'_{s,i})I_{qs,i} + T'_{0,i}(-\omega_s \frac{X_{m,i}}{X_{r,i}} V_{qr,i} + (\omega_s - \omega_{r,i})E'_{q,i})], \quad \forall i \in \mathcal{G} \tag{3.1a}$$

$$\dot{E}'_{q,i} = \frac{1}{T'_{0,i}}[-E'_{q,i} - (X_{s,i} - X'_{s,i})I_{ds,i} + T'_{0,i}(\omega_s \frac{X_{m,i}}{X_{r,i}} V_{dr,i} - (\omega_s - \omega_{r,i})E'_{d,i})], \quad \forall i \in \mathcal{G} \tag{3.1b}$$

where state-variables $E'_{q,i}, E'_{d,i} \in \mathbb{R}$ are the internal rotor voltages or flux linkages in the $d-q$ coordinate system, and $\omega_{r,i}$ the WG rotor-speed. The constant ω_s is the synchronous speed $2\pi 60$ $[\frac{rad}{s}]$ where the variables $V_{qr,i}$,$V_{dr,i} \in \mathbb{R}$ are the voltage components representing the control inputs directly controlled by the RSC. Further, the variables $I_{qs,i}, I_{ds,i} \in \mathbb{R}$ denote the stator currents of the WG. In the above equations, $T'_{0,i} \in \mathbb{R}_{++}$ is the transient open-circuit time constant, $X'_{s,i} \in \mathbb{R}_{++}$ the stator transient reactance, $X_{s,i} \in \mathbb{R}_{++}$ the stator reactance, $X_{r,i} \in \mathbb{R}_{++}$ the rotor reactance, $X_{m,i} \in \mathbb{R}_{++}$ the mutual reactance between stator and rotor.

3.3.2 Rotor Speed Dynamical Model

The rotor speed dynamical model also comes from [5] and captures the dynamics of the rotor speed $\omega_{r,i}$ with an ODE as follows:

$$\dot{\omega}_{r,i} = \frac{\omega_s}{2H_i}(T_{m,i} - T_{e,i}) \, , \qquad \forall i \in \mathcal{G} \tag{3.2a}$$

where the mechanical and electrical torque are respectively given by:

$$T_{e,i} = \frac{E'_{q,i} V_{s,i}}{X'_{s,i}}, \qquad \forall i \in \mathcal{G} \tag{3.2b}$$

$$T_{m,i} \triangleq \frac{1}{2} \frac{\rho \pi R_i^2 \omega_s}{S_{b,i} \omega_{r,i}} C_p(\lambda_i, \theta_i) v_{w,i}^3 \, , \qquad \forall i \in \mathcal{G} \tag{3.2c}$$

In the electrical torque equation, $V_{s,i}$ represents the voltage whereas in the mechanical torque equation, $\rho \in \mathbb{R}_{++}$ represents the air density $[\frac{kg}{m^3}]$, $R_i \in \mathbb{R}_{++}$ the radius of the turbine, $v_{w,i} \in \mathbb{R}_{++}$ the wind speed $[\frac{m}{s}]$, $S_{b,i} \in \mathbb{R}_{++}$ the base power and H_i the combined inertia of the turbine and the generator. Additionally, $C_{p,i} \in \mathbb{R}_{++}$ denotes the power coefficient that depends on the tip-speed ratio $\lambda_i \in \mathbb{R}_{++}$ and the pitch angle $\theta_i \in \mathbb{R}$. Concretely, $C_{p,i}$ can be analytically expressed in terms of $\lambda_i,\ \theta_i$ as [5]:

$$C_{p,i}(\lambda_i, \theta_i) \triangleq 0.22\Big[116(\frac{1}{\lambda_i + 0.08\theta_i} - \frac{0.035}{\theta_i^3 + 1})\Big] \cdot \mathrm{e}^{\left(-12.5(\frac{1}{\lambda_i + 0.08\theta_i} - \frac{0.035}{\theta_i^3+1})\right)}, \qquad \forall i \in \mathcal{G} \tag{3.3a}$$

where λ_i is given by:

$$\lambda_i \triangleq \frac{2k_i}{p_i} \frac{\omega_{r,i} R_i}{v_{w,i}} \, , \qquad \forall i \in \mathcal{G} \tag{3.4a}$$

3.3.3 Grid-side Converter (GSC) Dynamical Model

The grid-side converter (GSC) model can be described by the dynamics of its current output expressed in the $d-q$ coordinate system [31] as:

$$\frac{dI_{dg,i}}{dt} = -\omega_s\Big(\frac{R_{g,i}}{L_{g,i}}\Big)I_{dg,i}+\omega_s I_{qg,i}+\omega_s\Big(\frac{V_{dg,i}-V_{s,i}}{L_{g,i}}\Big), \qquad \forall i \in \mathcal{G} \tag{3.5}$$

$$\frac{dI_{qg,i}}{dt} = -\omega_s\Big(\frac{R_{g,i}}{L_{g,i}}\Big)I_{qg,i}-\omega_s I_{dg,i}+\omega_s\Big(\frac{V_{qg,i}}{L_{g,i}}\Big), \qquad \forall i \in \mathcal{G} \tag{3.6}$$

The state-variables $I_{dg,i},\ I_{qg,i}$ represent the current output of the GSC in the d and q axis respectively, whereas, $V_{dg,i}, V_{qg,i} \in \mathbb{R}$ are the controllable voltage inputs of the GSC [31]. The constants $R_{g,i}, L_{g,i} \in \mathbb{R}_+$ represent the losses of the GSC. The power output of the GSC is:

$$P_{g,i} = I_{dg,i}V_{s,i} \tag{3.7}$$

3.3.4 Interfacing Capacitor Dynamical Model

The dynamical model of the DC capacitor that interfaces the RSC and the GSC consists of the dynamics of its DC voltage $V_{dc,i}$, described by:

$$C_{dc,i}V_{dc,i}\dot{V}_{dc,i} = (P_{r,i}+P_{st,i}-P_{g,i}), \qquad i \in \mathcal{G} \tag{3.8}$$

where the state-variable $V_{dc,i}$ denotes the DC voltage, and $C_{dc,i} \in \mathbb{R}$ the capacitance of the capacitor. In addition, $P_{r,i}$ and $P_{st,i}$ are the RSC and storage power outputs, respectively. The RSC power output can be expressed in terms of local variables and parameters as:

a) **RSC power output**

$$P_{r,i} = -\frac{V_{dr,i}E'_{q,i}X_{s,i}}{X'_{s,i}X_{m,i}} - V_{qr,i}\Big[\frac{(X_{s,i}-X'_{s,i})V_{s,i}}{X_{s,i}} - E'_{d,i}\Big]\frac{X_{s,i}}{X'_{s,i}X_{m,i}} \tag{3.9}$$

In this thesis, the storage devices studied are supercapacitors due to their high efficiency and rapid response capability. Their power output can be expressed as:

b) **Storage power output**

$$P_{st,i} = V_{sc,i}\frac{(V_{sc,i}-u_{sc,i})}{R_{sc,i}} \tag{3.10}$$

where $V_{sc,i} \in \mathbb{R}$ denotes its DC voltage and $u_{sc,i} \in \mathbb{R}$ its control input. This control input represents the controllable, by the DC-DC converter (that interfaces the storage device and the capacitor), voltage through which the real power flowing from the storage device into the DC link can be regulated. By employing (3.9), (3.10), (3.7), equation (3.8) can be expanded as:

$$\begin{aligned}\dot{V}_{dc,i} = \frac{1}{C_{dc,i}V_{dc,i}}(&\underbrace{-\frac{V_{dr,i}E'_{q,i}X_{s,i}}{X'_{s,i}X_{m,i}} - V_{qr,i}[\frac{(X_{s,i}-X'_{s,i})V_{s,i}}{X_{s,i}} - E'_{d,i}]\frac{X_{s,i}}{X'_{s,i}X_{m,i}}}_{P_{r,i}} \\ &\underbrace{+V_{sc,i}\frac{(V_{sc,i}-u_{sc,i})}{R_{sc,i}}}_{P_{st,i}} - \underbrace{I_{dg,i}V_{s,i}}_{P_{g,i}})\end{aligned} \tag{3.11}$$

3.3.5 Supercapacitor Energy Storage Dynamical Model

The dynamical model of a supercapacitor energy storage is:

$$C_{sc,i}V_{sc,i}\dot{V}_{sc,i} = V_{sc,i}\frac{(u_{sc,i}-V_{sc,i})}{R_{sc,i}}, \qquad i \in \mathcal{G}$$

where $V_{sc,i}$ is the state-variable that denotes the DC voltage of the supercapacitor and $C_{sc,i},\ R_{sc,i} \in \mathbb{R}$ are constants that denote the capacitance and resistance of the supercapacitor respectively.

3.3.6 Time-constants of the WG Model

The above dynamical models involve several state-variables that are associated with both the mechanical and the electrical part of a SoA WG. To obtain some insight on the relevant time-scales that characterize these dynamics, we order their time-constants in a decreasing order.

$$\underbrace{T_{mech}[\omega_{r,i}]}_{slowest} > T_{rotor\ volt}[E'_{q,i}] > T_{supercap}[V_{sc,i}] > T_{cap}[V_{dc,i}] > \underbrace{T_{GSC}[I_{dg,i}]}_{fastest} \tag{3.12}$$

We underline that this ordering is valid for the specific parameters considered in this thesis.

3.3.7 Wind-speed Model

The wind speed model is from [32, 33]. In this model, the effective wind speed $v_{w,i}$ is obtained as the superposition of two components:

$$v_{w,i} \triangleq v_{m,i} + v_{s,i} \tag{3.13}$$

The first component $v_{m,i}$ corresponds to the average wind speed which can be assumed constant (at the turbulence time-scale), or slowly varying with the averaging usually being performed over a 10-min time window [34]. This particular component can be modeled with a Weibull distribution. The second component $v_{s,i}$ corresponds to the fast turbulence and can be modeled as a zero average random process. In this thesis, we assume that the mean wind speed $v_{m,i}$ is measured and therefore known. On the other hand, we take $v_{s,i}$ to be the output of a nonlinear model which represents the spectrum of the point wind and the spectrum of the area swept by the the rotor blades. For a specific frequency range, this nonlinear model can be well-approximated by a second-order linear filter whose state-space realization varies

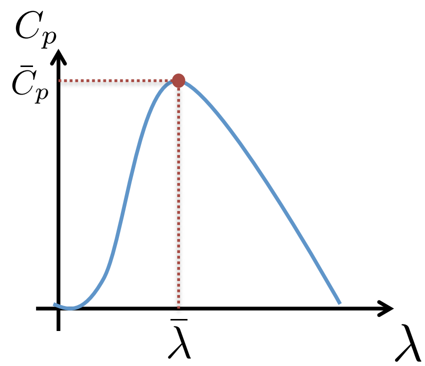

Figure 3.2: $C_p - \lambda$ characteristic under MPPT

with the mean wind speed $v_{m,i}$. This state-space realization can be expressed as:

$$\begin{pmatrix} \dot{v}_{s,i} \\ \ddot{v}_{s,i} \end{pmatrix} = \begin{pmatrix} 0 & 1 \\ -\frac{1}{p_{1,i}p_{2,i}} & -\frac{p_{1,i}+p_{2,i}}{p_{1,i}p_{2,i}} \end{pmatrix} \begin{pmatrix} v_{s,i} \\ \dot{v}_{s,i} \end{pmatrix} + \begin{pmatrix} 0 \\ \frac{k_i}{p_{1,i}p_{2,i}} \end{pmatrix} e \tag{3.14}$$

where the input driving the above dynamics $e \in \mathcal{N}(0,1)$ is a white noise process. The terms $p_{1,i}$, $p_{2,i}$, k_i depend on the mean wind speed $v_{m,i}$ so that $p_{1,i} \triangleq p_{1,i}(v_{m,i})$, $p_{2,i} \triangleq p_{2,i}(v_{m,i})$, $k_i \triangleq k_i(v_{m,i})$ [32, 33].

3.4 Problem Formulation

In this section, we analytically formulate two main problems that we seek to solve for the single-SoA-WG set-up. The first is provable maximum power extraction from the wind during low wind-speed conditions and the second is power output regulation.

3.4.1 Maximum Power Point Tracking (MPPT)

The fundamental equation for a WG is the one that describes the mechanical power extracted from the wind. This can be stated as:

$$P_{m,i} \triangleq \frac{1}{2}\rho C_{p,i} A_i v_{w,i}^3, \quad \forall i \in \mathcal{G} \tag{3.15}$$

Now, for specified θ_i^*, the relation between the power coefficient $C_{p,i}$ and the tip-speed ratio λ_i is captured by equation (3.3a) which can be plotted as shown in Fig. 3.2. When $C_{p,i}$ attains its maximum value $\overline{C}_{p,i} = \max_{\lambda_i}\{C_{p,i}(\lambda_i, \theta_i^*)\}$, the mechanical power of the WG becomes the maximum possible for the particular wind speed conditions, i.e $\overline{P}_{m,i} = \max_{C_{p,i}}\{P_{m,i}(C_{p,i})\} = P_{m,i}(\overline{C}_{p,i})$. That can be seen from:

$$\overline{P}_{m,i} \triangleq \frac{1}{2}\rho\overline{C}_{p,i}A_i v_{w,i}^3, \quad \forall i \in \mathcal{G} \tag{3.16}$$

A WG i that is operated such that $C_{p,i} = \overline{C}_{p,i}$ and $P_{m,i} = \overline{P}_{m,i}$ is said to be operated under a *Maximum Power Point Tracking (MPPT)* strategy. We state this formally as follows.

Problem Formulation 3 (Maximum power point tracking (MPPT)). *For given θ_i^*, a WG is operated under a MPPT strategy, extracting maximum power from the wind, when $C_{p,i}(\overline{\lambda}_i, \theta_i^*) = \overline{C}_{p,i}$ where $\frac{\partial C_{p,i}}{\partial \lambda_i}(\overline{\lambda}_i, \theta_i^*) = 0$.*

MPPT can be achieved through control of the RSC. To see this, recall that λ_i depends on $\omega_{r,i}$ as shown in (3.4a). Thus, the RSC can regulate λ_i to $\overline{\lambda}_i$ by regulating the rotor speed $\omega_{r,i}$ to:

$$\overline{\omega}_{r,i} = \frac{\overline{\lambda}_i p_i v_{w,i}}{2k_i R_i} \tag{3.17}$$

which depends on the wind speed conditions. The RSC regulates $\omega_{r,i}$ through the following mechanism. By controlling the voltage $V_{dr,i}$ which adjusts the internal voltage $E'_{q,i}$ and through that the electrical torque $T_{e,i}$. The variations of the $T_{e,i}$ are translated into variations of the generator speed $\omega_{r,i}$ through the relation in (3.2a).

At this point, we emphasize that the rotor speed dynamics are highly nonlinear due to the relation (3.3a). This motivates the nonlinear control design that we will introduce in later sections.

3.4.2 Power Output Regulation

The second control objective for the WG system is power output reference tracking. Let the total power output of a WG i be given by:

$$P_{t,i} = P_{g,i}+P_{e,i} \tag{3.18}$$

The above objective can be formally stated as follows.

Problem Formulation 4 (Power Output Regulation). *Given a total power reference $P^*_{t,i}$, a WG i attains power reference tracking or i.e power output regulation, when* $\lim_{t\to\infty} P_{t,i} = P^*_{t,i}$.

In our analysis, we assume that $P_{e,i}$ is known and corresponds to the electrical power of the WG originating from the wind. Hence, we realize the power reference tracking control objective through the GSCs by designing appropriate control for their voltage input $V_{dg,i}$. In more detail, we properly design a control input $V_{dg,i}$ that enables GSCs to regulate $I_{dg,i}$ and ultimately $P_{g,i}$ to $(P^*_{t,i}-P_{e,i})$.

3.5 Nonlinear Energy-Based Control

In this section, we analytically construct a novel nonlinear controller for a SoA WG. In the first place, we assemble the individual models which we already introduced in a compact standard state-space form. Subsequently, we use new energy state-variables to recast the WG model in a new standard state-space form. We eventually define the control objectives in this new model and construct Control Lyapunov Function (CLF)-based controllers to achieve them.

3.5.1 State-Space Model of a DFIG With Integrated Storage

Altogether, the interdependent models in (3.1a), (3.1b), (3.2a), (3.5), (3.6), (3.8), (3.12) constitute the model of a DFIG with a supercapacitor energy storage device. This can be expressed in compact *state-space form* as:

$$\dot{x}_i = f_i(x_i, y_i, u_i, d_i), \quad i \in \mathcal{G} \tag{3.19}$$

where $f_i : \mathbb{R}^7 \times \mathbb{R}^3 \times \mathbb{R}^5 \times \mathbb{R} \mapsto \mathbb{R}^7$ is the vector field:

$$f_i := \begin{pmatrix} \frac{1}{T'_{0,i}}[-E'_{d,i}+(X_{s,i}-X'_{s,i})(I_{qs,i})+T'_{0,i}(-\omega_s\frac{X_{m,i}}{X_{r,i}}V_{qr,i}+(\omega_s-\omega_{r,i})E'_{q,i})] \\ \frac{1}{T'_{0,i}}[-E'_{q,i}-(X_{s,i}-X'_{s,i})(I_{ds,i})+T'_{0,i}(\omega_s\frac{X_{m,i}}{X_{r,i}}V_{dr,i}-(\omega_s-\omega_{r,i})E'_{d,i})] \\ \frac{\omega_s}{2H_i}(\frac{1}{2}\frac{\rho\pi R_i^2\omega_s}{S_{b,i}\omega_{r,i}}C_p(\lambda_i,\theta_i)v_{w,i}^3-\frac{E'_{q,i}V_{s,i}}{X'_{s,i}}) \\ \frac{1}{C_{dc,i}V_{dc,i}}(-\frac{V_{dr,i}E'_{q,i}X_{s,i}}{X'_{s,i}X_{m,i}}-V_{qr,i}[\frac{(X_{s,i}-X'_{s,i})V_{s,i}}{X_{s,i}}-E'_{d,i}]\frac{X_{s,i}}{X'_{s,i}X_{m,i}}+V_{sc,i}\frac{(V_{sc,i}-u_{sc,i})}{R_{sc,i}}-I_{dg,i}V_{s,i}) \\ -\omega_s\left(\frac{R_{g,i}}{L_{g,i}}\right)I_{dg,i}+\omega_s I_{qg,i}+\omega_s\left(\frac{V_{dg,i}-V_{s,i}}{L_{g,i}}\right) \\ -\omega_s\left(\frac{R_{g,i}}{L_{g,i}}\right)I_{qg,i}-\omega_s I_{dg,i}+\omega_s\left(\frac{V_{qg,i}}{L_{g,i}}\right) \\ V_{sc,i}\frac{(u_{sc,i}-V_{sc,i})}{R_{sc,i}} \end{pmatrix} \text{ and}$$

x_i the WG state-vector:

$$x_i = [E'_{d,i},\ E'_{q,i},\ \omega_{r,i},\ V_{dc,i},\ I_{dg,i},\ I_{qg,i},\ V_{sc,i}]^\top,\ x_i \in \mathbb{R}^7 \tag{3.20}$$

The control input vector u_i consists of the RSC, storage and GSC controllable voltages:

$$u_i = [u_{RSC}^\top,\ u_{stor}^\top,\ u_{GSC}^\top]^\top,\ u_i \in \mathbb{R}^5 \tag{3.21}$$

$$u_{RSC} = [V_{qr,i},\ V_{dr,i}]^\top, \qquad u_{RSC} \in \mathbb{R}^2 \tag{3.22}$$

$$u_{stor} = u_{sc,i}, \qquad u_{stor} \in \mathbb{R} \tag{3.23}$$

$$u_{GSC} = [V_{dg,i},\ V_{qg,i}]^\top, \qquad u_{GSC} \in \mathbb{R}^2 \tag{3.24}$$

The subsystem (3.19) is interconnected with the rest of the system through the variables:

$$y_i = [I_{ds,i},\ I_{qs,i},\ V_{s,i}]^\top, \quad y_i \in \mathbb{R}^3 \tag{3.25}$$

where $I_{ds,i},\ I_{qs,i},\ V_{s,i}$ are the current output components and voltage of each WG respectively. The wind-speed is treated as an exogenous input:

$$d_i = v_{w,i}, \ \ d_i \in \mathbb{R} \tag{3.26}$$

3.5.2 Energy-based State-Space Model of a Wind DFIG

In this section, we introduce new energy state-variables which we use to recast the WG model (3.19) in a new standard state-space form. The reason for performing such a transformation are twofold. First, the main control objectives can be explicitly expressed as reference tracking for these new energy state-variables. In general, most of the control objectives related to power systems operation can be very easily defined with the notions of energy and power [35]. Second, the action of controllers on these physical quantities is more intuitive. In summary, energy state-space modeling enables a more direct definition of the control objectives and lends itself to a more intuitive control design. We now define the first energy state-variable $E_{g,i}$ as:

$$E_{g,i} = \int_0^\tau (P_{e,i} + P_{g,i} - P^*_{t,i}) d\tau, \quad E_{g,i} \in \mathbb{R} \tag{3.27}$$

This variable represents an additional undesired accumulated disturbance energy that is channeled from the WG i to the grid. Given a WG power reference $P^*_{t,i}$, its dynamics are:

$$\dot{E}_{g,i} = (\underbrace{\frac{E'_{q,i} V_{s,i}}{X'_{s,i}} + I_{dg,i} V_{s,i}}_{WG\ Total\ Power\ Output} - P^*_{t,i}) \tag{3.28}$$

The second energy state-variable we consider here is the kinetic energy $E_{k,i}$ of WG i::

$$E_{k,i} = H_i \omega_{r,i}^2, \qquad E_{k,i} \in \mathbb{R}_+ \tag{3.29}$$

This kinetic energy (KE) is stored in the shaft of the WG which is rotating with speed $\omega_{r,i}$. The dynamics of the KE can be described by:

$$\dot{E}_{k,i} = \omega_s \omega_{r,i}(T_{m,i} - T_{e,i}) \tag{3.30}$$

The third state-variable that we employ is the energy stored in the interfacing capacitor. This is denoted by the variable $E_{dc,i}$ and expressed as:

$$E_{dc,i} = \frac{1}{2} C_{dc,i} V_{dc,i}^2, \; E_{dc,i} \in \mathbb{R}_+ \tag{3.31}$$

The dynamics of this energy state-variable can be represented as:

$$\dot{E}_{dc,i} = (P_{r,i} + P_{st,i} - P_{g,i}) \tag{3.32}$$

To proceed, we restrict the domains of $\omega_{r,i}$ and $V_{dc,i}$ to lie in $\mathbb{R}_+$ so that the functions $E_{k,i}$ and $E_{dc,i}$ become *bijections* with inverses:

$$\omega_{r,i} = \sqrt{\frac{E_{k,i}}{H_i}}, \qquad \omega_{r,i} \in \mathbb{R}_+ \tag{3.33}$$

$$V_{dc,i} = \sqrt{\frac{2E_{dc,i}}{C_{dc,i}}}, \qquad V_{dc,i} \in \mathbb{R}_+ \tag{3.34}$$

Finally, we augment the initial state-vector:

$$x_i = [E_{d,i}^{'}, \; E_{q,i}^{'}, \; \omega_{r,i}, \; V_{dc,i}, \; I_{dg,i}, \; I_{qg,i}, \; V_{sc,i}]^\top, \quad x_i \in \mathbb{R}^7 \tag{3.35}$$

with the state-variable $E_{g,i}$ and replace the state-variables $\omega_{r,i},\ V_{dc,i}$ with their corresponding $E_{k,i},\ E_{dc,i}$. All these actions finally lead to the *new state-vector*:

$$\tilde{x}_i = [E^{'}_{d,i},\ E^{'}_{q,i},\ E_{k,i},\ E_{dc,i},\ I_{dg,i},\ I_{qg,i},\ V_{sc,i},\ E_{g,i}]^{\top}, \qquad \tilde{x}_i \in \mathbb{R}^8 \tag{3.36}$$

The *new transformed state-space* model corresponding to the state-vector $\tilde{x}_i$ is:

$$\dot{\tilde{x}}_i = \tilde{f}_i(\tilde{x}_i, y_i, u_i, d_i) \tag{3.37}$$

with the new vector field $\tilde{f}_i : \mathbb{R}^8{\times}\mathbb{R}^3{\times}\mathbb{R}^5{\times}\mathbb{R} \mapsto \mathbb{R}^8$ defined as:

$$\tilde{f}_i := \begin{pmatrix} \frac{1}{T^{'}_{0,i}}[-E^{'}_{d,i}+(X_{s,i}-X^{'}_{s,i})(I_{qs,i})+T^{'}_{0,i}(-\omega_s\frac{X_{m,i}}{X_{r,i}}V_{qr,i}+(\omega_s-\sqrt{\frac{E_{k,i}}{H_i}})E^{'}_{q,i})] \\ \frac{1}{T^{'}_{0,i}}[-E^{'}_{q,i}-(X_{s,i}-X^{'}_{s,i})(I_{ds,i})+T^{'}_{0,i}(\omega_s\frac{X_{m,i}}{X_{r,i}}V_{dr,i}-(\omega_s-\sqrt{\frac{E_{k,i}}{H_i}})E^{'}_{d,i})] \\ \frac{\omega_s\sqrt{\frac{E_{k,i}}{H_i}}}{2H_i}(\frac{1}{2}\frac{\rho\pi R_i^2\omega_s}{S_{b,i}\sqrt{\frac{E_{k,i}}{H_i}}}C_p(\lambda_i,\theta_i)v^3_{w,i}-\frac{E^{'}_{q,i}V_{s,i}}{X^{'}_{s,i}}) \\ (-\frac{V_{dr,i}E^{'}_{q,i}X_{s,i}}{X^{'}_{s,i}X_{m,i}}-V_{qr,i}[\frac{(X_{s,i}-X^{'}_{s,i})V_{s,i}}{X_{s,i}}-E^{'}_{d,i}]\frac{X_{s,i}}{X^{'}_{s,i}X_{m,i}}+V_{sc,i}\frac{(V_{sc,i}-u_{sc,i})}{R_{sc,i}}-I_{dg,i}V_{s,i}) \\ -\omega_s\left(\frac{R_{g,i}}{L_{g,i}}\right)I_{dg,i}+\omega_s I_{qg,i}+\omega_s\left(\frac{V_{dg,i}-V_{s,i}}{L_{g,i}}\right) \\ -\omega_s\left(\frac{R_{g,i}}{L_{g,i}}\right)I_{qg,i}-\omega_s I_{dg,i}+\omega_s\left(\frac{V_{qg,i}}{L_{g,i}}\right) \\ V_{sc,i}\frac{(u_{sc,i}-V_{sc,i})}{R_{sc,i}} \\ (\frac{E^{'}_{q,i}V_{s,i}}{X^{'}_{s,i}}+I_{dg,i}V_{s,i}-P^{*}_{t,i}) \end{pmatrix} \tag{3.38}$$

where $y_i,\ u_i,\ d_i$ denote the interconnection vector, control input and exogenous disturbance as already defined in (3.25), (3.21), (3.26), respectively.

3.5.3 Control Objectives

a) **Maximum Power Point Tracking (MPPT)**

In Section 3.4.1, we explained that MPPT can be attained when the rotor speed $\omega_{r,i}$ is tracking the reference $\overline{\omega}_{r,i}$ (3.17), equivalently when $\overline{\omega}_{r,i}$ is an *asymptotically stable* equilibrium of (3.2a). By employing equation (3.29), we now translate this requirement into a corresponding one for the kinetic energy $E_{k,i}$ variable through the following claim.

Claim 1. *For given θ_i^*, WG i is operating under a MPPT strategy, extracting maximum power from the wind, when its kinetic energy $E_{k,i}$ is tracking $\overline{E}_{k,i}$, which is explicitly given by:*

$$\overline{E}_{k,i} = H_i \overline{\omega}_{r,i}^2 \overset{(3.17)}{=} \frac{H_i \overline{\lambda}_i^2 p_i^2 v_{w,i}^2}{4k_i^2 R_i^2} \tag{3.39}$$

In other words, when $\overline{E}_{k,i}$ is an asymptotically stable equilibrium point of (3.30)*.*

Proof. To prove this claim, it is sufficient to formally show that *asymptotic stability* of $\overline{E}_{k,i}$ implies *asymptotic stability* of $\overline{\omega}_{r,i}$. For this scope, we invoke the next theorem.

Theorem 3.1 ([10])**.** *Let $\dot{y} = f(y)$, where $f : \mathbb{R}^n \mapsto \mathbb{R}^n$. Consider the change of variables $z = T(y)$, where $T(\mathbf{0}_n) = \mathbf{0}_n$ and $T : \mathbb{R}^n \mapsto \mathbb{R}^n$ is a diffeomorphism in the neighborhood of the origin; that is, the inverse map $T^{-1}(\cdot)$ exists, and both $T(\cdot)$ and $T^{-1}(\cdot)$ are continuously differentiable. The transformed system is $\dot{z} = \hat{f}(z)$. Then $y = 0$ is stable (asymptotically stable) iff $z = 0$ is stable (asymptotically stable).*

Practically, the above theorem states that, if we have two systems which are interrelated through a sufficiently smooth transformation then, establishing stability (asymptotic stability) of one of them is sufficient to infer stability (asymptotic stability) of the other. In our case, we consider the mapping $\mathcal{T} : \omega_{r,i} \mapsto E_{k,i}$ as $\mathcal{T}(\omega_{r,i}) = H_i \omega_{r,i}^2$ where $\mathcal{T}(\overline{\omega}_{r,i}) = \overline{E}_{k,i}$. In a neighborhood around $\overline{\omega}_{r,i}$, the inverse map $\mathcal{T}^{-1}(\cdot)$ exists, and both $\mathcal{T}(\cdot)$ and $\mathcal{T}^{-1}(\cdot)$ are continuously differentiable, i.e $\mathcal{T}$ is a diffeomorphism. From Theorem 3.1, we have that, the equilibrium point $\omega_{r,i} = \overline{\omega}_{r,i}$ is *asymptotically stable if and only if* the equilibrium point $E_{k,i} = \overline{E}_{k,i}$ is *asymptotically stable.* ■

In brief, the above analysis reduced the problem of achieving MPPT, which is a standard capability for a WG [16], into a nonlinear control design problem for the RSC with the objective to guarantee *asymptotic stability* of the equilibrium point $E_{k,i} = \overline{E}_{k,i}$.

b) **Power Output Reference Tracking**

The power output reference tracking is realized by regulating the power output of a WG such that it asymptotically matches a prespecified reference. Equivalently, by regulating the accumulated disturbance energy originating from the WG side to zero. The latter is formally stated as follows.

Claim 2. *WG i attains power output reference tracking and generates predictable power $P^*_{t,i}$ when $E_{g0,i} = 0$ is an asymptotically stable equilibrium of* (3.28).

Proof. At the equilibrium of $E_{g,i}$ it holds that $E_{g,i} = E_{g0,i}$ and $\dot{E}_{g,i} = 0$. Further, that the total power $P_{e,i}+P_{g,i}$ matches the power reference $P^*_{t,i}$, i.e $P_{e,i}+P_{g,i} = P^*_{t,i}$. ■

Intuitively, power output reference tracking is attained when all the disturbances that contribute to fluctuations of the WG's power output are counterbalanced. In our analysis, these are quantified through the energy that they carry. This quantification enables posing of the power output reference tracking problem as a control design problem for the GSC with objective to guarantee *asymptotic stability* of the equilibrium point $E_{g,i} = E_{g0,i}$. Practically, GSCs accomplish this objective by properly regulating their power outputs $P_{g,i}$ through the control input $V_{dg,i}$.

c) **Power Balancing on The Interfacing Capacitor**

The previous section focused on the GSC's control objective, which is power output regulation. The GSC can carry out this objective despite not being a generating source. In fact, the way the GSC carries out this objective is by drawing from the energy stored in the DC capacitor that interfaces RSC and GSC. However, an insignificant amount of energy is stored in this capacitor. On the other hand, we can use the energy stored in the supercapacitor to replenish the energy stored in the interfacing capacitor. By performing that, we indirectly supply the GSC with the required energy to attain its goal. Technically, we can achieve that by eliminating any power imbalance at the capacitor, i.e by maintaining the energy stored in the interfacing capacitor $E_{dc,i}$ at a specific equilibrium $E_{dc0,i}$. The combined actions of the DC-DC converter and the GSC facilitate energy/power flow from the storage through the GSC and into the grid [16]. Consider an equilibrium value for the $E_{dc,i}$ as:

$$E_{dc0,i} = \tfrac{1}{2} C_{dc,i} V_{dc0,i}^2$$

where $V_{dc0,i}$ is the equilibrium of the DC voltage that corresponds to this particular energy level. Formally, power balancing at the capacitor can be posed as the following control problem.

Claim 3. *At the interfacing capacitor, power balancing and regulation of the DC voltage $V_{dc,i}$ to $V_{dc0,i}$ are jointly guaranteed when $E_{dc,i}$ is tracking $E_{dc0,i}$, i.e when $E_{dc0,i}$ is an asymptotically stable equilibrium of* (3.32).

Proof. There two main arguments that need to be proved. The first is that, regulation of the $E_{dc,i}$ to $E_{dc0,i}$ results to power balancing on the capacitor. This is easy to see by noticing that, at the equilibrium, $E_{dc,i} = E_{dc0,i}$, which gives $\dot{E}_{dc,i} = 0$ and $P_{r,i}+P_{st,i}-P_{g,i} = 0$. Simply put, the capacitor's stored energy remains constant when the sum of powers at the capacitor (with the right sign convention) equals zero, i.e there is power balancing at the capacitor. The second argument is that asymptotic stability of $E_{dc0,i}$ implies asymptotic stability of $V_{dc0,i}$. To prove it, we first define the mapping $\mathcal{P} : V_{dc,i} \mapsto E_{dc,i}$ as $\mathcal{P}(V_{dc,i}) = \frac{1}{2} C_{dc,i} V_{dc,i}^2$, where $\mathcal{P}(V_{dc0,i}) = E_{dc0,i}$. Notice that, in a neighborhood around the equilibrium $V_{dc0,i}$, the inverse map $\mathcal{P}^{-1}(\cdot)$ exists, and both $\mathcal{P}(\cdot)$ and $\mathcal{P}^{-1}(\cdot)$ are continuously differentiable, i.e $\mathcal{P}$ is a diffeomorphism. By invoking *Theorem* 3.1, we deduce that, the equilibrium $V_{dc,i} = V_{dc0,i}$ is *asymptotically stable* if and only if the equilibrium point $E_{dc,i} = E_{dc0,i}$ is *asymptotically stable*. This establishes that $V_{dc,i}$ will converge toward its desired equilibrium $V_{dc0,i}$ when $E_{dc,i}$ converges toward its corresponding equilibrium $E_{dc0,i}$. ∎

To put it simply, Claim 3 guarantees that regulation of the capacitor's stored energy also leads to regulation of its DC voltage as well as power balancing.

In the forthcoming analysis, we review the necessary theoretical basis for designing our controllers.

3.5.4 Control Lyapunov Functions

Consider a nonlinear system:

$$\dot{x} = f(x, u), \;\; x \in \mathcal{D} \subseteq \mathbb{R}^n, \; u \in \mathcal{U} \subseteq \mathbb{R}^m \tag{3.40}$$

where x, u are the state vector and the control input vector respectively. Consider now the following definition.

Definition 3.1 ([36, 37, 38])**.** For the nonlinear dynamical system given by (3.40), a continuously differentiable positive-definite function $V : \mathcal{D} \to \mathbb{R}$ satisfying:

$$\inf_{u \in \mathcal{U}} \frac{\partial V}{\partial x} f(x, u) < 0, \;\; x \in \mathcal{D}, \;\; x \neq \mathbf{0}_n \tag{3.41}$$

is called a *Control Lyapunov Function* (CLF).

Simply put, a CLF is a positive-definite function whose derivative along the trajectories of the system can be rendered negative by an appropriate choice of the control input u i.e a Lyapunov function. Note that, if there exists a CLF for the system (3.40), then there also exists a feedback control law u which makes the equilibrium $x = \mathbf{0}_n$ of the closed-loop nonlinear system (3.40) asymptotically stable. Conversely, if there exists a control law u

that renders the equilibrium $x = \mathbf{0}_n$ asymptotically stable then, from standard converse Lyapunov theorems, there also exists a continuously differentiable positive-definite function $V : \mathcal{D} \mapsto \mathbb{R}$ satisfying (3.41) or, equivalently, there exists a CLF for the nonlinear system (3.40). Thus, a nonlinear system in the form (3.40) is feedback asymptotically stabilizable *if and only if* there exists a CLF satisfying (3.41). When $\mathcal{D} = \mathbb{R}^n$ and $u = \mathbb{R}^m$, $x = \mathbf{0}_n$ is globally asymptotically stable *if and only if* V is radially unbounded which is equivalent to $V(x) \to \infty$ as $\|x\| \to \infty$.

Moreover, for nonlinear input affine systems of the form:

$$\dot{x} = f(x)+g(x)u, \quad x \in \mathcal{D} \subseteq \mathbb{R}^n,\ u \in \mathcal{U} \subseteq \mathbb{R}^m \tag{3.42}$$

where $f : \mathbb{R}^n \mapsto \mathbb{R}$, $f(0) = 0$ and $g : \mathbb{R}^n \to \mathbb{R}^{n\times m}$ we have the following theorem.

Theorem 3.2 ([36, 37, 38])**.** *A continuously differentiable positive definite and radially unbounded function $V : \mathbb{R}^n \mapsto \mathbb{R}$ is a Control Lyapunov Function of (3.42) if and only if:*

$$\frac{\partial V}{\partial x} f(x) < 0, \quad x \in \mathcal{R} \tag{3.43}$$

where $\mathcal{R} \triangleq \{x \in \mathbb{R}^n,\ x \neq \mathbf{0}_n \mid \frac{\partial V}{\partial x} g(x) = 0\}$.

Therefore, the equilibrium $x = \mathbf{0}_n$ of a nonlinear system is globally feedback asymptotically stabilizable *if and only if* there exists a continuously differentiable positive definite and radially unbounded function $V : \mathbb{R}^n \mapsto \mathbb{R}$ satisfying (3.43).

3.5.5 Controller Design

We now devise several Control Lyapunov Functions (CLFs) to construct control laws for the RSC, GSC and storage (DC-DC converter) of a SoA WG. We present our results through a series of theorems which state the nonlinear stabilizing control laws which guarantee global asymptotic stability of the energy equilibria $\overline{E}_{k,i},\ E_{g0,i},\ E_{dc0,i}$.

a) **RSC Controller Design**

The control objective of the RSC controller is to guarantee global asymptotic stability of the kinetic energy equilibrium $\overline{E}_{k,i}$ given by (3.39). A particular RSC control law which can attain that is provided in the next theorem. Let the following assumption to be true.

Assumption 1. *During regulation of $E_{k,i}$ to $\overline{E}_{k,i}$, $\overline{E}_{k,i}$ is constant.*

Recall that $\overline{E}_{k,i}$ is a function of the wind speed. Thus, the above assumption simply states that the wind-speed is considered constant during the tracking process. This is a reasonable assumption since, as we will verify through our numerical simulations, the tracking dynamics evolve on a timescale of seconds while the fastest variations of the wind speed evolve on a timescale of minutes.

Theorem 3.3. *Under assumption 1, the equilibrium $(\overline{E}_{k,i},\ \overline{E}^{'}_{q,i})$ of the closed-loop form of the system described by (3.30), (3.1b) is globally asymptotically stable with the RSC control law:*

$$V_{dr,i} = \Big[-k_{2,i}(E^{'}_{q,i}-\overline{E}^{'}_{q,i})+\frac{\omega_{r,i}\omega_s V_{s,i}}{X^{'}_{s,i}}(E_{k,i}-\overline{E}_{k,i})+\dot{\overline{E}}^{'}_{q,i}-\frac{1}{T^{'}_{0,i}}(-(E^{'}_{q,i}+(X_{s,i}-X^{'}_{s,i})I_{ds,i})) \\ +(\omega_s-\omega_{r,i})E^{'}_{d,i}\Big]\frac{X_{r,i}}{X_{m,i}\omega_s},\quad \forall i\in\mathcal{G} \tag{3.44}$$

where $\overline{E}_{k,i}$ is given by (3.39) and $\overline{E}^{'}_{q,i}$ by:

$$\overline{E}^{'}_{q,i} = \Big(\frac{k_{1,i}(E_{k,i}-\overline{E}_{k,i})+\omega_s\omega_{r,i}T_{m,i}}{\omega_s\omega_{r,i}}\Big)\frac{X^{'}_{s,i}}{V_{s,i}} \tag{3.45}$$

and $\dot{\overline{E}}^{'}_{q,i}$ is the derivative of $\overline{E}^{'}_{q,i}$.

Proof. The direct way to prove this theorem is by first, form the closed-loop system with the control input in (3.44) and then, establish global asymptotic stability of its equilibrium $(\overline{E}_{k,i},\ \overline{E}^{'}_{q,i})$. Instead, here, we wish to provide more insight so we analytically design the controller that leads to asymptotic stability of $(\overline{E}_{k,i},\ \overline{E}^{'}_{q,i})$. To carry out this, we leverage a particular CLF.

Initially, consider a quadratic function $\mathcal{V}_{k,i} : \mathbb{R}_+ \mapsto \mathbb{R}_+$ with domain $\overline{\mathcal{D}}_{k,i} = \mathcal{D}_{k,i} \setminus \{\overline{E}_{k,i}\}$, $\mathcal{D}_{k,i} \subseteq \mathbb{R}$:

$$\mathcal{V}_{k,i} = \frac{1}{2}(E_{k,i} - \overline{E}_{k,i})^2, \ \ \mathcal{V}_{k,i} > 0, \ \ \forall E_{k,i} \in \overline{\mathcal{D}}_{k,i} \tag{3.46}$$

Now, a proper control input $V_{dr,i}$ will be the one which guarantees that:

$$\dot{\mathcal{V}}_{k,i} < 0, \ \ \forall E_{k,i} \in \overline{\mathcal{D}}_{k,i} \tag{3.47}$$

i.e that $\mathcal{V}_{k,i}$ is a CLF and an asymptotic stability certificate of $\overline{E}_{k,i}$ [37]. To construct such a proper controller, we perform time-differentiation of (3.46) while taking into account (3.2a). Since the actual control input $V_{dr,i}$ does not appear in this derivative, we employ the *backstepping method* [10] to derive its expression. The reason for resorting to this control method is the particular structure of the nonlinear system, i.e the nonlinear system lends itself to backstepping control design. Briefly, the basic idea behind backstepping is that, we can recursively construct controllers for cascade systems by first treating some state-variables as inputs; we call these virtual control inputs, and design stabilizing "*control laws*" for them. Then, we can design control laws for the actual inputs so that these virtual control inputs track their desired stabilizing "*control laws*". In our particular case, we treat $E^{'}_{q,i}$ as a virtual control input. By defining the desired form of the electrical torque as:

$$\overline{T}_{e,i} = \frac{k_{1,i}(E_{k,i} - \overline{E}_{k,i}) + \omega_s \omega_{r,i} T_{m,i}}{\omega_s \omega_{r,i}} \tag{3.48}$$

and consider the relation:

$$T_{e,i} = \frac{P_{e,i}}{\omega_0} = \frac{(V_{s,i} E^{'}_{q,i})}{X^{'}_{s,i}} \tag{3.49}$$

where $\omega_0 = 1$ is the per unit synchronous speed and $P_{e,i}$ is stator's electrical power output, we come up with the following virtual "control law":

$$\overline{E}'_{q,i} = (\frac{k_{1,i}(E_{k,i}-\overline{E}_{k,i})+\omega_s\omega_{r,i}T_{m,i}}{\omega_s\omega_{r,i}})\frac{X'_{s,i}}{V_{s,i}} \tag{3.50}$$

This is a stabilizing virtual control law since it leads to:

$$\dot{\mathcal{V}}_{k,i} = -k_{1,i}(E_{k,i}-\overline{E}_{k,i})^2 \ < \ 0, \quad E_{k,i} \in \overline{\mathcal{D}}_{k,i} \tag{3.51}$$

The last task is to ensure that $E'_{q,i}$ is tracking $\overline{E}'_{q,i}$ asymptotically. To this end, we augment $\mathcal{V}_{k,i}$ with the new variable $\xi_i = (E'_{q,i}-\overline{E}'_{q,i})$ to obtain the candidate CLF $\mathcal{V}_{\xi,i} : \mathbb{R}_+ \times \mathbb{R} \mapsto \mathbb{R}_+$ as:

$$\mathcal{V}_{\xi,i} = \frac{1}{2}(E_{k,i}-\overline{E}_{k,i})^2+\frac{1}{2}\xi_i^2, \quad \mathcal{V}_{\xi,i} > 0, \quad \forall(E_{k,i},\ \xi_i) \in \overline{\mathcal{D}}_{k,i}\times\overline{\mathcal{D}}_{\xi,i} \tag{3.52}$$

where $\overline{\mathcal{D}}_{\xi,i} = \mathcal{D}_{\xi,i}\backslash\{0\}, \quad \mathcal{D}_{\xi,i} \subseteq \mathbb{R}$. Before proceeding to the RSC control design, we state the following Lemma.

Lemma 3.1. *The function $\mathcal{V}_{\xi,i}$ is a CLF for the system* (3.30), (3.1b)*.*

Proof. Time differentiation of $\mathcal{V}_{\xi,i}$ with respect to time yields:

$$\dot{\mathcal{V}}_{\xi,i} = (E_{k,i}-\overline{E}_{k,i})(\dot{E}_{k,i}-\dot{\overline{E}}_{k,i})+\xi_i\dot{\xi}_i$$

Using (3.30), (3.1b) this equation can be further expanded to:

$$\begin{aligned}\dot{\mathcal{V}}_{\xi,i} &= (E_{k,i}-\overline{E}_{k,i})(\omega_s\omega_{r,i}(T_{m,i}-T_{e,i})) \\ &+\xi_i\Big(\frac{1}{T'_{0,i}}[-E'_{q,i}-(X_{s,i}-X'_{s,i})(I_{ds,i})+T'_{0,i}(\omega_s\frac{X_{m,i}}{X_{r,i}}V_{dr,i}-(\omega_s-\omega_{r,i})E'_{d,i})]-\dot{\overline{E}}_{q,i}\Big)\end{aligned} \tag{3.53}$$

Taking the $\mathbf{inf}(\cdot)$ of (3.53) finally yields:

$$\mathbf{inf}\ \dot{\mathcal{V}}_{\xi,i} = \begin{cases} -k_{1,i}(E_{k,i} - \overline{E}_{k,i})^2, & \xi_i = 0 \\ -\infty, & \xi_i \neq 0 \end{cases} \tag{3.54}$$

By invoking Theorem 3.2, we establish that $\mathcal{V}_{\xi,i}$ is a CLF for the system (3.30), (3.1b) and the equilibrium point $(\overline{E}_{k,i},\ \overline{E}'_{q,i})$ is feedback asymptotically stabilizable. ■

Next, we proceed to contruct a control law $V_{dr,i}$ that leads to:

$$\dot{\mathcal{V}}_{\xi,i} < 0, \ \ \forall (E_{k,i},\ \xi_i) \in \overline{\mathcal{D}}_{k,i} \times \overline{\mathcal{D}}_{\xi,i} \tag{3.55}$$

Substituting equations (3.49), (3.50) into (3.53), and imposing the equation:

$$\left(\frac{-\omega_s \omega_{r,i} V_{s,i}(E_{k,i} - \overline{E}_{k,i})}{X'_{s,i}} + \dot{\xi}_i\right) = -k_{2,i}\xi_i \tag{3.56}$$

yields:

$$\dot{\mathcal{V}}_{\xi,i} = -k_{1,i}(E_{k,i} - \overline{E}_{k,i})^2 - k_{2,i}\xi_i^2 < 0, \quad \forall (E_{k,i},\ \xi_i) \in \overline{\mathcal{D}}_{k,i} \times \overline{\mathcal{D}}_{\xi,i} \tag{3.57}$$

The full expression for $\dot{\xi}_i$ can be obtained from (3.1b) and the derivative of (3.50) as:

$$\dot{\xi}_i = (\dot{E}'_{q,i} - \dot{\overline{E}}'_{q,i}) \tag{3.58}$$

where:

$$\dot{\overline{E}}'_{q,i} = \left(\frac{k_{1,i}\omega_s^2 \omega_{r,i}^2 (T_{m,i} - T_{e,i}) - k_{1,i}(E_{k,i} - \overline{E}_{k,i})\omega_s}{\omega_s^2 \omega_{r,i}^2}\right) \frac{X'_{s,i}}{V_{s,i}} + \dot{T}_{m,i} \frac{X'_{s,i}}{V_{s,i}} \tag{3.59}$$

and $\dot{T}_{m,i}$ given by:

$$\dot{T}_{m,i} = \frac{\partial T_{m,i}}{\partial C_{p,i}} \frac{\partial C_{p,i}}{\partial \lambda_i} \frac{\partial \lambda_i}{\partial \omega_{r,i}} \dot{\omega}_{r,i} + \frac{\partial T_{m,i}}{\partial \omega_{r,i}} \dot{\omega}_{r,i} \tag{3.60}$$

The additional terms involved in the above equation are analytically expressed as:

$$\frac{\partial T_{m,i}}{\partial C_{p,i}} = \frac{\rho \pi R_i^2 \omega_s v_{w,i}^3}{2 S_{b,i} \omega_{r,i}} \tag{3.61}$$

$$\frac{\partial C_{p,i}}{\partial \lambda_i} = 0.22 \Big[116 (\frac{-1}{\lambda_i^2}) \Big] \cdot \mathrm{e}^{\left(-12.5(\frac{1}{\lambda_i} - 0.035)\right)} \tag{3.62}$$

$$+0.22 \Big[116 (\frac{1}{\lambda_i} - 0.035) \Big] \cdot \mathrm{e}^{\left(-12.5(\frac{1}{\lambda_i} - 0.035)\right)} \frac{12.5}{\lambda_i^2} \tag{3.63}$$

$$\frac{\partial \lambda_i}{\partial \omega_{r,i}} = \frac{2 k_i R_i}{p_i v_{w,i}} \tag{3.64}$$

$$\frac{\partial T_{m,i}}{\partial \omega_{r,i}} = \frac{1}{2} \frac{\rho \pi R_i^2 \omega_s}{S_{b,i}} C_{p,i} v_{w,i}^3 \Big(\frac{-1}{\omega_{r,i}^2} \Big) \tag{3.65}$$

Lastly, by combining equations (3.56) and (3.1b) we derive the control input for the RSC as:

$$\begin{aligned} V_{dr,i} = {} & [-k_{2,i} \xi_i + \frac{\omega_{r,i} \omega_s V_{s,i}}{X'_{s,i}} (E_{k,i} - \overline{E}_{k,i}) + \dot{\overline{E}}'_{q,i} - \frac{1}{T'_{0,i}} (-(E'_{q,i} + (X_{s,i} - X'_{s,i}) I_{ds,i})) \\ & + (\omega_s - \omega_{r,i}) E'_{d,i}] \frac{X_{r,i}}{X_{m,i} \omega_s}, \qquad \forall i \in \mathcal{G} \end{aligned} \tag{3.66}$$

which is the one in (3.44). This control law establishes *global asymptotic stability* of $(\overline{E}_{k,i}, \overline{E}'_{q,i})$ as follows from equations (3.52), (3.57) and the fact that $\mathcal{V}_{\xi,i}$ is radially unbounded. To be precise, *global exponential stability* since $\dot{\mathcal{V}}_{\xi,i} \leq -\underline{k}_{12,i} \mathcal{V}_{\xi,i}$, where $\underline{k}_{12,i} = 2 \min\{k_{1,i}, k_{2,i}\}$. In addition, exploiting Claim 1, we conclude that the control law in (3.66) guarantees MPPT. To practically realize the controller in (3.66), the local variables $T_{m,i},\ T_{e,i},\ \omega_{r,i},\ E'_{d,i},\ E'_{q,i},\ V_{s,i},\ I_{ds,i}$ need to be available through measurements as depicted in Fig. 3.3. ■

b) **GSC Controller Design**

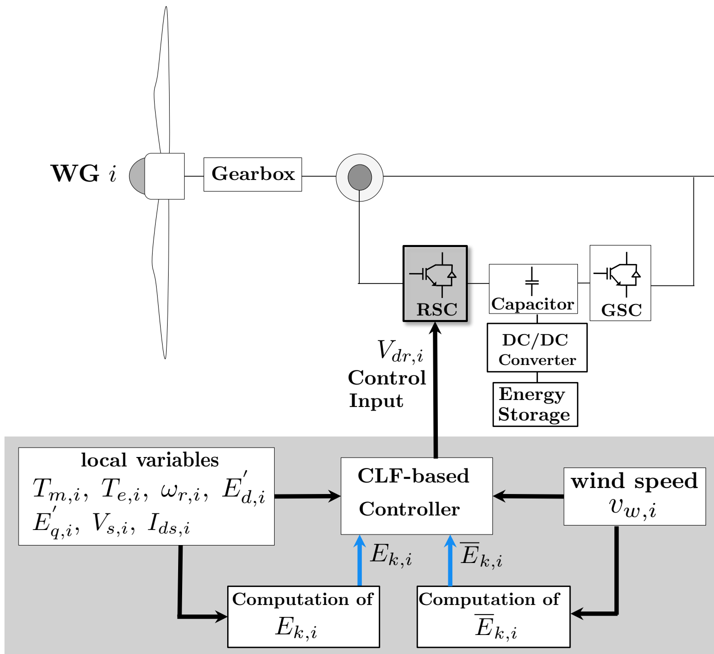

Figure 3.3: CLF-based RSC controller

The control objective of the GSC is to attain global asymptotic stability (GAS) of the equilibrium $E_{g0,i} = 0$. A particular GSC control law which can do that is presented in the next theorem.

Theorem 3.4. *The equilibrium $(E_{g0,i},\ I^*_{dg,i})$ of the closed-loop form of the system (3.28), (3.5) is globally asymptotically stable with the GSC control law:*

$$V_{dg,i} = (-(E_{g,i}-E_{g0,i})V_{s,i}-k_{4,i}(I_{dg,i}-I^*_{dg,i})+\dot{I}^*_{dg,i}-(-\omega_s\frac{R_{g,i}}{L_{g,i}}I_{dg,i}+\omega_s I_{qg,i}))\frac{L_{g,i}}{\omega_s}+V_{s,i},\quad \forall i \in \mathcal{G} \tag{3.67}$$

where $I^*_{dg,i}$ is given by:

$$I^*_{dg,i} = \Big(\frac{-P_{e,i}+P^*_{t,i}-k_{3,i}(E_{g,i}-E_{g0,i})}{V_{s,i}}\Big) \tag{3.68}$$

and $\dot{I}^*_{dg,i}$ by the derivative of $I^*_{dg,i}$.

Proof. We follow the same steps as in the RSC control design, introducing first the candidate CLF $\mathcal{V}_{g,i} : \mathbb{R} \mapsto \mathbb{R}$ as:

$$\mathcal{V}_{g,i} = \frac{1}{2}(E_{g,i}-E_{g0,i})^2, \;\; \mathcal{V}_{g,i} > 0, \;\; \forall E_{g,i} \in \overline{\mathcal{D}}_{g,i} \tag{3.69}$$

where $\overline{\mathcal{D}}_{g,i} = \mathcal{D}_{g,i} \backslash \{E_{g0,i}\}, \; \mathcal{D}_{g,i} \subseteq \mathbb{R}$. Now, the GSC controller has to guarantee that:

$$\dot{\mathcal{V}}_{g,i} < 0, \;\; \forall E_{g,i} \in \overline{\mathcal{D}}_{g,i} \tag{3.70}$$

in order for the equilibrium $E_{g0,i}$ to be GAS. Subsequently, we perform time differentiation of (3.69) and notice that, $V_{dg,i}$ does not appear in the resulted expression. To proceed, we treat $I_{dg,i}$ as a virtual control input and construct its control law $I^*_{dg,i}$ by taking into account (3.28) as:

$$I^*_{dg,i} = \Big(\frac{-P_{e,i}+P^*_{t,i}-k_{3,i}(E_{g,i}-E_{g0,i})}{V_{s,i}}\Big) \tag{3.71}$$

This virtual control law leads to:

$$\dot{\mathcal{V}}_{g,i} = -k_{3,i}(E_{g,i}-E_{g0,i})^2 < \; 0, \;\; \forall E_{g,i} \in \overline{\mathcal{D}}_{g,i}$$

Again, the structure of the above dynamics guide us to employ the *backstepping control method*. In particular, it is left to compute a control law for the actual input $V_{dg,i}$ which will ensure that $I_{dg,i}$ is asymptotically tracking $I^*_{dg,i}$. To do that, we augment $\mathcal{V}_{g,i}$ with the variable $z_i = (I_{dg,i}-I^*_{dg,i})$ to obtain the candidate CLF $\mathcal{V}_{z,i} : \mathbb{R}\times\mathbb{R} \mapsto \mathbb{R}$:

$$\mathcal{V}_{z,i} = \frac{1}{2}(E_{g,i}-E_{g0,i})^2+\frac{1}{2}z_i^2, \;\; \mathcal{V}_{z,i} > 0, \;\; \forall (E_{g,i}, \; z_i) \in \overline{\mathcal{D}}_{g,i}\times\overline{\mathcal{D}}_{z,i} \tag{3.72}$$

where $\overline{\mathcal{D}}_{z,i} = \mathcal{D}_{z,i} \backslash \{0\}, \; \mathcal{D}_{z,i} \subseteq \mathbb{R}$. The following Lemma can be stated for the CLF in (3.72).

Lemma 3.2. *The function $\mathcal{V}_{z,i}$ is a CLF for the system* (3.28), (3.5).

Proof. The proof of this lemma is direct. Time-differentiating (3.72) yields:

$$\dot{\mathcal{V}}_{z,i} = (E_{g,i}-E_{g0,i})(\dot{E}_{g,i}-\dot{E}_{g0,i})+z_i\dot{z}_i$$

which, can be further expanded using the expressions (3.28), (4.1) as:

$$\dot{\mathcal{V}}_{z,i} = (E_{g,i}-E_{g0,i})(P_{e,i}+P_{g,i}-P^*_{t,i})+z_i\Big(-(\omega_s\frac{R_{g,i}}{L_{g,i}})I_{dg,i}+\omega_s I_{qg,i}+\omega_s(\frac{V_{dg,i}-V_{s,i}}{L_{g,i}})-\dot{I}^*_{dg,i}\Big) \quad (3.73)$$

Taking the $\mathbf{inf}(\cdot)$ of (3.73) yields:

$$\mathbf{inf}\ \dot{\mathcal{V}}_{z,i} = \begin{cases} -k_{3,i}(E_{g,i}-E_{g0,i})^2, & z_i = 0 \\ -\infty, & z_i \neq 0 \end{cases} \quad (3.74)$$

Finally, by exploiting Theorem 3.2 it can be concluded that $\mathcal{V}_{z,i}$ is a CLF for the system (3.28), (3.5) and that the equilibrium point $(E_{g0,i}, I^*_{dg,i})$ is feedback asymptotically stabilizable. ■

An appropriate control law $V_{dg,i}$ will be one which guarantees:

$$\dot{\mathcal{V}}_{z,i} < 0,\ \ \forall(E_{g,i},\ z_i) \in \overline{\mathcal{D}}_{g,i}\times\overline{\mathcal{D}}_{z,i} \quad (3.75)$$

One such controller can be designed by imposing the equation:

$$V_{s,i}(E_{g,i}-E_{g0,i})+\dot{z}_i = -k_{4,i}z_i \quad (3.76)$$

such that it holds:

$$\dot{\mathcal{V}}_{z,i} = -k_{3,i}(E_{g,i}-E_{g0,i})^2-k_{4,i}z_i^2 < 0, \quad \forall(E_{g,i},\ z_i) \in \overline{\mathcal{D}}_{g,i}\times\overline{\mathcal{D}}_{z,i} \tag{3.77}$$

We can obtain the expression of the term $\dot{z}_i$, involved in (3.76), from equations (3.5) and (3.68) and by taking into account equations (3.28), (3.49) and (3.1b). Eventually, this term is obtained as:

$$\dot{z}_i = (\dot{I}_{dg,i}-\dot{I}^*_{dg,i}) \tag{3.78}$$

where

$$\begin{aligned}
\dot{I}^*_{dg,i} &= \Big(-\frac{\dot{E}'_{q,i}V_{s,i}}{X'_{s,i}}-k_{3,i}\dot{E}_{g,i}\Big)\frac{1}{V_{s,i}} \\
&= \Big(-\frac{1}{T'_{0,i}}[-E'_{q,i}-(X_{s,i}-X'_{s,i})(I_{ds,i})+T'_{0,i}(\omega_s\frac{X_{m,i}}{X_{r,i}}V_{dr,i}-(\omega_s-\omega_{r,i})E'_{d,i})]\frac{V_{s,i}}{X'_{s,i}} \\
&-k_{3,i}(\frac{E'_{q,i}V_{s,i}}{X'_{s,i}}+I_{dg,i}V_{s,i}-P^*_{t,i})\Big)\frac{1}{V_{s,i}}
\end{aligned} \tag{3.79}$$

We obtain the GSC control law by combining equations (3.76) and (3.5) as:

$$V_{dg,i} = (-(E_{g,i}-E_{g0,i})V_{s,i}-k_{4,i}(I_{dg,i}-I^*_{dg,i})+\dot{I}^*_{dg,i}-(-\omega_s\frac{R_{g,i}}{L_{g,i}}I_{dg,i}+\omega_s I_{qg,i}))\frac{L_{g,i}}{\omega_s}+V_{s,i}, \quad \forall i \in \mathcal{G} \tag{3.80}$$

which is the one in (4.87). This control law establishes *global asymptotic stability* of $(E_{g0,i}, I^*_{dg,i})$ or more precisely, *global exponential stability* since $\dot{\mathcal{V}}_{z,i} \leq -\underline{k}_{34,i}\mathcal{V}_{z,i}$, where $\underline{k}_{34,i} = 2\min\{k_{3,i}, k_{4,i}\}$. This follows from (3.72), (3.77) and the fact that $\mathcal{V}_{z,i}$ is radially unbounded. Moreover, Claim 2 enables us to conclude that the control law (3.80) guarantees power output reference tracking (predictable WG power output) or, i.e that zero accumulated disturbance

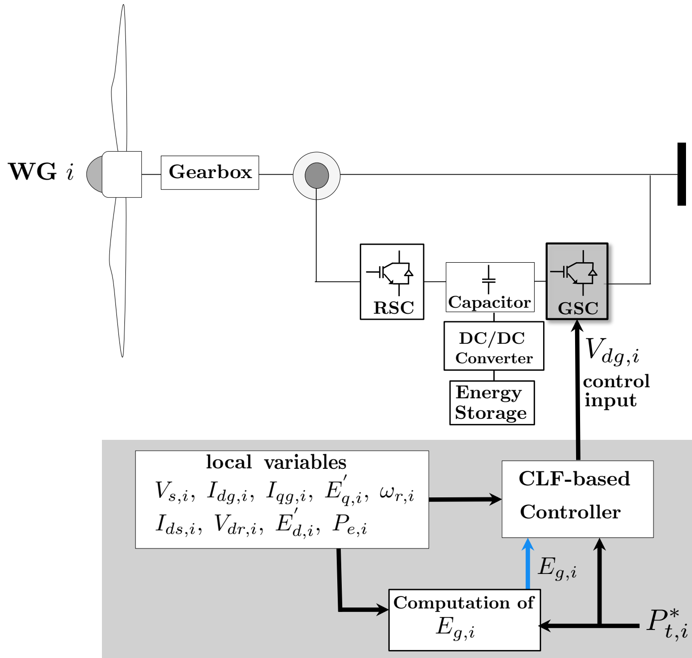

Figure 3.4: CLF-based GSC controller

energy is flowing from the WG side to the grid. On the practical side, this GSC controller can be implemented when the local variables $V_{s,i},\ I_{dg,i},\ I_{qg,i},\ E'_{q,i}, \omega_{r,i},\ I_{ds,i},\ V_{dr,i},\ E'_{d,i},\ P_{e,i}$ are available as depicted in Fig. 3.4. ■

c) **Storage Controller Design**

The aim of the controller for the DC-DC converter is to enable the storage to supply real power required to the GSC so that the latter effectively attains power reference tracking. As already explained, practically, the DC-DC converter can accomplish that when it can balance out any power mismatch in the interfacing capacitor or equivalently when it can cause the equilibrium of the stored energy $E_{dc0,i}$ to be globally asymptotically stable (GAS). A particular control law of this type is presented in the next theorem.

Theorem 3.5. *The equilibrium $E_{dc0,i}$ of the closed-loop form of the system (3.32) is globally* *asymptotically stable with the DC-DC converter control law:*

$$u_{sc,i} = (P_{g,i} - P_{r,i} - k_{5,i}(E_{dc,i} - E_{dc0,i}))\frac{R_{sc,i}}{V_{sc,i}} - V_{sc,i}, \qquad \forall i \in \mathcal{G} \tag{3.81}$$

Proof. To design the controller in (3.81), we start from a candidate CLF $\mathcal{V}_{dc,i} : \mathbb{R} \to \mathbb{R}$:

$$\mathcal{V}_{dc,i} = \frac{1}{2}(E_{dc,i} - E_{dc0,i})^2, \;\; \mathcal{V}_{dc,i} > 0, \;\; \forall E_{dc,i} \in \overline{\mathcal{D}}_{c,i} \tag{3.82}$$

where $\overline{\mathcal{D}}_{c,i} = \mathcal{D}_{c,i} \backslash \{E_{dc0,i}\}, \; \mathcal{D}_{c,i} \subseteq \mathbb{R}$ and state the following lemma.

Lemma 3.3. *The function $\mathcal{V}_{dc,i}$ is a CLF for the system (3.32).*

Proof. To prove this lemma, we compute the derivative of (3.82) with respect to time as:

$$\dot{\mathcal{V}}_{dc,i} = (E_{dc,i} - E_{dc0,i})(\dot{E}_{dc,i} - \dot{E}_{dc0,i})$$

By substituting equations (3.32) and (3.10) we further expand it as:

$$\dot{\mathcal{V}}_{dc,i} = (E_{dc,i} - E_{dc0,i})(P_{r,i} + V_{sc,i}(\frac{u_{sc,i} - V_{sc,i}}{R_{sc,i}}) - P_{g,i}) \tag{3.83}$$

The $\mathbf{inf}(\cdot)$ of (3.83) yields:

$$\mathbf{inf} \;\; \dot{\mathcal{V}}_{dc,i} = -\infty, \;\; E_{dc,i} \neq E_{dc0,i} \tag{3.84}$$

By applying Theorem 3.2, it can be concluded that $\mathcal{V}_{dc,i}$ is a CLF for the system (3.32) and that $E_{dc0,i}$ is feedback asymptotically stabilizable. ■

A control input $u_{sc,i}$ will lead to asymptotic stability of $E_{dc0,i}$ when the inequality:

$$\dot{\mathcal{V}}_{dc,i} < 0, \;\; \forall E_{dc,i} \in \overline{\mathcal{D}}_{c,i} \tag{3.85}$$

holds along the trajectories of the closed-loop system. One way to realize that, is by designing the controller so that an equation of the form:

$$P_{r,i}+P_{st,i}-P_{g,i} = -k_{5,i}(E_{dc,i}-E_{dc0,i}) \tag{3.86}$$

holds. That being the case, $\dot{\mathcal{V}}_{dc,i}$ becomes:

$$\dot{\mathcal{V}}_{dc,i} = -k_{5,i}(E_{dc,i}-E_{dc0,i})^2, \;\; \dot{\mathcal{V}}_{dc,i} < 0, \; \forall E_{dc,i} \in \overline{\mathcal{D}}_{c,i} \tag{3.87}$$

Finally, by combining (3.10) with (3.86) we arrive at the storage control law:

$$u_{sc,i} = (P_{g,i}-P_{r,i}-k_{5,i}(E_{dc,i}-E_{dc0,i}))\frac{R_{sc,i}}{V_{sc,i}}-V_{sc,i} \quad \forall i \in \mathcal{G} \tag{3.88}$$

which is the one given in (3.81). This control law results to global asymptotic stability of $E_{dc0,i}$ as follows from (3.82), (3.87) and the fact that $\mathcal{V}_{dc,i}$ is radially unbounded. In exact terms, global exponential stability since $\dot{\mathcal{V}}_{dc,i} = -2k_{5,i}\mathcal{V}_{dc,i}$. Combining that with Claim 3, we conclude that the storage control law given by (3.81) attains power balancing on the interfacing capacitor. ■

Implementation of this controller requires that the local variables $V_{dr,i}$, $E'_{q,i}$, $V_{qr,i}$, $V_{s,i}$, $E'_{d,i}$ $I_{dg,i}$, $V_{dc,i}$, $V_{sc,i}$ are available feedback signals as shown in Fig. 3.5.

3.6 Case Studies

The performance of the proposed controllers is demonstrated via numerical simulations on the 3-bus power system depicted in Fig. 3.6. At bus 3 of this system, a DFIG with integrated storage is placed as depicted in Fig. 3.1. Its RSC, GSC and DC-DC converters are controlled according to the control laws (3.66), (3.80) and (3.88), respectively. The simulations are conducted under the following scenarios.

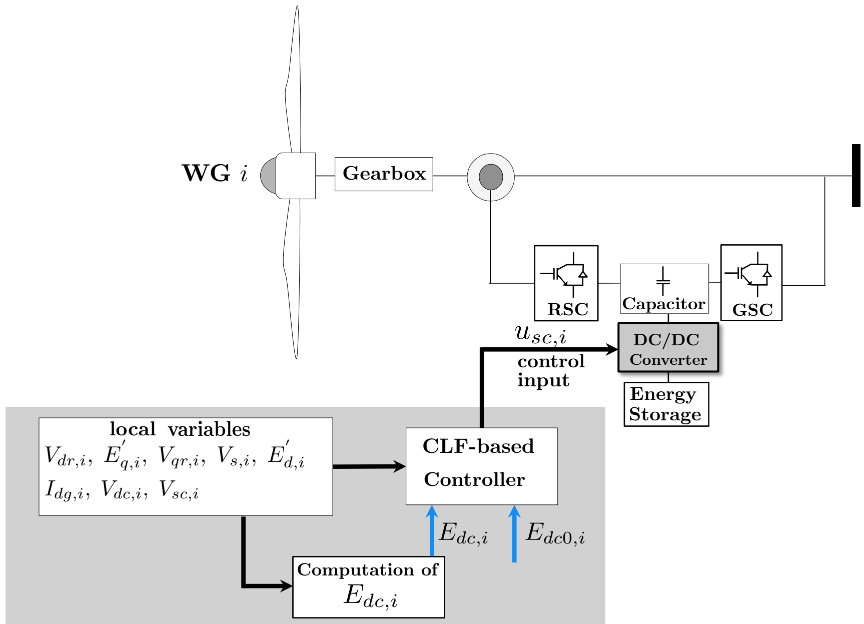

Figure 3.5: CLF-based DC-DC Converter Controller

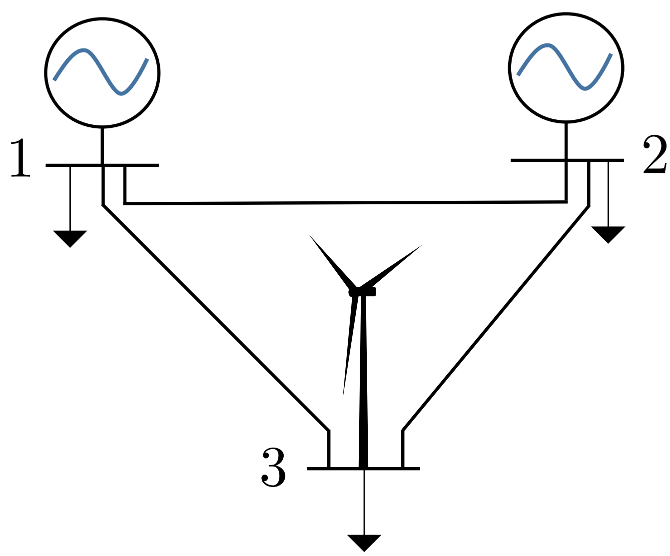

Figure 3.6: Test system

- **Scenario 1**: In the time interval $t = 0{-}25s$, step-wise variations in the average wind speed take place, as shown in Fig. 3.7a.
- **Scenario 2**: In the time interval $t = 0{-}20s$, the mean wind speed is constant and only the fast wind speed variations are present (turbulence), as shown in Fig. 3.8a.
- **Scenario 3**: In the time interval $t = 0{-}15s$, the power reference for the WG changes in a step-wise manner as shown in Fig. 3.10a.

Below, the dynamic response of the WG under these scenarios is presented and analyzed.

3.6.1 Performance Evaluation

Under *Scenario 1*, the response of the WG's rotor speed is depicted in Fig. 3.7b. It can be observed that this response is very much alike and in complete synchrony with the response of the wind speed since the rotor speed reference is proportional to the wind speed. Therefore, the proposed controller enables the rotor speed to track the desired quasistatic equilibrium rapidly and precisely, ensuring that the WG is operating under a MPPT strategy during these mean wind speed variations. Technically, the controller carries out its objective, i.e regulating the WG's rotor speed to its equilibrium, by regulating the kinetic energy of the WG to a corresponding equilibrium.

Under *Scenario 2*, observe that although the wind speed variations are rapid (turbulence) (Fig. 3.8a), the power output of the WG remains constant. This is achieved by the controllers of the GSC and DC-DC converter through power reference tracking (Fig. 3.8b). In particular, the GSC adjusts the power output P_g to counterbalance wind intermittency as depicted in Fig. 3.9 (green) while, the DC-DC converter continuously regulates the storage power output P_{st} to meet the power demand of the GSC, as shown in Fig. 3.9 (blue). With the RSC power P_r not significantly varying, the power outputs P_{st} and P_g manifest almost identical responses as shown in Fig. 3.9. This verifies the effectiveness of the proposed control design logic.

Scenario 3 is characterized by rapid step variations of the WG's power reference, as seen in Fig. 3.10a. The objective for the WG's controllers is power output tracking of this varying reference using power from the storage device. Focusing on Fig. 3.10b, we observe that the power output of the WG is closely tracking the reference with good dynamic performance, e.g no oscillations, no overshoot. The GSC and DC-DC converters jointly accomplished that via the following mechanism. The GSC continuously adjusts its power output, as shown in Fig. 3.11 (green), in order to regulate the total power output of the WG to the desired reference. Concurrently, the DC-DC converter rapidly adjusts its power output, as shown in Fig. 3.11 (blue), to meet the GSC's power demand. These actions can be realized by observing that P_{st} and P_g manifest identical (neglecting the sign convention) dynamical responses.

In summary, the proposed controllers effectively reached their objectives, MPPT and power output reference tracking for a wide-range of operating conditions and under all the studied scenarios.

3.7 Conclusion

In this chapter, we analytically designed nonlinear energy-based control laws for the RSC, GSC and DC-DC converter of a DFIG with an integrated storage. The proposed controllers can be leveraged by a WG to attain MPPT during low wind speed conditions and power reference tracking using stored energy. Further, since they are nonlinear and derived based on Control Lyapunov Functions (CLFs), their performance is guaranteed for a wide range of operating conditions. Their performance is evaluated via numerical simulations under critical scenarios on a proof-of-concept 3-bus system.

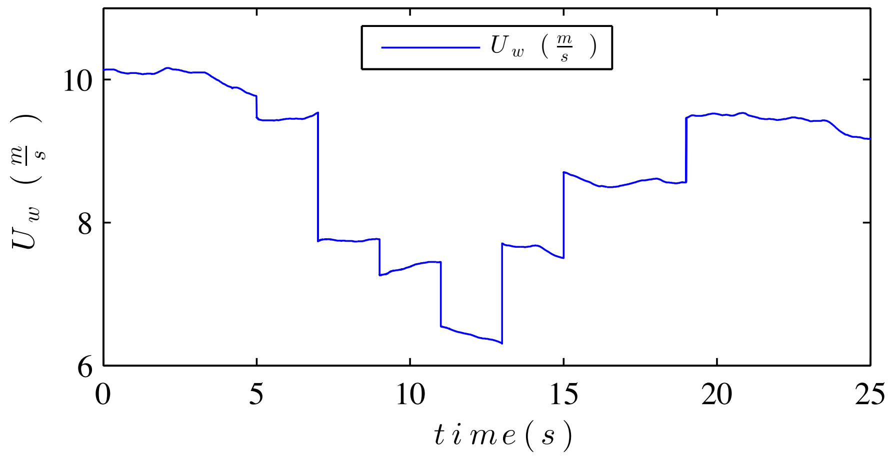

(a)

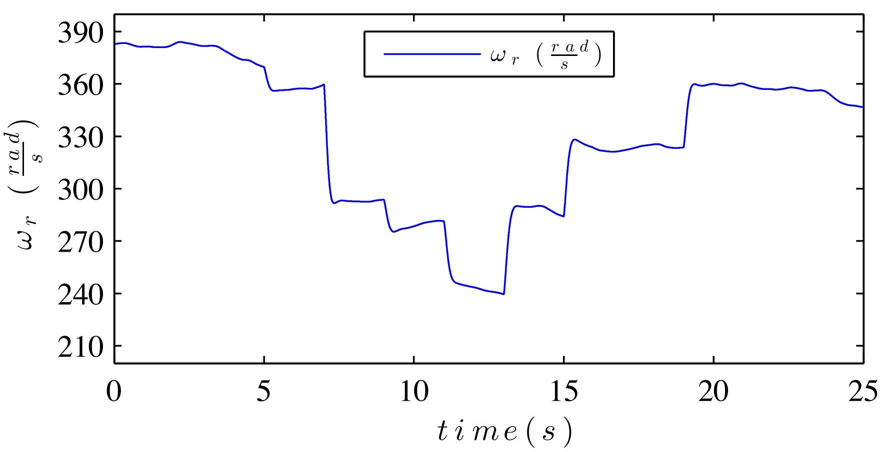

(b)

Figure 3.7: *Scenario 1* (a): Wind speed (v_w) scenario (b): Rotor speed (ω_r) with proposed controller

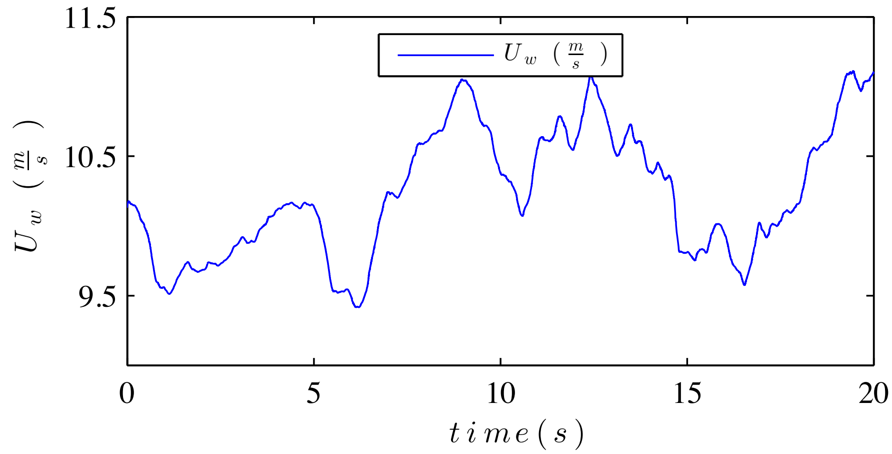

(a)

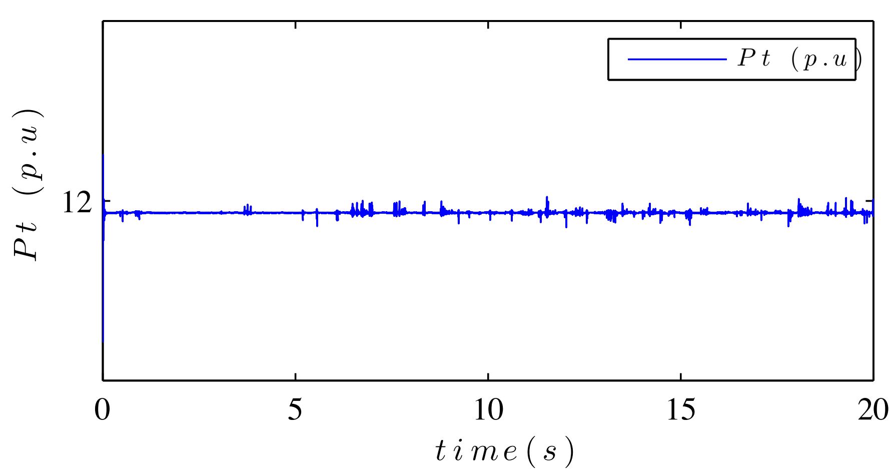

(b)

Figure 3.8: *Scenario 2* (a): Wind speed (v_w) scenario where $v_m = v_{m,nom}$ (b): Total power output (P_t) of WG

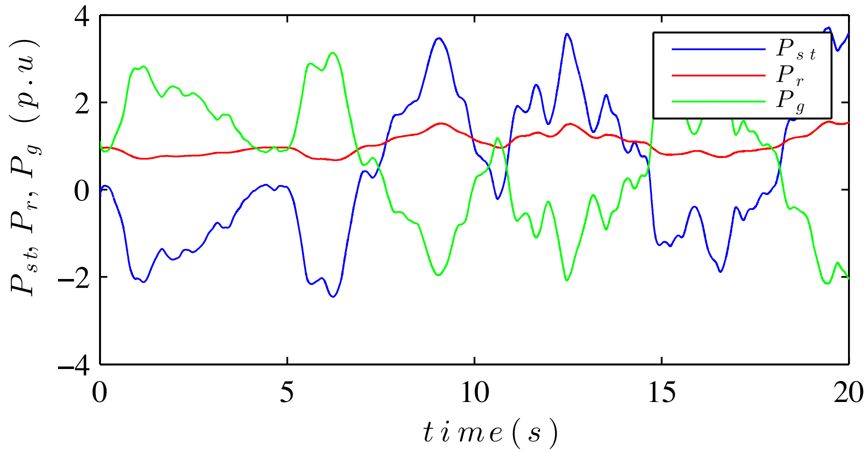

Figure 3.9: *Scenario 2* : Storage device's power output (P_{st}), GSC's power output (P_g) and RSC's power output (P_r)

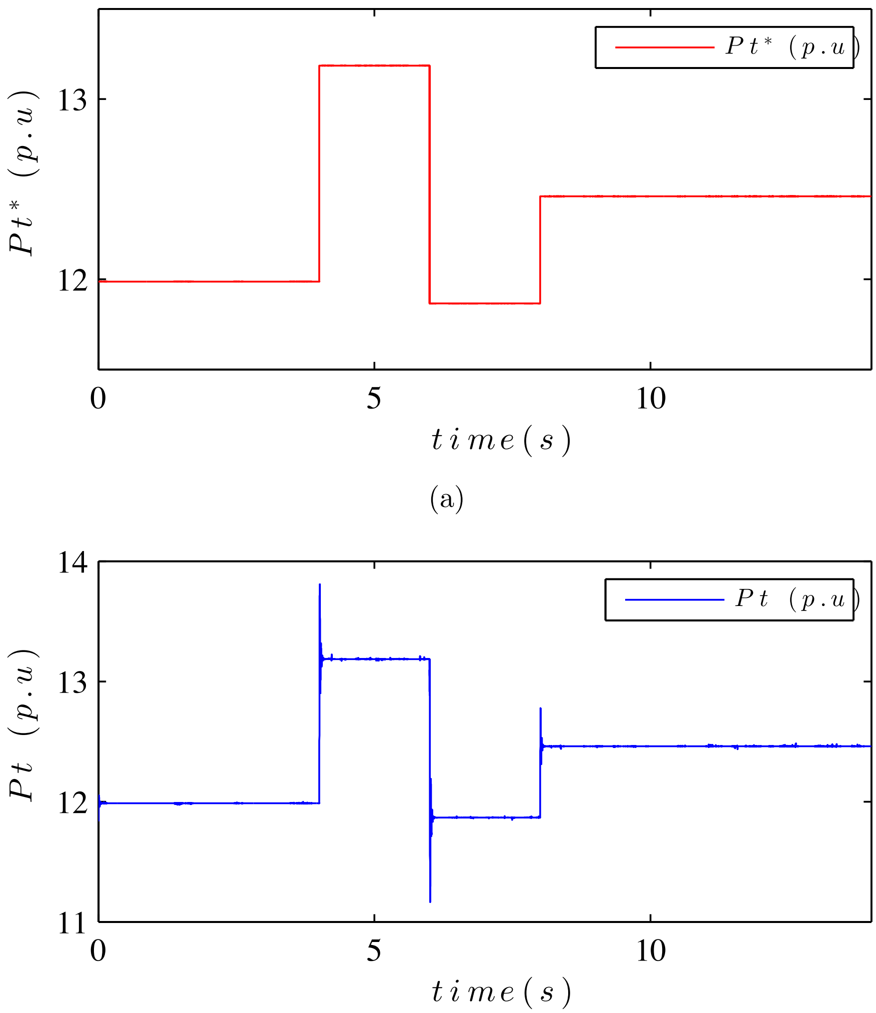

(a)

(b)

Figure 3.10: *Scenario 3* (a): Step-wise variations of reference P_t^* (b): Power output response (P_t)

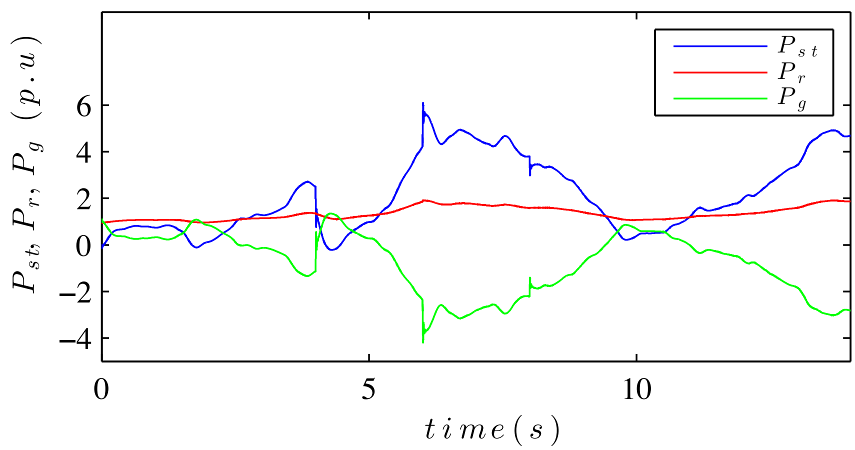

Figure 3.11: *Scenario 3* : Power output of the energy storage (P_{st}), the GSC (P_g) and the RSC (P_r)

Chapter 4

Distributed Control of Wind Generators with Integrated Storage

4.1 Introduction

As already discussed, several studies elaborate on a worldwide tendency for integrating large amounts of wind power into power systems today, with these integration levels challenging power systems' stability, reliability and robustness [2]. At the same time, the current regulations for the operation of WGs impose that WGs progressively provide multiple ancillary services to the grid through proper design of their controllers [2]. Some of these are frequency regulation, inertial response, power output smoothing, Low Voltage Ride-Through (LVRT) and voltage control [2]. Albeit all of these services contribute to the secure operation of power systems, the most crucial is indisputably power output regulation.

In the previous Chapter, we introduced the gold standard on WG technology which is considered to be the wind DFIG with an integrated energy storage. Further, we elaborated on how, a WG of this type can provide predictable power output (at the component level[1]) by harnessing the stored energy through a decentralized CLF energy-based control scheme.

[1] component refers to a single WG

Notice that, a group of WGs of this type that adopt this proposed control method can ultimately provide power output reference tracking at the WF level. WGs can accomplish this particular objective more efficiently and effectively by employing other methods that enable them to coordinate their actions. The reason for which decentralized control approaches might not be the most efficient ones for WF power output regulation is the following. Aggregating the power outputs of several WGs naturally reduces the temporal volatility that is present on their individual power outputs so that, at the WF level, the variability on the total wind power output becomes comparably much less than at the WG level [39]. Consequently, the amount of total storage power that will be required to achieve WF total power reference tracking by employing decentralized power output regulation of WGs will be the highest one. On the other hand, a more efficient solution and, in general, one that will lead to less amount of total storage power, will be the WGs to employ distributed control methods which leverage coordination to attain WF power output reference tracking. In this case, it is not necessary for the individual power outputs of the WGs to match particular references.

Realizing WF power output regulation presumes knowledge of the following information: the total power output, which can be measured locally, and the desired power reference, which can be obtained by the system operator (SO). In particular, WGs with integrated storage devices can reach this global objective by leveraging this information in the coordination and control of their storage devices through limited communication. To achieve that, they have to solve the following problem: given the total power and power reference, to compute appropriate individual power set-points for their storage devices under dynamical conditions and regulate their storage power outputs to these using coordination that is realized through communication, i.e to coordinately dispatch and regulate their storage power outputs.

Currently, the proposed methods for dispatching and controlling storage devices of a group of SoA WGs rest on centralized control. Concretely, local wind speed conditions prevalent at the location of the WGs as well as information about their stored energy, are communicated to a centralized controller. Then, the centralized controller uses this information to compute the available total wind power and the total storage power that is needed to meet a particular total power reference and, eventually, to compute two power set-points for each WG. The latter computation is carried out through some pre-specified allocation rule. The first set-point corresponds to the mechanical power that each WG has to extract from the wind while the second one to the power that its storage device has to provide. Finally, these two power set-points are communicated to the WGs which employ their local wind turbine and storage controllers to meet them.

In general, centralized control approaches carry several drawbacks that are too critical to be ignored. To mention a few, they exhibit slow response and are not robust to single-point failures, they demand high computational effort and extensive communication network [40]. In the case of WGs, the slow response can be a hurdle compromising a timely dispatch and regulation of their power outputs when these have to be performed rapidly under highly dynamic conditions to attain fast power balancing of supply and demand, e.g in low-inertia microgrids.

In dispatching and controlling SoA WGs, the real challenge lies into enabling them to compute both the power set-points for the wind turbine and storage device in a fast, robust and computationally efficient manner. In particular, it is very important for SoA WGs to be able to retrieve their power set-points fast since that, combined with the storage devices being able to respond fast, can allow them to attain fast total power output regulation. In this case, the range of services that can be provided by the WF will be much broader. In addition, the power set-points of the WGs have to be retrieved in a robust and efficient fashion, so that the WF total power output regulation is reliable and requires minimal computational effort.

Recognizing that the above challenges can be effectively addressed through distributed control methods, in this chapter, a particular distributed control design is proposed. The proposed control design solves the problem of WF power output regulation through dynamic dispatch and control of the storage devices of a group of SoA WGs.

Our main contribution is a distributed control methodology for the grid-side converter (GSC) and DC-DC converter that enables SoA WGs to regulate their total power to a reference by self-organizing and controlling their storage devices in an equal sharing fashion. In our context, self-organization and control of the storage devices in an equal sharing manner refers to the storage devices continuously adjusting their power outputs while these remain equal when the total power reference tracking is attained.

4.2 Related Work

The problem of WF power output regulation via dispatching and controlling a group of SoA WGs has been only studied in [15] where a centralized control system is proposed. In particular, a two-layer centralized constant power control system where, at the high-layer, a wind farm supervisory controller combines information about the reference and available wind power to generate the power set-points for both the wind turbine and the storage device of each WG. In the low-layer, proportional integral (PI) controllers for the RSCs and the DC-DC converters make sure that the power set-points are realized through regulation of the respective power outputs.

To the best of our knowledge, distributed control methods for dealing with the above problem have not been proposed in the literature. On the other hand, the centralized approach in [15] inherits all the weaknesses of centralized control approaches which are already discussed.

In our work, we develop a distributed control scheme that first allows, the GSCs to coordinatively and dynamicallly regulate their power outputs using communication so that WF power output regulation is attained and second, the DC-DC converters to dynamically self-organize and control the storage devices and ultimately supply the power demanded by the GSCs. In contrast with centralized approaches, our control method allows dynamic and distributed fast WF power output regulation.

4.3 Model of a Wind Generator With Storage

Here, SoA WGs are considered to have supercapacitor storage devices into their systems. The dynamical models which are related to the control of these storage devices are the GSC model and the supercapacitor model. Hence, we restate those next for completeness. Let the set of SoA WGs be denoted by $\mathcal{G} \triangleq \{1, ..., n\}$ and each SoA WG be indexed by i such that $i \in \mathcal{G}$.

4.3.1 GSC Model

The GSC model can be represented by the current output dynamics expressed in a $d-q$ coordinate system as [31]:

$$\frac{dI_{dg,i}}{dt} = -\omega_s\Big(\frac{R_{g,i}}{L_{g,i}}\Big)I_{dg,i}+\omega_s I_{qg,i}+\omega_s\Big(\frac{V_{dg,i}-V_{s,i}}{L_{g,i}}\Big), \quad \forall i \in \mathcal{G} \tag{4.1}$$

$$\frac{dI_{qg,i}}{dt} = -\omega_s\Big(\frac{R_{g,i}}{L_{g,i}}\Big)I_{qg,i}-\omega_s I_{dg,i}+\omega_s\Big(\frac{V_{qg,i}}{L_{g,i}}\Big), \qquad \forall i \in \mathcal{G} \tag{4.2}$$

The constants $R_{g,i}, L_{g,i} \in \mathbb{R}_+$ represent the losses of the GSC whereas, $V_{s,i} \in \mathbb{R}$ represents the terminal voltage of WG i. Moreover, $V_{dg,i}, V_{qg,i} \in \mathbb{R}$ represent the GSC-controlled voltage inputs [31].

4.3.2 Supercapacitor Energy Storage Model

Today, General Electric (GE) incorporates batteries into DFIGs. To get a sense of their relative size, the GE's batteries for 2.5MW wind DFIGs have energy capacity of 50kWh. That means they can provide 1/50 of the wind generator's nominal power output for one hour. Alternatively, in our work, we explore the application of supercapacitor storage devices into DFIGs for the following reasons: *a*) they have high efficiency and *b*) they have rapid

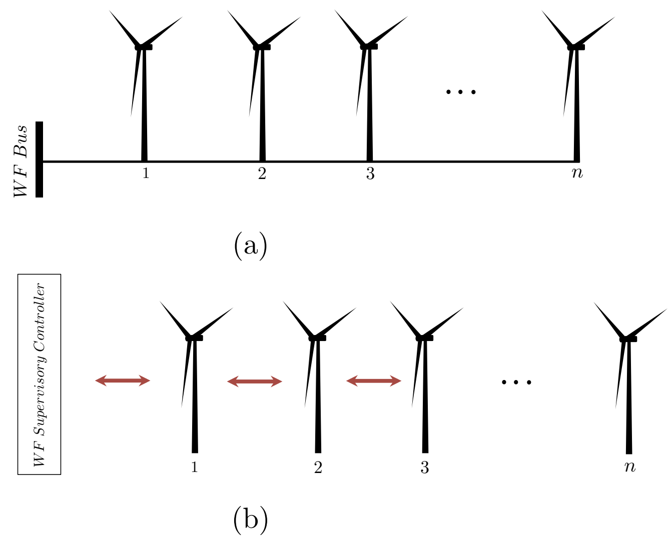

Figure 4.1: a) Physical topology b) Communication topology of the WF

response capability [23]. Their model can be stated as:

$$(C_{sc,i}V_{sc,i})\frac{dV_{sc,i}}{dt} = V_{sc,i}\frac{(u_{sc,i} - V_{sc,i})}{R_{sc,i}}, \quad \forall i \in \mathcal{G} \tag{4.3}$$

where $u_{sc,i} \in \mathbb{R}$ is the voltage controlled by the DC-DC converter whereas, $C_{sc,i}, V_{sc,i}, R_{sc,i} \in \mathbb{R}_+$ are the capacitance, the DC voltage and the losses of the supercapacitor, respectively. Throughout our analysis, the supercapacitors are assumed to be sufficiently charged and no bounds are imposed on their DC voltages $V_{sc,i}$. The storage power output of each WG is given by:

$$P_{st,i} = V_{sc,i}\frac{(V_{sc,i} - u_{sc,i})}{R_{sc,i}}, \qquad \forall i \in \mathcal{G} \tag{4.4}$$

Realize that, this can be regulated by the DC-DC converter through the input $u_{sc,i}$.

4.4 Problem Formulation

Consider a WF with n SoA WGs incorporating supercapacitor energy storage devices that receives a power reference P_d from a system operator (SO). This power reference corresponds to the WF's committed power output toward the SO and is the outcome of a wind forecasting method and an economic dispatch (ED) process.

Our main problem is formulated around a particular goal for the SoA WGs. This goal is coordination of their storage devices for total WF power reference (P_d) tracking, i.e predictable WF power output, with equal contribution from each storage power to the power mismatch required to meet the demand P_d, i.e fair load sharing. The reason for imposing fair load sharing among WGs will be explained later.

Let the variables $P_{e,i}$, $P_{g,i}$, $P_{r,i}$ and $P_{st,i}$ denote respectively the electric power output of the stator, the grid-side converter (GSC), the rotor-side converter (RSC) and the storage device, as seen in Fig. 3.1. Now, the dynamics of the capacitor that interfaces the RSC and the GSC (Fig. 3.1) can be stated as:

$$(C_{dc,i}V_{dc,i})\frac{dV_{dc,i}}{dt} = (P_{r,i}+P_{st,i}-P_{g,i}), \qquad i \in \mathcal{G} \tag{4.5}$$

Observe that, when the storage is not generating any power, at the equilibrium, we have:

$$P_{g,i} = P_{r,i}, \quad i \in \mathcal{G} \tag{4.6}$$

In this case, the total WF power output is approximately equal to the total mechanical power available from the wind, i.e:

$$\sum_{i\in\mathcal{G}}(P_{e,i}+P_{r,i}) \approx \sum_{i\in\mathcal{G}} P_{m,i} \tag{4.7}$$

This total mechanical power $\sum_{i\in\mathcal{G}} P_{m,i}$ is highly variable because it depends on the wind speed conditions. Accordingly, the total WF electrical power output is also highly variable and in the scenario that the WF is requested to meet a particular power reference P_d, it might happen that:

$$\sum_{i\in\mathcal{G}}(P_{e,i}+P_{r,i}) < P_d \tag{4.8}$$

i.e the WF cannot meet system operator's request. This is based on the following reason. There is a significant time-delay between the moment the SO issues the scheduled power reference P_d until the moment that this is implemented by the WF. Precisely, this time-delay is around 13 minutes according to [7]. This, combined with the wind-speed minute to minute variability, might cause the WF to be not able to meet SO's request and generate power that matches the reference P_d. On the other hand, the WF can manage the wind variability and time-delays and meet SO's request even with the available wind power being inadequate, when it is comprised of WGs with incorporated storage devices into their systems. Specifically, given that the storage devices have sufficient stored energy, the WGs can meet the reference P_d since:

$$\sum_{i\in\mathcal{G}}(P_{e,i}+P_{r,i}+P_{st,i}) = P_d \tag{4.9}$$

given that they have sufficient stored energy. In this case, each storage device generates power so that, at the equilibrium of (4.5) we have:

$$P_{st,i} = (P_{g,i}-P_{r,i}), \quad i \in \mathcal{G} \tag{4.10}$$

In total, the storage devices can provide additional or draw excess power so that the WF power output regulation objective is realized. Mathematically, this can be described by the following condition.

Condition 1 (Total storage power regulation).

$$\sum_{i\in\mathcal{G}} P_{st,i} = P_d - \sum_{i\in\mathcal{G}}(P_{e,i}+P_{r,i}) \tag{4.11}$$

The available storage devices are utilized more efficiently when they are controlled to contribute equally to the total storage power. This can be described by the following condition on the storage power outputs.

Condition 2 (**Fair load sharing among storage devices**).

$$P_{st,i} = P_{st,j} \ , \quad \forall i, j \in \mathcal{G} \tag{4.12}$$

With the desired conditions for the storage power outputs being fully defined, we now state the following definition.

Definition 1. WF power output regulation with fair utilization of the storage devices is attained when *Conditions* 1 and 2 *are jointly met.*

From this definition, it springs that SoA WGs can reach their goal by properly designing their controllers so that asymptotically they fulfill *Conditions* 1 and 2. Given that, the main problem can be formulated as:

Problem 1. *Coordinate and control the energy storage devices of a group of SoA WGs in a distributed way, to dynamically realize WF power output regulation with fair utilization of the storage devices..*

4.5 Proposed Methodology

We propose the next methodology for solving Problem 1, which is partitioned into five main steps.

- **Step 1**: We pose Problem 1 as a twofold control problem, a constrained consensus problem for the GSCs on the variable $z_i \triangleq (P_{g,i} - P_{r,i})$, and a tracking problem for the storage power outputs, i.e to ensure that $\lim_{t\to\infty} P_{st,i} = z_i, \ \forall i \in \mathcal{G}$.
- **Step 2**: We introduce a leader-follower consensus protocol that GSCs can incorporate

into their control systems to distributively reach consensus on their z_i's and a desired closed-loop form for the interfacing capacitor dynamics that the DC-DC converters can attain to ensure storage power output regulation.

- **Step 3**: We perform time-scale separation analysis of the coupled consensus protocol and closed-loop capacitor dynamics and derive conditions on the GSC and DC-DC converter control gains under which three time-scales arise in these dynamics.
- **Step 4**: Given that the GSC's and DC-DC converter's control gains fulfill the Conditions in Step 3, we first employ singular perturbation theory to conduct temporal decomposition of the above dynamics. Then, we perform compositional stability analysis of the decomposed subsystems and prove conditional asymptotic stability of the equilibrium of the full coupled consensus protocol and closed-loop capacitor system.
- **Step 5**: We design a distributed controller for the GSC and a decentralized controller for the DC-DC converter which respectively guarantee that, the closed-loop dynamics of z_i are identical to the consensus protocol dynamics and the closed-loop dynamics of the capacitor have the desired form defined in Step 2.

4.6 Constrained Consensus Among GSC-controlled Variables and Storage Power Output Regulation

In Section 4.4, the problem of WF power output regulation with fair load sharing of the storage devices is formulated as a control problem for the storage devices with objective their power outputs to meet *Conditions* 1 and 2. We realize that, instead of controlling the storage power outputs such that *Conditions* 1 and 2 are fulfilled, we can, alternatively control each storage power $P_{st,i}$ so that equation $P_{st,i} = (P_{g,i} - P_{r,i})$ is satisfied and then map *Conditions* 1 and 2 into the two conditions for the power difference (among GSC and RSC) $z_i = (P_{g,i} - P_{r,i})$ stated below.

Condition 3 (**Total power difference (z_i) regulation**).

$$\sum_{i \in \mathcal{G}} z_i = \Big(P_d - \sum_{i \in \mathcal{G}} (P_{ei} + P_{ri})\Big) \tag{4.13}$$

Condition 4 (**Fair load sharing among the GSCs**).

$$z_i = z_j, \quad \forall i, j \in \mathcal{G} \tag{4.14}$$

With these conditions, the initial control problem can be transformed to two equivalent control problems for the storage devices, one with objective for their GSCs to reach consensus on the variable $z_i = (P_{g,i} - P_{r,i})$ and one with objective for their DC-DC converters to regulate the storage power outputs to their respective z_i's. These problems are stated as follows.

Problem 2 (**Constrained Consensus Among GSCs**). *Coordinate and control the GSCs so that the variables z_i asymptotically reach consensus, i.e fulfill Condition 4, while respecting the contraint given in Condition 3.*

Problem 3 (**Storage Power Output Regulation**). *Control the storage devices so that their power outputs $P_{st,i}$'s are regulated to their respective z_i's, i.e $\lim_{t\to\infty} P_{st,i} = z_i$, $\forall i \in \mathcal{G}$.*

4.7 Leader-Follower Consensus Protocol and Desired Closed-loop Capacitor Dynamics

In this Section, we introduce a leader-follower consensus protocol that GSCs can adopt into their control design to reach consensus on their z_i's while respecting the constraint (4.13), i.e asymptotically fulfill the conditions given in Problem 2. Moreover, we introduce a desired closed-loop form for the capacitor dynamics that the storage devices can realize (through their DC-DC converters) to guarantee regulation of the storage power to the variable z_i, i.e asymptotically fulfill the condition provided in Problem 3.

4.7.1 Leader-Follower Consensus Protocol

The proposed leader-follower consensus protocol is stated below where, without loss of generality WG l with $l \triangleq 1$ is assigned as the leader and the set of followers is denoted by $\overline{\mathcal{G}} \triangleq \{2, ..., n\}$.

Consensus Protocol $\mathcal{P}_1$

Leader WG

$$\frac{d\xi_h}{dt} = \Big(P_d - \sum_{i\in\mathcal{G}}(P_{e,i}+P_{g,i})\Big) \qquad \xi_h \in \mathbb{R} \tag{4.15a}$$

$$\frac{dz_l}{dt} = -k_{\alpha,l}(z_l - \xi_h) \ , \qquad z_l \in \mathbb{R},\ z_l \triangleq z_1 \tag{4.15b}$$

WG i

$$\frac{dz_i}{dt} = -k_{\alpha,i}(z_i - z_{i-1}) \ , \qquad z_i \in \mathbb{R},\ \forall i \in \overline{\mathcal{G}} \tag{4.15c}$$

The state variables are the differences among the power outputs of the GSCs and RSCs $z_i \triangleq (P_{g,i} - P_{r,i})$ and an additional auxiliary variable of the leader ξ_h. The variable ξ_h is the one that drives the protocol and guarantees regulation of the total WF power to the reference P_d. Notice that, every WG is allowed to communicate with its two neighbors [2] as depicted in Fig. 4.1b. Further, observe that, the consensus protocol dynamics are defined in the continuous time-domain. Thus, to practically implement the protocol a communication network with *high bandwidth* is required. Alternatively, this requirement can be relaxed by defining the above dynamics in the discrete time-domain with sufficiently large time-step. Nevertheless, the forthcoming analysis will be conducted in the continuous time-domain.

[2] Here, with neighbors we refer to the WGs that have direct physical connection with the particular WG.

The execution of the protocol $\mathcal{P}_1$ can be conducted in the following way. The leader WG obtains information about the total power reference P_d from the WF supervisory controller. Combining this information with the global information $\sum_{i\in\mathcal{G}}(P_{e,i}+P_{g,i})$, the leader WG controls the dynamics of the state-variables z_1 and ξ_h and continuously communicates z_1 to its neighbors. Synchronized with the leader, all followers control the dynamics of their state-variables z_i by exploiting information from their respective neighbors while they communicate to them their z_i's. We underline that the information $\sum_{i\in\mathcal{G}}(P_{e,i}+P_{g,i})$ can be retrieved by the leader through indirect information passing from all WGs or can be physically measured.

4.7.2 Communication Topology

In this thesis, without loss of generality a row-connected communication topology is studied. Nevertheless, we recognize that this communication network is the most fragile in the sense that if one of the communication links is compromised then, the consensus protocol will not be able to converge, i.e this communication network is not robust to single point failures. In general, to have a sufficiently robust performance and fast convergence of the consensus protocol, a communication network with redundant communication links is required. Exploring more complicated communication networks and their interdependency with the convergence rate and robustness of the consensus protocol lies beyond the scope of the current work. However, we recognize that this is an interesting direction for future work.

4.7.3 Desired Closed-loop Capacitor Dynamics

Next, a desired closed-loop form for the interfacing capacitor dynamics is stated. Each DC-DC converter can respectively shape its capacitor's closed-loop dynamics so that they have this form and the storage power output $P_{st,i}$ tracks the variable z_i. Foremost, let the stored energy in the capacitor be:

$$E_{dc,i} = \frac{1}{2}C_{dc,i}V_{dc,i}^2, \qquad \forall i \in \mathcal{G} \tag{4.16}$$

We state the *desired closed-loop form* of the capacitor's dynamics with respect to the variable $\Delta E_{dc,i} = (E_{dc,i} - E_{dc0,i})$ that denotes the deviation of energy around the equilibrium $E_{dc0,i}$, as:

$$\frac{d(\Delta E_{dc,i})}{dt} = -k_{2,i}(\Delta E_{dc,i}), \qquad \forall i \in \mathcal{G} \tag{4.17}$$

On the other hand, the open-loop dynamics of the above equation are:

$$\frac{d(\Delta E_{dc,i})}{dt} = (P_{r,i} + P_{st,i} - P_{g,i}), \qquad \forall i \in \mathcal{G} \tag{4.18}$$

When the closed-loop dynamics of the capacitor are identical to (4.17), the dynamical equation for the storage power $x_i = P_{st,i}$ can be obtained, by differentiating equations (4.17) and(4.18) and letting them be equal, as:

$$\frac{dx_i}{dt} = \frac{dz_i}{dt} - k_{2,i}(x_i - z_i), \qquad \forall i \in \mathcal{G} \tag{4.19}$$

where $(P_{g,i} - P_{r,i}) \triangleq z_i$ is used. By substituting the term dz_i/dt from (4.15c), this equation can be further expanded to:

Storage power dynamics

$$\frac{dx_i}{dt} = -k_{\alpha,i}(z_i - z_{i-1}) - k_{2,i}(x_i - z_i), \qquad \forall i \in \mathcal{G} \tag{4.20}$$

The consensus protocol dynamics in (4.15c) represent the desired closed-loop dynamics of the variable z_i and can be realized by the GSC while, the dynamics in (4.20), the desired closed-loop dynamics of the storage power $P_{st,i}$, that can be realized by the DC-DC converter. Altogether, the model comprised of the equations (4.15a), (4.15c) and (4.20) describes the main dynamical system that will be extensively studied throughout this chapter.

4.8 Time-scale Separation Analysis

The desired closed-loop dynamics of the GSC-controlled variable z_i and the storage power x_i can be written more compactly in vector form as:

$$\frac{d\xi_h}{dt} = \Big(P_d - \sum_{i\in\mathcal{G}}(P_{e,i} + P_{g,i})\Big) \tag{4.21a}$$

$$\frac{d\mathbf{z}}{dt} = \mathbf{g}_z \tag{4.21b}$$

$$\frac{d\mathbf{x}}{dt} = \mathbf{g}_x \tag{4.21c}$$

where:

$$\mathbf{z} = [z_1, ..., z_n]^\top \in \mathbb{R}^n \tag{4.22}$$

$$\mathbf{x} = [x_1, ..., x_n]^\top \in \mathbb{R}^n \tag{4.23}$$

$$\mathbf{g}_z = [-k_{\alpha,1}(z_1 - \xi_h), ..., -k_{\alpha,n}(z_n - z_{n-1})]^\top, \quad \mathbf{g}_z \in \mathbb{R}^n \tag{4.24}$$

$$\mathbf{g}_x = \mathbf{g}_z - [k_{2,1}(x_1 - z_1), ..., -k_{2,n}(x_n - z_n)]^\top, \quad \mathbf{g}_x \in \mathbb{R}^n \tag{4.25}$$

The dynamics of the above system are characterized by three distinct time-scales, i.e they possess a three time-scales property, when the gains $k_{\alpha,i},\ k_{2,i}$ respect the conditions stated in the next Lemma.

Lemma 4.1. *The dynamics of the system (4.21a)-(4.21c) manifest three distinct time-scales when $k_{\alpha,i} \gg 1,\ \ k_{2,i} \gg\ k_{\alpha,i},\ \forall i \in \mathcal{G}$.*

Proof. Without loss of generality we set:

$$k_{\alpha,1} = ... = k_{\alpha,i} = ... = k_{\alpha,n} = \frac{1}{\varepsilon_1} \tag{4.26}$$

$$k_{2,1} = ... = k_{2,i} = ... = k_{2,n} = \frac{1}{\varepsilon_2} \tag{4.27}$$

Further, we express equations (4.21b), (4.21c) in scalar form and divide them by $k_{\alpha,i}$. This yields:

$$\frac{1}{k_{\alpha,i}}\frac{dz_i}{dt} = -(z_i - z_{i-1})\ ,\ z_0 = \xi_h, \qquad \forall i \in \mathcal{G} \tag{4.28}$$

$$\frac{1}{k_{\alpha,i}}\frac{dx_i}{dt} = -(z_i - z_{i-1}) - \frac{k_{2,i}}{k_{\alpha,i}}(x_i - z_i)\ , \qquad \forall i \in \mathcal{G} \tag{4.29}$$

Multiplying both sides of (4.29) by $(k_{\alpha,i}/k_{2,i})$ yields:

$$\frac{1}{k_{\alpha,i}}\frac{dz_i}{dt} = -(z_i - z_{i-1})\ ,\ z_0 = \xi_h, \qquad \forall i \in \mathcal{G} \tag{4.30}$$

$$\frac{1}{k_{2,i}}\frac{dx_i}{dt} = -\frac{k_{\alpha,i}}{k_{2,i}}(z_i - z_{i-1}) - (x_i - z_i)\ , \qquad \forall i \in \mathcal{G} \tag{4.31}$$

Finally, by substituting the gains from (4.26) and (4.27), the system (4.30) and (4.31) can be transformed to:

$$\varepsilon_1\frac{dz_i}{dt} = -(z_i - z_{i-1})\ ,\ z_0 = \xi_h, \qquad \forall i \in \mathcal{G} \tag{4.32}$$

$$\varepsilon_2\frac{dx_i}{dt} = -\frac{\varepsilon_2}{\varepsilon_1}(z_i - z_{i-1}) - (x_i - z_i)\ , \qquad \forall i \in \mathcal{G} \tag{4.33}$$

Altogether, we finally obtain the system:

$$\frac{d\xi_h}{dt} = \Big(P_d - \sum_{i\in\mathcal{G}}(P_{e,i} + P_{g,i})\Big) \tag{4.34a}$$

$$\varepsilon_1\frac{d\mathbf{z}}{dt} = \bar{\mathbf{g}}_z \tag{4.34b}$$

$$\varepsilon_2\frac{d\mathbf{x}}{dt} = \bar{\mathbf{g}}_x \tag{4.34c}$$

where the new vector fields are:

$$\bar{\mathbf{g}}_z = \mathbf{g}_z\varepsilon_1, \quad \bar{\mathbf{g}}_x = \mathbf{g}_x\varepsilon_2 \tag{4.35}$$

When $\varepsilon_1 \ll 1,\ \varepsilon_2 \ll \varepsilon_1$, the form of this system is the *standard singularly perturbed* one with three distinct time-scales $t,\ \tau = t/\varepsilon_1,\ \tilde{\tau} = t/\varepsilon_2$ where $\varepsilon_2 \ll \varepsilon_1$. Subsequently, ξ_h is the slow state-variable, $\mathbf{z}$ are the fast and $\mathbf{x}$ the very fast state-variables. ■

Lemma 4.1 can be practically useful in the following way. The conditions involved in the lemma can guide the choice of appropriate control gains for the GSCs ($k_{\alpha,i}$) and the DC-DC converters ($k_{2,i}$) that will grant three distinct time-scales in the dynamics of the system (4.21a), (4.21b),(4.21c).

4.9 Stability Analysis

Given that the control gains of the GSCs and DC-DC converters meet the conditions stated in Lemma 4.1, we employ singular perturbation theory to perform compositional stability analysis of this system.

4.9.1 Equilibrium and Desired Properties

Taking into account that $P_{g,i} \triangleq z_i + P_{r,i}$, we can state the model (4.21a)-(4.21c) as:

$$\frac{d\xi_h}{dt} = \Big(P_d - \sum_{i\in\mathcal{G}}(P_{e,i} + P_{r,i} + z_i)\Big) \tag{4.36a}$$

$$\frac{d\mathbf{z}}{dt} = \mathbf{g}_z \tag{4.36b}$$

$$\frac{d\mathbf{x}}{dt} = \mathbf{g}_x \tag{4.36c}$$

where the vectors fields $\mathbf{g}_z,\ \mathbf{g}_x$ are given by (4.24), (4.25), respectively. Recall that, this model represesents the coupled consensus protocol and storage power system. The equilibrium of this system is:

$$\xi_{h0} = \frac{\left(P_d - \sum_{i\in\mathcal{G}}(P_{e,i}+P_{r,i})\right)}{n} \tag{4.37a}$$

$$\mathbf{z}_0 = \xi_{h0}\cdot\mathbf{1}_n \tag{4.37b}$$

$$\mathbf{x}_0 = \xi_{h0}\cdot\mathbf{1}_n \tag{4.37c}$$

We set the vector $\boldsymbol{\phi}$ as the state-vector of the full system, concretely:

$$\boldsymbol{\phi} = \begin{pmatrix} \xi_h \\ \\ \mathbf{z} \\ \\ \mathbf{x} \end{pmatrix} \in \mathbb{R}^{2n+1} \tag{4.38}$$

It is convenient for the rest of our analysis to define a *consensus subspace* as [41]:

$$\mathcal{S} \triangleq \{\boldsymbol{\phi} \in \mathbb{R}^{2n+1} \mid \boldsymbol{\phi} = \beta\cdot\mathbf{1}_{2n+1}\ ,\quad \beta \in \mathbb{R}\} \tag{4.39}$$

WF power output regulation with fair load-sharing among the storage devices is guaranteed when the equilibrium $\boldsymbol{\phi}_0$ of the full system (4.36a)-(4.36c) possesses the following properties.

Property 4.1. $\boldsymbol{\phi}_0 \in \mathcal{S}$.

Property 4.2. $\boldsymbol{\phi}_0$ *is asymptotically stable.*

The system's equilibrium readily has property 4.1, since $\boldsymbol{\phi}_0 = (\xi_{h0}\cdot\mathbf{1}_{2n+1})$. It is left to show that the system possesses property 4.2 as well. By defining the new shifted state-variables:

$$\psi_h \triangleq (\xi - \xi_{h0}) \tag{4.40}$$

$$\mathbf{y} \triangleq (\mathbf{z} - \xi_h \cdot \mathbf{1}_n), \qquad \mathbf{y} = [y_1, ..., y_n]^\top \in \mathbb{R}^n \tag{4.41}$$

$$\boldsymbol{\eta} \triangleq (\mathbf{x} - \mathbf{z}), \qquad \boldsymbol{\eta} = [\eta_1, ..., \eta_n]^\top \in \mathbb{R}^n \tag{4.42}$$

the system (4.36a)-(4.36c) is transformed to:

$$\frac{d\psi_h}{dt} = -n\psi_h - \sum_{i=1}^{n} y_i \tag{4.43a}$$

$$\varepsilon_1 \frac{dy_i}{dt} = -(y_i - y_{i-1}) - \varepsilon_1 \frac{d\psi_h}{dt}, \quad y_0 \triangleq 0, \qquad \forall i \in \mathcal{G} \tag{4.43b}$$

$$\varepsilon_2 \frac{d\eta_i}{dt} = -\eta_i, \qquad \forall i \in \mathcal{G} \tag{4.43c}$$

or more compactly in vector form:

$$\frac{d\psi_h}{dt} = -n\psi_h - \mathbf{1}_n^\top \mathbf{y} \tag{4.44a}$$

$$\varepsilon_1 \frac{d\mathbf{y}}{dt} = \mathbf{g}_y \tag{4.44b}$$

$$\varepsilon_2 \frac{d\boldsymbol{\eta}}{dt} = \mathbf{g}_\eta \tag{4.44c}$$

where the vector fields are:

$$\mathbf{g}_y \triangleq [-y_1, ..., -(y_i - y_{i-1}), ..., -(y_n - y_{n-1})]^\top - \varepsilon_1 \frac{d\psi_h}{dt} \cdot \mathbf{1}_n \tag{4.45}$$

$$\mathbf{g}_\eta \triangleq -\boldsymbol{\eta} \tag{4.46}$$

We set the vector:

$$\bar{\boldsymbol{\phi}} = \begin{pmatrix} \psi_h \\ \mathbf{y} \\ \boldsymbol{\eta} \end{pmatrix} \in \mathbb{R}^{2n+1} \tag{4.47}$$

to denote the state-vector of the transformed system (4.44a)-(4.44c) with equilibrium:

$$\bar{\boldsymbol{\phi}}_0 = \mathbf{0}_{2n+1} \tag{4.48}$$

i.e the origin. The aim of the forthcoming analysis is to derive conditions under which $\bar{\boldsymbol{\phi}}_0$ is asymptotically stable. But first, realize that, in the transformed system, the consensus protocol dynamics (4.44a), (4.44b) are decoupled from the storage power dynamics (4.44c). This facilitates the stability analysis of these dynamics since by merely establishing stability of (4.44a), (4.44b) and independently of (4.44c), is sufficient to infer stability of the full system (4.44a)-(4.44c). In other words, if:

$$\tilde{\mathbf{y}}_0 = \begin{pmatrix} \psi_{h0} \\ \mathbf{y}_0 \end{pmatrix} = \mathbf{0}_{n+1}, \quad \boldsymbol{\eta}_0 = \mathbf{0}_n \tag{4.49}$$

are asymptotically stable equilibria of (4.44a), (4.44b) and (4.44c) respectively, then $\bar{\boldsymbol{\phi}}_0$ will be asymptotically stable equilibrium of (4.44a)-(4.44c).

4.9.2 Stability of the Consensus Protocol Dynamics

We first study stability of the consensus protocol dynamics (4.44a)-(4.44b) that have a standard singular perturbation form with two distinct time-scales, the slow one t and the fast one τ. The state-variable ψ_h is the slow one while the state-variables $\mathbf{y}$ the fast ones. Stability of this system is established in the following way. Initially, we perform temporal decomposition to obtain fast and slow decoupled subsystems and establish their asymptotic stability. Then, these stability certificates for the decoupled systems are assembled into a composite Lyapunov function which is employed to derive a condition under which asymptotic stability of the full consensus protocol system is guaranteed.

a) **Stability of Fast-boundary Layer Subsystem**

Here, we prove asymptotic stability of the equilibrium of the protocol's decoupled fast subsystem, $\mathbf{y}_0 = \mathbf{0}_n$. This fast boundary-layer system can be obtained by approximating the slow state-variable ψ_h in equation (4.43b) as constant, i.e $d\psi_h/d\tau = 0$:

Fast-boundary Layer Subsystem

$$\frac{dy_i}{d\tau} = -(y_i - y_{i-1}), \quad \forall i \in \mathcal{G} \tag{4.50}$$

where $\tau = t/\varepsilon_1$. Stability of this system is established through the following lemma.

Lemma 4.2. *The equilibrium $\mathbf{y}_0 = \mathbf{0}_n$ of the fast boundary-layer system (4.50) is asymptotically stable.*

Proof. The system (4.50) in matrix form can be written as:

$$\frac{d\mathbf{y}}{d\tau} = \mathbf{A}_f \mathbf{y}, \quad \mathbf{A}_f \in \mathbb{R}^{n\times n} \tag{4.51}$$

$$\mathbf{A}_f = \begin{bmatrix} -1 & 0 & \cdots & 0 & 0 \\ \vdots & \ddots & & & \vdots \\ 0 & 0 & \cdots & 1 & -1 \end{bmatrix}$$

We denote the eigenvalues of this matrix by $\boldsymbol{\lambda} = [\lambda_l, ..., \lambda_n]^\top$. The matrix $\mathbf{A}_f$ is lower triangular so it holds that:

$$\det(\mathbf{A}_f - \lambda \cdot \mathbf{I}_{n\times n}) = (-1)^n (\lambda + 1)^n \tag{4.52}$$

and $\boldsymbol{\lambda} = -\mathbf{1}_n \preceq 0$. From this, we conclude that $\mathbf{A}_f$ is *Hurwitz*. It also follows from Theorem 4.5 ([10]) that $\mathbf{y}_0$ is asymptotically stable. With this, we complete the proof. ■

The stability property established above will be useful in proving asymptotic stability of the full system (4.43a)-(4.43c). Therefore, a parameterized Lyapunov function that captures this property and serves as a stability certificate of the fast boundary-layer system can be defined as:

$$V_f = \mathbf{y}^\top \mathbf{P} \mathbf{y}, \quad V_f > 0, \;\; \forall \mathbf{y} \in \overline{\mathcal{D}}_y \tag{4.53}$$

where $\overline{\mathcal{D}}_y = \mathcal{D}_y \backslash \{\mathbf{0}_n\}$, $\mathcal{D}_y \subset \mathbb{R}^n$ and $\mathbf{P} \in \mathbb{R}^{n\times n}$ is a positive definite matrix satisfying the Lyapunov equation:

$$\mathbf{P}\mathbf{A}_f + \mathbf{A}_f^\top \mathbf{P} = -\mathbf{Q} \tag{4.54}$$

for a particular choice of $\mathbf{Q} \succ 0$. Later on, we will use among others this parameterized Lyapunov function V_f to derive a condition under which, asymptotic stability of $\mathbf{y}_0$ is guaranteed. Thus, this condition will be expressed in terms of the elements of the matrix $\mathbf{P}$.

b) **Stability of Slow Reduced-order Subsystem**

We will now establish asymptotic stability of ψ_{h0}, equilibrium of the protocol's slow reduced-order susbystem. Focusing on the slow time-scale t and approximating the fast state-variables $\mathbf{y}$ with their quasisteady state values $\mathbf{y} = \mathbf{0}_n$, yields the slow reduced-order subsystem:

Slow Reduced-order Subsystem

$$\frac{d\psi_h}{dt} = -n\psi_h \tag{4.55}$$

Stability of (4.55) is established through the following lemma.

Lemma 4.3. *The equilibrium point $\psi_{h0} = 0$ of the slow reduced system (4.55) is asymptotically stable.*

Proof. A candidate Lyapunov function for the system (4.55) is:

$$V_h = \psi_h^2, \quad V_h > 0, \quad \forall \psi_h \in \overline{D}_{\psi_h} \tag{4.56}$$

where $\overline{D}_{\psi_h} = D_{\psi_h} \backslash \{0\}$, $D_{\psi_h} \subseteq \mathbb{R}$. The time-derivative of (4.56) along the trajectories of (4.55) is:

$$\dot{V}_h = -2n\psi_h^2 < 0, \; \forall \psi_h \in \overline{D}_{\psi_h}, \;\; n > 0 \tag{4.57}$$

Applying Lyapunov's stability theorem yields that $\psi_{h0} = 0$ is asymptotically stable. ∎

With the stability properties of the decoupled subsystems established, we are now ready to derive conditions under which asymptotic stability of $\tilde{\mathbf{y}}_0$ is guaranteed.

c) **Stability of the Full Consensus Protocol System**

The stability properties of the fast boundary-layer and slow reduced-order subsystems just established can be exploited through their respective Lyapunov functions V_f and V_h to derive a condition for asymptotic stability of the equilibrium $\tilde{\mathbf{y}}_0$ of the full consensus protocol system (4.44a), (4.44b). In particular, we assemble the Lyapunov functions V_f and V_h through their linear combination to form a composite Lyapunov function for the full system (4.44a)-(4.44c) as:

$$V_c = \frac{1}{2}\mathbf{y}^\top \mathbf{P}\mathbf{y} + \frac{\psi_h^2}{2}, \quad V_c > 0, \quad \forall(\mathbf{y}, \psi_h) \in \overline{\mathcal{D}}_y \times \overline{\mathcal{D}}_{\psi_h} \tag{4.58}$$

Without loss of generality the matrix $\mathbf{P} = [p_{ji}]$ is assumed to be symmetric, i.e $\mathbf{P} = \mathbf{P}^\top$. The derivative of V_c can be analytically computed as:

$$\begin{aligned}
\frac{dV_c}{dt} &= \frac{1}{2}\dot{\mathbf{y}}^\top \mathbf{P}\mathbf{y} + \frac{1}{2}\mathbf{y}^\top \mathbf{P}\dot{\mathbf{y}} + \psi_h \dot{\psi}_h \\
&= \frac{1}{2}\mathbf{y}^\top (\frac{\mathbf{A}_f^\top \mathbf{P} + \mathbf{P}\mathbf{A}_f}{\varepsilon_1})\mathbf{y} + [-\frac{d\boldsymbol{\psi}_h}{dt}^\top \mathbf{P}\mathbf{y} + \mathbf{y}^\top \mathbf{P}\frac{d\boldsymbol{\psi}_h}{dt}]\frac{1}{2} + \psi_h(-n\psi_h - \sum_{i=1}^{n} y_i) \\
&= -\mathbf{y}^\top (\frac{\mathbf{Q}}{2\varepsilon_1})\mathbf{y} + [-\frac{d\boldsymbol{\psi}_h}{dt}^\top \mathbf{P}\mathbf{y}] - n\psi_h^2 - \psi_h \sum_{i=1}^{n} y_i
\end{aligned} \tag{4.59}$$

where $\dot{\mathbf{y}} = \frac{d\mathbf{y}}{dt}$ and $\frac{d\boldsymbol{\psi}_h}{dt} = \frac{d\psi_h}{dt} \cdot \mathbf{1}_n$. Futher, the term $[-\frac{d\boldsymbol{\psi}_h}{dt}^\top \mathbf{P}\mathbf{y}]$ can be expanded as:

$$[-\frac{d\boldsymbol{\psi}_h}{dt}^\top \mathbf{P}\mathbf{y}] = n\psi_h + \sum_{i=1}^{n}\Big(y_i \sum_{j=1}^{n} p_{ji}\Big) + \sum_{i=1}^{n}\Big(y_i^2 \sum_{j=1}^{n} p_{ij}\Big) + \sum_{i=1}^{n}\sum_{j=1}^{n} y_i y_j \Big(\frac{p_{ii} + p_{jj} + 2p_{ij}}{2}\Big) \tag{4.60}$$

Defining the vector:

$$\tilde{\mathbf{y}} = \begin{pmatrix} \psi_h \\ \\ \mathbf{y} \end{pmatrix} \in \mathbb{R}^{n+1} \tag{4.61}$$

facilitates expressing the equation (4.59) in the compact form:

$$\frac{dV_c}{dt} = \tilde{\mathbf{y}}^\top \, \mathbf{G} \, \tilde{\mathbf{y}} \tag{4.62}$$

where the matrix $\mathbf{G}$ is given by:

$$\mathbf{G} = \begin{bmatrix} \mathbf{A} & \mathbf{B} \\ \\ \mathbf{B}^\top & \mathbf{C} \end{bmatrix} \in \mathbb{R}^{(n+1)\times(n+1)} \tag{4.63}$$

and the submatrices $\mathbf{A} \in \mathbb{R},\ \mathbf{B}^\top \in \mathbb{R}^n,\ \mathbf{C} \in \mathbb{R}^{n\times n}$ by:

$$\mathbf{A} = -n \tag{4.64}$$

$$\mathbf{B} = \begin{bmatrix} -\frac{1}{2}+\frac{n}{2}\sum_{j=1}^{n} p_{j1} & \cdots & -\frac{1}{2}+\frac{n}{2}\sum_{j=1}^{n} p_{jn} \end{bmatrix} \tag{4.65}$$

$$\mathbf{C} = \begin{bmatrix} -\frac{q_{11}}{2\varepsilon_1}+\sum_{j=1}^{n} p_{1j} & \cdots & \frac{p_{11}+p_{nn}+2p_{1n}}{2} \\ \\ \vdots & \ddots & \\ \\ \frac{p_{nn}+p_{11}+2p_{n1}}{2} & \cdots & -\frac{q_{nn}}{2\varepsilon_1}+\sum_{j=1}^{n} p_{nj} \end{bmatrix} \tag{4.66}$$

Stability of $\tilde{\mathbf{y}}_0$ is established through the following theorem.

Theorem 4.1. *The equilibrium* $\tilde{\mathbf{y}}_0 = \mathbf{0}_{n+1}$ *of* (4.44a) - (4.44b) *is asymptotically stable when* $\varepsilon_1 < \overline{\varepsilon}_1$ *where,* $\overline{\varepsilon}_1 = \min\{\overline{\varepsilon}_{1,i}\}_{i\in\mathcal{G}}$ *and* $\overline{\varepsilon}_{1,i}$ *is given by:*

$$\overline{\varepsilon}_{1,i} = \frac{q_{ii}}{2\Big[\sum_{j=1}^{n} p_{ij}+\frac{1}{n}\|\mathbf{B}\|_2^2+\sum_{j=1}^{n}|-\frac{(p_{ii}+p_{jj}+2p_{ij})}{2}-\frac{1}{n}\|\mathbf{B}\|_2^2|\Big]}$$

and $p_{ij},\ q_{ij}$ *are elements of the matrices* $\mathbf{P},\ \mathbf{Q}$ *respectively.*

Proof. Asymptotic stability of $\tilde{\mathbf{y}}_0$ follows from $\mathbf{G} \prec 0$ or $-\mathbf{G} \succ 0$. In light of that, we focus next on deriving a sufficient condition under which $-\mathbf{G} \succ 0$. As we will show, this condition will be reduced to be an upper bound on the parameter ε_1. The *Schur complement* of $-\mathbf{G}$

is:

$$\mathbf{S} = -\mathbf{C} + \mathbf{B}^{\top}\mathbf{A}^{-1}\mathbf{B} \tag{4.67}$$

with the corresponding Schur complement conditions being:

$$-\mathbf{G} \succ 0 \Leftrightarrow \mathbf{S} \succ 0 \text{ and} -\mathbf{A} \succ 0 \tag{4.68}$$

Using this equivalence we will proceed to derive conditions which guarantee that $\mathbf{S} \succ 0, -\mathbf{A} \succ 0$ hold. The second inequality immediately holds as can be realized from $-\mathbf{A} = n > 0$. Hence, it is left to find a condition under which $\mathbf{S} \succ 0$ holds. By expanding (4.67), we obtain:

$$\mathbf{S} = -\mathbf{C} - \frac{1}{n}\|\mathbf{B}\|_2^2 \tag{4.69}$$

where $\|\cdot\|_2$ is the standard Euclidean norm. The matrix $\mathbf{S}$ can be written as:

$$\mathbf{S} = [s_{ij}], \quad s_{ij} = -c_{ij} - \frac{1}{n}\|\mathbf{B}\|_2^2 \tag{4.70}$$

At this point, the following matrix property can be used: *a Hermitian (symmetric) matrix with all positive eigenvalues is positive definite*. The matrix $\mathbf{S}$ is symmetric, i.e $\mathbf{S} = \mathbf{S}^{\top}$, since $\mathbf{C}$, $\mathbf{P}$ are symmetric. Therefore, it only left to find a condition which will guarantee positivity of the eigenvalues of $\mathbf{S}$. To this end, we employ the *Gershgorin's Circle Theorem* [42] which in our case gives that, the eigenvalues λ_i of $\mathbf{S}$ belong to the following set:

$$\mathcal{D} = \bigcup_{i \in \mathcal{G}} \mathcal{D}_i \tag{4.71}$$

where each subset $\mathcal{D}_i$ is given by:

$$\mathcal{D}_i \triangleq \{\chi \in \mathbb{R} : |\chi - s_{ii}| \leq \sum_{j=1, j\neq i}^{n} |s_{ij}|\}, \quad \forall i \in \mathcal{G} \tag{4.72}$$

Since $\mathbf{S}$ is symmetric, the eigenvalues $\boldsymbol{\lambda}$ are real and therefore the above subsets lie on the real axis. Further, $\mathbf{S}$ is positive definite when $\boldsymbol{\lambda}$ are also positive. To establish that, we find conditions under which the sets $\mathcal{D}_i$ become subsets of $\mathbb{R}_+$. In this direction, we start from (4.72) and derive an upper and a lower bound for the eigenvalues $\chi \in \mathcal{D}_i$ corresponding to each subset $\mathcal{D}_i$ as:

$$\underbrace{s_{ii} - \sum_{j=1}^{n} |s_{ij}|}_{\underline{\chi}_i} \leq \chi \leq \underbrace{s_{ii} + \sum_{j=1}^{n} |s_{ij}|}_{\overline{\chi}_i} \tag{4.73}$$

Then, to guarantee that $\chi > 0$ holds, the inequality $\underline{\chi}_i > 0$, $\forall i \in \mathcal{G}$ can be forced to hold. That can be achieved by first noticing from (4.70) that the diagonal elements of the matrix $\mathbf{S}$ (s_{ii}) depend explicitly on the parameter ε_1. Then, from each inequality $\underline{\chi}_i > 0$ an upper bound on ε_1, $\overline{\varepsilon}_{1,i}$, can be resulted. To compute this upper bound we start from the inequality:

$$\underline{\chi}_i > 0 \Leftrightarrow s_{ii} - \sum_{j=1}^{n} |s_{ij}| > 0$$

and substitute s_{ii} and s_{ij} from (4.70), (4.65), (4.66) to obtain:

$$\frac{q_{ii}}{2\varepsilon_1} - \Big[\sum_{j=1}^{n} p_{ij} + \frac{1}{n}\|B\|_2^2 + \sum_{j=1}^{n} \Big| -\frac{(p_{ii} + p_{jj} + 2p_{ij})}{2} - \frac{1}{n}\|B\|_2^2 \Big|\Big] > 0$$

Rearranging this inequality such that ε_1 appears on the left side leads to:

$$\varepsilon_1 < \underbrace{\frac{q_{ii}}{2\Big[\sum_{j=1}^{n} p_{ij} + \frac{1}{n}\|B\|_2^2 + \sum_{j=1}^{n}\Big|-\frac{(p_{ii}+p_{jj}+2p_{ij})}{2} - \frac{1}{n}\|B\|_2^2\Big|\Big]}}_{\bar{\varepsilon}_{1,i}}$$

The expression on the right side of this inequality corresponds to the upper limit on ε_1 for the particular subset $\mathcal{D}_i$. When the minimum of all these bounds $\bar{\varepsilon}_1 = \min\{\bar{\varepsilon}_{1,i}\}_{i\in\mathcal{G}}$ is respected, i.e $\varepsilon_1 < \bar{\varepsilon}_1$, it holds that $\mathcal{D} \subset \mathbb{R}_+$ and $\forall \chi \in \mathcal{D} \Rightarrow \chi > 0$, i.e. that the eigenvalues of $\mathbf{S}$ are positive. Equivalently, that $\mathbf{S}$ is positive definite. From the *Schur complement conditions*, it can be further concluded that $-\mathbf{G} \prec 0$ and that $\tilde{\mathbf{y}}_0 = \mathbf{0}_{n+1}$ is asymptotically stable. With this, the proof is completed. ■

The above bound provides a sufficient and not a necessary condition for asymptotic stability of $\tilde{\mathbf{y}}_0 = \mathbf{0}_{n+1}$. Nonetheless, it can be used in choosing suitable GSC control gains $k_{\alpha,i}$ that will guarantee this stability property. This can be accomplished as follows. First, for a particular positive definite diagonal matrix $\mathbf{Q}$, a corresponding matrix $\mathbf{P}$ satisfying (4.54) can be computed. Then by resorting to Theorem 4.1 a corresponding upper bound $\bar{\varepsilon}_1$ can be explicitly computed. Eventually, a specific value for the gains $k_{\alpha,i}$ can be chosen which satisfies $(1/k_{\alpha,i}) < \bar{\varepsilon}_1$ and guarantees asymptotic stability of $\tilde{\mathbf{y}}_0 = \mathbf{0}_{n+1}$ through Theorem 4.1.

4.9.3 Stability of the Storage Power Dynamics

Having established stability of the consensus protocol dynamics (4.44a),(4.44b), we proceed to establish stability of the storage power dynamics:

$$\varepsilon_2 \frac{d\eta_i}{dt} = -\eta_i, \quad \forall i \in \mathcal{G} \tag{4.74}$$

via the next Lemma.

Lemma 4.4. *The equilibrium $\boldsymbol{\eta}_0 = \mathbf{0}_n$ of the storage power dynamics (4.74) is asymptotically* *stable.*

A candidate Lyapunov function for this system is the function:

$$V_\eta = \|\boldsymbol{\eta}\|_2^2, \;\; V_\eta > 0, \;\; \forall \boldsymbol{\eta} \in \overline{\mathcal{D}}_\eta \tag{4.75}$$

where $\overline{\mathcal{D}}_\eta = \mathcal{D}_\eta \backslash \mathbf{0}_n, \;\; \mathcal{D}_\eta \subseteq \mathbb{R}^n$. Along the trajectories of the system (4.74), the derivative of V_η is:

$$\dot{V}_\eta = -\frac{2}{\varepsilon_2}\|\boldsymbol{\eta}\|_2^2, \;\; \dot{V}_\eta < 0, \;\; \forall \boldsymbol{\eta} \in \overline{\mathcal{D}}_\eta \tag{4.76}$$

Applying *Lyapunov's stability theorem* results to V_η being a Lyapunov function and $\boldsymbol{\eta}_0 = \mathbf{0}_n$ an asymptotically stable equilibrium point.

4.9.4 Stability of the Full Consensus Protocol & Storage System

The consensus protocol and storage power subsystems appear decoupled in the transformed state-space (4.44a)-(4.44c). Here, this is leveraged by deploying the already established stability properties for these subsystems to infer stability of the full system comprised of the protocol and storage power dynamics through the next Theorem.

Theorem 4.2. *The equilibrium $\bar{\boldsymbol{\phi}}_0 = \mathbf{0}_{2n+1}$ of the full consensus protocol and storage power output system (4.44a)-(4.44c) is asymptotically stable for $\varepsilon_1 < \overline{\varepsilon}_1$ where, $\overline{\varepsilon}_1$ is the upper bound stated in Theorem 4.1.*

Proof. Intuitively, a candidate Lyapunov function for the full system can be defined as:

$$V_{full} = V_c + V_\eta, \;\; V_{full} > 0, \;\; \bar{\boldsymbol{\phi}} \in \overline{\mathcal{D}}_{\bar{\phi}} \tag{4.77}$$

where $\overline{\mathcal{D}}_{\bar{\phi}} = \mathcal{D}_{\bar{\phi}} \backslash \{\mathbf{0}_{2n+1}\},\ \ \mathcal{D}_{\bar{\phi}} \subseteq \mathbb{R}^{2n+1}$. The time-derivative of V_{full} is:

$$\dot{V}_{full} = \dot{V}_c + \dot{V}_\eta = \tilde{\mathbf{y}}^\top \mathbf{G} \tilde{\mathbf{y}} - \frac{2}{\varepsilon_2} \|\boldsymbol{\eta}\|_2^2 \tag{4.78}$$

Recall that, $\mathbf{G} \prec 0$ when $\varepsilon_1 < \bar{\varepsilon}_1$ (Theorem 4.1). such that:

$$\dot{V}_{full} < 0,\ \ \forall \bar{\boldsymbol{\phi}} \in \overline{\mathcal{D}}_{\bar{\phi}},\ \ \forall \varepsilon_1 < \bar{\varepsilon}_1 \tag{4.79}$$

From Lyapunov's stability theorem, it can be concluded that $\bar{\boldsymbol{\phi}}_0 = \mathbf{0}_{2n+1}$ is asymptotically stable. This completes the proof. ■

The intuition behind the above results is that stability of the coupled consensus protocol and storage power output system is certified when the GSC gains (consensus protocol's gains) respect the inequality $\varepsilon_1 < \bar{\varepsilon}_1$ (Theorem 4.1). That being the case, provable WF power output regulation and asymptotic consensus on the variables $\mathbf{z}$ will be reached. On the other hand, the role of the DC-DC converters is to shape the closed-loop storage power dynamics such that they are identical to the dynamics in (4.20). When that is secured, the storage power outputs $\mathbf{x}$ will be provably regulated to the consensus state-variables $\mathbf{z}$, i.e $\lim_{t\to\infty} \boldsymbol{\eta} = \mathbf{0}_n \Rightarrow \lim_{t\to\infty} \mathbf{x} = \mathbf{z}$, as long as the control gains $k_{2,i}$ are positive. This has the implication that the variables $\mathbf{x}$ will also reach consensus through tracking of the variables $\mathbf{z}$. Albeit tracking will be attained as long as the gains $k_{2,i}$ are positive, ideally, high enough gains $k_{2,i}$ should be chosen so that the storage power regulation occurs much faster than the consensus on the variables $\mathbf{z}$. In this case, consensus on the variables $\mathbf{z}$ will directly lead to consensus on the variables $\mathbf{x}$.

Corollary 4.1. *When $\varepsilon_1 < \bar{\varepsilon}_1$, the GSC-controlled power variables $\mathbf{z}$ will reach consensus on the vector $[\frac{P_d - \sum_{i=1}^n (P_{e,i} + P_{r,i})}{n}] \cdot \mathbf{1}_n$ and the total WF power ($\sum_{i=1}^n P_{e,i} + P_{g,i}$) will be regulated to P_d (WF power output regulation). Additionally, the storage power outputs $\mathbf{x}$ will also reach* *consensus on the vector* $[\frac{P_d - \sum_{i=1}^{n}(P_{e,i}+P_{r,i})}{n}]\cdot\mathbf{1}_n$ *(fair load-sharing among the storage devices).*

Proof. It follows directly from Theorem 4.1 that $\mathbf{z}$ reach consensus on $(\xi_{h0}\cdot\mathbf{1}_n)$. Fulfillment of the WF power output regulation objective can be realized by considering the total WF power as:

$$\begin{aligned} P_{WF,tot} &= \sum_{i=1}^{n}(P_{e,i}+P_{g,i}) \\ &= \sum_{i=1}^{n}(P_{e,i}+P_{r,i}+\underbrace{P_{g,i}-P_{r,i}}_{z_i}) \\ &= \sum_{i=1}^{n}(P_{e,i}+P_{r,i}+z_i) \end{aligned} \tag{4.80}$$

Taking limits on both sides yields:

$$\lim_{t\to\infty} P_{WF,tot} = \lim_{t\to\infty}\sum_{i=1}^{n}\Big(P_{e,i}+P_{r,i}+n[\frac{P_d - \sum_{i=1}^{n}(P_{e,i}+P_{r,i})}{n}]\Big) \tag{4.81}$$

$$= P_d \quad (\textbf{WF power output regulation}) \tag{4.82}$$

Moreover, that the storage power outputs will also reach consensus follows directly from Lemma 4.4 which certified that:

$$\begin{aligned} \lim_{t\to\infty}\mathbf{x} &= \lim_{t\to\infty}\mathbf{z} \\ &= (\xi_{h0}\cdot\mathbf{1}_n) \ \ (\textbf{Consensus among storage power outputs}) \end{aligned} \tag{4.83}$$

Equivalently, that fair load-sharing among the storage devices will be reached. ■

4.10 Design of the Controllers

We now proceed to design the controllers for the GSC and the DC-DC converter which respectively realize the closed-loop consensus protocol and storage power output dynamics.

4.10.1 Design of the GSC Controller

The control objective of the GSC is to shape the physical closed-loop dynamics of z_i so that they are identical to the consensus protocol dynamics $\dot{z}_i$. These physical dynamics can be derived as:

$$\dot{z}_i = (\dot{P}_{g,i} - \dot{P}_{r,i}), \quad \forall i \in \mathcal{G} \tag{4.84}$$

where $P_{g,i}$ is the power output of the GSC:

$$P_{g,i} = I_{dg,i} V_{s,i}, \quad \forall i \in \mathcal{G} \tag{4.85}$$

Now, let the following assumptions to be true.

Assumption 2. *$dP_{r,i}/dt = 0,\ dV_{s,i}/dt = 0,\ \ \forall i \in \mathcal{G}$.*

Intuitively, these assumptions can be justified by the fact that the power output of the RSC ($P_{r,i}$) and the terminal voltage ($V_{s,i}$) vary in a much slower time-scale than that of the $\dot{z}_i$ dynamics. Thus, they can be considered as being constant in the time-scale of the $\dot{z}_i$ dynamics. By deploying equation (4.85) and under these assumptions, equation (4.84) can be expanded as:

$$\dot{z}_i = V_{s,i}\Big[-\omega_s\Big(\frac{R_{g,i}}{L_{g,i}}\Big)I_{dg,i} + \omega_s I_{qg,i} + \omega_s\Big(\frac{V_{dg,i} - V_{s,i}}{L_{g,i}}\Big)\Big], \ \ \forall i \in \mathcal{G} \tag{4.86}$$

The control input of the GSC is represented by the term $V_{dg,i}$. Lastly, the closed-loop physical dynamics of z_i match the consensus protocol dynamics (4.15c) with the *distributed GSC control law*:

$$V_{dg,i} = \Big(\frac{-k_{\alpha,i}(z_i - z_{i-1})}{V_{s,i}} + \omega_s\Big(\frac{R_{g,i}}{L_{g,i}}\Big)I_{dg,i} - \omega_s I_{qg,i}\Big)\frac{L_{g,i}}{\omega_s} + V_{s,i}$$

$\forall i \in \mathcal{G}$ and where $z_0 \triangleq \xi_h$. This controller is pictorially represented in Fig 4.2.

4.10.2 Design of the Storage Controller

The control objective of the DC-DC converter is to shape the physical closed-loop dynamics of the interfacing capacitor to the ones given by equation (4.17). Next, we provide more insight on the particular choice of the closed-loop capacitor dynamics by showing how these can be analytically derived from a CLF to lead asymptotic stability of $\Delta E_{dc,i}$. First, consider the related candidate CLF function $\mathcal{V}_{dc,i} : \mathbb{R} \mapsto \mathbb{R}$ as:

$$\mathcal{V}_{dc,i} = \frac{1}{2}\Delta E_{dc,i}^2, \qquad \forall i \in \mathcal{G} \tag{4.87}$$

and the corresponding lemma.

Lemma 4.5. *$\mathcal{V}_{dc,i}$ is a CLF for the system* (4.18).

Proof. The derivative of $\mathcal{V}_{dc,i}$ can be computed as:

$$\dot{\mathcal{V}}_{dc,i} = \Delta E_{dc,i}(P_{r,i} - P_{g,i} + \frac{(u_{sc,i} - V_{sc,i})V_{sc,i}}{R_{sc,i}}) \tag{4.88}$$

Taking the $\mathbf{inf}(\cdot)$ on both sides of (4.88) and assuming that the DC voltage of the supercapacitor lies in a domain $V_{sc,i} \in (0, \overline{V}_{sc,i}]$, yields:

$$\mathbf{inf}\,\dot{\mathcal{V}}_{dc,i} = \begin{cases} -\infty, & \Delta E_{dc,i} \neq 0 \\ 0, & \Delta E_{dc,i} = 0 \end{cases} \tag{4.89}$$

The bilateral relation (4.89) certifies that $\mathcal{V}_{dc,i}$ is a CLF and that there exists a control law $V_{dg,i}$ for the DC-DC converter that renders $\Delta E_{dc0,i} = 0$ asymptotically stable. ■

A control law $V_{dg,i}$ can be constructed by imposing the inequality:

$$\dot{V}_{dc,i} < 0, \quad \Delta E_{dc,i} \neq 0, \quad \forall i \in \mathcal{G} \tag{4.90}$$

to hold along the dynamics of $\Delta E_{dc,i}$. This can be realized by enforcing a constraint on the capacitor dynamics of the form:

$$(P_{r,i}+P_{st,i}-P_{g,i}) = -k_{2,i}(\Delta E_{dc,i}) \tag{4.91}$$

Notice that, this constraint will lead to the desired closed-loop capacitor dynamics in (4.17) which are chosen so that:

$$\dot{V}_{dc,i} = -k_{2,i}\Delta E_{dc,i}^2 < 0, \;\; \forall \Delta E_{dc,i} \neq 0, \;\; \forall i \in \mathcal{G}. \tag{4.92}$$

i.e so that $\Delta E_{dc0,i} = 0$ becomes asymptotically stable. Finally, the control law for the DC-DC converter can be derived from equation (4.91) as:

$$u_{sc,i} = \Big(P_{g,i}-P_{r,i}-k_{2,i}\Delta E_{dc0,i}\Big)\frac{R_{sc,i}}{V_{sc,i}}+V_{sc,i}, \qquad \forall i \in \mathcal{G} \tag{4.93}$$

This controller is depicted in Fig. 4.3.

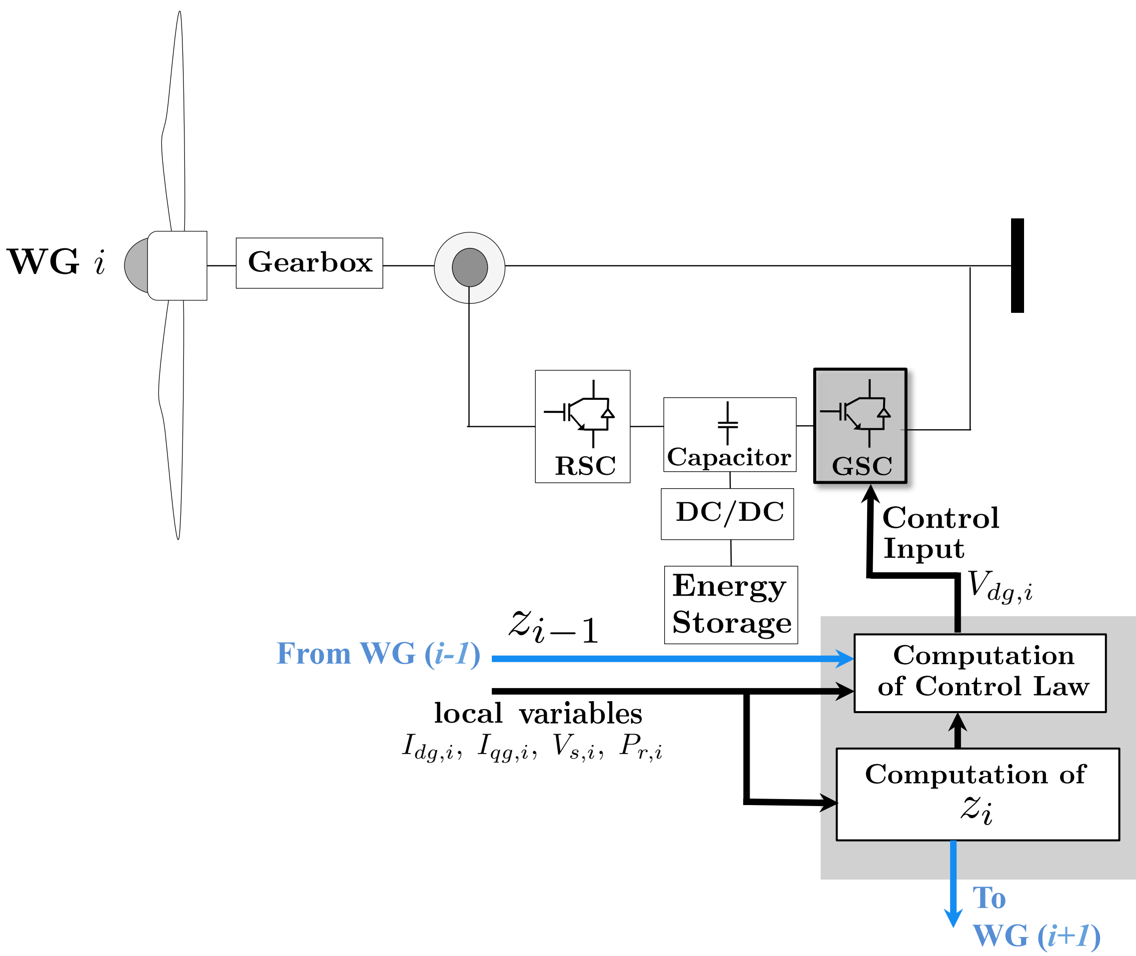

Figure 4.2: Distributed GSC controller

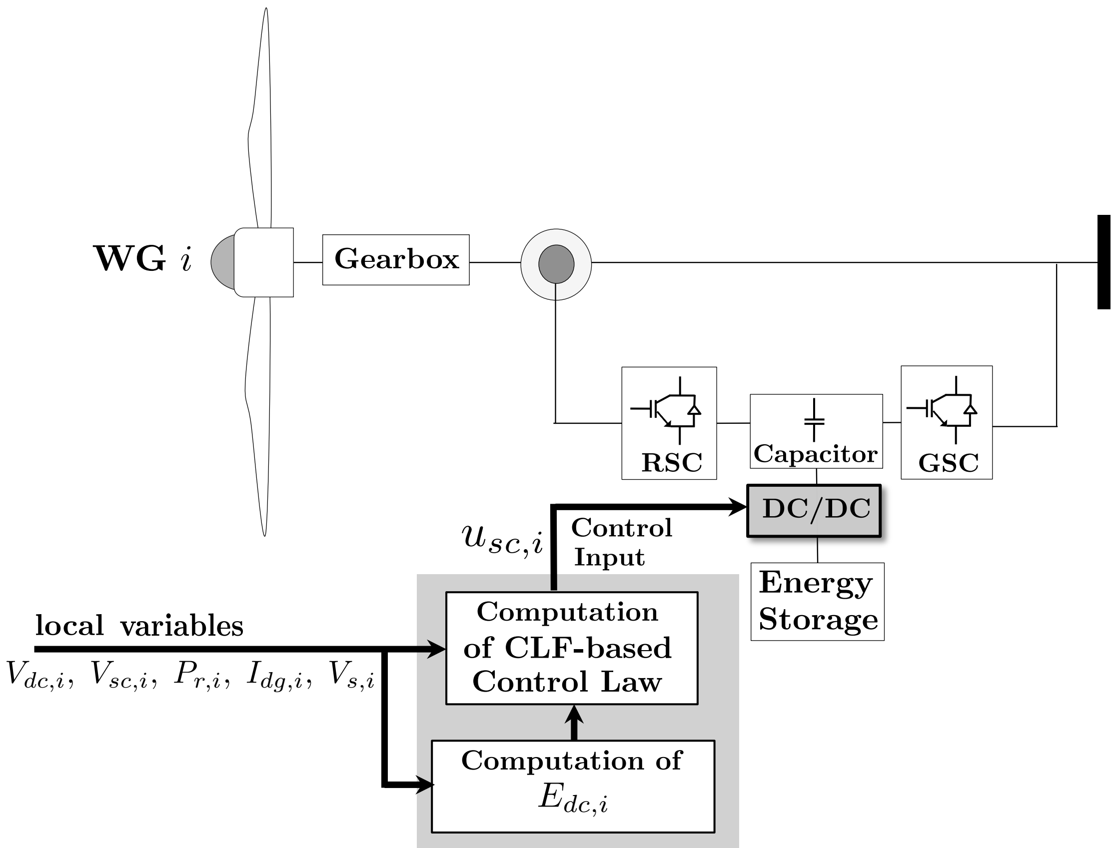

Figure 4.3: Storage controller

4.11 Case Studies

The theoretical results presented will now be numerically verified through simulations. In particular, we evaluate the performance of the proposed controllers and corresponding consensus protocol and closed-loop interfacing capacitor dynamics on solving the problem of WF power output regulation with fair load-sharing of the storage power outputs. For this purpose, a modified version of the IEEE 24-bus reliability test system is adopted where, at bus 22, a WF comprised of 10 SoA WGs with supercapacitor energy storage devices is placed. The physical and communication topologies are depicted in Fig. 4.1a, 4.1b. The GSCs and DC-DC converters of the WGs are controlled according to the distributed control law (4.87) and the CLF-based control law (4.93), respectively. The simulations are conducted under the following two critical scenarios.

Scenario 1: The WF power reference P_d varies in a step-wise manner as shown in Fig. 4.4a.

Scenario 2: The WF power reference P_d is constant.

Observe from Fig. 4.4a that, the distributed controllers for the GSCs and the CLF-based controllers for the storage controllers are able to attain WF power reference tracking with good performance as the total WF power is rapidly and closely tracking the fast-varying reference without exhibiting an overshoot.

Proceeding to Fig. 4.4b, we realize that the GSCs regulate their power outputs according to the proposed protocol and in response to the reference changes causing in that way their corresponding z_i variables to dynamically respond. These variables manifest indistinguishable dynamical responses throughout their trajectories since, at any point on their trajectory (Fig.4.4b) they rapidly reach consensus and converge to the variable ξ_h which is quasistatic. In the slow time-scale, this variable converges to the equilibrium ξ_{h0} (which depends on P_d) driving the variables $\mathbf{z}$ to the equilibrium ξ_{h0}. Particularly, these slower dynamics are depicted in Fig. 4.4b where the variables $\mathbf{z}$ and ξ_h are together driven to the quasistatic equilibrium ξ_{h0} while they already reached consensus between each other.

From Fig. 4.5a, it can be observed that the responses of the variables $\mathbf{x}$ are one-to-one identical to the responses of the variables $\mathbf{z}$ while they are also indistinguishable between them throughout their trajectories. This can be explained as follows. The CLF-based controllers for the DC-DC converters regulate the storage power outputs $\mathbf{x}$ to their corresponding $\mathbf{z}$ in order to continuously meet the power demands of the GSCs, needed to attain WF power output regulation. Through that, the storage power outputs $\mathbf{x}$ eventually reach consensus as well, carrying out in that way the fair load-sharing objective.

In Scenario 2, it can be observed from Fig. 4.6b that the total WF power output regulation is also accomplished with good performance with the WF power output being almost constant. To accomplish that, both the GSC-controlled variables $\mathbf{z}$ and the storage power outputs $\mathbf{x}$ are dynamically varying while reaching consensus at every point of their trajectories as depicted in Fig. 4.7a and Fig. 4.7b, respectively. Therefore, the GSCs and the DC-DC converters succeeded in regulating the WF power output with the storage devices being deployed under a fair load-sharing regime.

In conclusion, the proposed distributed GSC controllers and CLF-based storage controllers effectively carried out the WF power output regulation objective with fair utilization of the storage devices by correspondingly realizing the closed-loop protocol and capacitor dynamics.

4.12 Conclusion

In this Chapter, a distributed control design for SoA WGs with energy storage devices is introduced. The proposed control design can be adopted by a group of SoA WGs to attain WF power output regulaton by deploying their storage devices in a fair load-sharing manner. It is built upon a consensus protocol and a desired form for the closed-loop capacitor dynamics, realized by a distributed control law for the GSCs and a CLF-based control law for the DC-DC converters. We combined singular perturbation and Lyapunov theories to perform compositional stability analysis of the closed-loop dynamics and ultimately derive a condition under which asymptotic stability of their equilibrium is guaranteed. Finally, both the GSC's distributed control law that realizes the protocol with peer-to-peer communication and the DC-DC converter's control law that realizes the desired closed-loop capacitor dynamics are analytically derived. The performance of the controllers and the validity of the results are numerically tested and assessed via simulations on a modified version of the IEEE 24-bus RTS system.

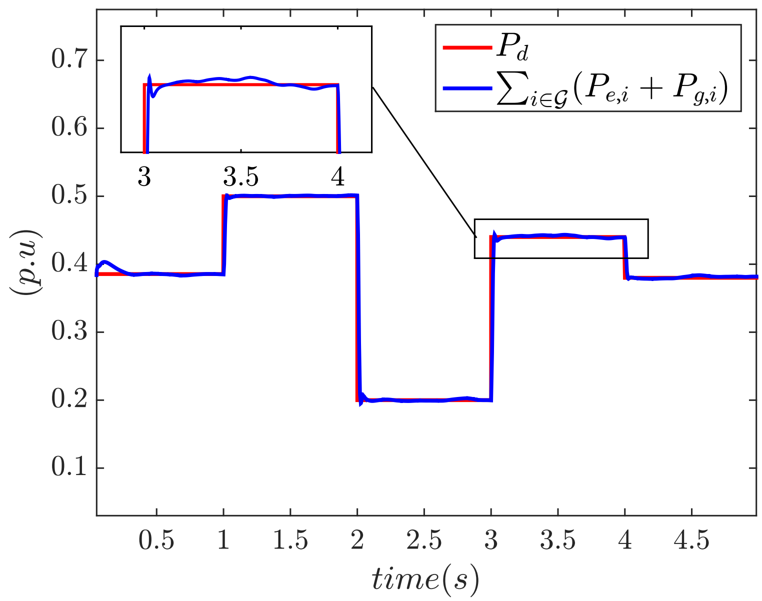

(a)

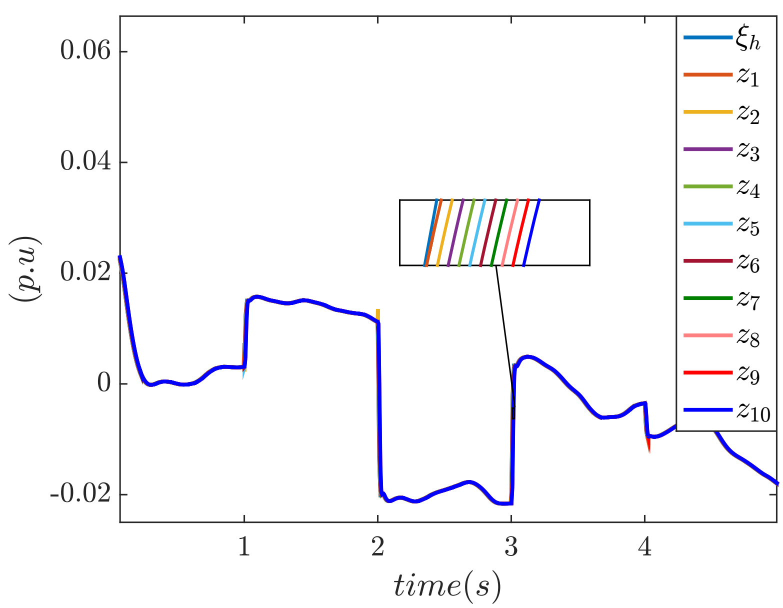

(b)

Figure 4.4: **Scenario 1** a) Total WF power output (*blue*) and reference (*red*), b) Consensus state-variables z_i

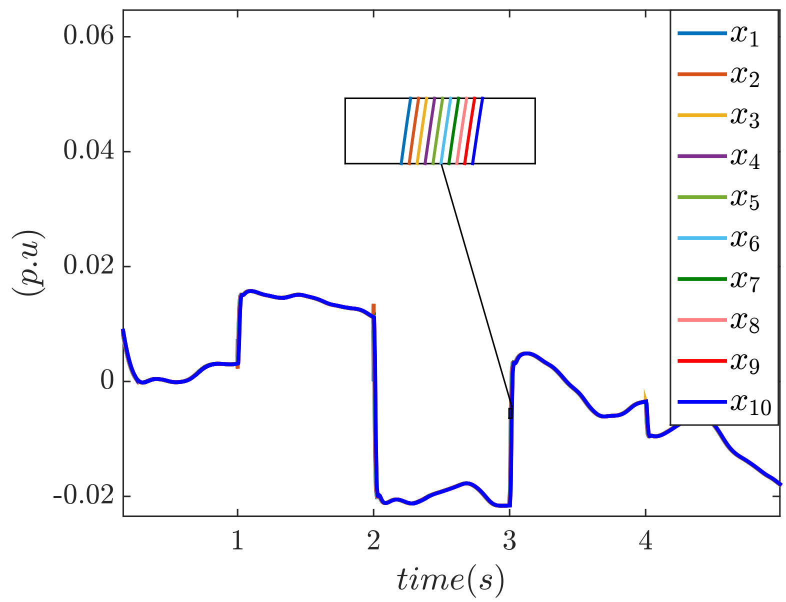

(a)

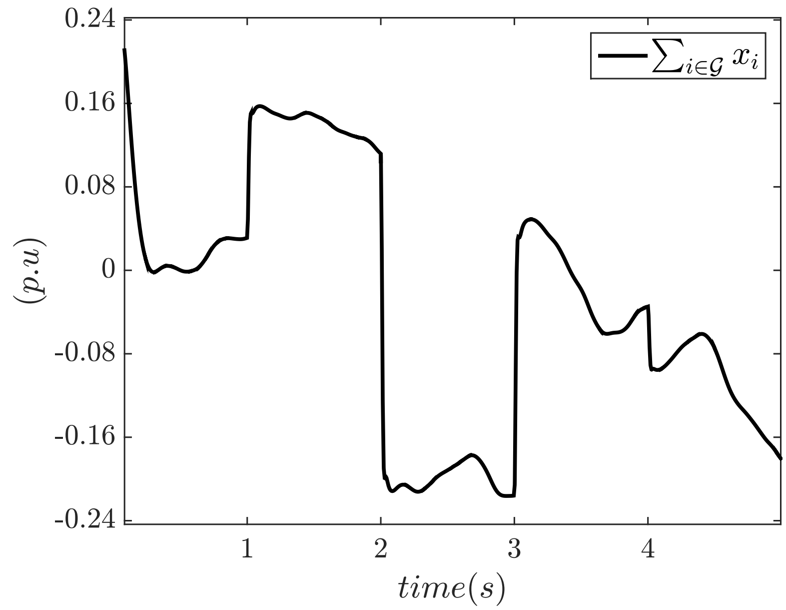

(b)

Figure 4.5: **Scenario 1** a) Storage power outputs x_i, b) Total storage power $\sum_{i\in\mathcal{G}} x_i$

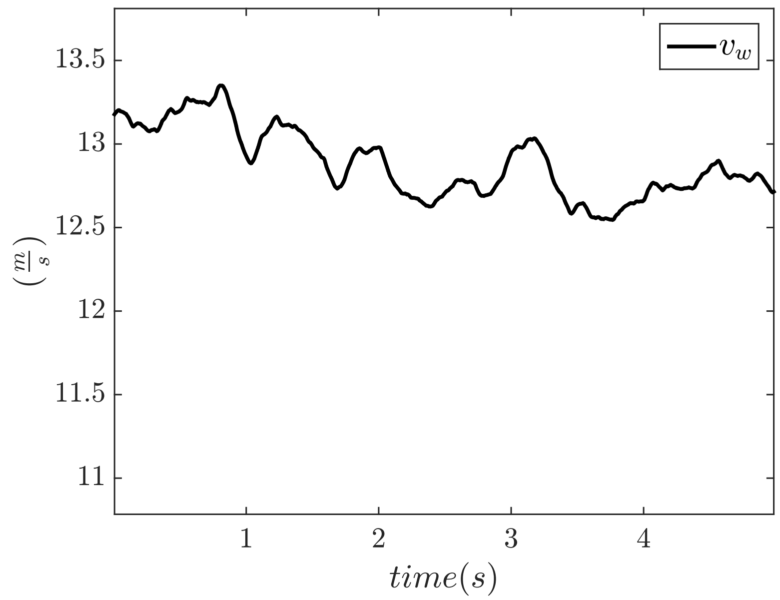

(a)

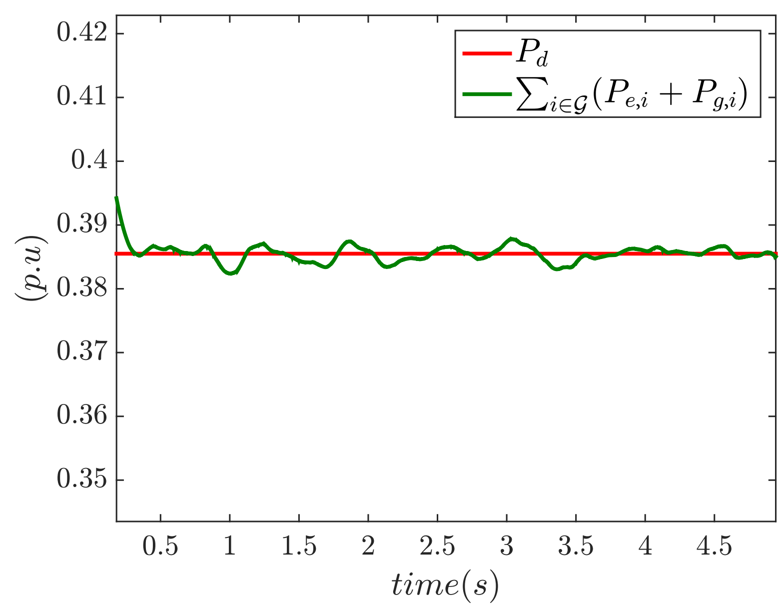

(b)

Figure 4.6: **Scenario 2** a) Wind speed v_w, b) Total WF power output

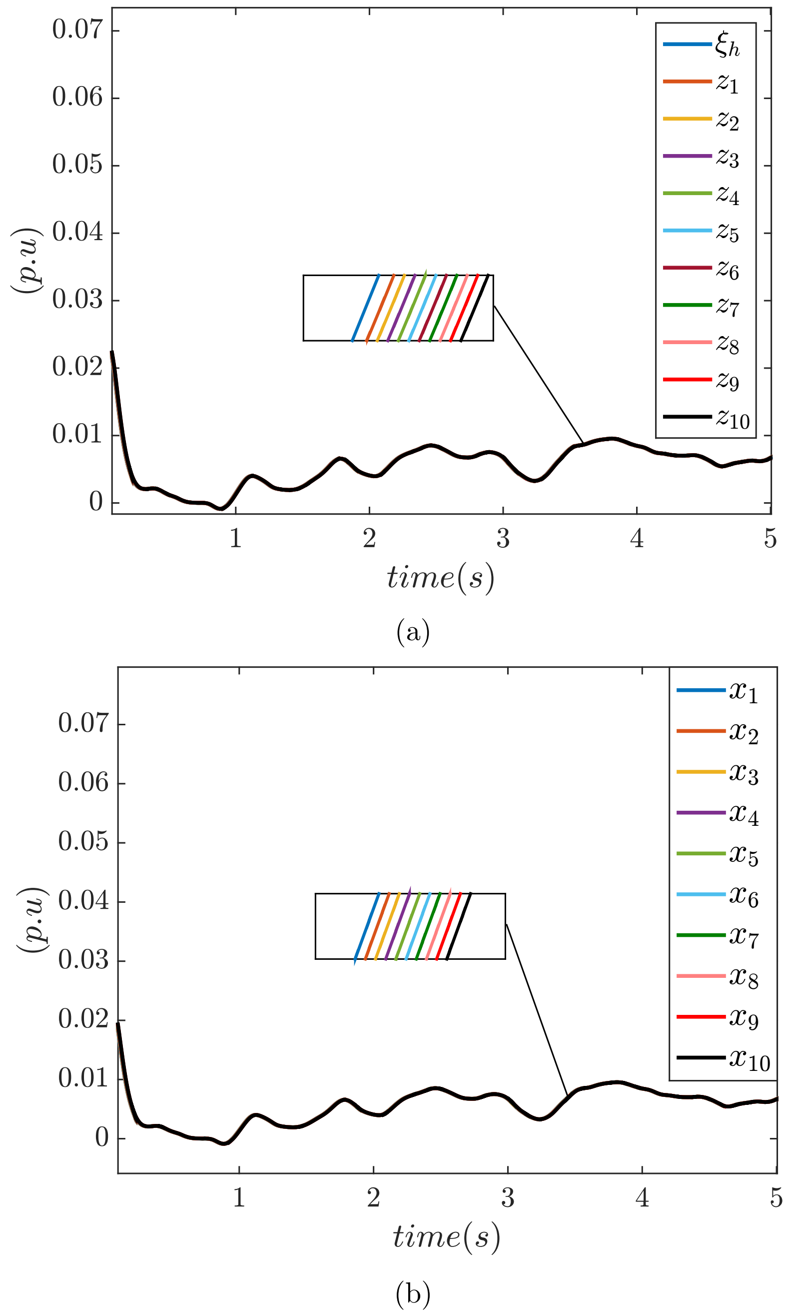

Figure 4.7: **Scenario 2** a) Consensus state-variables z_i, b) Storage power outputs x_i

Chapter 5

Distributed Torque Control of Deloaded Wind Generators

5.1 Introduction

As already discussed in previous chapters, one of the most critical capabilities that wind generators (WGs) are required to provide is predictable total power output at the wind farm (WF) level. WGs can distributively attain this through total power output regulation with limited communication among each other. In the previous chapter, we introduced a distributed control methodology for a group of DFIGs with storage which exploit peer-to-peer communication and harness their storage devices to attain total power output regulation [18]. These WGs are considered to be the State-of-the-Art (SoA) WGs and are currently under commercialization by General Electric (GE) [7]. However, nowadays, the majority of WGs that are operating worldwide are wind DFIGs that lack any kind of storage device, simply called wind DFIGs. Thus, it is also highly significant to develop distributed control designs for this type of WGs to realize WF power output regulation.

DFIGs can regulate their power output to meet a total power reference, i.e provide predictable power, when they operate under the so called deloading strategy, extracting wind power that is less than the maximum possible for specific wind speed conditions [29]. By operating in this mode, WGs retain some operating reserve and have the flexibility to raise their power outputs on command. In fact, a group of DFIGs having this flexibility can provide many services to the grid, directly related to real power control, e.g primary frequency control, inertial response, secondary frequency regulation [43].

For a group of DFIGs operating under a deloading mode to attain WF power output regulation, their individual power set-points have to be computed first. These power set-points can be computed by combining the information about the total WF power reference and the varying local wind speed conditions. Eventually, they have to be communicated to the WGs. This process is known as *dispatching of WGs*.

The traditional approach for dispatching WGs is by employing centralized control schemes. Centralized schemes presume that initially, local information, such as wind speed, is communicated to a central controller. Subsequently, the central controller deploys this information and knowledge of the total WF power output reference to compute the individual power set-points and transmit them to the WGs. Lastly, the local controller of each WG regulates its power output to the referenced power given by the power set-point [15].

In general, centralized control approaches carry several drawbacks which can compromise a timely, robust and efficient WG dispatching under highly dynamic conditions. Therefore, the real challenge in dispatching DFIGs is to obtain their power set-points timely, robustly and efficiently: timely, since in the future, WGs will have to respond and control their power output rapidly to maintain power balance between supply and demand, especially in microgrid settings; robustly, such that the performance of a group of WGs is also reliable and efficiently, such that the dispatching of WGs is cost-effective and can be realized in a fast time-scale, particularly when the number of WGs that has to be dispatched is very large.

In this chapter we effectively tackle this challenge by solving the problem of dispatching and controlling a group of deloaded WGs according to a designated total WF power reference and the local wind speed conditions, in a timely, robust and computationally efficient fashion.

Our main contribution is a distributed torque control scheme that can be adopted by a group of deloaded DFIGs to provide total power output regulation, i.e predictable power output, through dynamic adjustment of their power outputs in a fair load sharing manner. With the term dynamic adjustment, we refer to WGs continuously self-organizing and regulating their power outputs by driving them to dynamic power set-points that depend on the varying dynamical conditions. In particular, on the local wind-speed conditions and the total power reference which here are assumed to be quasistatic. On the other hand, with fair load sharing we refer to the WGs controlling their power outputs so that their loading (or utilization) levels reach a common value in steady state. In our case, the loading level of a WG is defined as the ratio of its mechanical power over its maximum mechanical power [19].

5.2 Related Work

We review the literature concerned with the problem of distributed dispatch and control of DFIGs, already discussed in the introduction of the thesis. This is summarized in the references [13] and [14]. In [13], a multi agent systems-based (MAS) control strategy for wind DFIGs in a microgrid is proposed. Each bus is assumed to have an agent which is allowed to exchange a particular information pattern with its two neighbor agents, as defined by two consensus protocols. In this way, each agent can retrieve the ratio defined by the total demand over the total available wind power in a distributed fashion. Subsequently, this information can be used by each DFIG to compute its set-point. A drawback of this method is that it is not dynamic. In more detail, the set-points are computed and communicated to the respective controllers at discrete time instants and not continuously, as the system conditions vary. Since the process that is characterized by the WGs receiving and implementing their power set-points evolves in a slow time-scale, power output regulation will also evolve in a slow time-scale. In settings where DFIGs are required to control their power outputs rapidly under highly dynamical fast-varying conditions, e.g in microgrids, they may not be able to respond timely with this control method. Reference [14] introduces a centralized and a distributed controller for WGs operating in a deloaded mode. Both controllers aim to regulate the set-points of the individual WGs such that the fatigue on wind turbines is minimized and at the same time a total power demand is met. In this work, linear WG models are considered therefore, regulation of the power set-points has performance guarantees close to the operating point around which the linear model is valid. This significantly bounds the operating region in which the power set-points can provably attain certain control objectives, with this approach having no guarantees in cases where the power set-points have to vary in a wide-range of operating conditions.

To the best of our knowledge, [13] and [14] are the only references that presented distributed methods for dispatching and controlling deloaded WGs according to a total power demand. Since the rotor-speed and the capacitor dynamics of wind DFIGs are highly nonlinear, the controllers proposed in the above references can only provide a limited range of capabilities.

In contrast with the control schemes proposed in [13] and [14], we introduce a distributed nonlinear control design. The proposed design enables deloaded WGs to dynamically and continuously self-dispatch and regulate their power outputs by tracking dynamic set-points with guaranteed performance for a wide-range of operating conditions.

5.3 Wind Generator Model

In this Chapter, control of the rotor-side dynamics will be considered. Thus, the dynamical models related to this part are restated next for completeness. These models are the rotor-voltages dynamical model with the RSC control input and the rotor-speed dynamical model of each WG. The set of deloaded WGs is denoted by $\mathcal{G} \triangleq \{1, ..., n\}$ and each WG is indexed by i so that $i \in \mathcal{G}$. The rotor-side dynamics of the wind DFIG can be fully described by three differential equations [5, 31].

5.3.1 Internal Rotor Voltages Dynamical Model

Two equations describe the dynamics of the rotor-voltage components, expressed as [5]:

$$\dot{E}'_{d,i} = \frac{1}{T'_{0,i}}\Big[-(E'_{d,i}-(X_{s,i}-X'_{s,i})I_{qs,i})+T'_{0,i}(-\omega_s\frac{X_{m,i}}{X_{r,i}}V_{qr,i}+(\omega_s-\omega_{r,i})E'_{q,i})\Big], \quad i \in \mathcal{G} \tag{5.1a}$$

$$\dot{E}'_{q,i} = \frac{1}{T'_{0,i}}\Big[-(E'_{q,i}+(X_{s,i}-X'_{s,i})I_{ds,i})+T'_{0,i}(\omega_s\frac{X_{m,i}}{X_{r,i}}V_{dr,i}-(\omega_s-\omega_{r,i})E'_{d,i})\Big], \quad i \in \mathcal{G} \tag{5.1b}$$

The rotor-voltage dynamics are given in a $d-q$ coordinate system where, d is the axis that is aligned with the terminal voltage phasor vector and, q is the axis that is orthogonal to d.

5.3.2 Rotor Speed Dynamical Model

The third dynamical equation describes the rotor-speed dynamics and is given by:

$$\dot{\omega}_{r,i} = \frac{\omega_s}{2H_i}(T_{m,i}-T_{e,i}), \qquad i \in \mathcal{G} \tag{5.1c}$$

where the mechanical torque can be written analytically as:

$$T_{m,i} \triangleq \frac{1}{2}\frac{\rho\pi R_i^2\omega_s}{S_{b,i}\omega_{r,i}}C_{p,i}(\lambda_i,\theta_i)v_{w,i}^3\ , \qquad i \in \mathcal{G} \tag{5.1d}$$

The power coefficient $C_{p,i}$ can be expressed in terms of the pitch angle θ_i and tip-speed λ_i as [5]:

$$C_{p,i}(\lambda_i,\theta_i) \triangleq 0.22\Big[116(\frac{1}{\lambda_i+0.08\theta_i}-\frac{0.035}{\theta_i^3+1})\Big]\cdot \mathrm{e}^{\left(-12.5(\frac{1}{\lambda_i+0.08\theta_i}-\frac{0.035}{\theta_i^3+1})\right)}, \qquad i \in \mathcal{G} \tag{5.1e}$$

Further, the tip-speed can be written in terms of the rotor speed and wind speed as [5]:

$$\lambda_i \triangleq \frac{2k_i}{p_i}\frac{\omega_{r,i}R_i}{v_{w,i}}\ , \quad i \in \mathcal{G} \tag{5.1f}$$

By focusing on the last three equations, it can be realized that the RSC can adjust the mechanical torque $T_{m,i}$ by controlling the rotor speed $\omega_{r,i}$ and through that the power coefficient $C_{p,i}$.

5.3.3 Dynamical Models of C_p and P_m

At this point, it is critical to derive the dynamical models of the power coefficient $C_{p,i}$ and the mechanical power $P_{m,i}$ and discuss their inderdependency. These constitute the main models that will be studied throughout this chapter. In our analysis the pitch angle is not considered controllable but constant and equal to zero. Given that, the dynamical model of the variable $C_{p,i}$ can be derived by applying the chain rule as:

$$\frac{dC_{p,i}}{dt} = \frac{\partial C_{p,i}}{\partial \lambda_i}\frac{\partial \lambda_i}{\partial \omega_{r,i}}\frac{\partial \omega_{r,i}}{\partial t} \tag{5.2}$$

The individual terms involved in the above expression are given by:

$$\frac{\partial C_{p,i}}{\partial \lambda_i} = 0.22\Big[116(\frac{-1}{\lambda_i^2})\Big]\cdot e^{\left(-12.5(\frac{1}{\lambda_i}-0.035)\right)} + 0.22\Big[116(\frac{1}{\lambda_i}-0.035)\Big]\cdot e^{\left(-12.5(\frac{1}{\lambda_i}-0.035)\right)}\frac{12.5}{\lambda_i^2} \tag{5.3}$$

$$\frac{\partial \lambda_i}{\partial \omega_{r,i}} = \frac{2k_iR_i}{p_iv_{w,i}} \tag{5.4}$$

while the dynamics of the rotor speed $\omega_{r,i}$ are given in (5.1c). By substituting the terms (5.3), (5.4) and (5.1c) into the equation (5.2), we finally obtain the dynamics of $C_{p,i}$ as:

$$\begin{aligned}\frac{dC_{p,i}}{dt} &= 0.22\Big[116(\frac{-1}{\lambda_i^2})\Big]\cdot e^{\left(-12.5(\frac{1}{\lambda_i}-0.035)\right)} + 0.22\Big[116(\frac{1}{\lambda_i}-0.035)\Big]\cdot e^{\left(-12.5(\frac{1}{\lambda_i}-0.035)\right)}\frac{12.5}{\lambda_i^2}\cdot\frac{2k_iR_i}{p_iv_{w,i}} \\ &\quad \cdot\frac{\omega_s}{2H_i}\Big(\frac{1}{2}\frac{\rho\pi R_i^2\omega_s}{S_{b,i}\omega_{r,i}}v_{w,i}^3C_{p,i} - T_{e,i}\Big)\end{aligned} \tag{5.5}$$

In the forthcoming analysis, $C_{p,i}$ is going to be one of the state-variables whose physical dynamics in (5.5) have to be shaped through appropriate control design. Alternatively, the mechanical power $P_{m,i}$ could be used as a state-variable where its dynamics can be explicitly derived from the dynamics of $C_{p,i}$. To this end, the wind speed is considered to be a slow-varying variable, i.e a quasistatic variable, such that the dynamics of $P_{m,i}$ are driven completely by the dynamics of $C_{p,i}$. This is substantiated by the fact that $C_{p,i}$ can vary much faster than the wind speed $v_{w,i}$. Under this assumption, the dynamical equation of $P_{m,i}$ can be expressed as:

$$\frac{dP_{m,i}}{dt} = \frac{1}{2}\rho A_i v_{w,i}^3 \frac{dC_{p,i}}{dt} \tag{5.6}$$

Utilizing (5.5), this can be further expanded as:

$$\frac{dP_{m,i}}{dt} = \frac{1}{2}\rho A_i v_{w,i}^3 0.22\Big[116(\frac{-1}{\lambda_i^2})\Big]\cdot \mathrm{e}^{\left(-12.5(\frac{1}{\lambda_i}-0.035)\right)} + 0.22\Big[116(\frac{1}{\lambda_i}-0.035)\Big]\cdot \mathrm{e}^{\left(-12.5(\frac{1}{\lambda_i}-0.035)\right)}\frac{12.5}{\lambda_i^2} \cdot\frac{2k_i R_i}{p_i v_{w,i}}\cdot\frac{\omega_s}{2H_i}(\frac{P_{m,i}}{S_{b,i}\omega_{r,i}} - T_{e,i}) \tag{5.7}$$

It is important to realize from (5.6) that, $dP_{m,i}/dt$ is linearly dependent on $dC_{p,i}/dt$. Thus, there is only one degree of freedom in controlling the dynamical equations $dP_{m,i}/dt$ and $dC_{p,i}/dt$, i.e only one of these equations can be independently altered. In our analysis, equation $dC_{p,i}/dt$ is the one that is controlled.

Discussion about the air density $\boldsymbol{\rho}$. In our analysis, the air density is assumed to be constant while, in general, it can vary as a function of the humidity and the temperature. This variation has to be taken into account when the mechanical power is computed and not measured in a control loop since, otherwise it might challenge the performance of the control design which we will present in later sections.

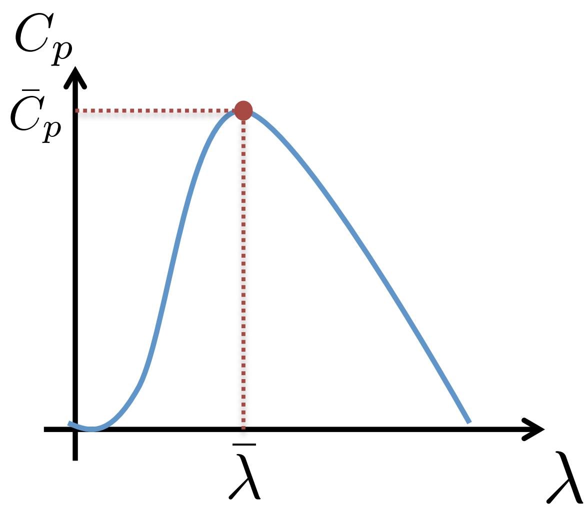

Figure 5.1: C_p−λ characteristic under MPPT

5.4 Problem Formulation

5.4.1 WF Power Output Regulation via Dynamic Dispatching and Control of WGs' Power Outputs

Consider a wind farm with n wind generators. The mechanical power that each WG i extracts from the wind is given by [5]:

$$P_{m,i} \triangleq \frac{1}{2}\rho C_{p,i} A_i v_{w,i}^3 \ , \qquad \forall i \in \mathcal{G} \tag{5.8}$$

where $C_{p,i} \in \mathbb{R}_+$ is the power coefficient, $\rho \in \mathbb{R}_{++}$ the air density (kg/m^3), $v_{w,i} \in \mathbb{R}_{++}$ the wind speed in (m/s) and $A_i = \pi R_i^2 \in \mathbb{R}_{++}$ the area swept by the blades with $R_i \in \mathbb{R}_+$ being the blade radius. Notice that, the only controllable variable in (5.8) is $C_{p,i}$, which can be regulated by the WG through the rotor speed $\omega_{r,i}$. Under low wind speed conditions, DFIGs usually operate under a Maximum Power Point Tracking (MPPT) strategy (Fig. 5.1) which was analyzed in Section 3.4.1. Under this strategy, a wind DFIG is controlled so that

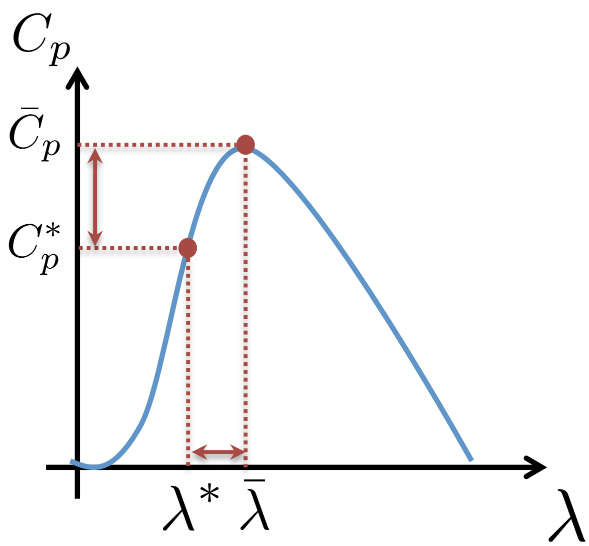

Figure 5.2: $C_p{-}\lambda$ characteristic under deloaded regime

$C_{p,i} = \overline{C}_{p,i}$, where $\overline{C}_{p,i} = \max\limits_{\lambda_i}\{C_{p,i}(\lambda_i, \theta_i^*)\}$ and $P_{m,i}$ in (5.8) is respectively equal to:

$$\overline{P}_{m,i} \triangleq \frac{1}{2}\rho\overline{C}_{p,i}A_i v_{w,i}^3 \,, \qquad \forall i \in \mathcal{G} \tag{5.9}$$

The term $\overline{C}_{p,i}$ is the maximum value of the power coefficient so it holds that $C_{p,i} \in [0, \overline{C}_{p,i}]$. Here, we consider a group of WGs operating in a deloading mode with $C_{p,i} < \overline{C}_{p,i}$, $P_{m,i} < \overline{P}_{m,i}$ so that they are able to vary their power coefficients in this range. This operating mode is depicted in Fig. 5.2. When WGs are operating under such regime, they can be controlled through their RSCs to extract mechanical power $P_{m,i}$ of any value in the set $[0, \overline{P}_{m,i}]$. On the other hand, the total power reference P_d for a WF originates from the system operator (SO) and is the outcome of a wind forecasting and an economic dispatch (ED) process conducted every several minutes. Further, it denotes the power that the WF is committed to supply to the grid in a 5-minute time-window.

Here, a set-up that includes a single WF comprised of n deloaded WGs that obtains a power reference P_d from the SO is considered. The reference satisfies $P_d \leq \sum_{i\in\mathcal{G}} \overline{P}_{m,i}$, i.e it is

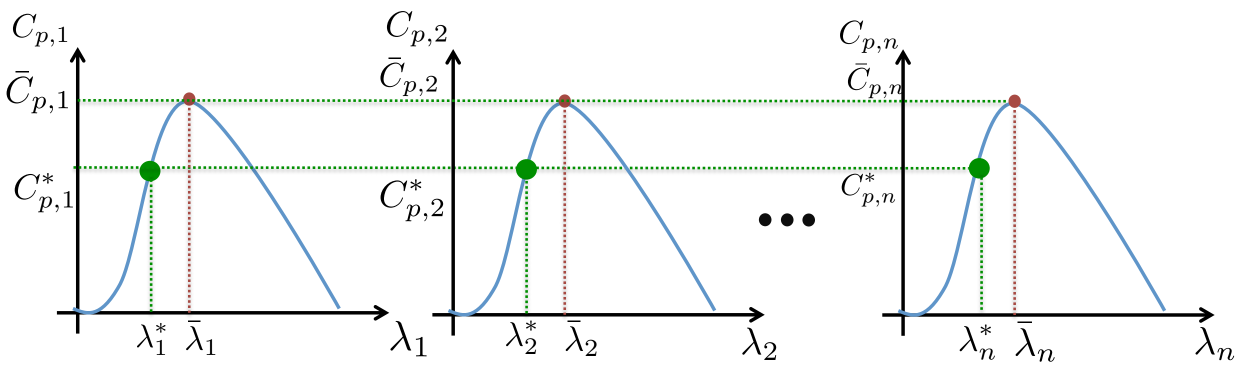

Figure 5.3: Fair dispatch of n WGs

realizable and can be met by WGs, considering the current prevalent wind-speed conditions at their locations. In fact, since deloaded WGs have more operational flexibility they can meet any total power request P_d as long as $P_d \in [0, \sum_{i\in\mathcal{G}} \overline{P}_{m,i}]$.

In our setting, the dispatch problem can be formulated as follows: *given* $v_{w,i}$, $\forall i \in \mathcal{G}$, *compute the set-points* $P^*_{m,i} \in [0, \overline{P}_{m,i}]$, $C^*_{p,i} \in [0, \overline{C}_{p,i}]$ *such that* $\sum_{i\in\mathcal{G}} P^*_{m,i} = P_d$. The combination of set-points that can satisfy the above constraints is not unique since any dispatching scenario $(P^*_{m,1}, ..., P^*_{m,n})$ that respects the above conditions is realizable. Ideally, the WGs should be dispatched in a more efficient way by requiring the set-points to also satisfy $(P^*_{m,1}/\overline{P}_{m,1}) = ... = (P^*_{m,n}/\overline{P}_{m,n})$. A dispatch that satisfies this condition is known as *"fair dispatch"* since WGs' power outputs are proportional to their maximum values which depend on the local wind speed conditions. This is equivalent to the WGs having the same loading levels (fair load sharing). A fair dispatching scenario is shown pictorially in Fig. 5.3 [40]. The conditions that the power outputs of WGs have to meet in order to realize a fair dispatching scenario are formally stated as follows.

Condition 5 (**Total power output regulation**).

$$\sum_{i\in\mathcal{G}} P^*_{m,i} = P_d \tag{5.10a}$$

Condition 6 (**Fair load sharing**).

$$\frac{P^*_{m,i}}{\overline{P}_{m,i}} = \frac{P^*_{m,j}}{\overline{P}_{m,j}}, \qquad \forall i, j \in \mathcal{G} \tag{5.10b}$$

Consider now the following definition.

Definition 5.1. Any dispatch of WGs' power outputs, $(P^*_{m,1}, ..., P^*_{m,n})$, that satisfies Conditions 5, 6 is called a *fair dispatch.*

At this point, we proceed with the following remark.

Remark 1.

$$\frac{P^*_{m,i}}{\overline{P}_{m,i}} = \frac{C^*_{p,i}}{\overline{C}_{p,i}}, \qquad \forall i \in \mathcal{G} \tag{5.11}$$

The ratio $(C^*_{p,i} \cdot \overline{C}^{-1}_{p,i})$ corresponds to the utilization (or loading level) of each WG. Through Remark 1, which is directly obtained by taking the ratio of (5.8) over (5.9), Condition 6 can be transformed to the new and equivalent condition below that also realizes the fair load sharing objective.

Condition 7 (**Fair load sharing**).

$$\frac{C^*_{p,i}}{\overline{C}_{p,i}} = \frac{C^*_{p,j}}{\overline{C}_{p,j}}, \qquad \forall i, j \in \mathcal{G}$$

Traditionally, the *fair dispatching* problem is solved in a centralized fashion where first the WGs communicate their wind-speed measurements to a central WF controller which then computes the power set-points for the individual WGs so that these meet the above two conditions. Here, we aim to solve the *fair dispatching* problem in a distributed set-up, formulated as follows.

Problem formulation (**Total Power Output Regulation via Distributed Dynamic**

Dispatching and Regulation of WGs' Power Outputs with Load Sharing). Develop a distributed control design for the RSCs with limited communication that WGs can employ to dynamically dispatch and regulate their power outputs so that these meet Conditions 5, 7. A methodology for solving this particular problem is proposed next.

5.5 Proposed Methodology

We first formulate the above problem as a constrained consensus problem for WGs where they have to agree on their loading levels while their total power is constrained to match a reference. To accomplish these objectives in a distributed and coordinated fashion, we *propose a leader-follower consensus protocol* that WGs can incorporate into their rotor-side converter (RSC) control design. Then, we study the asymptotic behavior of the protocol and establish certain stability properties as follows. We begin by employing singular perturbation theory to perform temporal decomposition of the protocol dynamics. Subsequently, we perform compositional stability analysis and establish, using Lyapunov-like arguments, asymptotic stability of the equilibria of the corresponding fast and slow decoupled subsystems. Thereafter, we assemble these stability certificates through a composite Lyapunov function and derive conditions on the time-scale separation parameter, under which, asymptotic stability of the equilibrium of the full protocol dynamics is guaranteed. In the final part of our stability analysis, we extend these results and establish, using a Lyapunov-Krasovskii functional, that the stability property is time-delay-independent. To realize the protocol in practice through peer-to-peer communication, we develop a distributed Control Lyapunov Function-based (CLF) torque controller for the rotor-side power electronics (RSC) of WGs. Practically, WGs that adopt this proposed control scheme can regulate their total power to track a reference, while their individual power outputs are driven to values proportional to their maximum power outputs available from the wind, with the proportionality coefficient being equal to all of them.

In summary, the proposed control scheme: 1) can be adopted by WGs to dynamically self-dispatch and regulate their power outputs based on local wind-speed conditions and in a distributed fashion, eliminating the need for a central wind farm controller that has to gather information and carry out numerous computations; 2) requires limited peer-to-peer communication among neighboring WGs; 3) enables WGs to dispatch and regulate their power outputs timely which is critical when these have to be performed under fast-varying dynamical wind and loading conditions to balance supply-demand, especially in autonomous power systems such as microgrids; 4) leads to guaranteed stability and performance of the associated dynamics.

5.6 Leader-Follower Consensus Protocol

The main problem can be solved by enabling WGs to distributively guarantee fulfillment of Conditions 5 and 7. Equivalently, to guarantee that their utilization levels $C_{p,i}/\overline{C}_{p,i}$ reach the same value while their total power tracks a reference P_d. This problem can be naturally posed as a *constrained consensus problem* among WGs, where they have to reach consensus on their utilization levels $C_{p,i}/\overline{C}_{p,i}$, constrained by the total power they have to extract. We propose the next *leader-follower consensus protocol*, that WGs can adopt in their RSC control scheme to dynamically self-dispatch and control their power outputs for meeting conditions 5, 7.

Consensus Protocol $\mathcal{P}_2$

Leader WG

$$\frac{d\xi_h}{dt} = (P_d - \sum_{i\in\mathcal{G}} P_{m,i}) \qquad \xi_h \in \mathbb{R} \tag{5.12a}$$

$$\frac{dz_l}{dt} = -k_{\alpha,l}(z_l - \xi_h)\,, \quad z_l \triangleq z_1 \qquad z_l \in \mathbb{R} \tag{5.12b}$$

WG i

$$\frac{dz_i}{dt} = -k_{\alpha,i}(z_i - z_{i-1}) \ , \quad i \in \overline{\mathcal{G}} \qquad\qquad z_i \in \mathbb{R} \tag{5.12c}$$

In the above protocol, without loss of generality WG 1 is assigned as the leader, *i.e* $l \triangleq 1$, and the set of followers is denoted by $\overline{\mathcal{G}} \triangleq \{2, ..., n\}$. The consensus protocol's state-variables are the utilization levels $z_l \triangleq C_{p,l}/\overline{C}_{p,l}$, $z_i \triangleq C_{p,i}/\overline{C}_{p,i}$ and the auxiliary variable ξ_h of the leader. Each WG is allowed to communicate with two other neighboring (physically) WGs, as shown in Figure 5.6.

The protocol is executed through the following mechanism. The supervisory WF controller attains a total power set-point P_d from the SO and communicates that to the leader WG. Subsequently, the leader WG controls the dynamics of its state-variables z_l and ξ_h, using the reference P_d and information (retrieved distributively via indirect information passing) from all WGs, and communicates only z_l and $\dot{z}_l$ to its neighbors. In synchrony with the leader, all the followers control the dynamics of their state-variables z_i, and communicate their respective z_i and $\dot{z}_i$ to their neighbors. It should be underlined that execution of the protocol $\mathcal{P}_2$ presumes that the leader is able to retrieve the information $\sum_{i\in\overline{\mathcal{G}}} P_{m,i}$.

5.7 Stability Analysis of the Consensus Protocol

In this section, we perform compositional stability analysis of the consensus protocol dynamics and prove conditional asymptotic stability of its equilibrium. This proof is carried out through the following steps. First, we show that the consensus protocol dynamics inherit two distinct time-scales when the protocol gains $k_{\alpha,i}$ meet certain conditions. Thereafter, by employing singular perturbation theory we decompose the system $\mathcal{P}_2$ into fast and slow subsystems, and prove asymptotic stability of their corresponding equilibria using separate Lyapunov functions as stability certificates. Finally, we combine these stability certificates to form a composite candidate Lyapunov function that we exploit to derive a condition under which, asymptotic stability of the full system's $\mathcal{P}_2$ equilibrium is guaranteed. This condition is characterized by an upper bound on the time-scale separation constant.

5.7.1 Leader-Follower Consensus Protocol in Standard Singularly Perturbed Form

The protocol $\mathcal{P}_2$ system inherits a two time-scales property for certain values of the gains $k_{\alpha,i}$. To show this, we recast this system into a parametric *standard singularly perturbed form* where the time-scale separation ratio is parameterized by the gains $k_{\alpha,i}$ [10]. First, we define the consensus state-vector as:

$$\mathbf{z} \triangleq [z_1,\ z_2,\ \dots,\ z_n]^\top, \qquad \mathbf{z} \in \mathbb{R}^n \tag{5.13a}$$

and the α_i coefficients as:

$$\alpha_i \triangleq \frac{1}{2}\rho \overline{C}_{p,i} A_i v_{w,i}^3, \qquad \alpha_i \in \mathbb{R}_+, i \in \mathcal{G} \tag{5.13b}$$

$$\boldsymbol{\alpha} \triangleq [\alpha_1, \alpha_2, \dots, \alpha_n]^\top, \qquad \boldsymbol{\alpha} \in \mathbb{R}_+^n \tag{5.13c}$$

The maximum value of $\boldsymbol{\alpha}$ is given by $\overline{\alpha} = \max\{\alpha_i\}_{i=1}^{|\mathcal{G}|}$. The two time-scales property of $\mathcal{P}_2$ is established through the following Claim.

Claim 4. The dynamics of the protocol system $\mathcal{P}_2$, given by (5.12a)-(5.12c), manifest two distinct time-scales when $k_{\alpha,1} = \dots = k_{\alpha,n} \gg \overline{\alpha}$.

Proof. To reveal the two times-scales property, a series of transformations is employed to recast equations (5.12a)-(5.12c) into a parametric *standard singularly perturbed form* [10]. To begin with, notice that $P_{m,i} = \alpha_i z_i,\ \forall i \in \mathcal{G}$. With that, equation (5.12a) is written as:

$$(5.12a)/\overline{\alpha} \Leftrightarrow \frac{1}{\overline{\alpha}}\frac{d\xi_h}{dt} = (\frac{P_d}{\overline{\alpha}} - \sum_{i\in\mathcal{G}} \frac{\alpha_i}{\overline{\alpha}} z_i) \tag{5.14}$$

with $(\alpha_i/\overline{\alpha}) \in [0,1],\ \forall i \in \mathcal{G}$. By defining a new time-scale $\tau = \overline{\alpha}\ t$, equation (5.14) can be written as:

$$\frac{d\xi_h}{d\tau} = (\frac{P_d}{\overline{\alpha}} - \sum_{i\in\mathcal{G}} \frac{\alpha_i}{\overline{\alpha}} z_i) \tag{5.15}$$

whereas, equations (5.12b), (5.12c) can be written as:

$$\frac{\overline{\alpha}}{k_{\alpha,i}}\frac{dz_i}{d\tau} = -(z_i - z_{i-1}), \quad z_0 = \xi_h,\ i \in \mathcal{G} \tag{5.16}$$

Letting $\overline{\alpha}/k_{\alpha,i} = \varepsilon,\ i \in \mathcal{G}$ and $\frac{d\mathbf{z}}{d\tau} \triangleq [\frac{dz_1}{d\tau},\ \dots\ , \frac{dz_n}{d\tau}]^\top \in \mathbb{R}^n$, equations (5.15) -(5.16) can be compactly expressed as:

$$\frac{d\xi_h}{d\tau} = g_h(\mathbf{z}) \tag{5.17}$$

$$\varepsilon\frac{d\mathbf{z}}{d\tau} = \mathbf{g}(\xi_h, \mathbf{z}) \tag{5.18}$$

where:

$$g_h(\mathbf{z}) = (\frac{P_d}{\overline{\alpha}} - \sum_{i\in\mathcal{G}} \frac{\alpha_i}{\overline{\alpha}} z_i), \quad g_h \in \mathbb{R} \tag{5.19}$$

$$\mathbf{g}(\xi_h, \mathbf{z}) = [-(z_1 - \xi_h),\ \dots\ , -(z_n - z_{n-1})]^\top,\ \mathbf{g} \in \mathbb{R}^n \tag{5.20}$$

Eventually, recognize that when $k_{\alpha,1} = \dots = k_{\alpha,n}$ and $\varepsilon \ll 1$, or equivalently $k_{\alpha,i} \gg \overline{\alpha}$, equations (5.17), (5.18) constitute a singularly perturbed system with two distinct time-scales, τ and $\tilde{\tau} = \tau/\varepsilon$. With this, the proof is completed. ■

It is important to realize that, the two times-scales property can be granted in the dynamics of $\mathcal{P}_2$ by choosing proper values for the gains $k_{\alpha,i}$, i.e it is not an innate property of the system $\mathcal{P}_2$ but it can be inherited.

5.7.2 Equilibrium and Desired Properties

Given that the dynamics of $\mathcal{P}_2$ possess two times-scales, the variable ξ_h is the *slow state-variable* and $\mathbf{z}$ are the *fast state-variables*. Their corresponding equilibria can be obtained from (5.12a) - (5.12c) as:

Slow state-variable (ξ_h) equilibrium

$$\xi_{h0} = \frac{P_d}{\left(\sum_{i\in\mathcal{G}} \alpha_i\right)}, \qquad \xi_{h0} \in \mathbb{R}_+ \tag{5.21a}$$

Fast state-variables ($\mathbf{z}$) equilibrium

$$\mathbf{z}_0 = \xi_{h0}\cdot\mathbf{1}_n, \qquad \mathbf{z}_0 \in \mathbb{R}_+^n \tag{5.21b}$$

The equilibrium of the full $\mathcal{P}_2$ system is then:

$$\tilde{\mathbf{z}}_0 = \begin{pmatrix} \xi_{h0} \\ \\ \mathbf{z}_0 \end{pmatrix}, \qquad \tilde{\mathbf{z}}_0 \in \mathbb{R}_+^{n+1} \tag{5.22}$$

Before assigning desired properties to the above equilibrium, it is convenient to define a *consensus subspace* as [41]:

$$\mathcal{S} \triangleq \{\mathbf{x} \in \mathbb{R}^{n+1} \mid \mathbf{x} = \beta\cdot\mathbf{1}_{n+1}\ ,\ \ \beta \in \mathbb{R}\} \tag{5.23}$$

The protocol $\mathcal{P}_2$ realizes the control objectives when, its equilibrium possesses the following two properties.

Property 5.1. $\tilde{\mathbf{z}}_0 \in \mathcal{S}$

Property 5.2. $\tilde{\mathbf{z}}_0$ *is asymptotically stable*

From equations (5.21a), (5.21b), observe that the equilibrium of $\mathcal{P}_2$ already possesses Property 5.1 with $\beta = \xi_{h0}$. In the next Sections, a particular condition for the protocol gains $k_{\alpha,i}$ will be derived which, if respected will lead to the equilibrium of $\mathcal{P}_2$ possessing Property 5.2 as well.

To prepare the ground for the coming stability analysis, we shift $\tilde{\mathbf{z}}_0$ to the origin $\mathbf{0}_{n+1}$ by employing the coordinates transformation:

$$\psi_h = (\xi_h - \xi_{h0}), \qquad \psi_h \in \mathbb{R} \tag{5.24}$$

$$\mathbf{y} = (\mathbf{z} - \xi_h\cdot\mathbf{1}_n), \qquad \mathbf{y} \triangleq [y_1,\ \dots\ , y_n]^\top \in \mathbb{R}^n \tag{5.25}$$

where $y_0 = (z_0 - \xi_h) = 0$. In the new coordinate system, (5.17) and (5.18) are transformed to:

$$\frac{d\psi_h}{d\tau} = -(\sum_{i\in\mathcal{G}} \frac{\alpha_i}{\overline{\alpha}})\psi_h - \sum_{i\in\mathcal{G}}(\frac{\alpha_i}{\overline{\alpha}} y_i) \tag{5.26}$$

$$\varepsilon\frac{d\mathbf{y}}{d\tau} = [-(y_1 - y_0) - \varepsilon\frac{d\psi_h}{d\tau}\ \ ,\ \ \dots\ \ ,\ \ -(y_n - y_{n-1}) - \varepsilon\frac{d\psi_h}{d\tau}]^\top \tag{5.27}$$

The equilibrium of this system is:

$$\tilde{\mathbf{y}}_0 = \begin{pmatrix} \psi_{h0} \\ \\ \mathbf{y}_0 \end{pmatrix} = \mathbf{0}_{n+1} \tag{5.28}$$

The following subsections are dedicated to deriving a condition under which, asymptotic stability of $\tilde{\mathbf{y}}_0$ is guaranteed, i.e under which the equilibrium of $\mathcal{P}_2$ possesses Property 5.2.

5.7.3 Stability of Fast Boundary-layer Subsystem

The fist step toward establishing asymptotic stability of $\tilde{\mathbf{y}}_0$ is to independently establish asymptotic stability of $\mathbf{y}_0$ and ψ_{h0}, equilibria of the decoupled fast and slow subsystems. In this Section, we focus on establishing asymptotic stability of $\mathbf{y}_0$. To this end, we obtain the fast boundary-layer dynamics by first, designating the fast time-scale as $\tilde{\tau} = (\tau/\varepsilon)$ and rewrite (5.27) in scalar form as:

$$\frac{dy_i}{d\tilde{\tau}} = -(y_i - y_{i-1}) - \frac{d\psi_h}{d\tilde{\tau}}, \qquad i \in \mathcal{G} \tag{5.29}$$

Then, we approximate the slow state-variable ψ_h as constant, i.e assume that $\frac{d\psi_h}{d\tilde{\tau}} = 0$. This leads to the following system:

Fast boundary-layer system

$$\frac{dy_i}{d\tilde{\tau}} = -(y_i - y_{i-1}), \qquad i \in \mathcal{G} \tag{5.30}$$

Stability of the fast boundary-layer system (5.30) is established through the next lemma.

Lemma 5.1. *The equilibrium $\mathbf{y}_0 = \mathbf{0}_n$ of the system (5.30) is asymptotically stable.*

Proof. The system (5.30) in matrix form can be expressed as:

$$\begin{bmatrix} \frac{dy_1}{d\tilde{\tau}} \\ \frac{dy_2}{d\tilde{\tau}} \\ \vdots \\ \frac{dy_n}{d\tilde{\tau}} \end{bmatrix} = \underbrace{\begin{bmatrix} -1 & 0 & \cdots & 0 & 0 \\ 1 & -1 & \cdots & 0 & 0 \\ \vdots & \ddots & & & \vdots \\ 0 & 0 & \cdots & 1 & -1 \end{bmatrix}}_{\mathbf{A_f} \in \mathbb{R}^{n \times n}} \begin{bmatrix} y_1 \\ y_2 \\ \vdots \\ y_n \end{bmatrix}$$

or, more compactly as:

$$\frac{d\mathbf{y}}{d\tilde{\tau}} = \mathbf{A_f}\mathbf{y} \tag{5.31}$$

Further, we denote the eigenvalues of $\mathbf{A_f}$ by $\boldsymbol{\lambda} = [\lambda_1, ..., \lambda_n]^\top$ and recognize that $\mathbf{A_f}$ is lower triangular therefore, we have:

$$\det(\mathbf{A_f} - \lambda \cdot \mathbf{I}_{n \times n}) = (-1)^n (\lambda + 1)^n \tag{5.32}$$

equivalently, $\boldsymbol{\lambda} = -\mathbf{1}_n$.

Since all of the eigenvalues of $\mathbf{A_f}$ lie on the left half of the complex plane, i.e $\mathrm{Re}(\lambda_i) < 0, \ \ \forall i$, it can be concluded that $\mathbf{A_f}$ is *Hurwitz*. By invoking Theorem 4.5 ([10]), it can be further concluded that $\mathbf{y}_0 = \mathbf{0}_n$ is *asymptotically stable*. With that, the proof of *Lemma* 5.1 is completed. ■

Later on, we will establish asymptotic stability of $\tilde{\mathbf{y}}_0$ by leveraging the stability property just proved. For this purpose, a parameterized Lyapunov function can be now constructed that serves as a stability certificate of (5.30) as:

$$V_f = \mathbf{y}^\top \mathbf{P} \mathbf{y}, \ \ V_f > 0, \ \ \forall \mathbf{y} \in \overline{\mathcal{D}}_\mathbf{y} \tag{5.33}$$

where $\overline{\mathcal{D}}_{\mathbf{y}} \triangleq \mathcal{D}_{\mathbf{y}}\backslash\{\mathbf{0}_n\},\ \mathcal{D}_{\mathbf{y}} \subset \mathbb{R}^n$ and $\mathbf{P} \in \mathbb{R}^{n\times n},\ \mathbf{P} \succ 0$ satisfying

$$\mathbf{P}\mathbf{A}_{\mathbf{f}}+\mathbf{A}_{\mathbf{f}}^{\top}\mathbf{P} = -\mathbf{Q} \tag{5.34}$$

for a given $\mathbf{Q} \succ 0$. Since $\mathbf{A}_{\mathbf{f}}$ is Hurwitz, there exists a unique $\mathbf{P}$, $\mathbf{P} \succ 0$, satisfying (5.34) for any given $\mathbf{Q}$, $\mathbf{Q} \succ 0$. Using this parameterized Lyapunov function V_f, we will derive conditions in terms of the matrix $\mathbf{P}$ under which, asymptotic stability of $\tilde{\mathbf{y}}_0$ is guaranteed.

5.7.4 Stability of Slow Reduced-order Subsystem

In this Section, we establish stability of ψ_{h0}, equilibrium of the decoupled slow reduced-order subsystem. By concentrating on the slow time-scale τ, the decoupled slow subsystem can be obtained by approximating the fast state-variables with their fast equilibrium manifold, $\mathbf{y} = \mathbf{0}_n$. In this case, equation (5.26) becomes:

Slow reduced-order subsystem

$$\frac{d\psi_h}{d\tau} = -(\sum_{i\in\mathcal{G}} \frac{\alpha_i}{\overline{\alpha}})\psi_h \tag{5.35}$$

Stability of (5.35) is established through the following lemma.

Lemma 5.2. *The equilibrium $\psi_{h0} = 0$ of the system (5.35) is asymptotically stable.*

Proof. First, we construct a candidate Lyapunov function as:

$$V_h = \psi_h^2,\ \ V_h > 0,\ \ \forall\psi_h \in \overline{D}_{\psi_h} \tag{5.36}$$

where $\overline{D}_{\psi_h} = D_{\psi_h}\backslash\{0\},\ D_{\psi_h} \subset \mathbb{R}$. Granted that, $(\sum_{i\in\mathcal{G}} \frac{\alpha_i}{\overline{\alpha}}) > 0$, the time-derivative of V_h

with respect to the time-scale τ along the trajectories of (5.35) becomes:

$$\frac{dV_h}{d\tau} = -2(\sum_{i\in\mathcal{G}} \frac{\alpha_i}{\overline{\alpha}})\psi_h^2, \quad \frac{dV_h}{d\tau} < 0, \quad \forall\psi_h \in \overline{D}_{\psi_h} \tag{5.37}$$

By applying *Lyapunov's stability theorem*, we conclude *asymptotic stability* of $\psi_{h0} = 0$. ■

In the next Section, this stability property will be leveraged through its Lyapunov function certificate V_h together with, the stability property of $\mathbf{y}_0$ through its Lyapunov function certificate V_f, to establish conditional asymptotic stability of $\tilde{\mathbf{y}}_0$.

5.7.5 Stability of the Full $\mathcal{P}_2$ System

Having established asymptotic stability of the fast boundary-layer subsystem and the slow reduced order subsystem, we will now proceed to derive conditions under which asymptotic stability of the full system (5.26)-(5.27) is guaranteed. By combining the stability certificates of (5.30) and (5.35) through a linear combination of V_f and V_h a candidate Lyapunov function for this system [10] can be formed as:

$$V_c = \frac{1}{2}\mathbf{y}^\top\mathbf{P}\mathbf{y}+\frac{\psi_h^2}{2}, \;\; V_c > 0, \;\; \forall(\mathbf{y},\psi_h) \in \overline{\mathcal{D}}_{\mathbf{y}}\times\overline{\mathcal{D}}_{\psi_h} \tag{5.38}$$

Further, we take $\mathbf{P} = [p_{ij}]$ where $\mathbf{P} = \mathbf{P}^\top$ and define the auxiliary coefficients:

$$\tilde{\alpha}_s \triangleq \sum_{i\in\mathcal{G}} \frac{\alpha_i}{\overline{\alpha}}, \quad \tilde{\alpha}_i \triangleq \frac{\alpha_i}{\overline{\alpha}}, \;\; \forall i \in \mathcal{G} \tag{5.39a}$$

The derivative of V_c with respect to τ is:

$$\begin{aligned}\frac{dV_c}{d\tau} &= \frac{1}{2}(\frac{d\mathbf{y}}{d\tau})^\top\mathbf{P}\mathbf{y}+\frac{1}{2}\mathbf{y}^\top\mathbf{P}(\frac{d\mathbf{y}}{d\tau})+\psi_h\frac{d\psi_h}{d\tau}\\ &= \frac{1}{2}\mathbf{y}^\top\underbrace{(\frac{\mathbf{A_f}^\top\mathbf{P}+\mathbf{P}\mathbf{A_f}}{\varepsilon})}_{-\frac{1}{\varepsilon}\mathbf{Q}}\mathbf{y}+(-\frac{d\boldsymbol{\psi_h}}{d\tau})^\top\mathbf{P}\mathbf{y}-\tilde{\alpha}_s\psi_h^2-\psi_h(\sum_{i\in\mathcal{G}}\tilde{\alpha}_i y_i)\end{aligned} \tag{5.40}$$

where $\frac{d\mathbf{y}}{d\tau} = [\frac{dy_1}{d\tau}, ..., \frac{dy_n}{d\tau}]^\top \in \mathbb{R}^{n\times n}$ and $\frac{d\boldsymbol{\psi_h}}{d\tau} = (\frac{d\psi_h}{d\tau})\cdot\mathbf{1}_n$, $\frac{d\boldsymbol{\psi_h}}{d\tau} \in \mathbb{R}^n$. The term $(-\frac{d\boldsymbol{\psi_h}}{d\tau})^\top\mathbf{P}\mathbf{y}$ can be expanded with algebraic manipulations as:

$$
\begin{aligned}
(-\frac{d\boldsymbol{\psi_h}}{d\tau})^\top\mathbf{P}\mathbf{y} = \tilde{\alpha}_s\psi_h \sum_{i=1}^{n}\Big(\sum_{j=1}^{n} p_{ji}\Big)y_i + \sum_{i=1}^{n}\Big(\sum_{j=1}^{n} p_{ji}\Big)\tilde{\alpha}_i y_i^2 \\
+ \sum_{i=1}^{n}\sum_{j=i+1}^{n}\Big((\tilde{\alpha}_i \sum_{k=1}^{n} p_{kj} + \tilde{\alpha}_j \sum_{k=1}^{n} p_{ki})y_i y_j\Big)
\end{aligned}
\tag{5.41}
$$

Further, by defining the vector:

$$
\tilde{\mathbf{y}} = \begin{pmatrix} \psi_h \\ \\ \mathbf{y} \end{pmatrix}, \quad \tilde{\mathbf{y}} \in \mathbb{R}^{n+1} \tag{5.42}
$$

equation (5.40) can be written in the compact form:

$$
\frac{dV_c}{d\tau} = \tilde{\mathbf{y}}^\top \, \mathbf{F} \, \tilde{\mathbf{y}} \tag{5.43}
$$

The matrix $\mathbf{F}$ is given by:

$$
\mathbf{F} \triangleq \begin{bmatrix} \mathbf{A} & \mathbf{B} \\ \\ \mathbf{B}^\top & \mathbf{C} \end{bmatrix} \in \mathbb{R}^{(n+1)\times(n+1)} \tag{5.44}
$$

and comprised of the submatrices $\mathbf{A} \in \mathbb{R}$, $\mathbf{B}^\top \in \mathbb{R}^n$, $\mathbf{C} \in \mathbb{R}^{n\times n}$ as defined below.

$$
\mathbf{A} = -\tilde{\alpha}_s, \tag{5.45}
$$

$$
\mathbf{B} = \begin{bmatrix} -\frac{\tilde{\alpha}_1}{2} + \frac{\tilde{\alpha}_s}{2}\sum_{j=1}^{n} p_{j1} & \cdots & -\frac{\tilde{\alpha}_n}{2} + \frac{\tilde{\alpha}_s}{2}\sum_{j=1}^{n} p_{jn} \end{bmatrix} \tag{5.46}
$$

$$\mathbf{C}=\begin{bmatrix} -\frac{q_{11}}{\varepsilon}+\tilde{\alpha}_1\sum\limits_{j=1}^{n}p_{j1} & \cdots & \frac{\tilde{\alpha}_1}{2}\sum\limits_{k=1}^{n}p_{kn}+\frac{\tilde{\alpha}_n}{2}\sum\limits_{k=1}^{n}p_{k1} \\ & \ddots & \\ \frac{\tilde{\alpha}_1}{2}\sum\limits_{k=1}^{n}p_{kn}+\frac{\tilde{\alpha}_n}{2}\sum\limits_{k=1}^{n}p_{k1} & \cdots & -\frac{q_{nn}}{\varepsilon}+\tilde{\alpha}_n\sum\limits_{j=1}^{n}p_{jn} \end{bmatrix} \tag{5.47}$$

Stability of $\tilde{\mathbf{y}}_0$ is now established via the next theorem.

Theorem 5.1. *The equilibrium $\tilde{\mathbf{y}}_0 = \mathbf{0}_{n+1}$ of (5.26) - (5.27) is asymptotically stable for $\varepsilon < \bar{\varepsilon}$ where $\bar{\varepsilon} = \min\{\bar{\varepsilon}_i\}_{i\in\mathcal{G}}$, and $\bar{\varepsilon}_i$ given by:*

$$\bar{\varepsilon}_i = \frac{q_{ii}}{\tilde{\alpha}_i\sum\limits_{j=1}^{n}p_{ji}+\frac{1}{\tilde{\alpha}_s}g_{ii}+\sum\limits_{\substack{k=1\\k\neq i}}^{n}\left|-\frac{\tilde{\alpha}_i}{2}\sum\limits_{j=1}^{n}p_{jk}-\frac{\tilde{\alpha}_k}{2}\sum\limits_{j=1}^{n}p_{ji}-\frac{1}{\tilde{\alpha}_s}g_{ik}\right|}$$

Further, $\mathbf{P}=[p_{ij}]$, $\mathbf{Q}=[q_{ij}]$ *and* $\mathbf{G}=\mathbf{B}^\top\mathbf{B}$ *such that* $\mathbf{G}=[g_{ij}]$ *with* $g_{ij}=b_i{\cdot}b_j$ $(\mathbf{B}=[b_i])$.

Proof. A sufficient condition for asymptotic stability of $\tilde{\mathbf{y}}_0 = \mathbf{0}_{n+1}$ can be found by requiring the inequality $\mathbf{F} \prec 0$ to hold. Given that, the forthcoming analysis is focused on deriving a sufficient condition under which $\mathbf{F} \prec 0$, eventually showing that its comes down to an upper bound on ε. Concretely, we derive conditions under which $-\mathbf{F} \succ 0$ holds. To this end, we first define the *Schur complement* of $-\mathbf{F}$ as:

$$\mathbf{S} = -\mathbf{C}+\mathbf{B}^\top\mathbf{A}^{-1}\mathbf{B} \tag{5.48}$$

From the Schur complement conditions we have that:

$$-\mathbf{F} \succ 0 \Leftrightarrow \mathbf{S} \succ 0 \textit{ and } -\mathbf{A} \succ 0 \tag{5.49}$$

Thus, the analysis can be simplified by deriving conditions under which $\mathbf{S} \succ 0, -\mathbf{A} \succ 0$ hold.

Immediately, we have that, $-\mathbf{A} = \tilde{\alpha}_s \succ 0$ so it is only left to guarantee that $\mathbf{S} \succ 0$. In this direction, first realize that by deploying $\mathbf{A} = -\tilde{\alpha}_s$, equation (5.48) becomes:

$$\mathbf{S} = -\mathbf{C} - (\tilde{\alpha}_s)^{-1}\mathbf{G}, \;\; where\ \mathbf{G} = \mathbf{B}^{\top}\mathbf{B} \tag{5.50}$$

With $\mathbf{G} = [g_{ij}]$ where $g_{ij} = b_i \cdot b_j$ (with $\mathbf{B} = [b_i]$), we can further write the matrix $\mathbf{S}$ more compactly as:

$$\mathbf{S} = [s_{ij}], \;\; s_{ij} = -c_{ij} - (\tilde{\alpha}_s)^{-1} b_i b_j \tag{5.51}$$

The next step is to find conditions that lead to $\mathbf{S} \succ 0$. This can be achieved by employing the following matrix property. *A Hermitian (symmetric) matrix with all positive eigenvalues is positive definite.* The matrix $\mathbf{S}$ is the sum of two symmetric matrices, $-\mathbf{C}$ and $-(\tilde{\alpha}_s)^{-1}\mathbf{G}$. Therefore, it is symmetric, i.e $\mathbf{S} = \mathbf{S}^{\top}$ holds. To meet the second requirement, we have to find conditions under which all eigenvalues of $\mathbf{S}$ are positive. To this end, we resort to *Gershgorin's Circle Theorem* [42] which in our particular case gives that, all the eigenvalues λ_i of the matrix $\mathbf{S}$ belong to the following set:

$$\mathcal{D} = \bigcup_{i \in \mathcal{G}} \mathcal{D}_i \tag{5.52}$$

where $\mathcal{D}_i$ is given by:

$$\mathcal{D}_i \triangleq \{\chi \in \mathbb{R} : |\chi - s_{ii}| \leq \sum_{j=1, j \neq i}^{n} |s_{ij}|\}, \quad \forall i \in \mathcal{G} \tag{5.53}$$

i.e $\lambda_i \in \mathcal{D}, \; \forall i \in \mathcal{G}$.

In the definition of the set $\mathcal{D}_i$, the eigenvalues λ_i are taken to be real since $\mathbf{S}$ is symmetric. For these to be also positive ($\lambda_i > 0$), all the subsets $\mathcal{D}_i$ have to satisfy $\mathcal{D}_i \subset \mathbb{R}_+$. To establish that, we first use (5.53) to derive a lower and an upper bound for the eigenvalues $\chi \in \mathcal{D}_i$, $\underline{\chi}_i$, $\overline{\chi}_i$ respectively, which corresponds to the particular subset $\mathcal{D}_i$, as:

$$\underbrace{s_{ii} - \sum_{j=1}^{n} |s_{ij}|}_{\underline{\chi}_i} \leq \chi \leq \underbrace{s_{ii} + \sum_{j=1}^{n} |s_{ij}|}_{\overline{\chi}_i} \tag{5.54}$$

To guarantee that $\chi > 0$, we only have to ensure that $\underline{\chi}_i > 0$, $\forall i \in \mathcal{G}$. Since s_{ii} depends on ε, this condition will be satisfied when ε respects an upper bound $\bar{\varepsilon}_i$. To see that, consider first the inequality:

$$\underline{\chi}_i > 0 \Leftrightarrow s_{ii} - \sum_{j=1}^{n} |s_{ij}| > 0 \tag{5.55}$$

which, by substituting s_{ii} and s_{ij} from (5.51), (5.46), (5.47), becomes:

$$\frac{q_{ii}}{\varepsilon} - \tilde{\alpha}_i \sum_{j=1}^{n} p_{ji} - \frac{g_{ii}}{\tilde{\alpha}_s} - \sum_{\substack{k=1 \\ k \neq i}}^{n} \left| -\frac{\tilde{\alpha}_i}{2} \sum_{j=1}^{n} p_{jk} - \frac{\tilde{\alpha}_k}{2} \sum_{j=1}^{n} p_{ji} - \frac{g_{ik}}{\tilde{\alpha}_s} \right| > 0$$

Ultimately, this inequality can be reformulated as:

$$\varepsilon < \underbrace{\frac{q_{ii}}{\tilde{\alpha}_i \sum_{j=1}^{n} p_{ji} + \frac{1}{\tilde{\alpha}_s} g_{ii} + \sum_{\substack{k=1 \\ k \neq i}}^{n} \left| -\frac{\tilde{\alpha}_i}{2} \sum_{j=1}^{n} p_{jk} - \frac{\tilde{\alpha}_k}{2} \sum_{j=1}^{n} p_{ji} - \frac{1}{\tilde{\alpha}_s} g_{ik} \right|}}_{\overline{\varepsilon}_i}$$

From the above, it is obvious that, by considering the inequality (5.55) for each set $\mathcal{D}_i$ a corresponding upper bound $\overline{\varepsilon}_i$ can be obtained. The minimum of all these bounds is the upper bound $\overline{\varepsilon} = \min\{\overline{\varepsilon}_i\}_{i \in \mathcal{G}}$ which, if respected by ε, i.e $\varepsilon < \bar{\varepsilon}$, leads to $\mathcal{D} \subset \mathbb{R}_+$, i.e $\forall \chi \in \mathcal{D}$, $\chi > 0$. Equivalently, that the eigenvalues of $\mathbf{S}$ are positive. In this case, $\mathbf{S}$ is positive definite and from the *Schur complement conditions* [42] we conclude that $-\mathbf{F} \prec 0$, i.e that $\tilde{\mathbf{y}}_0 = \mathbf{0}_{n+1}$ is asymptotically stable. That, concludes the proof. ■

Theorem 5.1 provides a *sufficient* but *not a necessary* condition for asymptotic stability of $\tilde{\mathbf{y}}_0 = \mathbf{0}_{n+1}$. Nevertheless, this theorem can be employed to design the gains $k_{\alpha,i}$ of the protocol $\mathcal{P}_2$ such that asymptotic stability of its equilibrium follows. This can be achieved in the following way. First we can choose any diagonal positive definite matrix $\mathbf{Q}$ and compute a positive definite matrix $\mathbf{P}$ satisfying (5.34). By having the information about the prevalent local wind-speed conditions at the location of each WG, i.e $v_{w,i},\ \forall i$, we can compute the coefficients $\tilde{\alpha}_i,\ \tilde{\alpha}_s$. Then, from Theorem 5.1, the upper bound $\overline{\varepsilon}$ can be computed and appropriate gains $k_{\alpha,i}$ that are equal and satisfy $(\overline{\alpha}/k_{\alpha,i}) < \overline{\varepsilon}$ can be chosen so that asymptotic stability of $\tilde{\mathbf{y}}_0 = \mathbf{0}_{n+1}$ is guaranteed.

5.7.6 Delay-Independent Stability

In the previous Sections we saw that, in the case of a system without time-delays, we can employ the Lyapunov method to determine stability properties of its equilibrium point. The basic idea behind this method is that, we can construct a Lyapunov function $V(t, x(t))$, which measures in some sense the deviation of $x(t)$ from its equilibrium 0, and check whether this function fulfills certain conditions. In the case that it does, we can directly establish certain stability properties of the system's equilibrium point through Lyapunov's theorem. Note that, in the case of systems without delay, this Lyapunov function is a function of $x(t)$, since only $x(t)$ is required to specify the evolution of the system's state beyond time t. On the other hand, in the case of a time-delayed system:

$$\dot{x}(t) = f(t, x_t) \tag{5.56}$$

where $x(t) \in \mathbb{R}^n$ and $f : \mathbb{R}\times\mathcal{C} \mapsto \mathbb{R}^n$ and $x_t = x(t+\theta),\ \ -r \leq \theta \leq 0$, the value of $x(t)$ in the interval $[t-r,\ t]$, i.e x_t, is required to determine its future evolution. Consequently, the corresponding Lyapunov function for a system with delays takes the form of a functional $V(t, x_t)$ which depends on x_t, measuring deviation of x_t from a trivial solution 0. This functional is known as *Lyapunov-Krasovskii functional* [44].

We now state the Lyapunov-Krasovskii Stability Theorem, which gives the conditions that this functional has to meet in order for the equilibrium point of (5.56) to have certain stability properties .

Theorem 5.2 (**Lyapunov-Krasovskii Stability Theorem**, [44])**.** *Suppose* $f : \mathbb{R}\times\mathcal{C} \mapsto \mathbb{R}^n$ *in* (5.56) *maps* $\mathbb{R}\times$(*bounded set in* $\mathcal{C}$) *into a bounded set in* $\mathbb{R}^n$*, and that* $u,\ v,\ w : \mathbb{R}_+ \mapsto \mathbb{R}_+$ *are continuous nondecreasing functions, where additionally* $u(s),\ v(s)$ *are positive for* $s > 0$*, and* $u(0) = v(0) = 0$*. If there exists a continuous differentiable functional* $V : \mathbb{R}\times\mathcal{C} \mapsto \mathbb{R}$ *such that:*

$$u(\|x(t)\|) \leq V(t, x_t) \leq v(\|x_t\|_c) \tag{5.57}$$

where $\|x_t\|_c = \max_{a\leq\theta\leq b} \|x(t+\theta)\|$ *and*

$$\dot{V}(t, x_t) \leq -w(\|x(t)\|) \tag{5.58}$$

then the trivial solution of (5.56) *is uniformly stable. If* $w(s) > 0$ *for* $s > 0$ *then it is uniformly asymptotically stable. If, in addition,* $\lim_{s\to\infty} u(s) = \infty$*, then it is globally asymptotically stable.*

Next, this theorem will be employed to establish a delay-independent stability property of the $\mathcal{P}_2$ consensus protocol's equilibrium point. This property certifies that the stability of the equilibrium point is robust with respect to any communication time-delays that may arise in the implementation of the consensus protocol in a practical setting. In our case, we consider a particular type of delays, namely fixed time-delays, and establish *delay-independent* *asymptotic stability* of the consensus protocol's fast sub-system equilibrium point. The delays are denoted by $r \in \mathbb{R}^+$ and it is assumed that under these delays, ξ_h remains constant in the time range $[\tilde{\tau}-r,\ \tilde{\tau}]$. That results to the value of the time-delayed slow state-variable $\xi_h(\tilde{\tau}-r)$ being equal to the present value of the state-variable $\xi_h(\tilde{\tau})$. This can be formally stated as follows.

Assumption 3. *For the considered time-delays r, it holds that $\xi_h(\tilde{\tau}-r) = \xi_h(\tilde{\tau})$.*

The time-delayed version of (5.29) under delays r takes the form:

$$\frac{d\mathbf{y}(\tilde{\tau})}{d\tilde{\tau}} = \mathbf{A}_0\mathbf{y}(\tilde{\tau}) + \mathbf{A}_1\mathbf{y}(\tilde{\tau}-r) \tag{5.59}$$

where $\mathbf{A}_0 \triangleq -\mathbf{I}_n$ and $\mathbf{A}_1$ defined as:

$$\mathbf{A}_1 \triangleq \begin{bmatrix} \mathbf{0}^\top_{(n-1)} & 0 \\ \mathbf{I}_{(n-1)} & \mathbf{0}_{(n-1)} \end{bmatrix} \tag{5.60}$$

Stability of the system (5.59) is established through the following theorem.

Theorem 5.3. *The equilibrium point $\mathbf{y}_0 = \mathbf{0}_n$ of the system (5.59) is delay-independent asymptotically stable.*

Proof. We first construct a candidate *Lyapunov-Krasovskii* functional for the system (5.59) [44] as:

$$V_1 = \mathbf{y}(\tilde{\tau})^\top \mathbf{P_1}\mathbf{y}(\tilde{\tau}) + \int_{\tilde{\tau}-r}^{\tilde{\tau}} \mathbf{y}(\eta)^\top \mathbf{Q_1}\mathbf{y}(\eta)d\eta \tag{5.61}$$

where $\mathbf{P_1}, \mathbf{Q_1} \in \mathbb{R}^{n\times n}$ and $\mathbf{P_1}, \mathbf{Q_1} \succ 0$. We have to prove that the functional V_1 meets conditions (5.57), (5.58) of the Lyapunov-Krasovskii theorem. To prove that it satisfies the first condition given by (5.57), we first use the inequality:

$$\lambda_{min}(\mathbf{P_1})\|\mathbf{y}(\tilde{\tau})\|_2^2 \leq \mathbf{y}(\tilde{\tau})^\top \mathbf{P_1}\mathbf{y}(\tilde{\tau}) \leq \lambda_{max}(\mathbf{P_1})\|\mathbf{y}(\tilde{\tau})\|_2^2 \tag{5.62}$$

to obtain that:

$$V_1 \geq \lambda_{min}(\mathbf{P_1})\|\mathbf{y}(\tilde{\tau})\|_2^2 + \int_{\tilde{\tau}-r}^{\tilde{\tau}} \mathbf{y}(\eta)^\top \mathbf{Q_1}\mathbf{y}(\eta) d\eta \tag{5.63}$$

where since $\mathbf{Q}_1$ is positive definite we finally get:

$$V_1 \geq \lambda_{min}(\mathbf{P_1})\|\mathbf{y}(\tilde{\tau})\|_2^2 \tag{5.64}$$

That proves the left part of the inequality (5.57) with $u(\|\mathbf{y}(\tilde{\tau})\|_2) = \lambda_{min}(\mathbf{P_1})\|\mathbf{y}(\tilde{\tau})\|_2^2$. This function is nondecreasing and continuous and also satisfies $u(0) = 0$. To prove the right part of the inequality (5.57), the next inequality is used:

$$\lambda_{min}(\mathbf{Q_1})\|\mathbf{y}(\eta)\|_2^2 \leq \mathbf{y}(\eta)^\top \mathbf{Q_1}\mathbf{y}(\eta) \leq \lambda_{max}(\mathbf{Q_1})\|\mathbf{y}(\eta)\|_2^2 \tag{5.65}$$

The right part of this twofold inequality together with the right part of (5.62) applied to (5.61) yield:

$$V_1 \leq \lambda_{max}(\mathbf{P_1})\|\mathbf{y}(\tilde{\tau})\|_2^2 + \int_{\tilde{\tau}-r}^{\tilde{\tau}} \lambda_{max}(\mathbf{Q_1})\|\mathbf{y}(\eta)\|_2^2 d\eta$$

where this inequality can be further expanded as:

$$V_1 \leq \lambda_{max}(\mathbf{P_1})\Big(y_1(\tilde{\tau})^2 + y_2(\tilde{\tau})^2 + \ldots + y_n(\tilde{\tau})^2\Big) + \int_{\tilde{\tau}-r}^{\tilde{\tau}} \lambda_{max}(\mathbf{Q_1})\Big(y_1(\eta)^2 + y_2(\eta)^2 + \ldots + y_n(\eta)^2\Big) d\eta$$

Now, the additional inequalities can be employed:

$$y_i(\tilde{\tau}) \leq \max_{\tilde{\tau}-r\leq\eta\leq\tilde{\tau}} \|y_i(\eta)\| = \|y_{i,\tilde{\tau}}\|_c, \quad \forall i \in \{1, ..., n\} \tag{5.66}$$

$$y_i(\eta) \leq \max_{\tilde{\tau}-r\leq\eta\leq\tilde{\tau}} \|y_i(\eta)\| = \|y_{i,\tilde{\tau}}\|_c, \quad \forall i \in \{1, ..., n\} \tag{5.67}$$

to finally obtain:

$$\begin{aligned} V_1 &\leq \lambda_{max}(\mathbf{P_1})\Big(\|y_{1,\tilde{\tau}}\|_c^2+\|y_{2,\tilde{\tau}}\|_c^2+...+\|y_{n,\tilde{\tau}}\|_c^2\Big)+\int_{\tilde{\tau}-r}^{\tilde{\tau}} \lambda_{max}(\mathbf{Q_1})\Big(\|y_{1,\tilde{\tau}}\|_c^2+\|y_{2,\tilde{\tau}}\|_c^2+...+\|y_{n,\tilde{\tau}}\|_c^2\Big)d\eta \\ &= \Big(\lambda_{max}(\mathbf{P_1})+r\lambda_{max}(\mathbf{Q_1})\Big)\Big(\|y_{1,\tilde{\tau}}\|_c^2+\|y_{2,\tilde{\tau}}\|_c^2, ..., \|y_{n,\tilde{\tau}}\|_c^2\Big) \end{aligned} \tag{5.68}$$

That, proves the right part of inequality (5.57) where:

$$v = \Big(\lambda_{max}(\mathbf{P_1})+r\lambda_{max}(\mathbf{Q_1})\Big)\Big(\|y_{1,\tilde{\tau}}\|_c^2+\|y_{2,\tilde{\tau}}\|_c^2, ..., \|y_{n,\tilde{\tau}}\|_c^2\Big)$$

or in a more compact form:

$$v(\|\mathbf{y}_{\tilde{\tau},c}\|_2) = \Big(\lambda_{max}(\mathbf{P_1})+r\lambda_{max}(\mathbf{Q_1})\Big)\Big\|\mathbf{y}_{\tilde{\tau},c}\Big\|_2^2 \tag{5.69}$$

where with $\mathbf{y}_{\tilde{\tau},c}$ we denote the vector $\mathbf{y}_{\tilde{\tau},c} = (\|y_{1,\tilde{\tau}}\|_c,\ \|y_{2,\tilde{\tau}}\|_c, ..., \|y_{n,\tilde{\tau}}\|_c)^\top$. Function v is nondecreasing and continuous and satisfies $v(0) = 0$. This, verifies that the inequality condition (5.57) is met. It is left to prove that condition (5.58) of the Lyapunov-Krasovskii Stability Theorem is fulfilled as well.

In this direction, the first step is to differentiate V_1 with respect to $\tilde{\tau}$. Performing that, yields:

$$\frac{dV_1}{d\tilde{\tau}} = \bar{\mathbf{y}}^\top \bar{\mathbf{Q}}_\mathbf{1} \bar{\mathbf{y}} \tag{5.70}$$

where

$$\bar{\mathbf{Q}}_{\mathbf{1}} \triangleq \begin{pmatrix} \mathbf{P_1 A_0} + \mathbf{A_0^\top P_1} + \mathbf{Q_1} & \mathbf{P_1 A_1} \\ \\ \mathbf{A_1^\top P_1} & -\mathbf{Q_1} \end{pmatrix} \tag{5.71}$$

and

$$\bar{\mathbf{y}} \triangleq \begin{pmatrix} \mathbf{y}(\tilde{\tau}) \\ \\ \mathbf{y}(\tilde{\tau}-r)) \end{pmatrix}, \ \bar{\mathbf{y}} \in \mathbb{R}^{2n} \tag{5.72}$$

Now, we have to prove that $\bar{\mathbf{Q}}_{\mathbf{1}}$ can be rendered negative definite [44], i.e $\bar{\mathbf{Q}}_{\mathbf{1}} \prec 0$, with suitable choice of the matrices $\mathbf{P_1}, \mathbf{Q_1}$ (LMI feasibility). This is established through the next lemma.

Lemma 5.3 (**LMI feasibility**). $\exists \mathbf{P_1}, \mathbf{Q_1} \succ 0$ *diagonal positive definite matrices such that the matrix* $\bar{\mathbf{Q}}_{\mathbf{1}}$ *given by* (5.71) *satisfies:*

$$\bar{\mathbf{Q}}_{\mathbf{1}} \prec 0 \tag{5.73}$$

Proof. Without loss of generality $\mathbf{P_1}, \mathbf{Q_1}$ are assumed to be positive definite diagonal matrices. The Schur complement conditions applied on the matrix $\bar{\mathbf{Q}}_{\mathbf{1}}$ give that the inequality $\bar{\mathbf{Q}}_{\mathbf{1}} \prec 0$ is satisfied when the inequalities $\mathbf{P_1 A_0} + \mathbf{A_0^\top P_1} + \mathbf{Q_1} \prec 0$ and $\mathbf{S_1} \prec 0$ are satisfied, where, $\mathbf{S_1}$ is the Schur complement matrix of $\bar{\mathbf{Q}}_{\mathbf{1}}$. Thus, we proceed to prove that $\exists \mathbf{P_1}, \mathbf{Q_1} \succ 0$ for which, the latter two inequalities are satisfied instead of the more involved $\bar{\mathbf{Q}}_1 \prec 0$. Performing basic matrix manipulations yields:

$$\mathbf{P_1 A_0} + \mathbf{A_0^\top P_1} + \mathbf{Q_1} =$$

$$\begin{bmatrix} q_1-2p_1 & 0 & \cdots & 0 \\ 0 & \ddots & 0 & 0 \\ 0 & q_i-2p_i & \cdots & 0 \\ 0 & 0 & \ddots & 0 \\ 0 & 0 & \cdot & q_n-2p_n \end{bmatrix}$$

This matrix is negative definite ($\prec 0$) when:

$$q_i-2p_i < 0, \quad \forall i \in \{1, ..., n\} \tag{5.74a}$$

Further, the Schur complement matrix of $\bar{\mathbf{Q}}_\mathbf{1}$ is obtained as:

$$\mathbf{S_1} = \begin{bmatrix} -q_1-\frac{p_2^2}{2p_2-q_2} & 0 & \cdots & 0 \\ 0 & \ddots & 0 & 0 \\ 0 & -q_i-\frac{p_{i+1}^2}{2p_{i+1}-q_{i+1}} & \cdots & 0 \\ 0 & 0 & \ddots & 0 \\ 0 & 0 & \cdots & -q_n \end{bmatrix}$$

which is negative definite ($\prec 0$) when:

$$-q_i-\frac{p_{i+1}^2}{2p_{i+1}-q_{i+1}} < 0, \quad \forall i \in \{1, ..., n-1\} \tag{5.74b}$$

$$-q_n < 0 \tag{5.74c}$$

Restricting $\mathbf{P}_1,\ \mathbf{Q}_1$ to be positive definite yields:

$$p_i > 0\ , \quad \forall i \in \{1, ..., n\} \tag{5.74d}$$

$$q_i > 0\ , \quad \forall i \in \{1, ..., n\} \tag{5.74e}$$

Eventually, we prove that $\exists p_i, q_i\ , \forall i \in \{1, ..., n\}$, that satisfy the inequalities (5.74a)-(5.74e), i.e LMI feasibility. Our proof is constructive and relies on the following methodology for computing p_i, q_i which provides a deterministic way for finding $p_i, q_i\ , \forall i \in \{1, ..., n\}$ that

Methodology 1 for computing p_i, q_i (LMI feasibility)

1: **Choose** $p_i,\ \forall i \in \{1, ..., n\}$ that satisfy (5.74d).
2: **Choose** q_n that jointly satisfies (5.74e), (5.74a).
3: **Choose** $q_i,\ \forall i \in \{1, ..., n-1\}$, starting from q_{n-1} and following a decreasing order of i, such that, at every step the corresponding q_i satisfies (5.74a), (5.74b).

satisfy the inequalities (5.74a)-(5.74e). Hence, the LMI in (5.73) is feasible. With this, we conclude the proof. ■

The final step in proving that V_1 is a Lyapunov-Krasovskii functional certifying delay-independent asymptotic stability of (5.59) is, to show that, when $\bar{\mathbf{Q}}_1 \prec 0$ holds, the inequality (5.58) holds as well, with a function w that is continuous nondecreasing and satisfies $w(s) > 0,\ s > 0$. To establish that, the next inequality is considered:

$$\lambda_{min}(\bar{\mathbf{Q}}_\mathbf{1})\|\bar{\mathbf{y}}\|_2^2 \leq \bar{\mathbf{y}}^\top \bar{\mathbf{Q}}_\mathbf{1}\bar{\mathbf{y}} \leq \lambda_{max}(\bar{\mathbf{Q}}_\mathbf{1})\|\bar{\mathbf{y}}\|_2^2 \leq 0 \tag{5.75}$$

where since $\bar{\mathbf{Q}}_\mathbf{1} \prec 0 \Rightarrow \lambda_{min}(\bar{\mathbf{Q}}_\mathbf{1}),\ \lambda_{max}(\bar{\mathbf{Q}}_\mathbf{1}) < 0$. Therefore, we can choose ε such that:

$$\lambda_{max}(\bar{\mathbf{Q}}_\mathbf{1})\|\bar{\mathbf{y}}\|_2^2 \leq -\varepsilon\|\bar{\mathbf{y}}\|_2^2 \leq 0 \tag{5.76}$$

Finally, using:

$$\|\bar{\mathbf{y}}\|_2 \geq \|\mathbf{y}(\tilde{\tau})\|_2 \Rightarrow \|\bar{\mathbf{y}}\|_2^2 \geq \|\mathbf{y}(\tilde{\tau})\|_2^2 \tag{5.77}$$

inequality (5.76) is reduced to:

$$\lambda_{max}(\bar{\mathbf{Q}}_\mathbf{1})\|\bar{\mathbf{y}}\|_2^2 \leq -\varepsilon\|\bar{\mathbf{y}}\|_2^2 \leq -\varepsilon\|\mathbf{y}(\tilde{\tau})\|_2^2 \leq 0 \tag{5.78}$$

which proves that the condition (5.58) is fulfilled with:

$$w(\|\mathbf{y}(\tilde{\tau})\|_2) = \varepsilon\|\mathbf{y}(\tilde{\tau})\|_2^2 \tag{5.79}$$

This function is nondecreasing and continuous with $w(\|\mathbf{y}(\tilde{\tau})\|_2) > 0$ for $\|\mathbf{y}(\tilde{\tau})\|_2 > 0$. In addition, it holds that $\lim_{\|\mathbf{y}(\tilde{\tau})\|_2 \to \infty} u(\|\mathbf{y}(\tilde{\tau})\|_2) = \infty$. Employing the Lyapunov-Krasovskii Theorem 5.2 [44], results to the equilibrium point $\mathbf{y}_0 = \mathbf{0}_n$ of (5.59) being *globally asymptotically stable.* ■

Theorem 5.3 guarantees that the equilibrium point of the fast boundary-layer system (5.29) is asymptotically stable independently of time-delays. Intuitively, that means that the fast consensus state-variables z_i, $\forall i \in \mathcal{G}$, converge to the slow state-variable ξ_h independently of any time-delays, as long as ξ_h remains "*frozen*" in the time interval $[\tilde{\tau}-r, \tilde{\tau}]$. That is of practical interest, since it certifies robust performance of the protocol $\mathcal{P}_2$ with respect to time-delays that are inherent in communication channels. Finally, Methodology 1 can be deployed to deterministically construct a Lyapunov-Krasovskii functional (5.61) for the system (5.59) that fulfills conditions (5.57), (5.58) of Theorem 5.2, and serves as a certificate of the above time-delays-robust stability property.

5.8 Distributed CLF-Based Torque Controller Design

In the previous Sections, we established asymptotic stability of the equilibrium of the system $\mathcal{P}_2$ and of the equilibrium of the time-delayed version of $\mathcal{P}_2$. Due to these properties, a group of WGs that adopts the protocol $\mathcal{P}_2$ can provably self-organize and control their power output in a fair load-sharing manner and under dynamical conditions to attain total power reference tracking. Practically, the protocol can be realized by appropriately designing the control laws for the RSCs which control the dynamics of $C_{p,i}/\overline{C}_{p,i}$. To this end, we develop a distributed CLF-based torque controller for the RSC of each WG which renders the closed-loop dynamics of $C_{p,i}/\overline{C}_{p,i}$ identical to (5.12c). We begin by considering equation (5.12c) in analytical form as:

$$\frac{1}{\overline{C}_{p,i}}\frac{dC_{p,i}}{dt} = -k_{\alpha,i}\left(\frac{C_{p,i}}{\overline{C}_{p,i}} - \frac{C_{p,i-1}}{\overline{C}_{p,i-1}}\right), \qquad i \in \mathcal{G} \tag{5.80}$$

This dynamical equation represents the desired closed-loop dynamics of the utilization level $C_{p,i}/\overline{C}_{p,i}$ as described by the consensus protocol dynamics (5.12c). On the other hand, the physical dynamics of $C_{p,i}/\overline{C}_{p,i}$ are:

$$\frac{1}{\overline{C}_{p,i}}\frac{dC_{p,i}}{dt} = \frac{1}{\overline{C}_{p,i}}\frac{\partial C_{p,i}}{\partial \lambda_i}\frac{\partial \lambda_i}{\partial \omega_{r,i}}\frac{\omega_s}{2H_i}(T_{m,i} - T_{e,i}), \quad i \in \mathcal{G} \tag{5.81}$$

The controller of the RSC has to ensure that the closed-loop physical dynamics in (5.81) become identical to the consensus dynamics in (5.80). This happens, when the electrical torque is equal to:

$$T^*_{e,i} = T_{m,i} - \left(\frac{1}{\overline{C}_{p,i}}\frac{\partial C_{p,i}}{\partial \lambda_i}\frac{\partial \lambda_i}{\partial \omega_{r,i}}\frac{\omega_s}{2H_i}\right)^{-1}\left[-k_{\alpha,i}\left(\frac{C_{p,i}}{\overline{C}_{p,i}} - \frac{C_{p,i-1}}{\overline{C}_{p,i-1}}\right)\right], \quad \forall i \in \mathcal{G}$$

The control objective of the RSC is to guarantee that the WG's electrical torque $T_{e,i}$ is asymptotically tracking the dynamical torque reference $T^*_{e,i}$. For this particular purpose, a distributed control law for the RSC is introduced through the theorem below under the following assumptions.

Assumption 4 (**Constant terminal voltage**). *$dV_{s,i}/dt$=0.*[1]

Assumption 5 (**Constant wind speed**). $(\partial^2\lambda_i/\partial t\partial\omega_{r,i}) = 0$.

Theorem 5.4. *Under assumptions 4 and 5, the electrical torque $T_{e,i}$ is asymptotically tracking the dynamical torque reference $T^*_{e,i}$ with the RSC control law:*

$$\begin{aligned} V_{dr,i} = {} & \frac{X'_{s,i}}{V_{s,i}}\Big[\dot{T^*_{e,i}} - k_{\beta,i}(T_{e,i} - T^*_{e,i})\Big] - \frac{1}{T'_{0,i}}\Big[-(E'_{q,i} \\ & + (X_{s,i} - X'_{s,i})I_{ds,i}) + T'_{0,i}(-(\omega_s - \omega_{r,i})E'_{d,i})\Big]\frac{X_{r,i}}{X_{m,i}\omega_s} \end{aligned} \tag{5.82}$$

where $T^*_{e,i}$ is given by (5.82) and $\dot{T}^*_{e,i}$ is the time derivative of $T^*_{e,i}$.

Proof. This theorem can be proved by analytically constructing the distributed RSC control law (5.82). First consider the candidate CLF as:

$$V_{e,i} = \frac{1}{2}(T_{e,i} - T^*_{e,i})^2, \; V_{e,i} > 0, \;\; \forall T_{e,i} \in \overline{\mathcal{D}}_{e,i}, \; \forall i \in \mathcal{G} \tag{5.83}$$

where $\overline{\mathcal{D}}_{e,i} \triangleq \mathcal{D}_{e,i} \backslash \{T^*_{e,i}\}$, $\mathcal{D}_{e,i} \subset \mathbb{R}$ and define the error $\Delta T_{e,i} = (T_{e,i} - T^*_{e,i})$. For this CLF, the next lemma is stated.

Lemma 5.4. *$V_{e,i}$ is a CLF for the system given by the error dynamics $\Delta\dot{T}_{e,i}$.*

Proof. Let the electrical torque be expressed as:

$$T_{e,i} = \frac{E'_{q,i}V_{s,i}}{X'_{s,i}}, \;\; \forall i \in \mathcal{G} \tag{5.84}$$

[1]This can be achieved through fast voltage control of the DFIG.

Computing the time derivative of $V_{e,i}$ gives us:

$$\dot{V}_{e,i} = (T_{e,i}-T^{*}_{e,i})\Big[\frac{V_{s,i}}{X^{'}_{s,i}}\frac{1}{T^{'}_{0,i}}[-(E^{'}_{q,i}+(X_{s,i}-X^{'}_{s,i})I_{ds,i})$$
$$+T^{'}_{0,i}(\omega_s\frac{X_{m,i}}{X_{r,i}}V_{dr,i}-(\omega_s-\omega_{r,i})E^{'}_{d,i})]-\dot{T}^{*}_{e,i}\Big] \quad (5.85)$$

Taking the $\mathbf{inf(\cdot)}$ of (5.85) we obtain:

$$\inf_{V_{dr,i}\in\mathcal{U}_i}\dot{V}_{e,i}\begin{cases}-\infty, & \Delta T_{e,i}\neq 0\\ 0, & \Delta T_{e,i}=0\end{cases} \quad (5.86)$$

From (5.86), it can be concluded that $V_{e,i}$ is a CLF and that there exists a control law $V_{dr,i}$ which guarantees that $\lim_{t\to\infty}\Delta T_{e,i}=0$, i.e $\lim_{t\to\infty}T_{e,i}=T^{*}_{e,i}$. With that, we complete the proof. ■

An appropriate control law $V_{dr,i}$ is the one that causes the next inequality to hold.

$$\dot{V}_{e,i}<0,\ \ \forall T_{e,i}\in\overline{\mathcal{D}}_{e,i},\ \forall i\in\mathcal{G} \quad (5.87)$$

One such controller can be constructed by imposing the constraint below on the error dynamics:

$$\Delta\dot{T}_{e,i} = -k_{\beta,i}\Delta T_{e,i} \quad (5.88)$$

Expanding this constraint yields:

$$\dot{T}_{e,i} = \dot{T}^{*}_{e,i}-k_{\beta,i}(T_{e,i}-T^{*}_{ei}),\ \ \forall i\in\mathcal{G} \quad (5.89)$$

With this constraint, the derivative of $V_{e,i}$ becomes:

$$\dot{V}_{e,i} = -k_{\beta,i}(T_{e,i} - T^*_{e,i})^2 < 0, \ \ \forall T_{e,i} \in \overline{\mathcal{D}}_{e,i} \tag{5.90}$$

where $\dot{T}^*_{e,i}$ is given by:

$$\begin{aligned} \dot{T}^*_{e,i} &= \dot{T}_{m,i} + k_{\beta,i}\overline{C}_{p,i}\Big(\frac{\omega_s}{2H_i}\frac{\partial \lambda_i}{\partial \omega_{r,i}}\Big)^{-1}\Big(\frac{\partial C_{p,i}}{\partial \lambda_i}\Big)^{-2} \cdot \Big[\Big(\frac{\dot{C}_{p,i}}{\overline{C}_{p,i}} - \frac{\dot{C}_{p,i-1}}{\overline{C}_{p,i-1}}\Big)\frac{\partial C_{p,i}}{\partial \lambda_i} \\ &- \Big(\frac{C_{p,i}}{\overline{C}_{p,i}} - \frac{C_{p,i-1}}{\overline{C}_{p,i-1}}\Big)\frac{\partial^2 C_{p,i}}{\partial \lambda_i^2}\frac{\partial \lambda_i}{\partial \omega_{r,i}} \cdot \dot{\omega}_{r,i}\Big], \ \ \forall i \in \mathcal{G} \end{aligned} \tag{5.91}$$

Finally, by substituting the electrical torque expression:

$$T_{e,i} = (E^{'}_{q,i}V_{s,i}) \cdot (X^{'}_{s,i})^{-1}, \ \ \forall i \in \mathcal{G} \tag{5.92}$$

into (5.89) and by employing equation (5.1b) the RSC control input can be obtained as:

$$\begin{aligned} V_{dr,i} &= \frac{X^{'}_{s,i}}{V_{s,i}}\Big[\dot{T}^*_{e,i} - k_{\beta,i}(T_{e,i} - T^*_{e,i})\Big] - \frac{1}{T^{'}_{0,i}}\Big[-(E^{'}_{q,i} \\ &+ (X_{s,i} - X^{'}_{s,i})I_{ds,i}) + T^{'}_{0,i}(-(\omega_s - \omega_{r,i})E^{'}_{d,i})\Big]\frac{X_{r,i}}{X_{m,i}\omega_s} \end{aligned} \tag{5.93}$$

Recall that, in the derivation of the above controller, Assumptions 4 and 5 are considered. The terms $\partial\lambda_i/\partial\omega_{r,i}$, $\partial C_{p,i}/\partial\lambda_i$ are already given in Chapter 3 by (3.64) and (3.62) while the term $\partial^2 C_{p,i}/\partial\lambda_i^2$ can be obtained by differentiating $\partial C_{p,i}/\partial\lambda_i$ with respect to λ_i as:

$$\frac{\partial^2 C_{p,i}}{\partial \lambda_i^2} = e^{-12.5(\frac{1}{\lambda_i} - 0.035)}\Big[\frac{12.5}{\lambda_i^2}\Big(-\frac{25.52}{\lambda_i^2} + \frac{319}{\lambda_i^2}\Big(\frac{1}{\lambda_i} - 0.035\Big)\Big) + \Big(\frac{51.04}{\lambda_i^3} - \frac{957}{\lambda_i^4} + \frac{22.33}{\lambda_i^3}\Big)\Big] \tag{5.94}$$

■

This completes the proof.

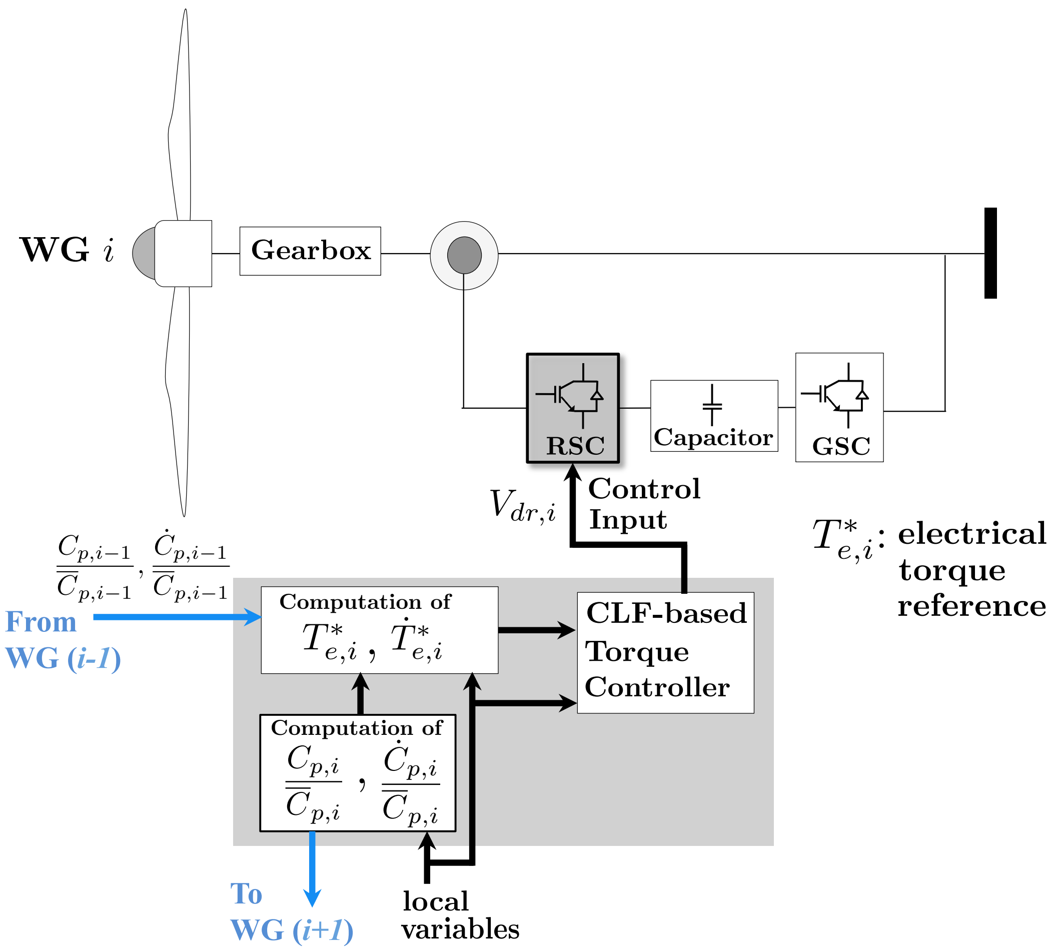

Figure 5.4: Distributed CLF-based torque controller of RSC i

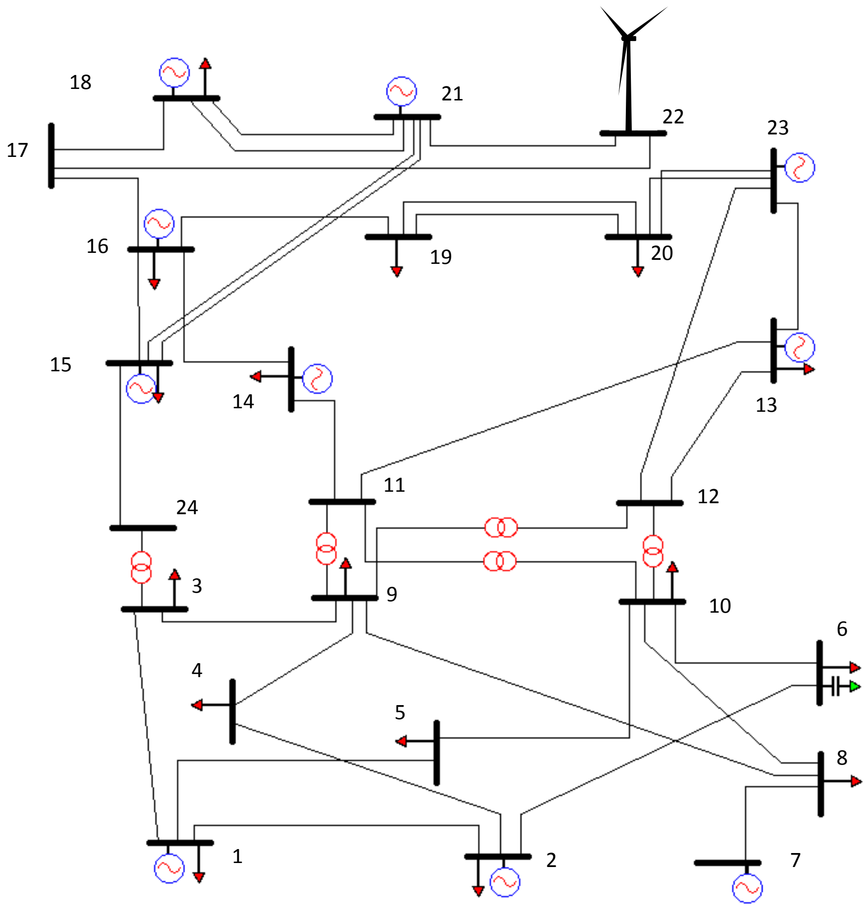

Figure 5.5: IEEE 24-bus RT system with a WF at bus 22

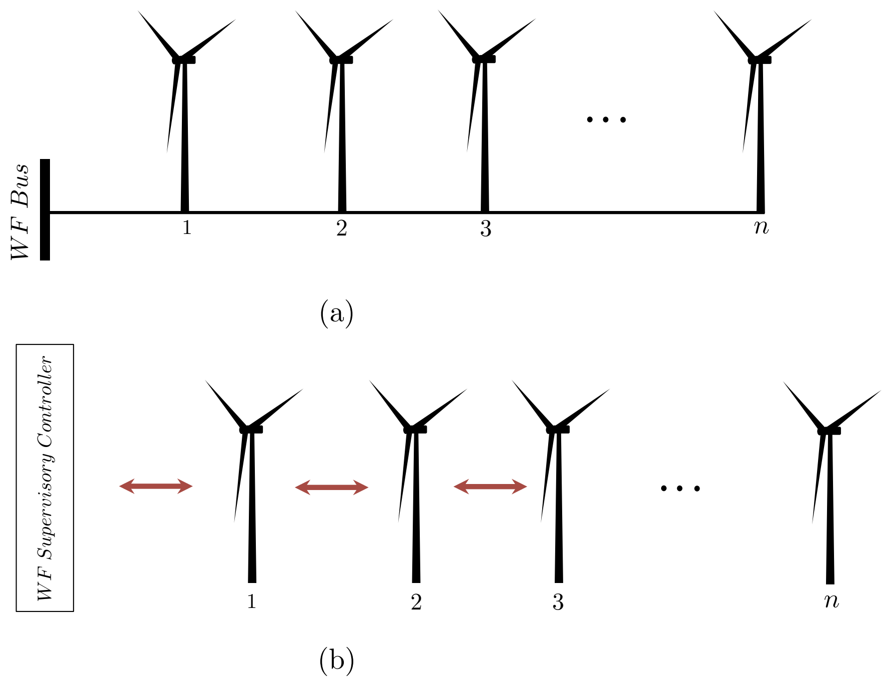

Figure 5.6: a) Physical and b) Communication interconnections among WGs

5.9 Case Studies

This Section presents numerical simulations verifying the theoretical results presented in this Chapter. Specifically, through simulations on the modified IEEE 24-bus RT system, the performance of the proposed protocol and corresponding distributed CLF-based torque controller are evaluated. The 24-bus system is modified such that on bus 22, a WF, comprised of 10 WGs and the physical and communication topologies depicted in Fig. 5.6, is placed . The initial local wind-speed conditions are assumed to be $v_{w,i} = 13.17\frac{m}{s}$ and homogeneous throughout the WF. In this set-up, simulations are conducted with the RSC of each WG implementing the distributed CLF-based torque controller in (5.93) under the following critical scenarios.

- **Scenario 1** (Reference P_d varies with constant wind speed $v_w = 13.17\ m/s$)
  - $t = 0s$: The WF power reference is constant at $P_d = 0.38\ p.u.$

- $t = 3s$: The WF power reference decreases to $P_d = 0.36\ p.u.$
- $t = 9s$: The WF power reference increases to $P_d = 0.40\ p.u.$

- **Scenario 2** (Wind speed v_w varies with constant reference $P_d = 0.38$)
  - $t = 0s$: The wind speed is constant at $v_w = 13.17\ m/s$.
  - $t = 2s$: The wind speed decreases to $v_w = 12\ m/s$.

- **Scenario 3** (Both the reference P_d and wind speed v_w vary)
  - $t = 0s$: The reference and wind speed are constant, $P_d = 0.38\ p.u$, $v_w = 13.17 m/s$.
  - $t = 3s$: The WF power reference increases to $P_d = 0.40\ p.u.$
  - $t = 9s$: The wind speed increases to $v_w = 14.17\ m/s$.
  - $t = 15s$: The WF power reference decreases to $P_d = 0.36\ p.u$ and at the same time the wind speed decreases to $v_w = 12.17\ m/s$.

For illustration purposes, step-wise variations of the reference and wind speed are considered in the above scenarios. First, the results of *Scenario 1* are discussed. From Fig. 5.8, observe that the distributed CLF-based torque controller succeeds in providing total WF power output regulation. Specifically, the WF total power output tracks the variations of P_d with very good dynamic performance e.g small response time, no overshoot. In order for the total WF power to closely track P_d while it varies quasistatically, the controllers everytime dynamically redispatch and readjust the power outputs of WGs through regulation of the loading levels (consensus states) to their new equilibria which depend on the reference P_d. In our particular case, two new equilibria arise for the loading levels, one at $t = 3s$ and one at $t = 9s$. These can be respectively computed as:

$$t = 3s: \qquad \xi_{h0} = \frac{P_d}{\sum_{i=1}^{10} \alpha_i} = \frac{0.36{\cdot}100{\cdot}10^6}{10{\cdot}(0.5{\cdot}1.225{\cdot}0.438{\cdot}\pi{\cdot}52^2{\cdot}13.17^3)} = 0.6915$$

$$t = 9s: \qquad \xi_{h0} = \frac{P_d}{\sum_{i=1}^{10} \alpha_i} = \frac{0.40 \cdot 100 \cdot 10^6}{10 \cdot (0.5 \cdot 1.225 \cdot 0.438 \cdot \pi \cdot 52^2 \cdot 13.17^3)} = 0.7684$$

The "fair dispath" or equivalently, the "load sharing" among the WGs can be observed in Fig. 5.7, where the loading levels (ratios $C_{p,i}/\overline{C}_{p,i}$) converge to a common value soon after each perturbation. The protocol accomplishes that through the following mechanism. The ratios $C_{p,i}/\overline{C}_{p,i}$ reach consensus and rapidly converge to the auxiliary state-variable ξ_h of the leader where ξ_h can be thought of as a quasistatic equilibrium for the fast state-variables $C_{p,i}/\overline{C}_{p,i}$. At the same time, the state-variable ξ_h converges to its equilibrium ξ_{h0}, which depends on the new reference P_d, in the slow time-scale as depicted in Fig. 5.7. Through that, ξ_h drives the consensus protocol dynamics since the state-variables $C_{p,i}/\overline{C}_{p,i}$ eventually converge to the equilibrium of ξ_h, ξ_{h0}.

The intuition driving the execution of the protocol and the above numerical simulations, can be analyzed as follows. First, the leader WG senses the variations of P_d through its auxiliiary state-variable ξ_h which decreases and increases at $t = 3s$ and at $t = 9s$, respectively. Correspondingly, the leader's consensus state-variable follows ξ_h and decreases at $t = 3s$ while it increases at $t = 9s$. In a concurrent and synchronized manner, the followers act in a similar fashion, decreasing and then increasing their utilization levels (consensus states) to reach consensus with the leader. Concretely, these actions lead to the loading levels converging to 0.6915 after $3s$ and to 0.7684 after $9s$, while initially departing from the value 0.73 (Fig. 5.7). Practically, the distributed CLF-based torque controllers accomplished that by initially accelerating and then decelerating the WGs as shown in Fig. 5.9. That facilitated the WGs to reduce and then increment their mechanical power outputs so that altogether, they closely tracked the desired power reference in both cases (Fig. 5.8).

Moving to the simulation results under *Scenario 2*, it can be realized from Fig. 5.12 that the total mechanical power $\sum_i P_{m,i}$ is initially constant while after the sudden drop in the wind-speed it dives to a lower value. The equilibrium of the WGs' loading levels and the

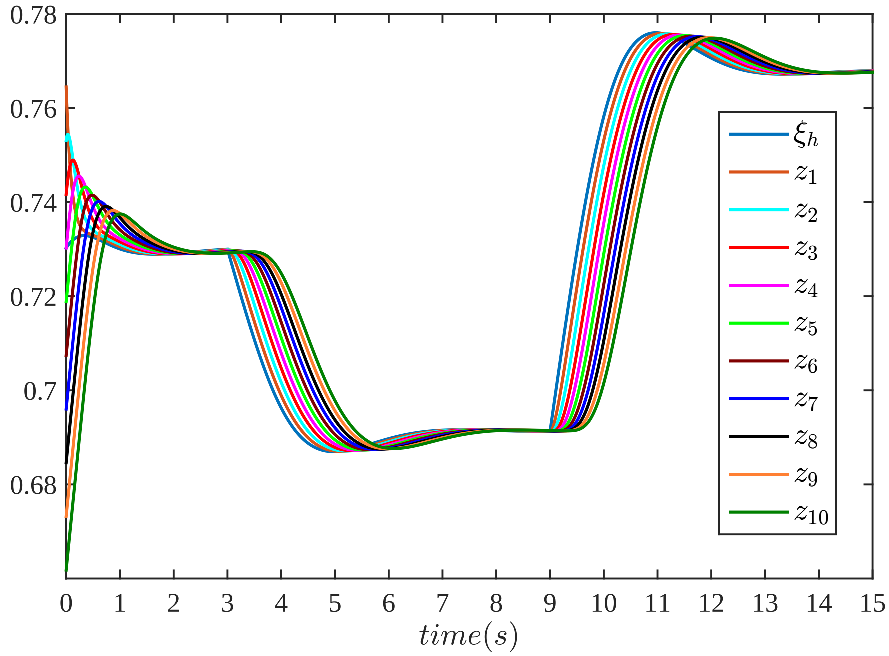

Figure 5.7: *Scenario 1*: Loading levels

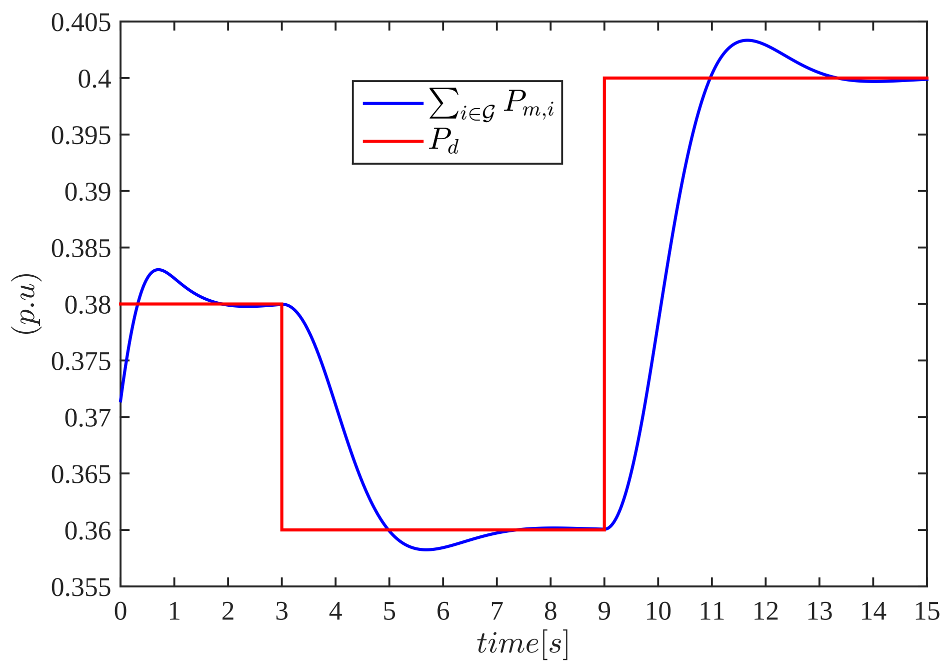

Figure 5.8: *Scenario 1*: Total mechanical power

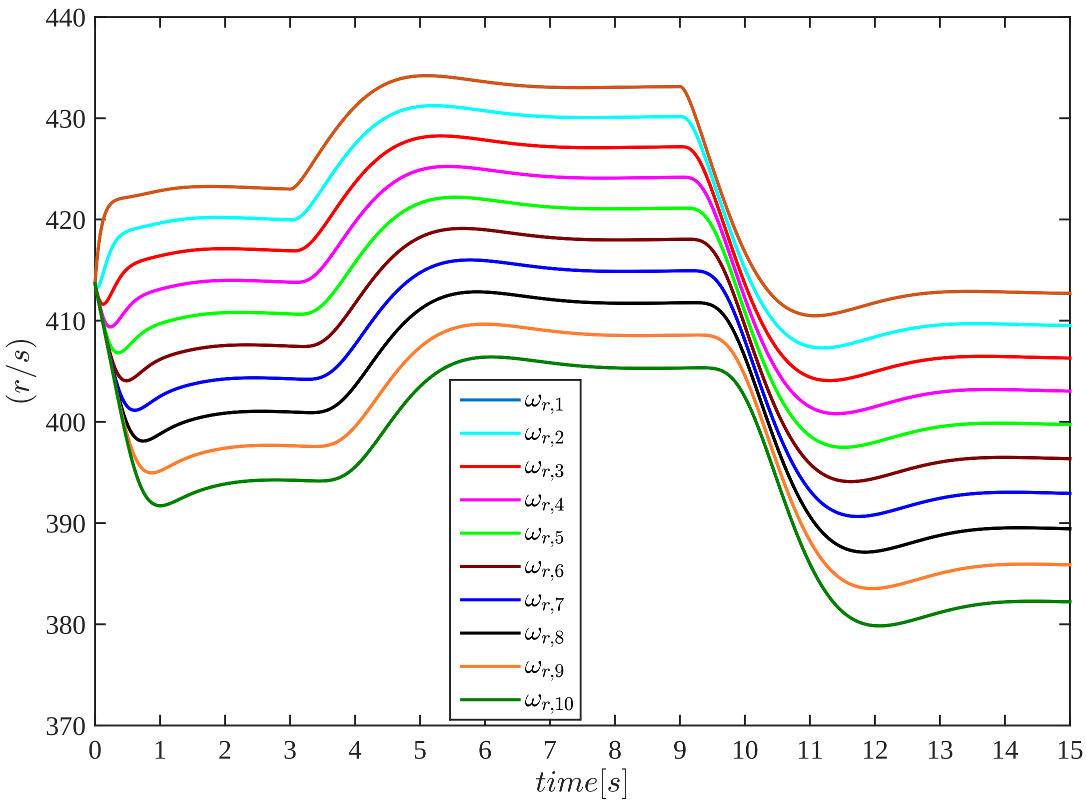

Figure 5.9: *Scenario 1*: Rotor speeds

auxiliary state-variable ξ_h, before the wind-speed disturbance (i.e in $t \in [0, 2s]$), is:

$$\xi_{h0} = \frac{P_d}{\sum_{i=1}^{10} \alpha_i} = \frac{0.38{\cdot}100{\cdot}10^6}{10{\cdot}(0.5{\cdot}1.225{\cdot}0.438{\cdot}\pi{\cdot}52^2{\cdot}13.17^3)} = 0.729$$

The loading levels starting from non equal values converge to this equilibrium asymptotically during the first 2 seconds, as can be seen in Fig. 5.11. Subsequently, the leader senses the wind-speed drop in the dynamics of the auxiliary variable ξ_h whose equilibrium, that is also the equilibrium for the loading levels, changes to:

$$\xi_{h0} = \frac{P_d}{\sum_{i=1}^{10} \alpha_i} = \frac{0.38{\cdot}100{\cdot}10^6}{10{\cdot}(0.5{\cdot}1.225{\cdot}0.438{\cdot}\pi{\cdot}52^2{\cdot}12^3)} = 0.965$$

Notice that, this equilibrium signifies that the WGs' loading levels have to increase in order for the WGs to generate the same power P_d but now with lower wind-speed, $v_w = 12$ (m/s) instead of $v_w = 13.17$ (m/s). The auxiliary state-variable of the leader first moves toward the new equilibrium. Concurrently and in synchrony with the leader, each of the followers exploit the peer-to-peer communication to regulate their loading levels to the loading levels of their respective neighbors. These actions ultimately lead to all loading levels converging to the new equilibrium ξ_{h0} as seen in Fig. 5.11. This verifies the fair load-sharing among the WGs. Practically, the WGs regulate their loading levels by controlling the rotational speeds of their shafts, i.e accelerating or decelerating their turbines. This can be seen in Fig. 5.13.

In *Scenario 3*, both variations on the reference P_d and the wind speed v_w are considered as can be seen in Fig. 5.14. First, at $t = 3s$ the WF power reference increases from 0.38 $p.u$ to 0.4 $p.u$, causing both the loading levels of WGs and correspondingly the total mechanical power to increase, with the latter tracking the new value of the reference. These responses are depicted in Fig. 5.15 and Fig.5.16 respectively. Practically, the RSCs realize that by slowing down the WGs as seen in Fig. 5.17. At $t = 9s$, the wind speed increases from

$13.17 m/s$ to $14.17\ m/s$ (Fig. 5.14). In this case, the controllers decrease WGs' loading levels (Fig. 5.15) such that they still generate total power equal to 0.4 $p.u$ but now with higher wind speed. To achieve that, the turbines accelerate in this case as shown in Fig. 5.17. The abrupt raise of the wind speed causes a spike in the response of the total mechanical power while at $t = 15s$, the sudden drop of the wind speed causes the mechanical power to dive as depicted in Fig. 5.16. In the latter case though, the loading levels increase in order to track their new equilibrium value that depends on both the reference P_d and the wind speed v_w. The reason is that the drop of P_d alone would cause the loading levels to decrease while the drop of the wind speed v_w alone, would cause the loading levels to increase. In our case, these variations combined eventually cause the loading levels to increment (Fig. 5.15) which means that the effect of the wind speed variation is more pronounced on the new equilibrium of the loading levels. In this case, the WGs decelerate in order to increase their total power departing from the nadir point that was reached because of the dive in the wind speed.

In all the above results, the small delay in the tracking response of the all the variables is due to the consensus/information dynamics and not due to the implementation of the consensus dynamics by the local controllers. The latter is achieved via tracking of the electrical torque reference almost instantaneously due to high control gains. Therefore, we speculate that if we run the above simulations by replacing the distributed consensus-based control scheme with a perfect centralized control scheme, i.e a scheme where the references can be provided to wind generators almost instantaneously, there would be no delay in the tracking response of the above variables. In future work, it would be interesting to normalize the performance of our proposed distributed control scheme over such a perfect centralized control scheme.

In summary, the proposed protocol and corresponding distributed CLF-based torque controller, as numerically verified by the above simulations under the three critical scenarios, are able to distributively and dynamically self-organize and control a group of deloaded WGs in a fair load sharing fashion so that their total power tracks a given reference.

5.10 Conclusion

In this Chapter, a control method that can be adopted by a fleet of deloaded WGs to distributively self-dispatch and regulate their power outputs such that they provide total power reference tracking, is proposed. Our methodology is comprised of a consensus protocol and a corresponding distributed CLF-based torque controller for the RSC of each WG. By invoking Lyapunov and singular perturbation theories [10] we provided theoretical guarantees for the asymptotic behavior of the consensus protocol and derived a specific condition under which asymptotic stability of its equilibrium is guaranteed. This result is further extended by proving delay-independent asymptotic stability of its equilibrium through a Lyapunov-Krasovskii functional. Lastly, we developed a distributed CLF-based torque controller for the RSC that implements the protocol in practice through peer-to-peer communication. The effectiveness of the proposed methodology is tested and evaluated through numerical simulations on the IEEE 24-bus RT system.

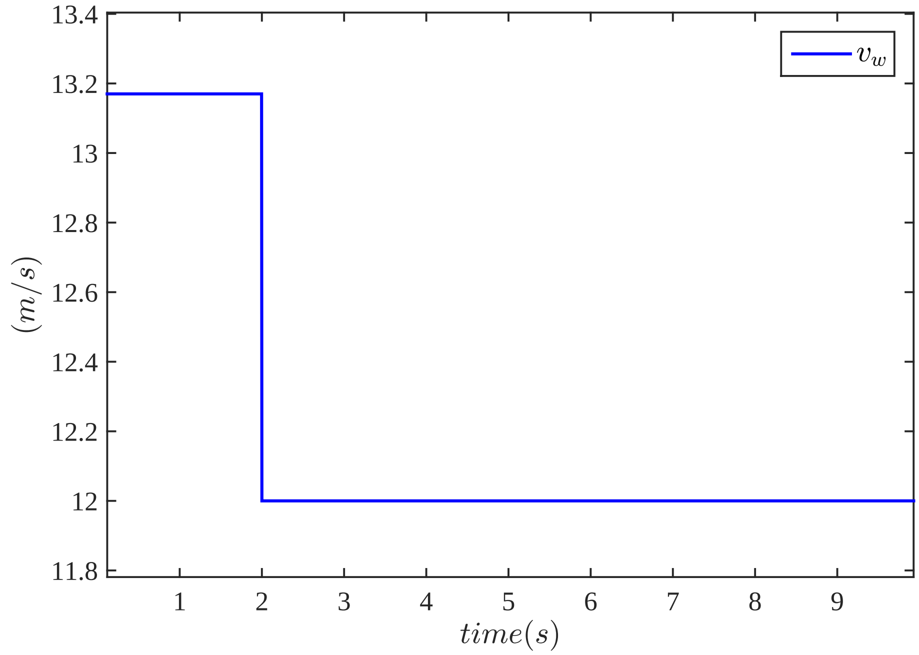

Figure 5.10: *Scenario 2*: Wind speed

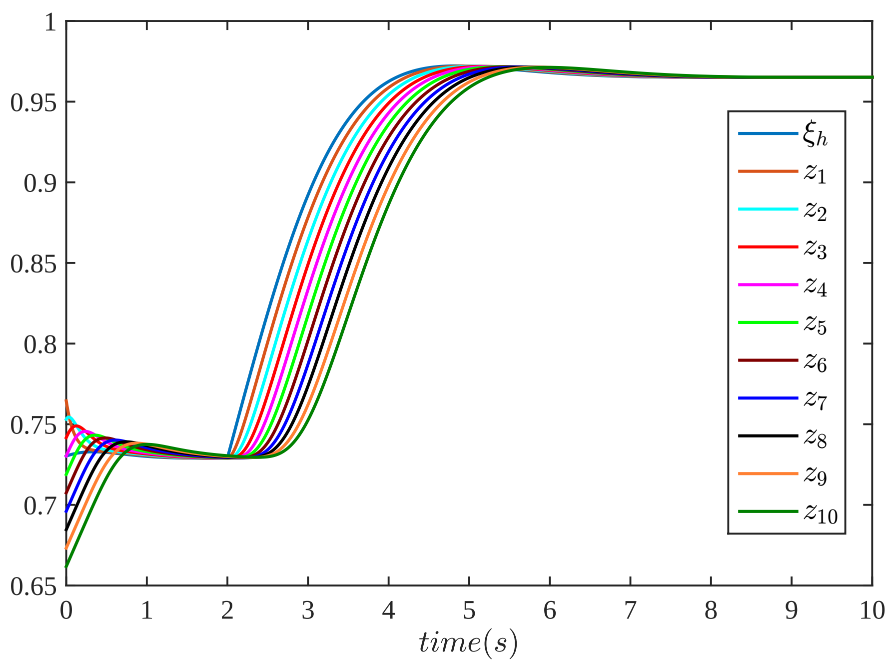

Figure 5.11: *Scenario 2*: Loading levels

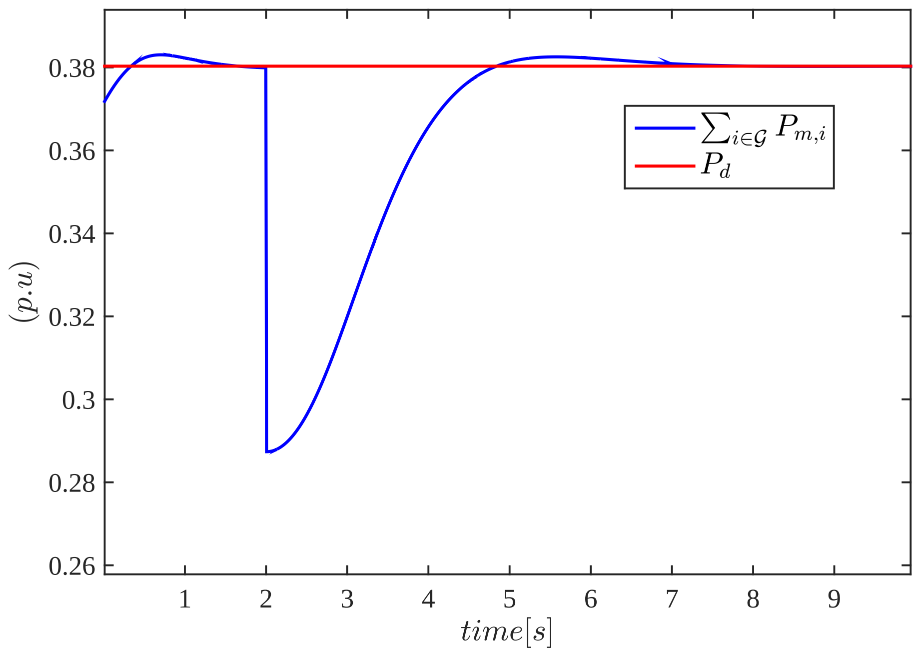

Figure 5.12: *Scenario 2*: Total mechanical power

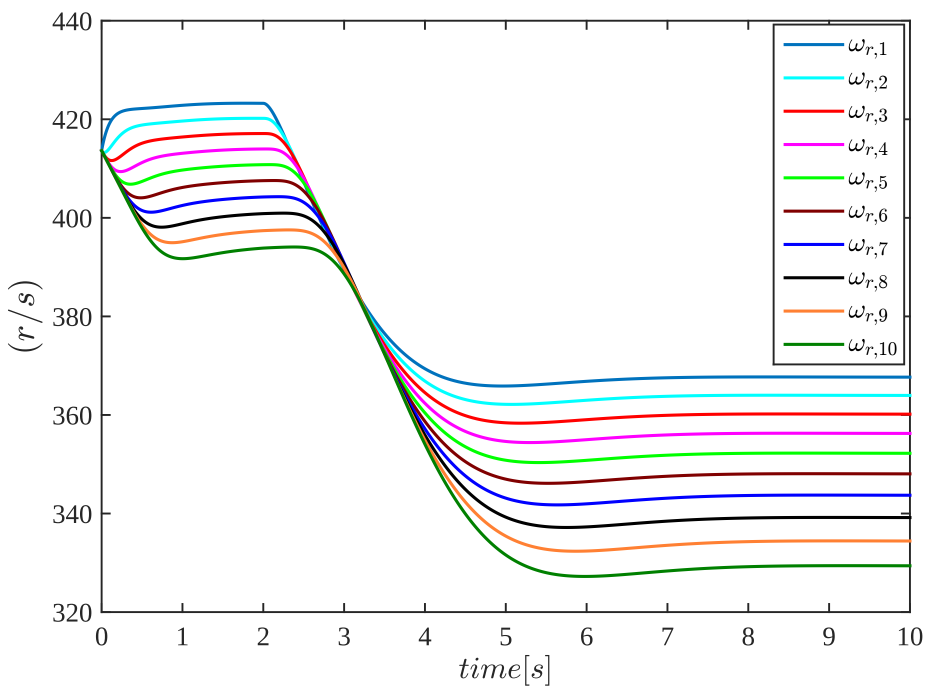

Figure 5.13: *Scenario 2*: Rotor speeds

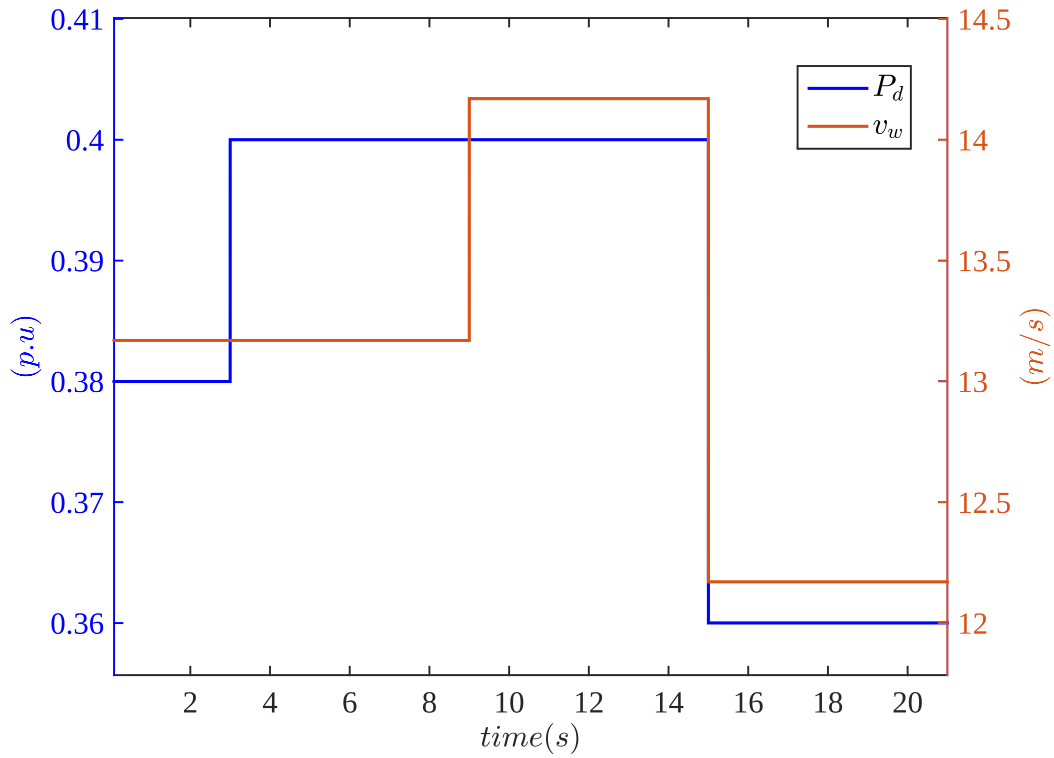

Figure 5.14: *Scenario 3*: Wind speed (v_w) and power reference (P_d) variations

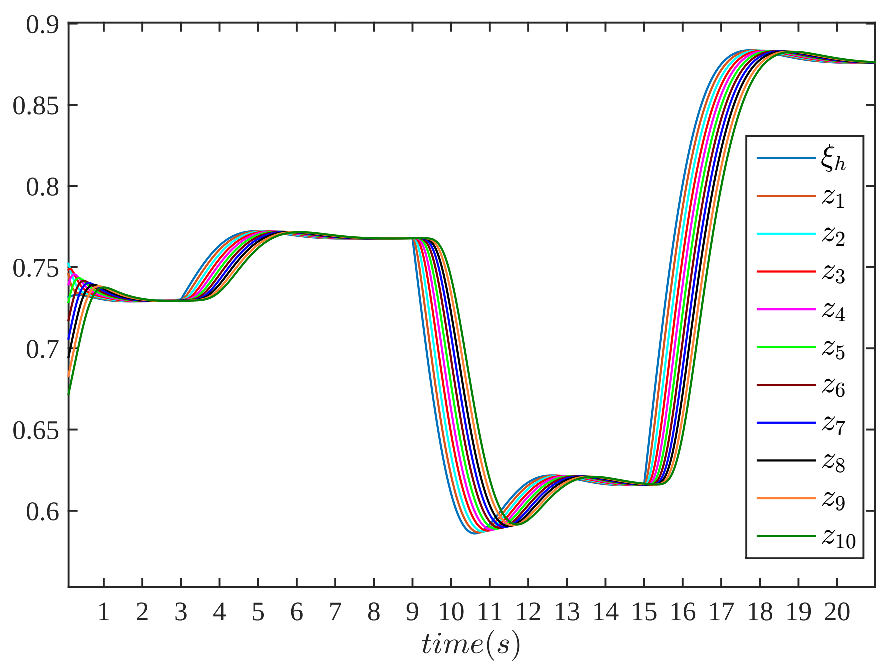

Figure 5.15: *Scenario 3*: Loading levels

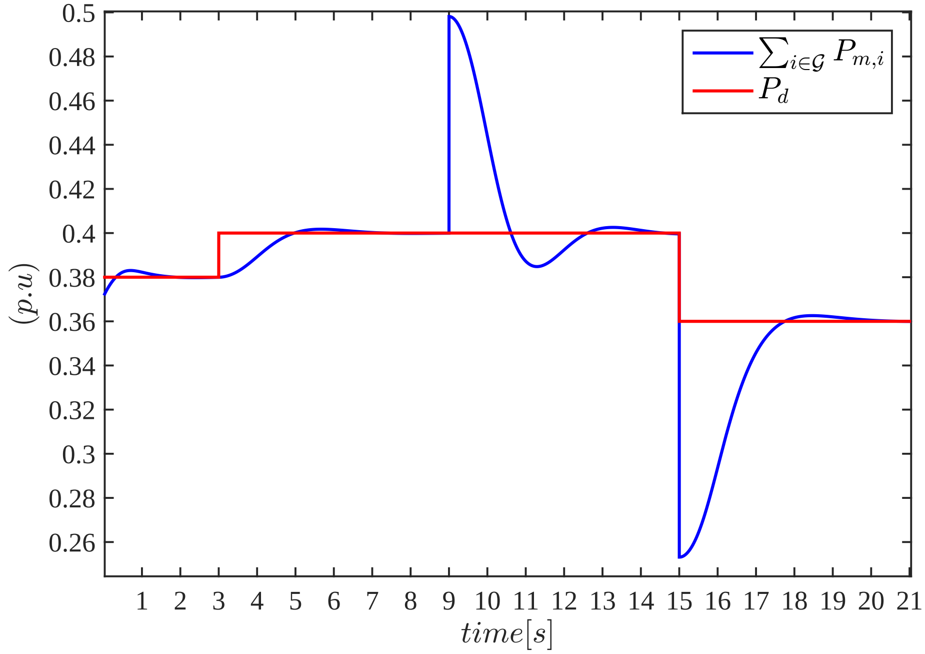

Figure 5.16: *Scenario 3*: Total mechanical power

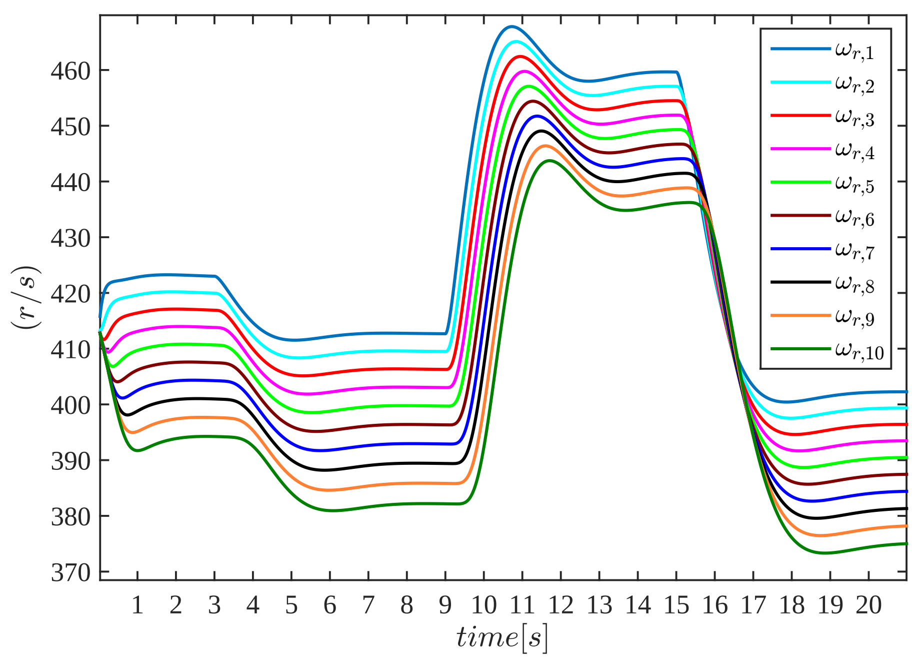

Figure 5.17: *Scenario 3*: Rotor speeds

Chapter 6

Conclusions and Future Work

In this Chapter, the research work presented in this dissertation is summarized and concluded, and directions for future work are pointed out.

6.1 Conclusions

In this dissertation, we first recognize that, modern power systems are characterized by the increasing influx of advanced sensing, communication, information technologies as well as high levels of penetration of renewable energy resources. On one side, these advanced technologies provide a new source of information and new means of contributing to power systems control and to the maintainance of normal operation of power systems. On the other side, the volatile nature of renewable energy resources causes fast and unpredictable variations on the generation side that challenge normal operation of power systems. In this context, two critical problems for modern power systems are identified and studied in this thesis, the problem of transient stabilization of conventional synchronous generators and the problem of WF power output regulation. These two problem can be naturally posed as nonlinear control problems due to the inherent nonlinear dynamics of conventional synchronous generators, storage devices and wind DFIGs involved. In this thesis, these control problems are effectively solved through the development of several sophisticated nonlinear control architectures that leverage the available communication, sensing and information technologies. By contributing to transient stabilization of SGs and to WF power output regulation, the proposed control schemes can lead to enhanced performance, stability, robustness and efficiency in power systems with high levels of wind power penetration. In this thesis, we particularly focus on developing decentralized and distributed control schemes for synchronous generators (SGs), energy storage devices and state-of-the-art wind generators (WGs) that effectively solve the above problems with theoretical guarantees on their performance. The effectiveness of the proposed control methods is demonstrated and the theoretical results are numerically verified, through numerical simulations on a proof-of-concept 3-bus system and the IEEE 24-bus Reliability Test System (RTS).

In the beginning of this dissertation the focus is on the transient stabilization problem where the following two facts are recognized: 1) excitation control of generators which is traditionally the one responsible for retaining their transient stabilization and terminal voltage regulation cannot effectively accomplish both objectives at the same time since they become conflicting [24]; 2) large disturbances trigger highly nonlinear power system dynamics for which standard linearization-based controllers are not able to guarantee stabilization or performance for a wide range of operating conditions. With this in mind, a nonlinear control law based on MIMO feedback linearization theory is proposed that provably attains transient stabilization and voltage regulation by coordinating the controller of a storage device, which can provide real and reactive power regulation, with the excitation controller of a synchronous generator. In this way, the proposed control scheme fully exploits the potential of both a generator and a storage device for real and reactive power regulation in a coordinated fashion, effectively accomplishing the above two control objectives. The proposed control scheme is novel since it is the first control scheme to provably attain concurrent transient stability and voltage regulation for a wide-range of operating conditions by effectively and efficiently exploiting the capabilities of existing power system technologies like synchronous generators with these of new technologies like storage devices.

The biggest part of this dissertation is dedicated to solving the WF power output regulation problem where several contributions are made. We identify this problem as an emerging problem in modern power systems for the following reason. In the near future and in many countries around the world, it is expected that a high portion of the total electricity demand will be met from energy coming from wind generators. The required high wind power integration levels that will achieve that, can be practically realized efficiently and securely when WGs are able to counterbalance wind intermittency and attain power output regulation together with capabilities such as frequency/inertial control. This is true because high wind power integration levels lead to significantly deteriorated power quality and increased cost of electricity for meeting a particular load pattern. The latter comes from the fact that expensive conventional generators are called to generate the mismatch between scheduled-predicted and actual available wind power. At the same time, with WGs replacing SGs and causing an overall decrease of system's effective inertia while not providing any frequency or inertial control capabilities, power systems stability, specifically transient and frequency stability, is greatly challenged. Having established that power output regulation from WGs is very important for the secure operation of power systems, we first study this problem at the component level, i.e enabling a single state-of-the-art (SoA) WG with a supercapacitor storage device to generate predictable power. To solve this problem in this set-up, we propose a nonlinear energy-based control scheme for the WG which can enable the WG to use its storage power in order to drive its power output to a constant or varying reference, i.e to achieve power output regulation. At the same time, the proposed control scheme attains the maximum power point tracking (MPPT) objective. This control scheme is the first decentralized nonlinear control scheme for this emerging technology of WGs which is expected to be widely deployed in the future, that can enable power output regulation through exploitation of their storage devices for a wide-range of operating conditions.

In the same direction, the problem of enabling a group of SoA WGs with supercapacitor storage devices to regulate their total power output is studied. We first emphasize that aggregating wind power outputs of several wind generators leads to reduced temporal volatility on their total power output (compared with that of their individual power outputs). Therefore, in this dissertation we develop a distributed control scheme that WGs can adopt to self-organize and regulate their total power output. With the proposed scheme, their individual power outputs do not have to necessarily match given references, as in the case of the decentralized control scheme mentioned above. Further, with the proposed distributed control scheme SoA WGs can regulate their total power output while at the same time deploy their storage devices in a fair load-sharing fashion, i.e all storage devices provide the same amount of power. The methodology for developing this control scheme can be described as follows. Initially, the main problem is posed as a constrained consensus problem for the power electronics controllers of SoA WGs and a distributed leader-follower consensus protocol whose equilibrium realizes the desired objectives is proposed. Thereafter, we employ singular perturbation and Lyapunov theories to conduct compositional stability analysis and establish asymptotic stability of the consensus protocol's equilibrium point, explicitly deriving sufficient conditions under which this is guaranteed. Eventually, we develop the distributed controller for the GSC and the CLF-based control law for the DC-DC converter that together enable WGs to attain WF power output regulation with fair load-sharing of the storage devices. The distributed power-electronics control design: 1) can contribute to total generation cost reduction especially in large power systems since it uses stored wind energy to balance wind intermittency, eliminating the need for utilizing fast ramping-up SGs; 2) is practically realizable, requiring WGs to exchange feedback signals that can be easily measured locally; 3) has stability and performance that are guaranteed for a wide range of operating conditions. The control methodology and the results related to this proposed scheme are novel in the following aspects:

1. For a specific class of leader-follower consensus protocols (e.g with the specific communication set-up analyzed here), it is the first work that employs singular perturbation and Gershgorin's circle theorem for stability analysis. By combining these two tools, a new methodology and approach to stability analysis for this particular class of distributed protocols is provided that: 1) provides valuable insight since singular perturbation reveals the control objectives that exist in different time-scales; 2) is computationally simpler than standard full-system stability methods since it is based on Lyapunov functions for lower-dimensional subsystems; 3) it gives an explicit way of deriving sufficient conditions for stability of this class of protocols by exploiting Gershgorin's circle theorem.
2. On the practical side, it is the first work to introduce a distributed power-electronics control architecture for SoA WGs that reveals and leverages their full potential by self-organizating and coordinating them so that they provide power output regulation.

It is worthwhile emphasizing that WGs of this particular type will become main power generating units in the coming years. Therefore, a crucial task that should precede their large-scale exploitation is to develop systematic methods for controlling them which are both practical and mathematically rigorous.

In the same spirit, another direction for effectively dealing with the WF power output regulation problem is explored. Particularly, solving the problem of enabling a group of wind double-fed induction generators (DFIGs) that lack storage devices to attain WF power output regulation. These WGs are the ones that are most commonly deployed today. In order for them to generate predictable power, they have to first operate in a deloaded operating regime, extracting less power than the maximum possible for given wind-speed conditions. Then, they have to self-dispatch according to a given total WF power reference and the local wind speed conditions, and regulate their power outputs dynamically to corresponding dynamic set-points. The real challenge for wind DFIGs is to perform all these actions in a timely, robust and computationally efficient fashion: timely, since in the future, WFs will have to respond faster to maintain supply-demand power balance, especially in microgrid settings; robust, such that the performance of WFs is also reliable and computationally efficient, to support timely and cost-effective operation (especially when the number of WGs is very large). In this dissertation, we resolve this challenge by developing a novel distributed control architecture that WGs can adopt to dynamically self-dispatch and control their mechanical power outputs extracted from the wind, so that their total extracted power tracks a pre-assigned reference and their utilization levels converge to a common value (i.e fair load-sharing). The methodology for developing this control scheme is outlined as follows. First, the main problem is formulated as a constrained consensus problem among WGs where they have to dynamically agree on their utilization levels (that depend on local wind-speed conditions) under the constraint that their total power tracks a power reference. Then, we introduce a suitable leader-follower consensus protocol that WGs can adopt through their RSC control scheme to carry out these objectives. We employ singular perturbation theory to temporarily decompose the protocol dynamics and perform compositional stability analysis to derive a condition under which asymptotic stability of the equilibrium of the full protocol dynamics is guaranteed. In the last step of our methodology, we analytically develop the distributed Control Lyapunov Function-based torque controller for the rotor-side power electronics of WGs that realizes the proposed protocol in practice through peer-to-peer communication. The proposed distributed control scheme: 1) can enable a group of WGs to self-dispatch and regulate their power outputs based on local wind-speed conditions, in that way eliminating the need for a central wind farm controller and leading to low computational cost; 2) requires minimum peer-to-peer communication among neighboring WGs; 3) enables WGs to be dispatched and regulate their power outputs timely which is critical when these actions have to be performed under fast-varying dynamical wind and loading conditions to balance supply-demand (especially in autonomous power systems such as microgrids); 4) has guaranteed stability and performance.

The dissertation results related to this part are the first to systematically and effectively solve the problem of dispatching and controlling the power outputs of a group of deloaded WGs in order to attain WF power output regulation, in a distributed, dynamic and efficient manner. In contrast with previous work [13], our method is dynamic in the sense that the proposed power electronics WG controllers reach consensus dynamically according to a given reference. We emphasize that solving the problem of dispatching WGs efficiently and distributively is as critical as solving the Economic Dispatch (ED) problem of SGs in a distributed fashion, which has already attracted a lot of attention in the power systems and control communities [20, 21, 22]. Therefore, our work provides first steps in this direction.

In summary, this dissertation makes several contributions to the effective solution of the transient stabilization and WF power output regulation problems, through comprehensive distributed control methodologies for storage devices, currently used WGs and SoA WGs with incorporated storage devices.

6.2 Future Work

There are several interesting directions that can be followed to extend the results of this dissertation.

6.2.1 Direction 1 - Distributed economic dispatch and frequency control with dispatchable SoA WGs

In the future, SoA WGs will have to provide services to power grids akin to the services that SGs provide today, e.g primary, secondary frequency control. Since the storage devices of these WGs render them dispatchable generating units, they can now be accounted for in the same manner as conventional synchronous generators in the formulation and solution of the two most important problems in power systems operation, the economic dispatch problem and the frequency control problem: 1) distributed economic dispatch problem has to be reformulated and solved by considering objective functions for dispatchable WGs together with the objective functions for SGs in a coupled optimization problem set-up,; 2) distributed optimal frequency control problem has to be reformulated and solved by considering also the SoA WGs' advanced frequency-regulation capabilities. Therefore, formulating and effectively solving these two main problems in high-wind integration settings arise as two core challenges for future power systems operation. Possible approaches for solving these challenges in a rigorous manner can be:

1. **Distributed economic dispatch with dispatchable SoA WGs**: First, this problem can be formulated under high-wind integration settings and then solved by deriving optimality and stability conditions that can be realized distributively with price-based controllers.
2. **Distributed optimal frequency control with SoA WGs**: We can solve the optimal secondary frequency regulation problem when WGs are also regulating units by deriving optimality and stability conditions that will ensure optimal frequency regulation in high-wind integration settings.
3. **Distributed economic dispatch and optimal frequency control with dispatchable SoA WGs**: Here, we can study, formulate and solve the above interrelated problems jointly.

Another interesting direction that can be pursued in the future is distributed stability and control of modern power systems. This direction is related to the results presented in this dissertation but is more generic and does not involve only stability and control aspects for wind farms but stability and control aspects for any type of new heterogeneous technologies that can be interconnected in power systems today.

6.2.2 Direction 2 - Distributed stability assessment and control of power systems

The heterogeneity and complexity of power systems are increasing due to the interconnection of new power generation, communication and information technologies. Moreover, the power system dynamics tend to evolve in faster time-scales due to decreasing system inertia caused by the power-electronically-interfaced generation technologies. Additionally, power systems experience more severe and uncertain power disturbances, originating from renewable energy resources. The implication of all the above is that *stability and normal operation of power systems are now more endangered but also harder to assess and guarantee.*

In this new power systems environment, conducting centralized stability assessment becomes computationally inefficient (due to huge amount of data), requires information and dynamical models from geographically distant control areas and also raises privacy concerns. At the same time, there are no systematic methods for decomposing the global control objectives for stability and performance of an interconnected power grid into simpler control objectives that its dynamical elements (e.g SGs, WGs, storage devices), have to accomplish [45, 46, 47]. This has the following crucial implications: 1) there are *no formal guarantees for stability and performance of the interconnected system* with all these integrated heterogeneous technologies; 2) there are *no specific control objectives which various technologies have to meet along with their controllers* that are also interrelated with the global objectives discussed above; 3) because of 2), there are *no incentives or requirements for the various technologies to participate in power systems control* through advancing their control methodologies; 4) also, the implications of 2), 3) are that, the way power systems are being operated today *does not promote the ongoing plug-and-play evolution of the grid and the integration of new technologies at value* since the control capabilities and value of each technology cannot be realized and leveraged in such environments [45, 46, 47]. The above challenges can be solved by:

1. **Developing distributed stability methods** that are: 1) *computationally efficient*, requiring power system agent-based components to exchange limited information and formally assess whether they satisfy simple stability criteria; 2) *privacy-preserving*, meaning they only require minimal communication among components and nonsensitive private information (e.g detailed dynamical models); 3) *provide faster system-wide stability assessment with guarantees*, something very important in modern grids with fast-varying loading conditions. Previous work toward distributed stability assessment and control design for nonlinear dynamical systems can be found in [48, 49, 50].

2. **Developing distributed stability criteria** based on sufficient conditions that single or group of components have to respect and, if met, guarantee system-wide stability and performance [45, 46, 47]. The significance of developing such criteria is that they will 1) *enable plug-and-play integration of various technologies* with simple and well-defined control objectives accomplished by their controllers; 2) *guide the control design* since the controllers have to comply with specific requirements; 3) *provide guarantees for system-wide performance and stability*; 4) *promote integration of various technologies at value*, since in the above framework their capabilities and potential can be realized and leveraged.

3. **Developing advanced distributed control architectures** for various technologies that will *guarantee stability and certain performance aligned with the criteria* in 2). Our previous work in this direction can be found in [51, 24, 30, 52, 18, 19].

Appendix A

3-Bus Power System with STATCOM and Storage

The 3-bus system presented in Chapter 2 is based on the parameters for the dynamical models of generators and the transmission lines from [53] and the parameters for the models of the Automatic Voltage Regulators (AVR) from [9] given below.

Gen #	Bus #	H	T'_{d0}	X_d	X_q	X'_d	X'_q
1	1	10	5	0.44	0.088	0.088	0.088
2	2	15	5	0.25	0.05	0.05	0.05
3	3	30	7	0.075	0.015	0.015	0.015

Table A1: Parameters of generators' dynamical models

Gen #	Bus #	K_A	T_A	K_E	T_E	K_F	T_F
1	1	20	0.2	1	0.314	0.063	0.35
2	2	20	0.2	1	0.314	0.063	0.35

Table A2: Parameters of the generators' Automatic Voltage Regulator (AVR) models

From Bus #	To Bus #	R	X
1	2	0.01	0.46
1	3	0.01	0.26
2	3	0.0086	0.0806

Table A3: Parameters of Transmission Lines

Storage #	Bus #	R_b	L_b
2	2	0.05	0.1

Table A4: STATCOM Battery Storage Parameters

Appendix B

3-Bus Power System with Wind Generator

The 3-bus system presented in Chapter 3 is based on the parameters for the dynamical models of generators and the transmission lines from [53] and the parameters for the models of the Automatic Voltage Regulators (AVR) from [9]. In addition, the parameters for the dynamical model of the double-fed induction wind generator are from [5]. All these parameters are provided below.

Gen #	Bus #	H	T'_{d0}	X_d	X_q	X'_d	X'_q
1	1	10	5	0.44	0.088	0.088	0.088
2	2	15	5	0.25	0.05	0.05	0.05

Table B1: Parameters of generators' dynamical models

Gen #	Bus #	K_A	T_A	K_E	T_E	K_F	T_F
1	1	20	0.2	1	0.314	0.063	0.35
2	2	20	0.2	1	0.314	0.063	0.35

Table B2: Parameters of the generators' Automatic Voltage Regulator (AVR) models

Gen #	Bus #	T_0	X_m	X_r	X_s	X_s'	R_s	R_r
3	3	1.088	3.5092	3.5547	3.5859	0.1206	0.01015	0.0088

Table B3: Parameters of double-fed induction wind generator's dynamical model

Gen #	Bus #	R_g	L_g	R_{sc}	C_{sc}	C_{dc}
3	3	0.05	0.1	0.1	0.05	0.0001

Table B4: Parameters of double-fed induction wind generator's GSC, capacitor and super-capacitor storage models

From Bus #	To Bus #	R	X
1	2	0.01	0.46
1	3	0.01	0.26
2	3	0.0086	0.0806

Table B5: Parameters of Transmission Lines

Appendix C

IEEE 24-Bus Reliability Test System with a Wind Farm

The parameters of the dynamical models of generators as well as of their AVRs are given below while the parameters of the transmission lines can be found in [54]. The impedance of the line segment among two neighboring wind generators is $Z_d = 1.3951e{-}04{+}1.9849e{-}04j\ \Omega$.

Gen #	Bus #	H	T'_{d0}	X_d	X_q	X'_d	X'_q
1	1	5.46	8.96	0.146	0.0608	0.0608	0.0608
2	2	2.67	6	0.25	0.05	0.05	0.05
3	7	3.304	5.89	1.3125	0.1813	0.1813	0.1813
4	13	6.496	6	0.8958	0.1198	0.1198	0.1198
5	14	2.5	5.89	1.3125	0.1813	0.1813	0.1813
6	15	5.46	8.96	0.146	0.0608	0.0608	0.0608
7	16	5.46	6	0.8958	0.1198	0.1198	0.1198
8	18	23.55	8.96	0.146	0.0608	0.0608	0.0608
9	21	23.55	8.96	0.146	0.0608	0.0608	0.0608
10	23	12.36	6	0.8958	0.1198	0.1198	0.1198

Table C1: Parameters of generators' dynamical models

Gen #	Bus #	K_A	T_A	K_E	T_E	K_F	T_F
1,...,10	1	20	0.2	1	0.314	0.063	0.35

Table C2: Parameters of the generators' Automatic Voltage Regulator (AVR) models

Wind Gen #	Bus #	T_0	X_m	X_r	X_s	X'_s	R_s	R_r	H
1,...,10	3	1.088	3.5092	3.5547	3.5859	0.1206	0.01015	0.0088	4

Table C3: Parameters of double-fed induction wind generator's dynamical model

Wind Gen #	Bus #	R_g	L_g	R_{sc}	C_{sc}	C_{dc}
1,...,10	3	0.05	0.1	0.1	0.05	0.0001

Table C4: Parameters of double-fed induction wind generator's GSC, capacitor and super-capacitor storage models

Bibliography

[1] U. Deparment of Energy, "Wind Vision: A New Era for Wind Power in the United States," tech. rep., U.S Deparment of Energy, March 2015.

[2] Thomas Ackermann, ed., *Wind Power in Power Systems*. John Wiley and Sons, second ed., 2012.

[3] P. Kundur, *Power System Stability and Control*. McGraw-Hill, 1994.

[4] G. Andersson, P. Donalek, R. Farmer, N. Hatziargyriou, I. Kamwa, P. Kundur, N. Martins, J. Paserba, P. Pourbeik, J. Sanchez-Gasca, R. Schulz, A. Stankovic, C. Taylor, and V. Vittal, "Causes of the 2003 Major Grid Blackouts in North America and Europe, and Recommended Means to Improve System Dynamic Performance," *IEEE Transactions on Power Systems*, vol. 20, pp. 1922–1928, November 2005.

[5] H. Pulgar Painemal and P. Sauer, "Dynamic Modeling of Wind Power Generation," in *Proceedings of the North American Power Symposium (NAPS)*, 2009.

[6] Y. Guo, D. J. Hill, and Y. Wang, "Global Transient Stability and Voltage Regulation for Power Systems," *IEEE Transactions on Power Systems*, vol. 16, pp. 678–688, November 2001.

[7] N. Miller, "GE Experience with Turbine Integrated Battery Energy Storage," in *IEEE PES General Meeting*, 2014.

[8] FERC, "Security Constrained Economic Dispatch: Definition, Practices, Issues and

Recommendations," tech. rep., FERC, July 2006.

[9] P. W. Sauer and M. A. Pai, *Power System Dynamics and Stability.* Stipes Publishing L.L.C, 2007.

[10] H. K. Khalil, *Nonlinear Systems.* Prentice Hall, 3rd ed., 2002.

[11] C. A. King, J. W. Chapman, and M. D. Ilic, "Feedback Linearizing Excitation Control on a Full-Scale Power System Model," *IEEE Transactions on Power Systems*, vol. 9, pp. 1102–1109, May 1994.

[12] K. Lingyi and L. Liying, "Multi-Index Nonlinear Coordinated Control for Battery Energy Storage System and Generator Excitation," in *Proceedings of the International Conference on Applied Physics and Industrial Engineering*, pp. 503–511, 2012.

[13] W. Zhang, Y. Xu, W. Liu, F. Ferrese, and L. Liu, "Fully Distributed Coordination of Multiple DFIGs in a Microgrid for Load Sharing," *IEEE Transactions on Smart Grid*, vol. 4, pp. 806–815, June 2013.

[14] B. Biegel, D. Madjidian, V. Spudic, A. Rantzer, and J. Stoustrup, "Distributed low-complexity controller for wind power plant in derated operation," in *Proceeding of 2013 IEEE International Conference on Control Applications (CCA)*, pp. 146–151, IEEE, 2013.

[15] L. Qu and W. Qiao, "Constant Power Control of DFIG Wind Turbines With Supercapacitor Energy Storage," *IEEE Transactions on Industry Applications*, vol. 47, pp. 359–367, January/February 2011.

[16] C. Abbey and G. Joos, "Integration of Energy Storage with a Doubly-Fed Induction Machine for Wind Power Applications," in *Proceedings of the 35th IEEE Annual on Power Electronics Specialists Conference*, vol. 3, pp. 1964–1968, June 2004.

[17] F. A. Bhuiyan and A. Yazdani, "Multimode Control of a DFIG-Based Wind-Power Unit

for Remote Applications," *IEEE Transactions on Power Delivery*, vol. 24, pp. 2079–2089, October 2009.

[18] S. Baros, "Predictable Wind Power via Distributed Control of Wind Generators with Integrated Storage," in *Proceedings of the American Control Conference*, 2016.

[19] S. Baros, "Distributed Torque Control of Deloaded Wind DFIGs: Power Reference Tracking via Fair Dynamic Dispatching," in *Proceedings of the American Control Conference*, 2016.

[20] N. Li, C. Zhao, and L. Chen, "Connecting Automatic Generation Control and Economic Dispatch from an Optimization View," in *Proceedings of the American Control Conference*, pp. 735 – 740, 2014.

[21] D. Cai, E. Mallada, and A. Wierman, "Distributed optimization decomposition for joint economic dispatch and frequency regulation," in *Proceedings of the 54th IEEE Conference on Decision and Control*, 2015.

[22] C. Zhao and S. Low, "Optimal Decentralized Primary Frequency Control in Power Networks," in *Proceedings of the 53rd IEEE Conference on Decision and Control*, pp. 2467 – 2473, 2014.

[23] C. Abbey and G. Joos, "Supercapacitor Energy Storage for Wind Energy Applications," *IEEE Transactions on Industry Applications*, vol. 43, pp. 769–776, May/June 2007.

[24] S.Baros and M. Ilic, "On Transient Stability and Voltage Regulation Through MIMO Feedback Linearizing Control of Generator and Energy Storage," in *Proceedings of the American Control Conference*, 2015.

[25] A. Isidori, *Nonlinear Control Systems (Communications and Control Engineering)*. Springer, 3rd ed., 1995.

[26] D. Gautam, V. Vittal, and T. Harbour, "Impact of Increased Penetration of DFIG-

Based Wind Turbine Generators on Transient and Small Signal Stability of Power Systems," *IEEE Transactions on Power Systems*, vol. 24, pp. 1426–1434, May 2009.

[27] L. Meegahapola and D. Flynn, "Impact on transient and frequency stability for a power system at very high wind penetration," in *Proceedings of the IEEE Power and Energy Society General Meeting*, 2010.

[28] C. Jauch, J. Matevosyan, and T. A. amd S. Bolik, "International Comparison of Requirements for Connection of Wind Turbines to Power Systems," *Wind Energy*, vol. 8, pp. 295–306, September 2005.

[29] Y. Bao and Y. Li, "On deloading control strategies of wind generators for system frequency regulation," *International Transactions on Electrical Energy Systems*, vol. 25, pp. 623–635, April 2015.

[30] S. Baros, "A Novel Ectropy-Based Control Scheme for a DFIG Driven by a Wind Turbine with an Integrated Energy Storage," in *Proceedings of the American Control Conference*, pp. 4345 – 4351, 2015.

[31] W. Qiao, "Dynamic Modeling and Control of Doubly Fed Induction Generators Driven by Wind Turbines," in *Proceedings of the Power Systems Conference and Exposition (PSCE)*, 2009.

[32] A. Larsen and T.S Mogensen, "Individuel Pitchregulering af Vindmølle," Master's thesis, Technical University of Denmark., 2006.

[33] S. Thomsen, "Nonlinear Control of a Wind Turbine," Master's thesis, Technical University of Denmark, 2006.

[34] I. Munteanu, A. Bratcu, N. Cutululis, and E. Ceanga, *Optimal Control of Wind Energy Systems - Towards a Global Approach*. Springer, 2008.

[35] M. Cvetkovic, *Power-Electronics-Enabled Transient Stabilization of Power Systems*.

PhD thesis, Carnegie Mellon University, December 2013.

[36] W. M. Haddad and V. Chellaboina, *Nonlinear Dynamical Systems and Control: A Lyapunov-Based Approach.* Princeton University Press, 2008.

[37] E. D. Sontag, *Mathematical Control Theory: Deterministic Finite Dimensional Systems.* No. 6 in Textbooks in Applied Mathematics, Springer, 2nd ed., 1998.

[38] R. A. Freeman and P. V. Kokotovic, *Robust Nonlinear Control Design: State-Space and Lyapunov Techniques.* Birkhauser, January 2008.

[39] M. Albadi and E. El-Saadany, "Overview of wind power intermittency impacts on power systems," *Electric Power Systems Research*, vol. 80, pp. 627–632, June 2010.

[40] H. Xin, Z. Qu, J. Seuss, and A. Maknouninejad, "A Self-Organizing Strategy for Power Flow Control of Photovoltaic Generators in a Distribution Network," *IEEE Transactions on Power Systems*, vol. 26, pp. 1462–1473, August 2011.

[41] S. Kar and J. M. Moura, "Distributed Consensus Algorithms in Sensor Networks With Imperfect Communication: Link Failures and Channel Noise," *IEEE Transactions on Signal Processing*, vol. 57, pp. 355–369, January 2009.

[42] R. Horn and C. Johnson, *Matrix Analysis.* Cambridge University Press, 2013.

[43] R. G. de Almeida and J. A. P. Lopes, "Participation of Doubly Fed Induction Wind Generators in System Frequency Regulation," *IEEE Transactions on Power Systems*, vol. 22, pp. 944–950, August 2007.

[44] K. Gu, V. L. Kharitonov, and J. Chen, *Stability of Time-Delay Systems.* Springer Science+Business Media, 2003.

[45] M. Ilic and Q. Liu, "Toward Standards for Model-based Control of Dynamic Interactions in Large Electric Power Grids," in *Proceedings of the 2012 Signal and Information Processing Association Annual Summit and Conference (APSIPA ASC)*, 2012.

[46] M. Ilic, "Toward Standards for Dynamics in Electric Energy Systems," White Paper, Power Systems Engineering Research Center, 2012.

[47] M. Ilic, "Toward Plug-and-Play Standards for Dynamics in the Changing Electric Energy Systems." PSERC Webinar Slides, http://pserc.wisc.edu/education/archived_tele_seminars/systems_webinars.aspx, November 2015.

[48] S. Kundu and M. Anghel, "Distributed Coordinated Control of Large-scale Nonlinear Networks," in *Proceedings of the 5th IFAC Workshop on Distributed Estimation and Control in Networked Systems*, pp. 240–245, 2015.

[49] S. Kundu and M. Anghel, "An iterative expanding-contracting ring algorithm for decentralized stability analysis," in *Proceedings of the 54th IEEE Conference on Decision and Control*, 2015.

[50] S. Kundu and M. Anghel, "A sum-of-squares approach to the stability and control of interconnected systems using vector lyapunov functions," in *arXiv:1501.05266*, 2015.

[51] S.Baros and M.Ilic, "Multi-objective Lyapunov-based Control of a STATCOM/BESS," in *Proceedings of the Innovative Smart Grid Technologies Conference (ISGT)*, 2015.

[52] S.Baros and M. Ilic, "Robust Ectropy-based Cooperative Control of a Wind DFIG for Transient Stabilization and Mppt," in *Proceedings of the IEEE Power and Energy Society General Meeting*, 2015.

[53] J. W. Chapman, *Power system control for large-disturbance stability : security, robustness and transient energy*. PhD thesis, Massachusetts Institute of Technology, 1996.

[54] R. T. S. T. Force, "The IEEE Reliability Test System - 1996," *IEEE Transactions on Power Systems*, vol. 14, pp. 1010–1020, August 1999.

[55] S.Baros and M. Ilic, "Robust Ectropy-based Cooperative Control of a Wind DFIG for Transient Stabilization and Mppt," in *Proceedings of the IEEE Power and Energy*

Society General Meeting, 2015.

[56] J. W. Chapman, M. D. Ilic, C. A. King, L. Eng, and H. Kaufman, "Stabilizing a Multimachine Power System via Decentralized Feedback Linearizing Excitation Control," *IEEE Transactions on Power Systems*, vol. 8, pp. 830–839, August 1993.

[57] L. Fan and A. Feliachi, "Decentralized Stabilization of Nonlinear Electric Power Systems Using Local Measurements and Feedback Linearization," in *Proceedings of the 43rd IEEE Midwest Symposium on Circuits and Systems*, 2000.

[58] M. Cvetkovic and M. Ilic, "Ectropy-based Nonlinear Control of FACTS for Transient Stabilization," *IEEE Transactions on Power Systems*, vol. 29, November 2014.

[59] *Focus on 2030: EWEA aims for 22% of Europe's Electricity by 2030*, November/December 2006.

[60] A. Bidram, A. Davoudi, F. Lewis, and J. Guerrero, "Distributed Cooperative Secondary Control of Microgrids Using Feedback Linearization," *IEEE Transactions on Power Systems*, vol. 28, pp. 3462–3470, August 2013.

[61] P. S. Georgilakis, "Technical challenges associated with the integration of wind power into power systems," *Renewable and Sustainable Energy Reviews*, vol. 12, pp. 852–863, April 2008.

[62] W. M. Haddad, V. Chellaboina, and S. G. Nersesov, *Thermodynamics: A Dynamical Systems Approach.* Princeton Series in Applied Mathematics, Princeton University Press, July 2005.

[63] A. D.Dominguez Garcia and C. N. Hadjicostis, "Coordination and Control of Distributed Energy Resources for Provision of Ancillary Services," in *Proceedings of the IEEE International Conference on Smart Grid Communications (SmartGridComm)*, pp. 537–542, 2010.

[64] A. D.Dominguez-Garcia and C. N. Hadjicostis, "Resilient Networked Control of Distributed Energy Resources," *IEEE Journal on Selected Areas in Communications*, vol. 30, pp. 1137–1148, May 2012.

[65] S. Kar and G. Hug, "Distributed Robust Economic Dispatch in Power Systems: A Consensus + Innovations approach," in *Proceedings of the IEEE Power and Energy Society General Meeting*, 2012.

[66] Z. Yang, C. Shen, L. Zhang, M. L. Crow, and S. Atcitty, "Integration of a StatCom and Battery Energy Storage," *IEEE Transactions on Power Systems*, vol. 16, pp. 254–260, May 2001.

[67] A. Bidram, A. Davoudi, F. L. Lewis, and J. M. Guerrero, "Distributed Cooperative Secondary Control of Microgrids Using Feedback Linearization," *IEEE Transactions on Power Systems*, vol. 28, pp. 3462–3470, March 2013.

[68] M. Cvetkovic and M. Ilic, "A Two-level Approach to Tuning FACTS for Transient Stabilization," in *Proceedings of the IEEE Power and Energy Society General Meeting*, 2014.

[69] M. Cvetkovic and M. Ilic, "Cooperative Line-flow Power Electronics Control for Transient Stabilization," in *Proceedings of the 53rd IEEE Conference on Decision and Control*, pp. 3280 – 3285, 2014.

[70] R. Olfati Saber, J. A. Fax, and R.M. Murray, "Consensus and Cooperation in Networked Multi-Agent Systems," *Proceedings of the IEEE*, vol. 95, pp. 215–233, January 2007.

[71] North American Electric Reliability Coorporation, "Special Report: Potential Reliability Impacts of Emerging Flexible Resources," tech. rep., NERC, November 2010.

[72] M. Mahmud, H. Pota, and M. Hossain, "Full-order nonlinear observer-based excitation controller design for interconnected power systems via exact linearization approach," *International Journal of Electric Power and Energy Systems*, vol. 41, pp. 54–62, October

2012.

[73] J. G. Slootweg and W. L. Kling, “Modelling and Analysing Impacts of Wind Power on Transient Stability of Power Systems,” *Wind Engineering*, vol. 25, no. 6, pp. 3–20, 2001.

[74] D. J. Hill, T. Liu, and G. Verbic, “Smart Grids as Distributed Learning Control,” in *Proceedings of the IEEE Power and Energy Society General Meeting*, 2012.

[75] O. Francis, D. Louis A, and A. Ouassima, “Power System Stability Enhancement Using a Wide-Area Signals Based Hierarchical Controller,” *IEEE Transactions on Power Systems*, vol. 20, August 2005.